# INVESTIGATIONS ON STATIC CONTROLLERS FOR SELF-EXCITED INDUCTION GENERATORS

**A THESIS**

***Submitted in fulfillment of the***

***requirements for the award of the degree***

***of***

**DOCTOR OF PHILOSOPHY**

***in***

**ELECTRICAL ENGINEERING**


***By***

**Yogesh Kumar Chauhan**

**ELECTRICAL AND INSTRUMENTATION ENGINEERING DEPARTMENT**

**THAPAR UNIVERSITY**

**PATIALA-147004**

**PUNJAB-INDIA**



**October, 2010**

# CERTIFICATE

This is to certify that the thesis entitled "**Investigations on Static Controllers for Self-Excited Induction Generators**" being submitted by Mr. Yogesh Kumar Chauhan for the award of the degree of **Doctor of Philosophy** is a record of bona fide research work carried out by him in the Electrical and Instrumentation Engineering Department of Thapar University, Patiala.

Mr. Yogesh Kumar Chauhan has worked under our guidance and supervision and has fulfilled the requirements for the submission of this thesis, which to our knowledge has reached the requisite standard. The results and work presented in this thesis have not been submitted by him for the award of any other degree of this or any other university.

(Dr. Sanjay K Jain)
Associate Professor
Electrical & Instrumentation Engg. Deptt.
Thapar University
Patiala-147004, India
Email: skjain@thapar.edu

(Dr. Bhim Singh)
Professor
Department of Electrical Engineering
Indian Institute of Technology, Delhi
New Delhi-110016, India
Email: bsingh@ee.iitd.ac.in

Dated: 08th oct 2010

# ACKNOWLEDGEMENTS

My foremost gratitude goes to my guides Dr. Bhim Singh, Professor, Department of Electrical Engineering, Indian Institute of Technology Delhi, New Delhi and Dr. Sanjay K. Jain, Assistant Professor, Electrical and Instrumentation Engineering Department, Thapar University, Patiala for their proficient guidance, continuous monitoring, motivating and helping nature, and useful criticism throughout the research work leading to this thesis in the present form.

It is my proud privilege of being a student of Prof. Bhim Singh since my M. Tech. His wide experience, prolific research knowledge on the subject, innovative and visionary approach and time management are very much inspiring to me. His continuous encouragement is always a force to reckon and to introspect. I have profound regards for him and express life time heartfelt thanks to Prof. Singh.

I am thankful to the chairman doctoral committee and HEIED Prof. S. Ghosh; doctoral committee members Prof. R. Agarwal and Prof. R. K. Sharma; Dean, Research and Sponsored Projects Prof. S. Mittal for motivation and constructive criticism.

My heart felt gratitude is due to Prof. K. K. Raina, Dean, Faculty Affairs and Deputy Director and Honorable Director, Dr. A. Mukherjee for encouragement and support to complete this work.

My sincere thanks are duo to All India Council for Technical Education (AICTE), New Delhi for granting the research project, which has facilitated me to acquire computational facility at the most crucial time.

I express my special gratitude to the Electric Machine Lab staff Mr. Shayam Lal, Mr. Dalvir Singh and Mr. Raj Kumar for their untiring assistance and motivation during initial glitches of the experimental setup and during conduction of experiment.

I acknowledge thanks to M.E. (Power Systems and Electric Drives) students Mr. Satnam Mahley, Mr. D.V. Krishna Kishore, Mr. Sailesh, Mr. Parveen Kumar, Mr. Sahil Gupta and Mr. Manoj Kumar Arya for their support in conducting the experiment during odd hours.

I extend my thanks to all those, who directly or indirectly contributed with their encouragement, suggestions and positive criticism.

My special heartfelt gratitude goes to my parents, my brother Er. Mahesh Kumar Chauhan, nieces Shivanshi and Nimisha for their consistent support and encouragement throughout the research duration.

My sincere very special thanks are due to my soul mate Dr. (Mrs) Poonam Rani, my children Shivam and Kishan for their emotional support and strength during this journey, which can not be forgotten in my life time.

(Yogesh Kumar Chauhan)

Roll. No. 9021154

# ABSTRACT

The fast depleting rate of fossils fuels such as coal, petroleum products, environment pollution and ecological concerns are drawing an attention to harness the renewable energy resources. Moreover, the challenges in extending the grid supply to far flung and hilly areas have forced the work on stand alone generating units. The self-excited induction generator (SEIG) is a strong candidate to extract electrical energy from renewable energy sources such as small hydro and wind due to various advantages over the conventional synchronous generator for small capacity applications. The SEIG is normally an externally driven three-phase squirrel cage induction machine with suitable capacitor bank at its stator terminals. The research on SEIG has got impetus after the energy crisis faced during seventies and various facets of SEIG have been investigated. The generated voltage of SEIG depends upon the speed of prime mover, shunt capacitance, magnetization characteristic of the machine and the nature of load. The SEIG terminal voltage droops with an increase in the load. Various conventional methods to improve the voltage regulation of SEIG include the use of series capacitors i.e. compensated SEIG configurations, constant voltage transformer (CVT), saturable core reactor etc. Although, the conventional methods are simple but their effectiveness, size, losses etc. have been the reasons to explore other methods. Moreover, the compensated SEIG configurations have resulted into unstable and oscillating behavior with the induction motor loads.

The advancements in the characteristics of power electronic devices, hardware support for higher switching frequency operation etc. have motivated to use the switching devices based voltage regulators such as switching capacitors, continuously controlled capacitors etc. for improving the performance of SEIG. Moreover, the improvement in power converter topologies, digital signal processors, controllers and control techniques have asserted the voltage source converter applications for improving the SEIG performance by improving the voltage regulation. The static shunt compensator (STATCOM) is normally a pulse width modulation (PWM) based voltage source converter (VSC) with a capacitor on DC bus for self support. The STATCOM can emulate as a controlled inductive or capacitive element, which can absorb or supply reactive power with the proper switching arrangement. The static synchronous series

compensator (SSSC), a synchronous voltage source converter connected in series with the line through a series transformer, has proven applicability in power system for power flow and damping control etc. The SSSC produces controllable compensating voltage, which can emulate a controlled capacitor or inductor independent to the line current.

This research work is carried out with the broad objective to investigate the performance of SEIG with static controllers namely STATCOM and SSSC for feeding various loads. The following investigations are made to achieve the set objectives.

Various regulating schemes for SEIG are discussed along with their relative suitability, and operational aspects. The voltage regulating schemes are categorized into shunt and series compensation schemes, which are sub classified into classical schemes, switching devices based schemes and converter based schemes. The frequency regulating schemes are based on arrangement for the active power control. The voltage-frequency regulating schemes, which are based on active and reactive power control arrangement, are also briefed for three-wire and four-wire systems.

The steady state performance of SEIG is investigated for feeding various linear loads. The steady state performance is analyzed for voltage regulation optimization with shunt capacitance and speed as variables. The objective function is subjected to various equality and inequality constraints related to successful operation. The combination of shunt capacitance and speed for the formulated problem is calculated using genetic algorithm (GA), a global search and optimization approach.

The transient performance of SEIG is studied for feeding linear and non-linear loads. The generalized induction machine model in q-d variables in stationary reference frame is developed and used for SEIG and an induction motor load, whereas, phase variables models are used for the non-linear loads. The balanced and unbalanced non-linear loads such as three-wire and four-wire uncontrolled rectifier fed resistive-capacitive loads are considered for the study. The effect of load harmonics on SEIG is estimated with total harmonic distortion (THD) and harmonic spectrum. For non-linear load, the THD in generator quantities are compared with permitted IEEE-519 standard.

The performance analysis of SEIG-STATCOM system is analyzed for feeding static resistive-inductive load and dynamic (induction motor load and fully controlled rectifier fed DC motor) loads. The equations to model each system component are

explained along with the equations for generating gating signals. A methodology is developed to decide the STATCOM rating and its associated parameters. Accordingly, the STATCOM is designed for voltage regulation of SEIG in two cases, namely full rating and reduced rating. A control technique is proposed for generating the gating signals for STATCOM devices. The control technique consists of two proportional-integral (PI) controllers, one for maintaining the DC bus voltage and other for maintaining the SEIG terminal voltage. The transient performance characteristics of the complete system are studied with both full rating and reduced rating STATCOM design parameters for voltage buildup, switching of STATCOM into the system, sudden application of the load and change of the loads. The power quality of the SEIG supply is estimated using harmonic spectrum and THD.

The modeling and transient performance analysis of three-phase, four-wire isolated SEIG-STATCOM system are presented for feeding various types of balanced/unbalanced linear and non-linear loads. The employed STATCOM is an insulated gate bipolar transistor (IGBT) based pulse width modulation (PWM) operated four-leg voltage source converter (VSC) with self supporting DC bus. Various studies are carried out on three-phase, four-wire stand alone supply system to address the problems of voltage regulation, unbalanced operation, harmonics and neutral current for linear and non-linear loads. For non-linear loads, harmonic spectrum and total harmonic distortion (THD) are analyzed to assess the quality of the generator voltage and currents.

The steady state performance analysis of series capacitor compensated SEIG, namely short shunt SEIG configuration is also studied for feeding static loads. The optimization problems, representing voltage regulation characteristic and performance characteristic of SEIG, as separate objective functions are formulated, subjected to various equality and inequality constraints arising due to operating conditions of SEIG. The objective function representing performance characteristic is taken as the weighted sum of voltage regulation characteristic and loadability of SEIG. The value of series and shunt capacitances at a specified speed are obtained for optimum voltage regulation and optimum performance using GA. The performance is studied for resistive and resistive-inductive loads.

The transient performance of SEIG with static synchronous series compensator (SSSC) is carried out for resistive, resistive-inductive and resistive-capacitive loads. The

performance has been investigated for SEIG-battery supported SSSC and SEIG-capacitor supported SSSC configurations. The employed SSSCs are IGBT based PWM operated current controlled-voltage source converters (CC-VSC). A methodology is proposed for the design of SSSC parameters and components for above mentioned SSSC configurations and static loads. The proposed control technique for battery supported SSSC consists of a proportional-integral (PI) controller that is employed to maintain the load voltage. The proposed control technique for capacitor supported SSSC consists of two PI controllers, one for regulating the DC bus voltage and other for regulating the SEIG terminal voltage. The transient performance of SEIG-SSSC system is investigated for feeding static loads.

The design, modeling and transient performance of SEIG-SSSC are investigated to feed an induction motor load to obtain stable operation. The performance of short shunt SEIG feeding an induction motor load is simulated and the unstable behavior under different conditions like voltage collapse, sustained oscillations, high voltage and current are studied. The capability of SSSC is demonstrated in mitigating the unstable and oscillating behavior resulting during the loading of compensated SEIG with an induction motor load.

The investigations summarized in this thesis on the regulating schemes for three-phase SEIGs, steady state and transient analysis of three-phase SEIG, SEIG operation with STATCOM feeding static and dynamic loads, SEIG-STATCOM operation as an isolated four-wire supply system, short shunt SEIG operation for optimum performance, SEIG operation with SSSC feeding static and induction motor load bring the objectives of thesis to a successful conclusion.

# CONTENTS

# LIST OF FIGURES

# LIST OF TABLES

# LIST OF SYMBOLS

The various symbols and variables, which are used, are defined at the first occurrence in various chapters. However, list of principal symbols is given herewith for reference.

$P$ : Number of poles of SEIG

$J$ : Moment of inertia of SEIG system (Kg-m$^2$)

$\omega_r$ : SEIG angular speed (Rad/sec.)

$T_{em}$ : Electromagnetic torque developed in SEIG (N-m)

$T_P$ : Prime mover torque of SEIG (N-m)

$P_m$ : Number of poles of induction motor load

$J_m$ : Moment of inertia of induction motor load system (Kg-m$^2$)

$\omega_{rm}$ : Induction motor load angular speed (Rad/sec.)

$T_{emm}$ : Electromagnetic torque developed in induction motor load (N-m)

$T_L$ : Mechanical load coupled to motor load (N-m)

$C_{dc}$ : DC bus capacitance of CC-VSC (F)

$V_{dc}$ : DC bus voltage of CC-VSC (V)

$e_B$ : Back emf induced in DC motor load (V)

$\omega_{rd}$ : DC motor load angular speed (Rad/sec.)

$T_{emd}$ : Electromagnetic torque developed in DC motor load (N-m)

$J_d$ : Equivalent moment of inertia of DC motor load system (Kg-m$^2$)

$v_a$ : Applied armature voltage of DC motor load (V)

$i_a$ : Armature current of DC motor load (A)

$V_{dc}$ : DC bus voltage of CC-VSC (V)

$i_d$ : DC side current of uncontrolled rectifier load (A)

$v_d$ : DC side voltage of uncontrolled rectifier load (V)

$V_{ps}$ : Peak source voltage (V)

$i_{lab}$, $i_{lbc}$, $i_{lca}$ : Load phase currents (A)

$i_{la}$, $i_{lb}$, $i_{lc}$ : Load line currents (A)

$i_{ln}$, $i_{sn}$ : Load and supply neutral current (A)

$i_{rla}$, $i_{rlb}$, $i_{rlc}$ : Line currents for static R-L load (A)

$i_{ma}$, $i_{mb}$, $i_{mc}$ : Induction motor load currents (A)

$i_{ca}$, $i_{cb}$, $i_{cc}$ : Compensation currents of CC-VSC (A)

$i_{ga}$, $i_{gb}$, $i_{gc}$ : SEIG line currents (A)

$i_{ua}$, $i_{ub}$, $i_{uc}$ : Load current of uncontrolled diode rectifier fed load (A)

$v_{ga}$, $v_{gb}$, $v_{gc}$ : SEIG phase voltages (V)

$v_{ab}$, $v_{bc}$, $v_{ca}$ : Line voltages for Δ-connected SEIG (V)

$R_f$, $L_f$, $C_f$ : AC side filter parameter of CC-VSC

$e_a$, $e_b$, $e_c$ : AC side phase voltage of VSC (V)

$R_a$, $L_a$ : DC motor armature resistance and inductance (Ω, H)

$i_{da}$, $i_{db}$, $i_{dc}$ : AC side current of controlled rectifier fed DC motor load (A)

$Q_{dc}$ : VAR requirement of uncontrolled rectifier fed DC motor (VAr)

$HB$ : Hysteresis band of current controller

$u_{sda}$ $u_{sdb}$ $u_{sdc}$ : In-phase current templates

$u_{sqa}$ $u_{sqb}$ $u_{sqc}$ : Quadrature current templates

$S_a$, $S_b$, $S_c$ : Switching functions of CC-VSC

$i_{sa}$, $i_{sb}$, $i_{sc}$ : Supply currents (A)

$V_{ps}^*$ : Reference peak source voltage (V)

$V_{dcr}$ or $V_{dc}^*$ : Reference DC bus voltage (V)

$I_{sd}^*$ : Reference peak in-phase supply current (V)

$I_{sq}^*$ : Reference peak quadrature supply current (A)

$i_{sda}^*$,$i_{sdb}^*$, $i_{sdc}^*$ : Reference in-phase supply currents (A)

$i_{sqa}^*$,$i_{sqb}^*$, $i_{sqc}^*$ : Reference quadrature supply currents (A)

$i_{sa}^*$,$i_{sb}^*$,$i_{sc}^*$ : Reference supply currents (A)

$K_p$, $K_i$ : Proportional and integral gains of PI controller

$v_{la}$, $v_{lb}$, $v_{lc}$ : Load voltages (V)

$v_{ia}$, $v_{ib}$, $v_{ic}$ : Injected voltage into the supply lines by SSSC (V)

$V_{id}^*$ : Peak in-phase SSSC voltage (V)

$V_{iq}^{*}$ : Peak quadrature SSSC voltage (V)

$v_{ida}^{*}, v_{idc}^{*}, v_{idc}^{*}$ : Reference in-phase SSSC voltages (V)

$v_{iqa}^{*}, v_{iqb}^{*}, v_{iqc}^{*}$ : Reference quadrature SSSC voltages (V)

$v_{la}^{*}, v_{lb}^{*}, v_{lc}^{*}$ : Reference load voltages (V)

$i_{fa}$, $i_{fb}$, $i_{fc}$ : Inductor currents of ripple filter for SSSC (A)

$V_{pl}$ : Peak load voltage (V)

$V_{pl}^{*}$ : Reference peak load voltage (V)

$v_{bat}$ : Battery voltage (V)

$C_{sh}$ : Shunt capacitance in the capacitor bank connected across SEIG (F)

$R_s$, $R_r$ : Stator and rotor resistance per phase (Ω)

$L_s$, $L_r$ : Self inductance of stator and rotor winding (H)

$X_{ls}$, $X_{lr}$ : Stator and rotor leakage reactance per phase (Ω)

$R_{sm}$, $R_{rm}$ : Stator and rotor resistance of induction motor (IM) load (Ω)

$X_{lsm}$, $X_{lrm}$ : Leakage reactance of stator and rotor winding of IM load (Ω)

$X_M$, $X_{Mm}$ : Magnetizing reactance of SEIG and IM load (Ω)

$F$, $v$ : pu frequency and pu prime mover speed of SEIG respectively

$X_{sh}$ : Shunt capacitive reactance per phases connected across SEIG terminal (Ω)

$v_m$ : pu speed of IM load

$R_l$, $L_l$, $C_l$ : Resistance, inductance and capacitance of static load respectively

$V_s$, $I_s$ : Steady state SEIG stator voltage and current (V, A)

$V_l$, $I_l$ : Steady state load voltage and current (V, A)

$V_g$ : Air gap voltage generated in SEIG (V)

$Z_{LS}$ : Loop impedance of SEIG (Ω)

$Z_{LH}$ : Loop impedance of short shunt SEIG (Ω)

$Z_b$ : Base impedance (Ω)

$X_M^{uns}$ : Unsaturated magnetizing reactance per phase (Ω)

$C_{es}$, $C_{hs}$ : Series and Shunt capacitance for short shunt SEIG configuration (F)

$X_{es}$, $X_{hs}$ : Series and shunt capacitive reactance (Ω)

| | |
|---|---|
| *npr* | : Load point representing rated capacity of the machine |
| *npm* | : Load point representing maximum loading without constraint violation |
| $P_l$ | : Actual loading of the SEIG (W) |
| $P_r$ | : Rated power of the SEIG (W) |
| $f_{obj}$ | : Objective function |
| $f_1, f_2$ | : Fitness function |
| *mx*, *mn* | : Superscript indicates maximum and minimum values |

# CHAPTER-I

# INTRODUCTION

## 1.1 GENERAL

The factors like environmental and ecological concerns due to phenomenal industrialization, urbanization, and energy crisis due to fast rate of depleting fossils fuels such as coal, petroleum products etc. are drawing an attention among the research fraternity to look for the clean renewable energy sources such as wind, small hydro, solar, tidal, biomass and industrial waste etc. The challenges in extending the national grid for the electrification of remote locations have forced to explore the stand alone power generating units. The self-excited induction generator (SEIG), first reported by Bassett and Potter [1] in 1935, is emerging as a strong candidate to extract electrical energy from renewable sources such as biomass, small hydro and wind. The use of SEIG is advantageous over the conventional synchronous generator for small capacity applications due to operational simplicity, brushless and rugged construction, reduced maintenance, lower unit cost, good dynamic response, self protection against faults, and ability to generate power at varying speeds. The SEIG is normally an externally driven three-phase squirrel cage induction machine with a suitable capacitor bank at its terminals. The SEIG is increasingly being used for small capacity isolated generating units with both conventional as well as renewable energy resources. In the last three decades, the research on SEIG has got momentum and various facets regarding steady state operation, transient state operation, voltage and frequency regulation, balance and unbalance operation, single-phase operation, design consideration, parallel operation, performance improvement through static compensators, and its usage for various applications have been prominently reported in the literature [1-230].

The terminal voltage of SEIG is governed by the speed of prime mover, shunt capacitance, magnetization characteristic of the machine and loads. Notwithstanding various advantages, the SEIG terminal voltage and frequency droop with the increase in the load even when SEIG is driven by constant speed prime movers such as biomass, diesel engine or fixed head hydro turbine. As the load increases, the difference between volt-ampere reactive (VARs) supplied by the shunt capacitors and VARs demanded by

the generator and loads increases. The rate of decrease in the terminal voltage is high for inductive loads. The poor voltage and frequency regulations are the major bottlenecks for its applicability as an isolated supply feeding various domestic or industrial loads. The various loads can be classified as static loads, dynamic motor loads and non-linear loads. The commonly used applications of non-linear loads are computers, uninterrupted power supply, adjustable speed drives etc. Further, the loads may be balanced or unbalanced. The conventional methods to improve the voltage regulation include use of series capacitors in conjunction with shunt capacitors as short shunt or long shunt SEIG [122-130], use of a constant voltage transformer (CVT) [137] or a saturable core reactor [134-136] etc. Although, the conventional methods are simple but their ineffectiveness, bulky size, higher losses etc. are the reasons to explore other methods [131-192]. Due to various advantages, the SEIG has been considered for numerous applications [193-230].

The factors like improvement in power electronic devices, their characteristics, hardware supports for higher operating frequency etc. have motivated to use the switching devices based voltage regulators for improving voltage regulation of SEIG such as switching capacitors, thyristor controlled inductors, continuously controlled capacitors consisting of a fixed capacitor in parallel with anti-parallel static switches, static VAR compensator (SVC) etc. The advancements in power converter topologies, digital signal processors and control techniques have pronounced the switching power converters such as static shunt compensator (STATCOM) [231-248], static synchronous series compensator (SSSC) [249-269] etc. applications for improving the SEIG performance.

The STATCOM is a shunt connected device. Normally, a STATCOM is a pulse width modulation (PWM) based voltage source converter (VSC) with a capacitor on its DC bus for self support. The voltage regulation can be achieved by regulating the reactive VARs in SEIG. Conventionally, the frequency regulation can be achieved by input control through the governor. The voltage and frequency of a SEIG system can be controlled through a static converter based circuit, which is a combination of STATCOM and electronic load controller (ELC). The SSSC has proven acceptability in power system for power flow control, line impedance control, damping control etc. The SSSC is a synchronous voltage source converter connected in series with the line through a series transformer and produces controllable compensating voltages. When the compensating voltage is in quadrature leading to the line current, it emulates a controlled series inductor

and when compensating voltage is in quadrature lagging to the line current, it emulates a controlled series capacitor. This research work is carried out with the objective to investigate the performance of SEIG with static controllers namely STATCOM and SSSC for feeding various linear and non-linear loads.

## 1.2 STATE OF ART

The phenomenon of self-excitation in the induction machine has been first reported by Bassett and Potter in 1935 [1]. It has been shown with the help of an experiment that a suitable capacitor bank across the externally driven induction machine has resulted into voltage buildup. Later, Wagner [2] has suggested an approximate method for steady state performance by obtaining the terminal voltage and slip for a given load, the prime mover speed and the shunt capacitance. The research contribution made by Bassett and Potter has been classical in nature [1]. The contemporary researchers have not foreseen the potentials of SEIG and the research on SEIG could not pick up at that time. The sincere efforts on the various aspects of the induction generator have been started in late seventies after the oil crisis faced the world over. The emphasis has been given on exploring and exploiting the renewable sources like wind, small hydro, tidal, biogas, industrial waste etc. and various facets of SEIG related to self-excitation phenomenon, steady state and transient state performance, operation with various type of linear (static and dynamic) and non-linear loads, design consideration, limits on capacitance and speed for self-excitation, balanced and unbalanced operation, parallel operation, compensated SEIG operation, voltage and frequency regulation, performance improvement through static converters and various applications have been investigated [1-230] in the literature.

The performance of SEIG is studied in terms of steady state and transient state analysis. The steady state analysis is important for selecting the generator rating, ensuring the power quality for particular application and SEIG configuration. Various methods such as loop impedance, admittance method etc. have been investigated for analyzing the steady state performance of SEIG by considering different set of unknown variables [16-42]. The state space q-d machine models with currents or flux linkages as state variables have been used for studying the transient performance of the induction machine [43-48]. The correctness of the q-d model depends upon the treatment of saturation in the magnetization characteristics of the machine [49-52], which is required for accurate

estimation of transient voltages and currents. The transient state analysis of SEIG [53-62] is vital for assessing the strength of insulation, machine winding, capacitor, and shaft and to develop protection strategy.

The majority of industrial loads are dynamic in nature such as an induction motor load. The investigation of SEIG with the induction motor loads is important as they cause excessive reactive power burden on SEIG. Moreover, the power factor of the induction motor is also varying with loading. The performance of SEIG feeding an induction motor load is presented by many researchers [63-67]. The advancements in power electronics devices, operating characteristics, power converter topology etc. have resulted in emerging a new category of non-linear loads. Due to excessive use of the converters, the non-linear loads are increasingly being used for domestic and industrial applications. The main concern of usage of non-linear loads is the injection of harmonics into the supply system, which causes additional losses, stresses on insulation, derating of the machine etc. The performance of SEIG has been investigated for feeding rectifier load [68, 69, 193-199].

The self-excitation in SEIG depends upon number of factors such as shunt capacitance, prime mover speed and magnetizing characteristics. For a specific load condition, there is a limiting prime mover speed for given capacitance or a limiting shunt capacitance for fixed prime mover speed for self excitation and successful operation of SEIG. Various criteria have been suggested for calculating the capacitive requirement and limiting values for the operation of SEIG [70-78].

The considerations like size of machine, routine maintenance, reliability and expansion plan have resulted into the research on the parallel operation of SEIGs. The parallel operation of SEIGs has the advantages such as no need of synchronization, no hunting like phenomenon etc. as in case of parallel operation of synchronous generators. The performance of parallely operated SEIGs has been studied on the basis of steady state equivalent circuit or q-d axis dynamic model [79-86].

The SEIG is reported for its suitability in remote and hilly tracts for supplying the power to sparsely distributed population due to availability of wind and small hydro potential in abundance in these locations. The every distribution system operates under varying degree of unbalance due to activities of large number of consumers. Due to the

unbalanced capacitors or load configuration, the voltage and current in different windings of SEIG are different. The unbalanced operation causes additional losses in SEIG and also results in pulsating torque which in turn reduces the efficiency and derates the machine. The performance during unbalanced operation can be analysed using the symmetrical component in the steady state conditions or using q-d model for transient conditions [87-99].

The operation of single-phase SEIG [100-110] or three-phase SEIG [111-116] supplying single phase loads has been reported in the literature. In small power applications up to 10 kW, the use of single-phase SEIG is preferred. The single phase SEIG operation can be achieved through either conventional single-phase induction machine or from the three-phase induction machine with appropriate arrangement of capacitors. In view of the importance of small power applications of single-phase SEIG driven by constant and variable speed prime movers, utilizing conventional and non-conventional power source, researchers have reported the steady state and transient performance analysis of single-phase SEIG system feeding various loads [100-116].

In spite of various advantages of SEIG for small power capacity, the poor SEIG performance remains a concern for researchers and a major hindrance for its wider utilization for domestic and industrial loads. The endeavors have been made from time to time to formulate the strategy to improve the performance of SEIG. Some researchers have redesigned the induction machine to obtain maximum output in generating mode and studied the effect of various design parameters on SEIG performance [117-121].

It is well evident that the SEIG exhibits poor voltage regulation under loading, due to increasing difference between VAR supplied by terminal capacitance and VAR required by the generator and loads. The voltage regulation of SEIG can be improved through shunt or series regulating schemes. These regulating schemes can be classical such as compensated SEIG configurations etc, switching device based schemes such as switching capacitors etc. and converter based schemes such as STATCOM etc.

Basset and Potter in 1935 [1] have experimentally shown that compounding in SEIG through series capacitors could improve the SEIG performance. The series compensation in SEIG is achieved through series capacitors and resulted into short shunt and long shunt SEIG configurations. Both these configurations have been investigated

thoroughly for feeding static and dynamic loads [122-130]. With the proper combination of series and shunt capacitances, both the configurations are resulting into improved performance with static loads. However, compensated SEIG exhibits unstable oscillating behaviour with dynamic loads.

Due to the development of thyristor and gate turn off thyristor (GTO) as a switch, various switching devices based voltage regulating schemes such as switching shunt capacitor, static VAR compensator etc. have been reported in the [131-153] literature. These schemes are having some disadvantages such as switching transients, lack of fast response, size of the inductor and cost. The advancement in self-commutating devices, converter topologies, digital processors etc. brings the converter based compensator at forefront of research. The self-commutating devices based voltage source converter (VSC) has several advantages over switching device based static VAR compensators (SVC) such as identical capacitive and inductive range operation, fast response and high switching frequency operation etc. The STATCOM, a shunt three-phase VSC with self-supporting DC bus is a proven technology for the power system. It produces a set of three-phase leading or lagging AC output voltage of controllable magnitude. These AC voltages are coupled to the corresponding AC system through a small inductive filter. With the proper switching arrangement, the STATCOM simply interconnects the three output terminals in such a way that the output reactive currents can flow freely among the phases. The STATCOM is effectively used for reactive power compensation, harmonic elimination, load balancing in the power system [231-248]. The use of STATCOM for improving the SEIG performance has been investigated from time to time [154-166].

The SEIG exhibits poor frequency regulation even when driven by constant speed prime mover such as diesel internal combustion (IC) engine, biomass driven engine etc. The frequency regulation in SEIG can be achieved by controlling the prime-mover speed and torque through speed governor system. In small power applications, the cost, control and operation of such speed governor system marginalize the simplicity of SEIG. For frequency regulation, the electronic load controller (ELC) has been employed in uncontrolled hydro turbine driven small SEIG based power systems [167-174]. The voltage and frequency regulation is achieved in SEIG by decoupled control of the active and reactive powers. Such schemes are employed for satisfactory performance of voltage

and frequency sensitive appliances using STATCOM and matrix converter based SEIG systems [175-192].

The series compensation in SEIG is achieved either through series capacitors as discussed above, or through static synchronous series compensator (SSSC). The SSSC, a synchronous voltage source converter (VSC) connected through an insertion transformer, is a proven flexible AC transmission system (FACTS) device and has been used in power system [249-269] for power flow control and mitigation of the oscillations. The SSSC is a three-phase gate turn off thyristor (GTO) / insulated gate bipolar transistor (IGBT) based PWM operated VSC with capacitor or energy source at DC bus (for exchanging the real power), and AC side inductive-capacitive (L-C) ripple filter.

The SEIG founds applications to obtain DC power by employing AC/DC converter [193-200] for applications such as battery charger etc. With the development of various controllers for SEIG, the wind and hydro applications of SEIG are on rise [201-220]. The issues related to wind farm for wind energy conversion system (WECS) have been investigated in detail [206-220]. The series compensation using FACTS controllers is applied for mitigation of subsynchronous resonance in a series-compensated wind farm [218, 219]. Numerous other applications of induction generator have been reported such as for aircraft, automobile applications; petroleum and chemical industry, cogeneration plants applications [221-230].

## 1.3 OBJECTIVES OF THE THESIS

From the available literature [1-230], it is observed that the research work on SEIG is very much diversified. However, little information is available on its operation with static controllers (STATCOM and SSSC) for feeding various static, dynamic and non-linear loads. The loads can be balanced or unbalanced as decided by consumers. The investigation with dynamic loads is important as they constitute majority of the industrial loads. The analysis of SEIG with nonlinear loads is important because they are injecting harmonics, causing additional losses and reactive power burden to the system. Therefore, the scope of this research work is identified to investigate the performance of SEIG with static controllers for feeding various linear/nonlinear/static/dynamic loads. The research work entitled **"**Investigations on Static Controllers for Self-Excited Induction Generators**"** is carried out with the following objectives,

- Investigations on the performance of SEIG for linear and non-linear loads.
- Investigations on the use of STATCOM with SEIG for improved performance for static and dynamic loads.
- Investigations on the suitability of STATCOM for SEIG to feed unbalanced and nonlinear loads.
- Investigations on the use of SSSC with SEIG for improved performance for static and dynamic loads.

## 1.4 ORGANIZATION OF THE THESIS

The specific contributions by the author to achieve the above mentioned objectives are summarized into nine chapters. The brief description of these chapters is outlined as follows.

***Chapter–I*** introduces the self-excited induction generator and details on the state-of-art on the area of research work. This chapter also enlists the objectives of the present study and outlines the organization of thesis.

***Chapter-II*** provides the brief literature review on various operational and control aspects of three-phase SEIG. The literature review mainly focuses on aspects like steady and transient state performance analysis of SEIG feeding various types of static and dynamic linear loads and non-linear loads, voltage regulation and remedial measures through compensated SEIG and static controllers namely STATCOM and SSSC. The contributions to identified research objectives are also described in this chapter.

***Chapter-III*** details the regulating schemes for performance improvement of three-phase SEIG systems. These regulating schemes are categorized into voltage, frequency and voltage-frequency regulating schemes. The voltage regulation of SEIG can be achieved by the shunt or series method of reactive power compensation. The shunt and series voltage regulating schemes are further sub categorized into conventional, switching devices based and converter based schemes. The frequency regulation schemes pertaining to load control are discussed briefly. The voltage-frequency regulating schemes applied for three-phase three-wire and three-phase four wire systems are also discussed in detail.

***Chapter-IV*** presents steady state and transient performance of three-phase SEIG feeding various types of loads. The equivalent circuit is used for investigating the steady state performance with resistive, resistive-inductive and induction motor loads. The optimum voltage regulation is formulated as an optimization problem and is solved using genetic algorithm (GA) to obtain optimum set of capacitance and speed for static loads under machine and performance constraints. The equality constraints are satisfied using Newton-Raphson (NR) method. The simulated results are validated experimentally.

The transient performance of three-phase SEIG is presented for feeding various linear and non-linear loads. The dynamic models of SEIG and induction motor load are expressed using q-d variables in stationary reference frame with current and voltage as state variables, considering the effect of main and cross flux saturation. The three-wire and four-wire uncontrolled rectifier fed resistive and resistive-capacitive loads are modeled in phase variables. The model equations are solved using fourth order Runge-Kutta method of integration. The transient performance of SEIG is studied for static resistive-inductive load, an induction motor load, three-wire uncontrolled rectifier fed resistive and resistive-capacitive loads, and four-wire uncontrolled rectifier fed resistive-capacitive load during various loading conditions. The power quality of loads and generator quantities is studied through harmonic spectrum and total harmonic distortion (THD).

***Chapter-V*** deals with the SEIG operation with STATCOM feeding static and dynamic loads. The STATCOM comprising PWM voltage source converter (VSC) with self supporting DC bus is considered for improving the voltage regulation of SEIG. A methodology to design STATCOM parameters is presented and the STATCOM parameters are designed for two cases namely full rating STATCOM and reduced rating STATCOM. The induction machines are modeled in q-d variables in stationary reference frame and the STATCOM is modeled in phase variables. A simplified proportional-integral (PI) controller based control technique employing two controllers is proposed for the STATCOM. One PI controller is applied to regulate the DC bus voltage of STATCOM to the reference value. The other PI controller is applied to regulate the terminal voltage of SEIG by regulating the required reactive power. With the designed STATCOM parameters, the transient performance of SEIG system is investigated for resistive-inductive, induction motor and the controlled rectifier fed DC motor loads. The

power quality aspects like total harmonic distortion (THD) and harmonic spectrum are estimated through Fast Fourier Transformation (FFT) of steady state waveforms.

***Chapter-VI*** deals with the modeling and performance of SEIG with STATCOM as four-wire isolated system feeding various static linear and nonlinear loads namely resistive, resistive-inductive, uncontrolled rectifier fed resistive load with and without DC side filter. Both three-phase and single-phase rectifier configurations are considered for the study. The SEIG is modeled in q-d axis with currents as state space variables. The non-linear loads are modeled in phase variables. The transient performance is computed and the power quality aspects are also presented for SEIG system. The STATCOM effectiveness in operating as a voltage regulator, a load balancer, a harmonic eliminator and a neutral current compensator has been investigated. The THD indices of voltages and currents of SEIG-STATCOM are calculated to assess the power quality performance.

***Chapter-VII*** details the operation of series compensated SEIG feeding static loads. The series compensation of SEIG is achieved using both series capacitor and SSSC. The steady state performance of SEIG is evaluated using the steady state equivalent circuit and the transient performance is studied using dynamic model. The series and shunt capacitances are calculated by formulating voltage regulation and performance characteristic as separate objective functions and the optimization problems subjected to various performance related constraints are solved using GA.

This chapter also reports the transient operation of static synchronous series compensator (SSSC) feeding static loads. The PWM controlled voltage source converter (VSC) with a battery or a capacitor at DC bus is considered as SSSC. The guidelines to decide the parameters of battery supported and capacitor supported SSSC configurations are also discussed. The simplified control strategy for the battery supported SSSC using a PI control loop is proposed to regulate the terminal voltage of SEIG. The battery supported SSSC effectiveness in providing flat voltage characteristic is investigated for resistive, resistive-inductive, and resistive-capacitive loads. The operation of SSSC in inductive and capacitive mode is also studied. The proposed control technique for capacitor supported SSSC consists of two PI controllers, one for maintaining the DC bus voltage and other for maintaining the SEIG terminal voltage. The THD indices of voltages and currents of SEIG-SSSC system are obtained to assess the power quality performance of the system.

***Chapter-VIII*** describes the operation of series compensated SEIG feeding an induction motor load. As described in Chapter-VII, the series compensation of SEIG is achieved using series capacitor and through SSSC. The methodology to design the SSSC parameters for feeding induction motor load is described. The performance of the SEIG systems is evaluated through dynamic model. The oscillating and unstable behavior of SEIG with series capacitors resulting in supplying an induction motor load is exhibited. The effectiveness of SEIG-SSSC system to dampen the oscillations and resulting into stable operation during starting and loading of induction motor load is investigated. The power quality performance is assessed through THD.

***Chapter-IX*** highlights the specific contribution and the main conclusions. It also enlists the scope for further research work in this area.

# CHAPTER-II

# LITERATURE REVIEW

## 2.1 GENERAL

The state of art, detailing the developments related to self-excited induction generators (SEIGs) to the present state has been presented in the previous chapter. The objectives of the research work are also summarized in the previous chapter. The SEIG operating as an isolated generating unit is suited for the electrification of the remote and far flung areas. For small capacity applications, SEIG is advantageous over conventional synchronous generator due to the advantages such as brushless and rugged construction, reduced maintenance, lower unit cost, good dynamic response, self protection against faults, and simplicity of control. Due to these advantages, SEIG is emerging a strong candidate to extract electrical energy form both conventional energy sources like diesel and renewable energy sources like small hydro and wind.

In last three decades, many facets regarding the operation, control and applications of SEIG have been investigated in detail [1-230]. The steady state analysis is used for estimating voltage regulation, losses, efficiency, design of the machine, assessing the suitability of configuration for given application. The transient analysis helps to estimate over current, over voltage, electro-magnetic torque during the balanced and unbalanced transient conditions. The transient analysis has been used to find the suitability of winding, insulation level, capacitor rating, guidelines for the control etc. The advancement in the power electronic devices, hardware support for higher switching frequency and their availability at low cost is the key to the application of switching devices and static converter based regulators and the increasing usage of non-linear loads. Several research review articles have been reported from time to time [5-9] on various aspects of SEIG.

## 2.2 LITERATURE REVIEW

The self-excited induction generator (SEIG) has been investigated extensively for the last three decades and various aspects have been explored. In view of the available vast literature on SEIG, it is not possible to review the literature exhaustively on every

aspect. The brief literature review on the performance analysis, operation and control, design aspects, performance improvement, and applications of SEIG is carried out with the objective of complementing the work done by various researchers on the issues of research interest. The capacitor excitation in the induction machine has been first reported by Bassett and Potter [1] in 1935 with the help of experimental study. Later, Wagner [2] has proposed an approximate method for evaluating SEIG performance. The terminal voltage and slip were obtained for given load, shunt capacitance and prime mover speed from the equivalent circuit.

After the oil crisis that has loomed over the world in seventies and the concern for the electrification of remote and far flung areas, the SEIG has attracted considerable attention from the contemporary researchers. The techniques to analyse the steady state performance of SEIG have been demonstrated in early eighties. The analysis of steady state performance of SEIG involves computation of unknown magnetizing reactance and frequency for specified speed, load and capacitance. Broadly, the methods to obtain magnetizing reactance and frequency can be classified in two categories namely loop impedance method [16] or nodal admittance method [21]. In loop impedance method, the equivalent loop impedance has been resolved into two polynomials by separating real and imaginary parts and these polynomials are solved to obtain magnetizing reactance and frequency. In nodal admittance method, the admittance across the nodes defining air gap voltage is considered. The frequency is computed by solving polynomial for real power balance across air gap and the magnetizing reactance is obtained by equating imaginary part of the admittance to zero.

Many researchers [16-42] have contributed towards the steady state operation of SEIG. The research papers [16-19] have considered the loop impedance method and solved the real and imaginary polynomial with Newton-Raphson method. Singh et al. [20] have compared the performance of commercially designed SEIG with the conventional induction machine operated as a SEIG. Quazene and McPherson [21] have reported the nodal admittance method for steady state performance. Singh et al. [24] have presented an algorithm for calculating number of capacitor steps to load the machine to its rated capacity while maintaining load voltage within the specified upper and lower limits of rated value. Ammasaigounden et al. [27] have computed the speed for specified frequency. Yegnanarayanan and Johny [28] have obtained the SEIG performance by

considering air gap voltage and frequency as variables. Alghuwainem [30, 31] has investigated the photo-voltaic (PV) powered DC motor driving a SEIG. Chan [32, 34] has introduced the iterative approach [32], symbolic programming approach [34] for finding the solution using loop impedance. Wang and Lee [35] have described the methods to study steady state performance of SEIG driven by regulated and unregulated prime movers.

The genetic algorithms (GAs), a global search and optimization technique [270-273] are having a number of advantages over the conventional optimization methods such as no requirement of good initial estimation of variables, ability to come out of local minima and find global optimum point. The GA based approach has been suggested by researchers [40, 181] to obtain the frequency and magnetizing reactance for given shunt capacitance and speed or combination of speed and shunt capacitance for maintaining the voltage and frequency. Alolah and Alkanhal [39] have suggested the multidimensional optimization based approach to obtain the frequency of SEIG. Haque [42] has proposed the numerical based method for constant voltage and constant current operation of SEIG.

The transient state analysis helps in finding the suitability of winding, insulation level, capacitor rating and suggesting the guidelines for control and protection switchgears for safe, reliable and efficient operation of SEIG. The Park transformation [43] has revolutionised the dynamic analysis of synchronous machine by eliminating all time varying inductances. Krause [44, 45] has suggested that referring both stator and rotor variables to an arbitrary reference frame eliminate all time varying inductances of the induction machine. The transient analysis of an induction machine is carried out in phase variables or d-q variables with either the currents or the fluxes as state variables. For most of the analysis, the d-q model with currents as state variables is found suitable. However, the accuracy of the model depends on appropriate treatment of saturation.

The effects of saturation and cross saturation on dynamic machine model have been investigated by many researchers in the induction machine and its operation as an induction generator [46-52]. It has also been observed that the saturation in one axis affects the saturation in other axis and due to cross saturation, the self-inductances of q-axis and d-axis attain different values. Melkebeek et al. [46, 47] have given an improved method for incorporating the main flux saturation in small signal model of the induction machine. Vas et al. [48] have explained that the effect of cross saturation in AC machine

is like the demagnetizing effect of the armature reaction. The effect of cross saturation in the dynamic model is incorporated using saturated magnetizing inductance and dynamic inductance [49-52].

Hallenius et al. [53] have stressed the importance of cross-saturation in self-excited induction generators. Wang and Su [56] have studied the dynamic performance of SEIG under different loading conditions. Bispo et al. [57] have reported a strategy to incorporate saturation effect by considering the magnetic harmonic function. It has been shown that the distortion in current and voltage is due to harmonic contents in the main flux caused by saturation. Wamkeue and Kamwa [58] have reported the unified generalized current and flux linkage models to account the saturation for various rotor circuit with neutral connection. Murthy and Pinto [59] have presented the generalized MATLAB model for transient performance. Kumar and Kishore [60, 61] have studied the transient performance using q-d state space model by considering the artificial neural network model for magnetizing inductance. Neam et al. [62] have analyzed the transient performance of SEIG driven by variable speed wind turbine.

The induction motor, which is referred as a dynamic load, comprises of a majority of the domestic and the industrial loads. During operation, the dynamic loads cause voltage dip, inrush current and moreover, their power factor do not remain constant throughout the loading range. The behaviour of SEIG feeding the induction motor is important for assessing the performance and suitability of configuration. Shridhar et al. [63] have given a method for evaluating the steady state performance of SEIG feeding the induction motor load and discussed the capacitance required for the start-up of the motor and for the steady state operation. Alghuwainem [64] has reported the analysis with the node admittance method for optimum selection of the generator, the motor, the mechanical load and the excitation capacitance for water pumping system. Kuo and Wang [65-67] have presented eigenvalue analysis based on synchronous reference frame to determine the critical operating conditions and dynamic stability of the studied machines.

Due to improvement in power electronic devices, ratings, characteristics, static converters topology, hardware circuitry etc., the usage of non-linear loads like controlled and uncontrolled rectifiers has increased for number of applications. The non-linear loads like computers, televisions, uninterrupted power supply (UPS), switch mode power supply (SMPS), adjustable speed drives (ASD) etc. are increasingly being used. However,

the literature on the operation of SEIG feeding non-linear loads is limited. Kuo and Wang [68] have examined the performance of SEIG feeding rectifier load. The hybrid model of machine has been considered for the analysis. The different arrangements for supplying the DC loads have been presented in [69, 193-199].

There is minimum value of capacitance and speed beyond which self-excitation is not possible [70-78]. Al-Jabri and Alolah [72] have reported the upper and lower limiting values of capacitance and speed for SEIG to maintain self-excitation. The upper limiting values are the characteristic indices, and the operation around these values may damage the system. The limiting values of the excitation capacitance, speed, load and different criteria for necessary self-excitation have been obtained using loop impedance and nodal admittance methods [73]. Wang and Su [75] have given a formula for minimum and maximum capacitance based on eigenvalue sensitivity approach. Eltamaly [76] has proposed a formula for minimum capacitance using nodal admittance method applied to steady state equivalent circuit. Seyoum et al. [77, 78] have presented the effect of voltage and frequency on loading with change of the speed and also minimum and maximum speeds necessary to initiate the self excitation in SEIG for known value of capacitance and load.

The size of machine, maintenance requirement, reliability consideration and expansion plan etc. are the main reasons for the parallel operation of SEIG. The parallel operation of induction generators has numerous advantages such as no need of synchronization and problems associated with hunting [79-86]. Al-Bahrani and Malik [79] have suggested that the voltage of a group of SEIGs is controlled by either controlling the speed or by controlling the shunt capacitance. Shilpakar et al. [80] have presented the dynamic model of SEIGs operating in parallel to feed a common load. Chakraborty et al. [82] have addressed the voltage regulation of multiple SEIGs connected to a common bus and concluded that given excitation capacitances and load sharing are influenced by machine parameters, speed and VAR requirement at a specified terminal voltage etc. The transient analysis based on eigenvalue approach for linear load [81] and motor load [84] has been applied to calculate the minimum and maximum value of capacitance for the successful parallel operated SEIG. Palle and Farret [85, 86] have suggested the parallel operated SEIG for isolated wind farms to generate the bulk electric power.

The SEIG, while supplying sparsely distributed loads in remote and rural areas, operates with some degree of unbalance as experienced with various distribution systems. The unbalance operation of three-phase SEIG is due to unbalanced excitation or due to unbalanced consumer load. Various researchers have analysed the unbalanced operation of SEIG using symmetrical components in steady state or q-d model in transient state [87-99]. The operation of three-phase SEIG feeding single-phase load has been reported in [87, 88]. The unbalanced operation causes additional losses and results in the pulsating torque of the machine. A methodology has been reported by Bhattacharya and Woodward [89] for selecting the capacitors, which is regarded as C-2C method to minimise the unbalancing and the derating of the machine. Rahim et al. [91] have reported the operation of three-phase SEIG excited by single capacitor and feeding single-phase load in same phase. The transient operation under different unbalanced capacitor conditions has been studied on a star connected generator with star connected capacitor bank in [93]. Wang and Cheng [94] have analyzed star connected three-phase SEIG behaviour for single-phase resistive load and used eigenvalues to determine minimum and maximum capacitances for self excitation of the SEIG. Chan and Lai [95, 96] have proposed the Smith connection for three-phase SEIG feeding single-phase loads which results good balancing. Jain et al. [97] have reported the transient performance during balanced and unbalanced faults and suggested the design guidelines for winding, shaft and protection strategy. Wang and Huang [98] have proposed a two port network based equivalent circuit model for SEIG supplying unbalanced loads. Elder et al. [133] have observed that the use of variable capacitor between unloaded phases results in balanced phase currents for maximum load.

The continuous efforts have been made to harness the renewable energy resources, available in abundance at various locations. Murthy [100] and Shridhar [101] have reported the basic system of self regulated single-phase SEIG for single-phase power generation. Anagreh [102] has used MATLAB inbuilt optimization function for finding unknown variables form the impedance directly. Ahmed et al. [103, 108] have proposed the static VAR compensator (SVC) based voltage regulator, which consists of fixed capacitor with thyristor switched capacitor (TSC) and thyristor controlled reactor (TCR) in parallel. Ojo [104-106] has investigated the steady state and transient performance for shunt, short shunt and long shunt excitation connections in single-phase SEIG. Palwalia

and Singh [110] have proposed a digital controller for improving the single-phase SEIG performance.

The single-phase SEIG operation can also be achieved using three-phase induction machine. Various researchers have studied the steady state and transient performance regarding different capacitor arrangement employed on three-phase induction machine to obtain single phase generation [111-116]. Shilpkar and Singh [111] have presented the transient behaviour of three-phase SEIG excited by C-2C capacitors for feeding single-phase load in d-q variables. Mahato et al. [113-115] have reported the transient analysis of single-phase SEIG and suggested the damping resistance for compensated single-phase SEIG feeding motor load for stable operation. The transient performance of series capacitor compensated single-phase SEIG under different load conditions is presented in [116].

Various researchers have explored the improvements in SEIG performance through redesigning of the machine by identifying the parameters affecting the SEIG performance. The effects of different machine design parameters on performance of SEIG have been discussed in [117-121]. Singh and Shridhar [117, 118] have reported the effect of parameters such as resistance, reactance and magnetizing reactance on voltage and reactive VARs. Faiz [119] has suggested the minimizing of rotor resistance and increasing the flux density, which are obtained by reducing the stator core length, for better voltage and frequency regulation. Sawetsakulanond and Kinnares [120, 121] have shown the effect of skewing on the performance of SEIG. The performance of standard and high efficiency induction machines operation as a SEIG has been compared [120].

The terminal voltage of SEIG decreases with the increase in the load even if it is driven by regulated prime mover such as internal combustion (IC) engine. The reduced voltage is due to the increased gap between the volt-ampere reactive (VAR) demanded by the machine and the load, and the VAR supplied by the external capacitor bank. The poor voltage regulation results in poor loading capacity and under utilization of SEIG. The short shunt and long shunt capacitor configurations of SEIG, which employ series capacitors, are popular arrangement for providing additional reactive power with increase in the load current. Both the configurations are simple, cost effective and provide improved voltage profile for static loads. The steady state and transient state performance of long shunt and short shunt SEIG feeding various static and dynamic loads have been

studied extensively by the researchers [122-130]. Shridhar et al. [123, 124] have presented the performance characteristics of short shunt SEIG and suggested the method to obtain the values of shunt and series capacitances for minimum voltage regulation. Bim et al. [122] have reported the approximate analysis of long shunt SEIG in which the values of series and shunt capacitances are selected by the interpolation of the magnetizing characteristic of machine. Chan [32] has used equivalent circuit for the analysis of long shunt SEIG for specified values of capacitances. The comparative study has been carried out by Wang and Su [127] for same values of series and shunt capacitances. The operation of compensated SEIG with dynamic load [128, 129] has drawn attention of the researchers because of varying power factor of dynamic load, complex selection of series and shunt capacitance. Moreover, compensated SEIG exhibits unstable oscillating behaviour with dynamic loads. Wang and Lee [128] have studied the operation of compensated SEIG feeding dynamic load during both steady state and transient condition with the help of eigenvalue analysis. Singh et al. [129] have shown that stable operation could be obtained using damping resistors across series capacitors. Haque [130] has optimized the series and shunt capacitances and proposed the switching shunt capacitors for improving the voltage regulation.

Since advent of thyristor in 1957, numerous developments have taken place in power electronics devices such as ratings, characteristic, self-commutation, high switching frequency firing circuit, protection circuit etc. The power electronic device can effectively operate as a static switch. Several shunt and series voltage regulating methods using passive element, power electronics device, static VAR compensators (SVC) etc. have been investigated in [131-152]. The various voltage regulators have been reported such as 6-pulse naturally commutated converter [132], thyristor controlled inductor [133], switched capacitors [133], naturally commutated inductively loaded AC-DC converter [133], saturable core reactor in parallel with fixed value capacitor [134-136]. The voltage regulator performance employing constant voltage transformer (CVT) has been reported for both single-phase and three-phase SEIG [137]. A static control method has been proposed [138] utilizing the concept of continuously controlled capacitor consisting fixed capacitor in parallel with anti-parallel GTO switches. Quispe et al. [139] have presented a voltage regulator using two additional capacitor banks and a reactor connected through a static switch. Chtchetinine [140] has presented a method of terminal voltage stabilization using a digital voltage control scheme. The solid-state lead-lag (VAR) compensator,

designed for single input single output control system for voltage control of SEIG, has been proposed in [141-144]. The voltage regulator employing fully controlled converter has been reported in [145]. The static control of series compensated SEIG has been analysed [146] using thyristor controlled series inductor in parallel with the capacitor. The static VAR controller (SVC) based voltage regulator has been reported by Ahmad et al. [148]. Wijaya et al. [149] have studied the SVC magnetic energy recovery switch (MERS) for voltage control. Some authors [150-152] have proposed the voltage control using integral cycle controller. Lee et al. [153] have proposed an automatic voltage regulator (AVR) based controller using low voltage self-starting circuit and instantaneous voltage detector for regulating the terminal voltage.

The STATCOM is generally a three-phase pulse width modulated - voltage source converter (PWM-VSC) with DC bus capacitor for self support that controls the reactive power by generating leading or lagging power factor current with respect to its terminal voltage. Due to the advantage of fast dynamic response by PWM control, it finds potential applications in improving the voltage regulation of SEIG [154-166]. Singh et al. [154, 156-160, 166] have proposed a system comprising of SEIG and STATCOM for feeding various loads. Kuo and Wang [155] have presented the analysis of voltage control for a SEIG using a current controlled voltage source converter. The current source converter based STATCOM reported by Karshenas and Abdolahi [161] has the current limiting capability during short circuit. Wekhande and Agarwal [162-164] have presented a control technique for PWM converter for voltage control. Singh and Kasal [166] have reported a neural network based voltage regulating scheme for SEIG-STATCOM feeding four-wire load.

The SEIGs driven by constant head uncontrolled water turbines are advantageous due to operational simplicity and less maintenance. The system frequency can be regulated through mechanical governor system or through electronic load controller (ELC). With ELC, the total power generated by SEIG is constant and equals to actual load power and power dissipated in a dump resistor of ELC. The static converter controlled ELC configurations have been discussed in [167-174]. Murthy et al. [167] have compared various ELC schemes for SEIG. The ELC proposed by Singh et al. [168, 173] is a combination of a three-phase insulated gate bipolar transistor (IGBT) based current controlled voltage source inverter (CC-VSl) and a high frequency DC chopper to keep the

generated voltage and frequency constant for changing three-phase and single-phase loads. Some authors [169, 172] have reported the transient performance of three-phase SEIG with uncontrolled rectifier using chopper controlled resistor based ELC for feeding three-phase and single-phase static and dynamic loads. Ramirez and Torres [174] have presented a bidirectional switch based ELC.

It is well evident that apart from terminal voltage drop, frequency also decreases when load is increased on SEIG. The change in frequency may affect the performance of frequency sensitive dynamic and non-linear loads. Various voltage and frequency regulating methods using voltage source converter have been proposed for three-phase SEIG system [175-192]. Hilloowala and Sharaf [176] have proposed a fuzzy logic controlled converter-inverter configuration to track down and extract the maximum power available from the wind energy system. Marra and Pomilio [177] have reported the constant voltage and frequency operation of SEIG using PWM bidirectional inverter on AC side. Suarez and Bortolotto [178] have presented the operation of a SEIG with permanently connected capacitor and electronically switched inductor for obtaining constant voltage and frequency operation. Pereira et al. [179] have used the PWM inverter for constant voltage and frequency operation of SEIG driven by a speed governor regulated internal combustion engine. The STATCOM along with servo motor control mechanism has been presented by Chen [180] for regulating SEIG voltage and frequency. Perumal and Chatterjee [183-187] have presented the operation of SEIG with STATCOM and generalized impedance controller. Lopes and Almeida [188] have studied the operation of cost effective reduced rating voltage source inverter for SEIG. Youssef et al. [189] have obtained the voltage and frequency control using PWM converter with variable DC link voltage. Kumar et al. [190] have presented the operation of SEIG with the matrix converter, which is a three-phase AC to AC converter employing nine back to back solid state switches without reactive power element. The voltage and frequency control of three-phase four wire loads has been proposed in [191, 192]. Kasal and Singh [191] have presented the decoupled voltage and frequency controller using current controlled-voltage source converter as a STATCOM and uncontrolled rectifier with chopper fed dump load as an ELC. Barrado et al. [192] have presented a controller comprises of an active filter, battery charger and ELC for independent control of voltage and frequency of three-phase four-wire load.

The developments in solid state devices and static power converters have contributed enormously to the growth of induction generators for various applications such as DC load and DC supply [193-200], small hydro power projects [201-205], wind energy conversion system (windmill and wind park) [206-220], industrial applications [221-228], aircraft system [229, 230] .

Some authors [193-195] have presented a SEIG with forced-commutated rectifier bridge system as a DC power supply. Chakraborty et al. [196] have obtained controllable DC power from SEIG through series connected single-phase forced commutated rectifier. Some authors [197-199] have reported the AC to DC conversion scheme for applications such as battery charging system or to supply DC loads. The AC and DC applications have been suggested by Nishida [200] using the induction generator with an active power filter.

Miranda et al. [201] have reported an alternative isolated electric pumping system using induction machine. Murthy [202] has shared his experience in field installation of a small SEIG system at hydro site. Ekanayake [203] has described various practical schemes for harnessing hydropower for the small capacity loads. Faria [204] has studied the run of river project using propeller type water current turbine. Singh et al. [205] have experimentally investigated a six-phase induction generator for small hydro power.

Raina and Malik [206] have proposed a scheme with fixed shunt capacitance in parallel with thyristor controlled reactor for terminal voltage regulation. Hafiz et al. [210] have presented the state space model of SEIG, incorporating the skin effect for utilizing the wind power. The cycloconverter excited squirrel cage machine in wind power application has been proposed by Al-Geelani and Gupta [211]. Datta and Ranganathan [212] have proposed a method to track the peak power points for a variable speed wind energy conversion system (WECS). Kishore et al. [213, 214] have reported the field oriented state space model of converter-PWM inverter scheme for wind power applications. Sousy et al. [215] have proposed the indirect field oriented control to maintain the DC bus voltage of current regulated PWM converter. Satish et al. [216] have reported matrix converter fed induction generator for variable speed wind turbine. Varma et al. [218, 219] have proposed the mitigation of subsynchronous resonance in a series compensated wind farm using static VAR compensator (SVC) and thyristorized controlled series capacitor (TCSC). Various power converter topologies used for wind generator have been encapsulated by Baroudi et al. [220].

Various industry applications of induction generators have been reported in the literature [221-230]. In process and chemical industries, its application in power recovery train applied to fluid catalytic cracking (FCC) unit has been discussed by Own and Griffith [221]. The operation of an induction generator driven by natural gas engine has been reported for refinery by Bolin [222]. The cogeneration or waste heat of process steam is harnessed through the induction generator and issues related to the installation, cost and control for different process industries have been reported in [223-227]. A low voltage low power automotive induction generator system using a diode bridge rectifier and a PWM inverter has been compared with a conventional alternator based system in [228]. The limitation of induction generator in constant frequency aircraft system [229] and use of induction generator in variable speed constant frequency aircraft system has been reported in [230].

The advancements in static switches, power converter topology, fast digital signal processors and improved control algorithms have opened new prospective for researchers in the field of flexible AC transmission systems (FACTS) devices such as static shunt compensation (STATCOM) for reactive power compensation, harmonic compensation, load balancing etc. in the power system [231-248]. During eighties, the basic scheme of static shunt compensation has been given [233, 234]. Later, the instantaneous reactive power theory proposed by Akagi et al. [235] has revolutionized the modelling of static shunt compensation. Walker [236] has proposed the current source converter to supply reactive power to improve the power factor for large rating dynamic load. Moran et al. [237] have presented the design and analysis of three-phase synchronous solid state VAR compensator. Galanos et al. [238] have reported a static compensator, which exchange both real and reactive power during power oscillations. Schauder and Mehta [239] have presented the vector analysis and performance during negative sequence and harmonic voltage condition. Some authors [241, 244] have suggested a control strategy for three-phase active power filter for power factor correction and balancing the loads. The selection criteria for passive elements for three-level inverter based static synchronous compensator have been presented by Ekanayaka and Jenkins [243]. Jain et al. [245, 246] have proposed a control scheme that can compensate harmonics and/or reactive power simultaneously. The fuzzy logic controller is used with three-phase shunt active power filter to improve power quality. Singh et al. [248] have encapsulated the configurations, control strategy etc. of hybrid filters for power quality improvement.

Power flow control in electric power network is crucial for electric power system. Traditionally, power flow is controlled using series inductors, fixed value capacitors, thyristorized controlled series reactors and capacitors. The Static Synchronous Series Compensator (SSSC), a series FACTS device, emulates a controlled series capacitor or a controlled series inductor, by injecting controllable voltage through series transformers has proven implementation in power and distribution system applications for power flow and damping control etc. [249-269]

Gyugyi et al. [249] have described the basic operation of SSSC and compared them with conventional thyristorized switched controlled series capacitors. Sen [251] has presented the SSSC using a 24-pulse harmonic neutralized inverter configuration. Mihalic [252] has presented the analysis of controllable reactive series compensation (CRSC) and signifies the difference between controllable series compensator (CSC) and static synchronous series compensator (SSSC). Singh et al. [255] have examined the workability of robust and adaptive sliding mode and fuzzy controllers for the SSSC. Papic [256] has presented the mathematical models of voltage source converter that can be operated in different modes with different connection. These models are useful to understand STATCOM, SSSC and unified power flow controller (UPFC) through steady state characteristics. Han et al. [254] and Sood [258] have described a switching level simulation model for SSSC using electromagnetic transient program (EMTP). The work of Sen [251] on SSSC with 24-pulse inverter has been extended by Huang et al. [259] to investigate the detailed EMTDC model of the SSSC regarding the resonant characteristics of the transmission line.

The current source converter based SSSC modelling and control has been discussed in [257]. Gabrijel et al. [260] have presented the assessment for transient stability in power systems comprising static devices. The usage of dynamic voltage restorer (DVR), a static series compensator used in distribution network, for mitigating the series compensation problems such as sag, swell, voltage harmonics, voltage unbalanced is extensively reported in the literature [261-269]. Zhan et al. [262] have presented the operation of DVR using voltage space vector PWM control technique. The lead acid battery models based on short term discharge and long term integration are used in battery supported DVR [263]. Ghosh et al. [264] have analyzed a design of capacitor supported DVR for unbalanced and distorted loads. Sasitharan et al. [265] have

deliberated on the rating and design issues of DVR injection transformer. The underrating of the transformer may lead to its saturation whereas overrating increases the cost and size of the DVR. The open-loop control strategy used in the DVR to regulate load voltage can produce poorly damped response due to the presence of the switching harmonic filter in the restorer. Valithgamuwa et al. [266] have presented multi-loop controller for enhancing the damping response to regulate the load voltage. Ho et al. [267] have proposed a scheme that consists of two control loops; the inner control loop has been used to dictate the gate signals and the outer control loop has been used to generate the reference for the inner loop. Jayaprakash et al. [268] have proposed an indirect control technique based on the supply current using synchronous reference frame theory (SRFT) for capacitor supported DVR. The reference supply currents have been estimated using the sensed load voltages and the dc bus voltage of DVR. A DVR control scheme based on four-leg voltage source converter has been proposed by Naidu et al. [269].

## 2.3 IDENTIFIED RESEARCH AREAS

After the comprehensive review on selected research interest topics of vastly available literature on SEIG, following areas have been identified for further investigations in this research work.

- It is well evident that SEIG suffers from poor voltage and frequency regulations even when driven by constant speed prime movers or fixed head hydro turbines. A number of voltage and frequency regulating schemes have been reported in the literature. The study of operational aspects, relative suitability and classification of various regulating schemes is considered vital for commercialization of SEIG.

- The performance of SEIG feeding linear load is identified to select capacitance and speed for optimum voltage regulation. The investigation on transient performance of SEIG feeding common linear and non-linear loads is identified to evaluate harmonics and their effects on health of the generator and to devise the strategy to mitigate them.

- The study of design, modelling and performance of STATCOM with SEIG feeding various static and dynamic loads is identified to evaluate the power quality performance and to make the SEIG-STATCOM system cost effective for far flung areas.

- The study of isolated four-wire SEIG-STATCOM system feeding various types of linear and non-linear loads is identified to extend the potential applications of SEIG in remote locations. It is identified to assess the effectiveness of SEIG-STATCOM system as an isolated generating system for voltage regulation, load balancing, harmonic elimination and neutral current compensation.

- The series compensation in SEIG is an effective approach for regulating the load voltage. For the series compensated SEIG using series capacitors i.e. short shunt SEIG, the selection of shunt and series capacitors at a specified speed is considered vital for optimum voltage regulation and for optimum performance, a combination of voltage regulation characteristic and loadability.

- It is identified to investigate the series compensation of SEIG through static synchronous series compensator (SSSC), a series connected pulse width modulated (PWM) voltage source converter (VSC) for improved performance. To the best of author knowledge, no work has been reported on SEIG-SSSC configuration.

- As reported in the literature, the oscillating and unstable behavior is resulted in when series capacitors compensated SEIG feeds the induction motor load. It is identified to investigate the SSSC in conjunction with SEIG for providing effective damping to oscillations and to provide satisfactory performance with an induction motor load during starting and mechanical loading on induction motor.

The investigations have been carried out in the identified research areas to achieve the research objectives. The specific contributions to accomplish those research objectives are presented herewith.

**1. Study on the classification and operational aspects of the regulating schemes**

- The regulating schemes have been classified on the basis of voltage, frequency and voltage-frequency regulation strategies.

- Based on shunt or series compensation of reactive VARs, the voltage regulating schemes have been subcategorized into classical, switching device based and

converter based voltage regulating schemes. The frequency regulating scheme and voltage-frequency regulating schemes have also been discussed in details.

- The various loads on SEIG are summarized. The loads classification is made on number of phases or nature of load (linear or non-linear) and balanced and unbalanced category. The broad industrial and commercial application areas of SEIG are summarized.

- The suitability and operational aspects of each regulating scheme have been summarized for SEIG.

**2. Steady state performance of SEIG feeding static and dynamic loads and the transient performance of SEIG feeding linear and non-linear loads**

- On the basis of steady state equivalent circuit, the problem of voltage regulation optimization has been formulated by considering various equality and inequality constraints related to satisfactory operation of SEIG with static loads.

- The optimum values of capacitance and speed have been selected by developing a strategy employing genetic algorithm. The steady state SEIG performance has been evaluated for static and dynamic loads. The simulated results have been verified experimentally for both static and dynamic loads.

- The dynamic model of SEIG system has been developed to study the performance with linear and non-linear loads. The induction machines are modeled in q-d axis with current and voltage as state variables model in stationary reference frame, by considering main and cross flux saturation. The commonly used non-linear loads are modeled in phase variables.

- The transient performance has been analyzed for both three-wire and four wire non-linear loads including unbalanced loads. The power quality and harmonics generated by these non-linear loads have been analyzed using total harmonic distortion (THD) and harmonic spectrum.

**3. SEIG-STATCOM system for feeding balanced static resistive-inductive, induction motor and three-phase fully controlled rectifier fed DC motor loads**

- A STATCOM employing three-phase pulse width modulated (PWM), voltage source converter (VSC) with self supporting DC bus has been considered as a voltage regulator.

- A methodology to design STATCOM parameters has been presented and the STATCOM parameters have been designed for two cases namely full rating STATCOM and reduced rating STATCOM.

- A simplified proportional-integral (PI) controller based control technique has been proposed for the STATCOM. The control technique consists of two PI controllers. One PI controller is applied to regulate the DC link voltage to the reference value. The other PI controller is applied to regulate the terminal voltage by controlling the required reactive power.

- To obtain the system model, the induction machines have been modeled in q-d variables in stationary reference frame; whereas, the STATCOM and controlled rectifier fed DC machine have been modeled in phase variables.

- The power quality aspects have been studied in terms of THD and harmonic spectrum through Fast Fourier Transformation (FFT) during steady state condition.

**4. SEIG-STATCOM system operating as a four-wire isolated supply system for feeding various static linear and nonlinear loads**

- The hybrid dynamic model of four-wire SEIG-STATCOM system has been developed to study its performance. The induction machine is modeled in q-d variables, whereas, shunt capacitance, STATCOM and load are modeled in phase variables to model complete system.

- The performance is investigated for three-wire, four-wire loads and practical non-linear loads. The three-wire uncontrolled rectifier fed resistive, three-wire uncontrolled rectifier fed resistive-capacitive and four-wire uncontrolled rectifier fed resistive-capacitive loads have been treated as non-linear loads.

- The capability of the STATCOM operating as a voltage regulator, load balancer, harmonic eliminator and neutral current compensator has been demonstrated with SEIG system.

- The quality of various voltages and current of the system has been studied on the basis of THD and harmonic spectrum during steady state condition and are compared with the standard IEEE-519.

**5. Operation of series compensated SEIG feeding static loads using series capacitors and static synchronous series compensator (SSSC)**

- The steady state performance of short shunt SEIG has been evaluated using the steady state equivalent circuit.

- The optimization problems have been formulated to obtain series and shunt capacitances for the optimization of voltage regulation characteristic and for the performance characteristic, a combination of voltage regulation and loadability characteristics, subjected to various equality and inequality constraints related to SEIG performance.

- The optimum values of capacitances are obtained by developing a strategy based on genetic algorithm at different speeds and for different static loads. The simulated results for static resistive and resistive-inductive loads have been experimentally validated at rated speed.

- The design procedure and guidelines to decide the battery supported and capacitor supported SSSC parameters have been briefed for feeding static loads.

- The hybrid dynamic model of SEIG-SSSC system has been developed. The induction machine is modeled in q-d variables, whereas, shunt capacitance, SSSC and load are modeled in phase variables.

- The transient performance of SEIG-battery supported SSSC system and SEIG-capacitor supported SSSC system have been studied for feeding static loads.

- A simplified control strategy using a PI control loop has been proposed to regulate the terminal voltage by SSSC. The transient performance of SEIG-battery supported SSSC system is studied for feeding resistive, resistive-inductive and

resistive-capacitive loads. The inductive mode operation of SSSC for capacitive load and capacitive mode operation for both resistive and inductive loads has been demonstrated for SEIG-battery supported SSSC system.

- The proposed control technique for capacitor supported SSSC consists of two PI controllers, one for regulating the DC bus voltage and other for regulating the SEIG terminal voltage. The transient performance of SEIG-capacitor supported SSSC system has been investigated for feeding static R-L load.

- The quality of various voltages and currents of the SEIG-SSSC system has been studied on the basis of THD and harmonic spectrum during steady state condition.

**6. SEIG-SSSC system feeding induction motor load for the stable operation**

- The dynamic models of SEIG-SSSC system and short shunt SEIG feeding induction motor load have been developed to study the transient performance of both the configuration.

- The hybrid model of SEIG-SSSC system has been used. The induction machine is modeled in q-d variables, whereas, shunt capacitance and SSSC are modeled in phase variables.

- The SSSC parameters have been designed for feeding induction motor load.

- The effects of series capacitors on the performance of short shunt SEIG feeding motor load have been studied in details.

- The performance of SEIG-SSSC has been studied for the starting and subsequent mechanical loading of the induction motor load.

- The quality of various voltages and currents of the SEIG-SSSC system has been studied on the basis of THD and harmonic spectrum during steady state condition.

## 2.4 CONCLUSIONS

The present chapter summarizes the contributions made by various researchers in developing the SEIG and its technology to the present status by carrying out the literature survey. Keeping in mind, SEIG utility for small capacity applications and emergence in

extracting the wind and small hydro renewable resources, the review has been carried out in investigating the steady and transient state performance, design aspects, voltage regulation aspects and remedial measures, frequency regulation aspects and voltage-frequency regulation. On the basis of literature survey, the broad research objectives have been identified, and specific contributions by the author have been summarized to achieve the objectives.

# CHAPTER-III

# REGULATING SCHEMES FOR THREE-PHASE SELF-EXCITED INDUCTION GENERATORS

## 3.1 GENERAL

The generation of electrical energy has been mainly from fossil fuels such as coal, gas etc. Factors like degrading environment, depleting fossil fuels and challenges in extending the national grid to remote locations have motivated research on stand alone generating units for harnessing renewable energy sources such as micro hydro in hilly tracts, river flow, wind, industrial waste etc. A self-excited induction generator (SEIG) is a strong candidate to harness these renewable sources like small hydro and wind energy resources. A SEIG is normally a squirrel cage induction machine excited through externally connected ac capacitor bank as shown in Fig. 3.1. The primary advantages of the SEIG over conventional synchronous generators are brush-less and rugged construction, less maintenance cost, small size and better transient performances etc. Furthermore, SEIG does not require a separate dc exciter and field breaker. After the oil crisis faced world over in the seventies, the research on the SEIG has got impetus and various facets on its operational, performance improvement aspects and applications have been investigated in the literature [1-230].

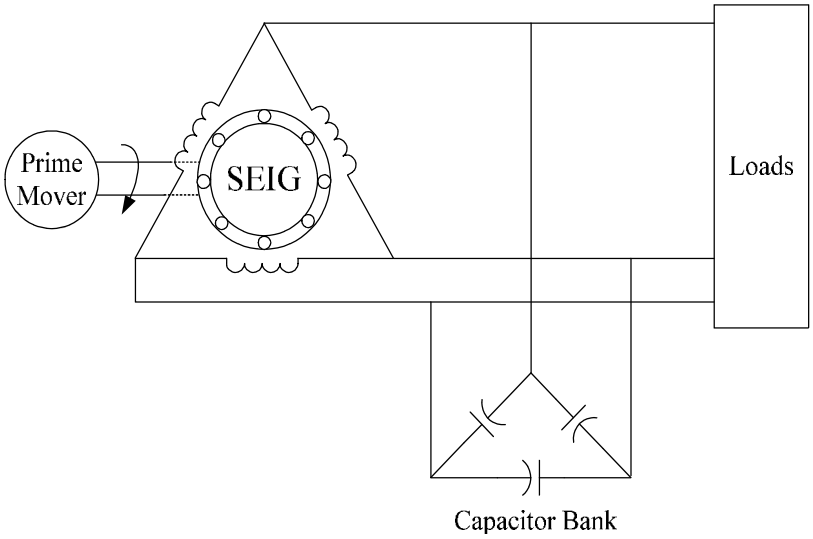


***Fig. 3.1 Schematic of a self-excited induction generator (SEIG)***

The terminal voltage of a SEIG is governed by an external shunt capacitance, the speed of the prime mover and the amount/power factor of the loads [16]. With the loading of the generator, its terminal voltage decreases due to the increasing difference between the VAR supplied by a capacitor bank and the VAR demanded by the generator and the loads. The poor voltage regulation exhibited by the SEIG can be improved by the shunt or series compensation using classical voltage regulating (VR) schemes [122-130]. Later, due to the development of the thyristor as a static switch, VR schemes like switching shunt capacitors etc. have appeared in the literature [131-153]. The advancements in power electronic switches, power converter circuits, digital signal processors and improved control algorithms have facilitated the researchers to employ a STATic COMpensator (STATCOM) for improving the performance of SEIGs [231-248] for feeding various linear and non-linear loads. Another VSC (voltage source converter) based power converter namely, a static synchronous series compensator (SSSC) has been used effectively in power systems [249-269] for improving voltage profile, power flow. The SSSC is referred by various names such as dynamic voltage restorer (DVR), series active filter (SAF), active power line conditioner (APLC), static series compensator (SSC) etc. in power system. The SSSC can also be employed with the SEIG to improve its performance for isolated applications. Various researchers have reported control schemes for frequency regulation [167-174], voltage and frequency control schemes [175-190] for three-phase systems and three-phase four-wire systems [191, 192].

The poor frequency regulation is also a concern for SEIG operating with uncontrolled turbine like micro and pico hydro generator. The frequency regulation can be achieved by speed governor control or by employing load controller. With load controllers [167-174], the total active power seen by the SEIG is maintained constant. The voltage and frequency control schemes [175-192] are important for converter fed applications like rectifier, battery charges, variable speed drives and thus the study of SEIG feeding these loads is important.

The present chapter is an endeavor focusing on voltage and frequency regulations aspects of three-phase SEIG supplying linear and non-linear loads. Various regulating schemes scattered in the literature are classified as voltage, frequency and voltage-frequency regulating schemes. Various voltage regulating schemes are classified on the basis of a shunt and a series compensations. The applications areas suited for SEIG and

various loads are also discussed separately. Various salient features and the control of regulating schemes are also encapsulated to facilitate in developing a new regulating schemes for commercial applications of SEIGs.

## 3.2 VARIOUS LOADS AND APPLICATIONS OF SEIG

The classification of loads on SEIGs is depicted in Fig. 3.2. The three-phase SEIG systems are classified on the basis of load phases i.e. three-phase or single phase loads [100-116]. The three-phase loads can be three-phase, three-wire loads or three-phase, four-wire loads [166]. These loads can be classified as linear or non-linear loads. The linear loads are static such as the heaters, lighting loads or dynamic loads (ac and dc motors). The majority of dynamic industrial loads are induction motor loads [63-67] used in fans, centrifugal pumps, compressors etc. Further, the loads may also be classified as balanced or unbalanced loads in three-phase systems.

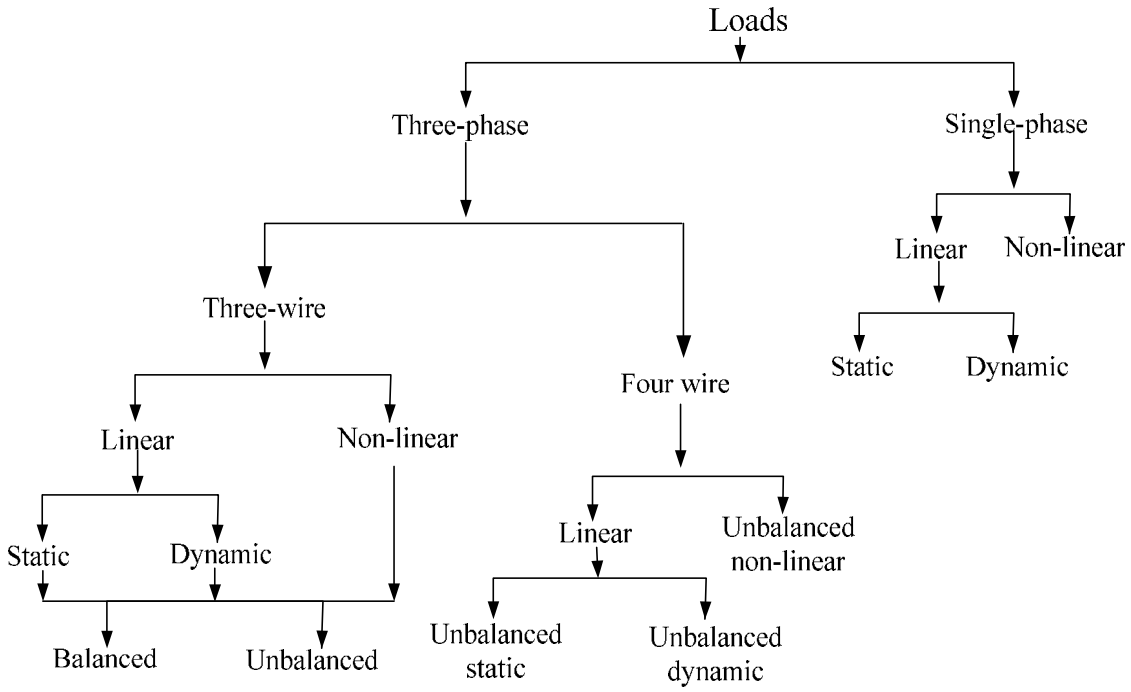


***Fig. 3.2 Classification of loads on SEIGs***

The percentage of non-linear loads fed by SEIG [68-69] is escalating due to increasing use of power electronic and converters based appliances such as rectifiers, battery chargers, uninterrupted power supplies (UPS), switch mode power supplies (SMPS), compact fluorescent lamps (CFLs), adjustable speed drives (ASDs) etc. The utilization of non-linear loads to be supplied by SEIGs is expected to increase in near

future. The reactive power burden, the harmonics generation, the power factor deterioration, the loss addition and an electro-magnetic interference etc. are few adverse effects of the non-linear loads.

Due to the various relative advantages, SEIGs may be used in the applications summarized [5-9] as follows-

- *Emergency power supplies* used for areas such as hospitals, libraries, telephone exchanges, railways bookings and signaling, computers and marketing complexes etc.

- *Small power generators* used in remote and isolated places to feed lighting and heating loads, domestic appliances and small agricultural appliances.

- *Portable source of power supplies* used for supplying decorative lightings, lighting for projects and at constructional sites, battery chargers and in vehicles such as tractors, buses etc.

- *Industrial applications of induction generators* have been reported in the literature [221-228]. In process and chemical industries, its application in power recovery train applied to fluid catalytic cracking (FCC) unit has been discussed in [221]. The operation of an induction generator driven by natural gas engine has been reported for refinery in [222]. The cogeneration or waste heat of process steam is harnessed through the induction generator and issues related to the installation, cost and control for different process industries have been reported in [223-227]. A low voltage low power automotive induction generator system using a diode bridge rectifier and a PWM inverter has been compared with a conventional alternator based system in [228].

## 3.3 REGULATING SCHEMES FOR SEIG

The improved performance of SEIG system is obtained by improving voltage and frequency regulation through various reactive and active power control schemes. A detailed classification of these schemes is depicted in Fig. 3.3. Broadly, the regulating schemes are classified into voltage, frequency and voltage-frequency regulating schemes. The voltage regulating schemes are further sub classified into shunt compensation and

series compensation based voltage regulating schemes, each of one is further subcategorized into classical, switching device based and converter based schemes.

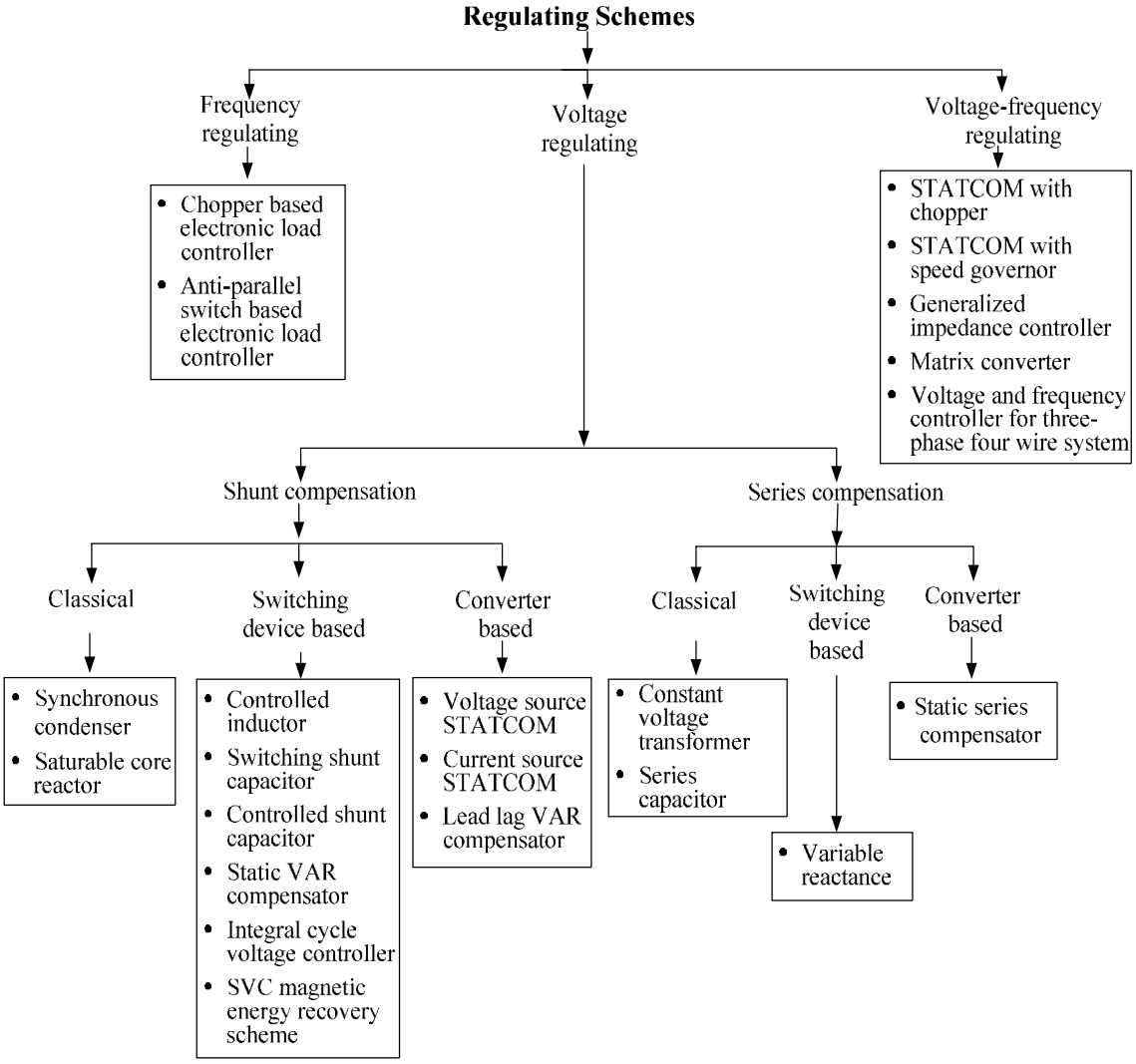


***Fig. 3.3 Classification of regulating schemes for SEIGs***

## 3.4 VOLTAGE REGULATING SCHEMES

The improved voltage regulation of SEIGs is obtained through the reactive power control schemes using shunt and series compensations. The voltage regulation of the SEIG based on shunt compensation schemes is achieved by the reactive power compensation provided by the compensator current. The improved voltage regulation of the SEIG based on series compensation is achieved by inserting a source of the reactive power or a passive reactive element. As the load is increased on the SEIG, the additional reactive power is injected into the lines. The shunt and series compensation schemes are classified into classical schemes, switching device based schemes and converter based

schemes. The operational aspects and relative suitability of these schemes are presented in the following discussion.

### 3.4.1 Classical Shunt Compensation Schemes

The classical compensation schemes are advantageous due to their operational simplicity and resulting no problems like harmonics, transients etc.

#### *3.4.1.1 Synchronous Condenser Based Scheme*

An over-excited synchronous machine (synchronous condenser) is connected across the SEIG terminals, which supplies additional VARs during an inductive loading to keep the load voltage constant, thus provides good voltage regulation. This scheme is simple and effective in providing the voltage regulation, but it requires high initial investment and results into large size and high cost.

#### *3.4.1.2 Saturable Core Reactor Based Scheme*

The saturable core reactor based VR scheme [134-136] is shown in Fig. 3.4. The saturable core reactor is connected in parallel with capacitor bank across the generator terminals. The shunt capacitor bank supplies the VAR requirement of the generator and a pure inductive load and the saturable core reactor absorbs the capacitive current under no load condition. The saturable core reactor works as an auto-excited magnetic amplifier and thus the terminal voltage is maintained at the rated value. It employs two control windings namely reference winding and feedback winding. The reference winding is given reference signal whereas the feedback winding is excited from derived feedback dc signals. The rating of saturable core reactor is decided to absorb the capacitive current under no load condition and to maintain rated terminal voltage.

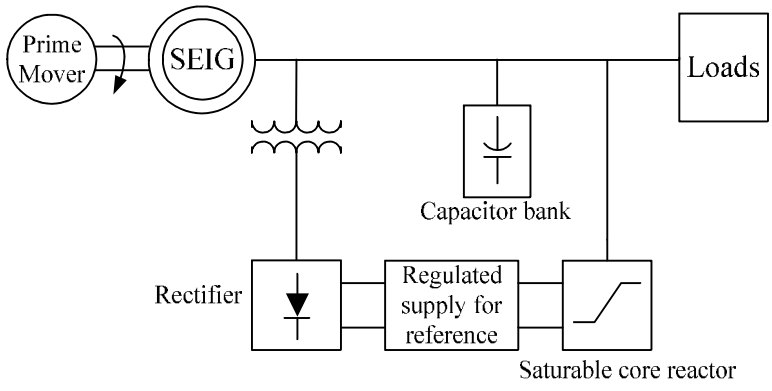


***Fig. 3.4 Saturable core reactor based VR scheme***

The terminal voltage reduces with the increase in the load, causing desaturation of the core. With the desaturation of the core, the effective inductance increases thus resulting in a decrease in the reactor current. Therefore, the capacitor current is transferred to the SEIG and it results in to an increased excitation and a higher terminal voltage. This VR scheme is advantageous because of the better operational stability and reliability over other classical VR schemes of SEIGs.

### 3.4.2 Switching Device Based Shunt Compensation Schemes

The shunt compensation VR schemes realized through solid state switching devices, which can adaptively control the reactive power required by the load and generator to regulate the terminal voltage, are briefed herewith.

#### *3.4.2.1 Solid State Switched Controlled Inductor Scheme*

A schematic of the voltage regulating scheme employing solid state switched controlled inductor [139] is shown in Fig. 3.5. A permanently connected capacitor bank $C_{min}$ is selected to obtain the rated voltage at no load. After the voltage buildup, the programmable logic controller (PLC) closes the contact $K_1$ and set the firing angle ($\alpha$) of static switch (S) by comparing the sensed terminal voltage ($V_t$) with the reference voltage ($V_{ref}$). A capacitor connected through $K_1$ provides the capacitive VAR when the SEIG is supplying the full load. The additional capacitive VARs are absorbed by the inductor connected through a static switch (S) controlled inductor and thus it results into a constant terminal voltage. The capacitor bank connected through $K_2$ is an optional and is used during the starting of induction motor loads.

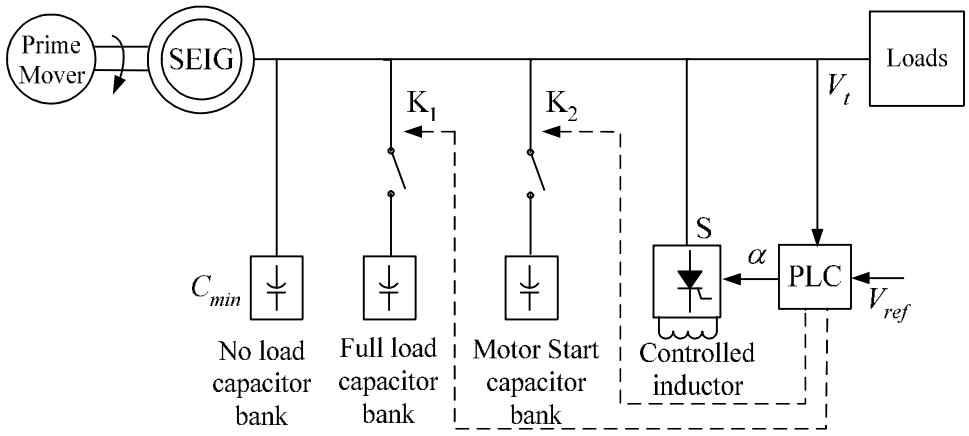


***Fig. 3.5 Solid state switched controlled inductor based VR scheme***

### *3.4.2.2 Switching Shunt Capacitor Based Scheme*

Fig. 3.6 shows a schematic of a voltage regulating scheme based on switched capacitors [137]. The capacitance is varied from a minimum $C_{min}$ to a maximum $C_{max}$. The $C_{min}$ and $C_{max}$ are capacitances needed to obtain the rated voltage at no load and at a lagging power factor full load. The $C_{min}$ is connected in parallel with binary weighted capacitors $C$, $2C$ and $4C$ which has a total value of ($C_{max}$-$C_{min}$). The load current is taken as a feed back signal and an appropriate switching is effected for the switching of the capacitors in binary steps. It has the advantage of distortion free waveforms, but its operation causes switching transients and the terminal voltage control in steps.

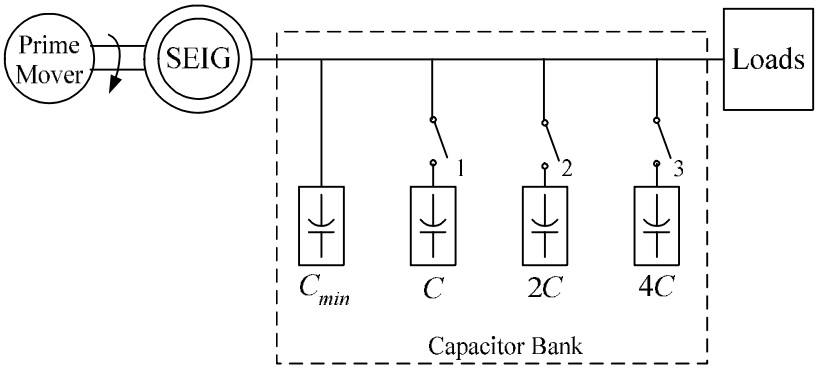


***Fig. 3.6 Switching shunt capacitor based VR scheme***

### *3.4.2.3 Controlled Shunt Capacitor Based Scheme*

A voltage regulating scheme employing continuously controlled shunt capacitance [138] is shown in Fig. 3.7. The effective capacitance is adjusted periodically by controlling the ON/OFF control of the self commutating switching device namely gate turn off (GTO) switch. The current flows through the capacitor when the switch is OFF. The switch is turned ON for a short period when the instantaneous capacitor voltage reaches the zero value and the current flows through the GTO. The voltage across the capacitor remains zero when the switch is ON**.** When the switch is closed for the longer duration, the fundamental component of voltage across the capacitor is reduced, which results into a higher effective capacitance independent of the current through the capacitor. Therefore, the minimum capacitance is the actual capacitance $C_{sh}$ in the circuit while the maximum capacitance is quite high depending upon the angle control of the GTO. This scheme can be applied for low power applications of the SEIG.

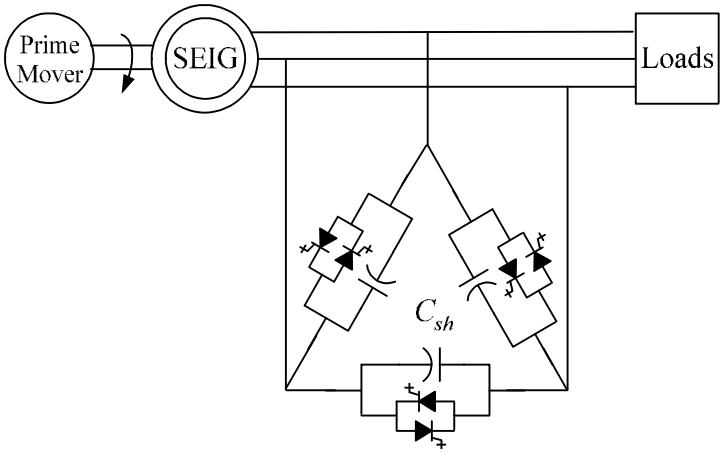


***Fig. 3.7 Controlled shunt capacitor based VR scheme***

### *3.4.2.4 Static VAR Compensator Based Scheme*

A VR scheme with the variable shunt reactance resulted in because of phase angle control of switching devices [146] is shown in Fig. 3.8. The current in the shunt branch is controlled to obtain the rated voltage at different loads. Another voltage regulating scheme employing a static VAR compensator (SVC) for the SEIG [147, 148] is depicted in Fig. 3.9. The SVC is composed of a fixed capacitor (FC) connected in parallel with the thyristor based phase controlled reactor (TCR) and thyristor based switched capacitor (TSC). The firing angle of the TCR is controlled and a TSC is switched in and out using feedback control in a closed loop manner. The error between the sensed and reference voltage is processed in Proportional-Integral (PI) controller and the voltage controller output is used to generate the control signals for controlling the TCR and a TSC.

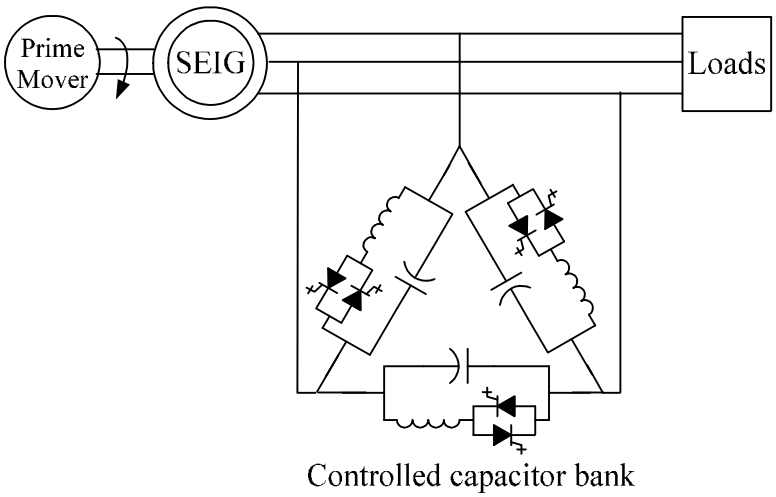


***Fig. 3.8 TCR-FC based VR scheme***

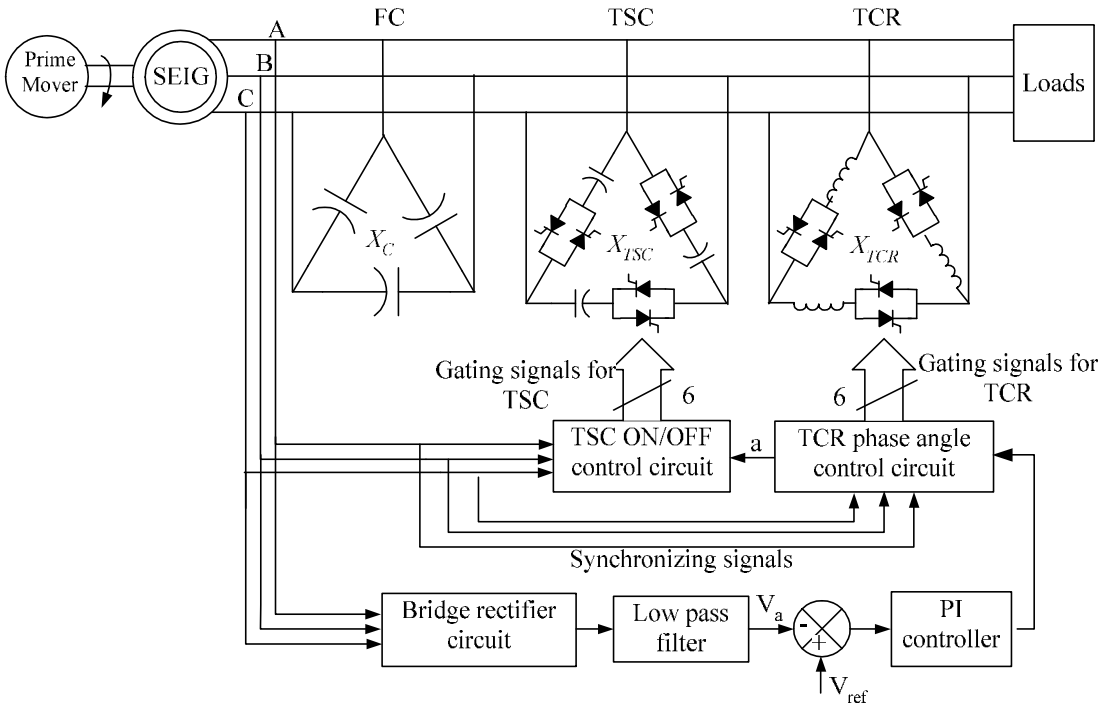


***Fig. 3.9 SVC based VR scheme***

### *3.4.2.5 Integral Cycle Voltage Regulating Scheme*

The excitation capacitor in each phase is switched individually by a set of insulated gate bipolar transistors (IGBTs) at the zero crossing of respective capacitor currents in an integral cycle voltage controller [150-152], as shown in Fig. 3.10. The terminal voltage is compared continuously with the reference value of the terminal voltage. The switching of the capacitors at high or low voltage is implemented at the zero crossing of the capacitor current and thus a snubber circuit is not required. The reduced switching loss is an advantage of this scheme.

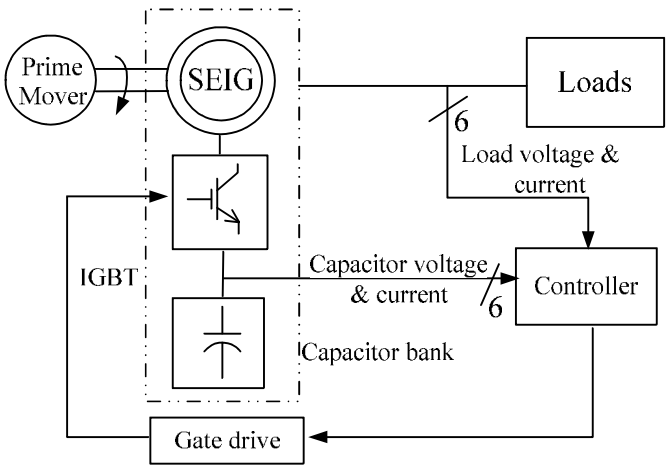


***Fig. 3.10 Integral cycle control based VR scheme***

### *3.4.2.6 Static VAR Compensation Magnetic Energy Recovery Scheme*

The static VAR compensation scheme based on a magnetic energy recovery switch (SVC-MERS) for the SEIG [149] is shown in Fig. 3.11. The SVC-MERS can control the SEIG terminal voltage with the advantage of low switching frequency, low switching losses and the fast control. The SVC-MERS consists of bidirectional switches made from IGBTs, a DC capacitor and an inductor and thus functions as a variable reactive power compensator.

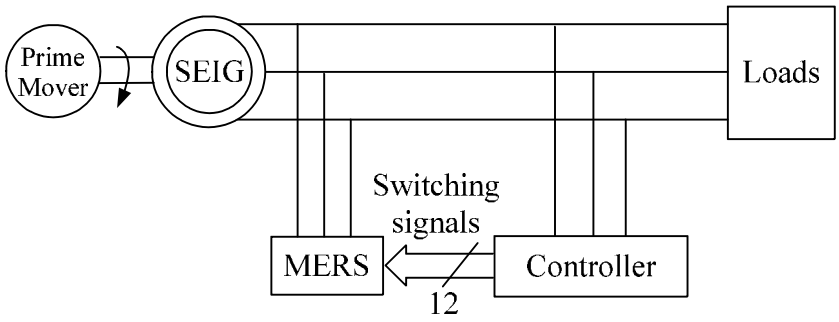


***Fig. 3.11 SVC-MERS based VR scheme***

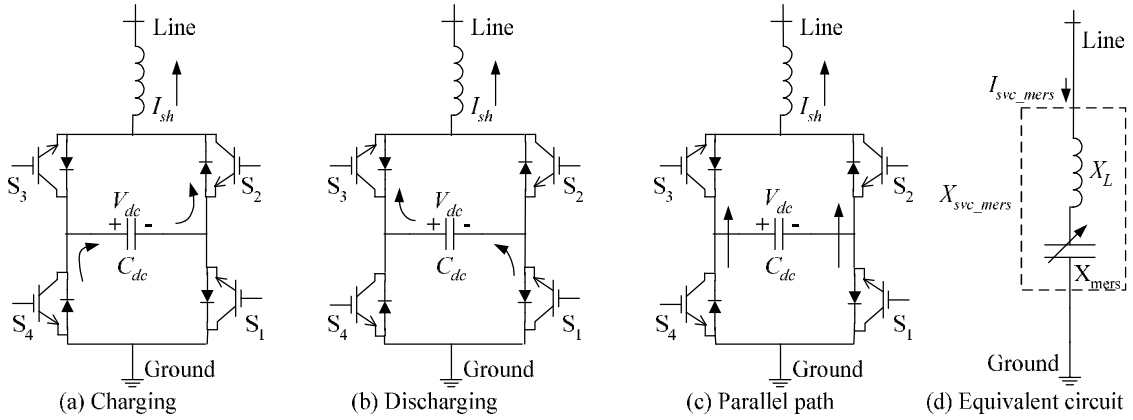


***Fig. 3.12 Operational states and equivalent circuit of SVC-MERS***

The operational states of SVC-MERS during charging, discharging, and a parallel path with the equivalent circuit are shown in Fig. 3.12 (a), Fig. 3.12 (b), Fig. 3.12 (c), and Fig. 3.12 (d) respectively. In the positive half cycle, the IGBTs ($S_2$, and/or $S_4$) are conducting and in other half cycle, the IGBTs ($S_1$ and/or $S_3$) are conducting. Each pair of IGBTs are switched ON and OFF once in a cycle. In the negative half cycle, when current $i_{sh}$ is upward, the charging of the capacitor is in the direction of the arrow. During switching ON of $S_1$, $S_3$, the capacitor is discharged with the same direction of the current. When the voltage of capacitor is zero, the current flows in a parallel path created by the

conduction of IGBTs. In the next half cycle, the polarity of capacitor charging remain same, however the direction of current $i_{sh}$ is reversed. The varying compensation current is obtained by controlling the current flowing in the DC capacitor by appropriate gate control signal.

### 3.4.3 Converter Based Shunt Compensation Schemes

A STATic COMpensators (STATCOM) is basically a three-phase pulse width modulated (PWM), voltage source converter (VSC) connected in shunt to control the reactive power by generating leading or lagging current with respect to terminal voltage. A STATCOM can be constructed either through voltage or current source PWM based converter. Various static compensators based on voltage source converters (VSC) and current source converters (CSC) shunt compensation based VR schemes are presented herewith.

#### *3.4.3.1 Voltage Source STATCOM Based Scheme*

The schematic with associated control arrangement of STATCOM (static compensator) based voltage regulator for SEIG [154-160] is shown in Fig. 3.13. The current controlled – voltage source converter (CC-VSC), as shown in Fig. 3.14, comprises of IGBTs ($I_1$-$I_6$) with anti-parallel diodes ($D_1$-$D_6$). In this scheme, there are two control loops; one for controlling the terminal voltage of SEIG ($V_0$) and other for maintaining the DC link voltage of STATCOM ($V_{dc}$). The controlled lagging or leading reactive currents are injected by the VSC and the scheme is found to be effective and suitable to feed nonlinear loads [158] also. The main advantages of voltage source converter based STATCOM are its fast response and ability to operate at a high switching frequency.

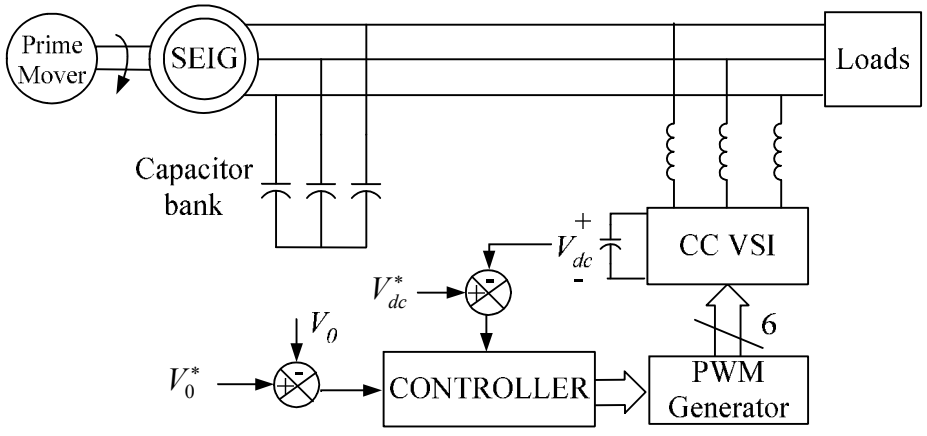


***Fig. 3.13 STATCOM based VR scheme***

With the current source converter (CSC) based STATCOM (CSC-STATCOM) in place of voltage source converter (VSC) based STATCOM and its DC link current control loop in place of the DC link voltage control loop [161], the basic scheme remains same as shown in Fig. 3.13.

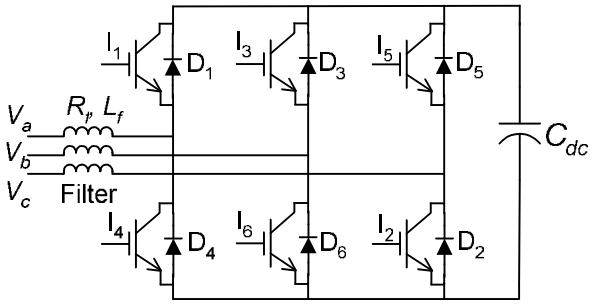


***Fig. 3.14 Voltage source STATCOM***

### *3.4.3.2 Current Source STATCOM Based Scheme*

The CSC-STATCOM, as shown in Fig. 3.15, consists of IGBTs ($I_1$-$I_6$) with series diodes ($D_1$-$D_6$). The operation of CSC-STATCOM with the SEIG is advantageous for resulting in rugged and short circuit proof operation. Without complicated control circuitry, it directly produces reactive current that can be fed to the SEIG. This VR scheme introduces high frequency harmonics that are absorbed by the capacitor bank to some extent and does not flow into the SEIG system.

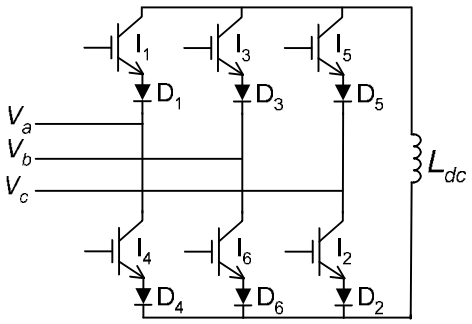


***Fig. 3.15 Current source STATCOM (CS-STATCOM)***

### *3.4.3.3 Solid State Lead Lag VAR Compensator Based Scheme*

The schematic and a control loop of an inductively loaded current controlled solid-state lead-lag compensator [141-144] are shown in Fig. 3.16 and Fig. 3.17 respectively. In this VR scheme, the compensator operates as a variable current source. The firing angle delay ($\alpha$) of the lead lag VAR compensator devices is estimated in the

closed loop manner from a PI controller over the sensed terminal voltage ($V_0$) and the reference voltage ($V_0^*$).

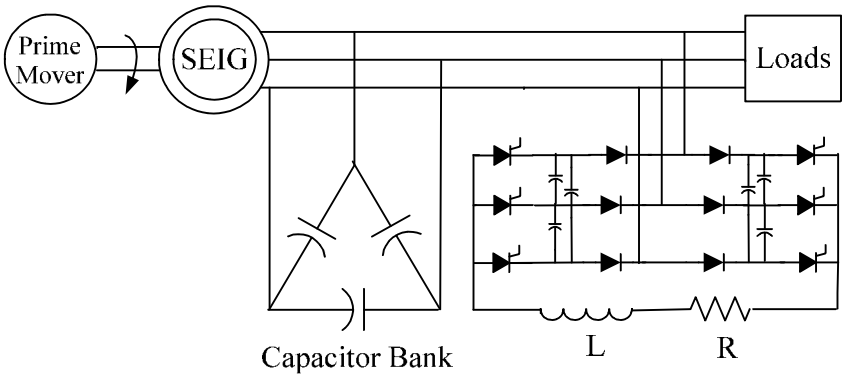


***Fig. 3.16 Lead lag VAR compensator based VR scheme***

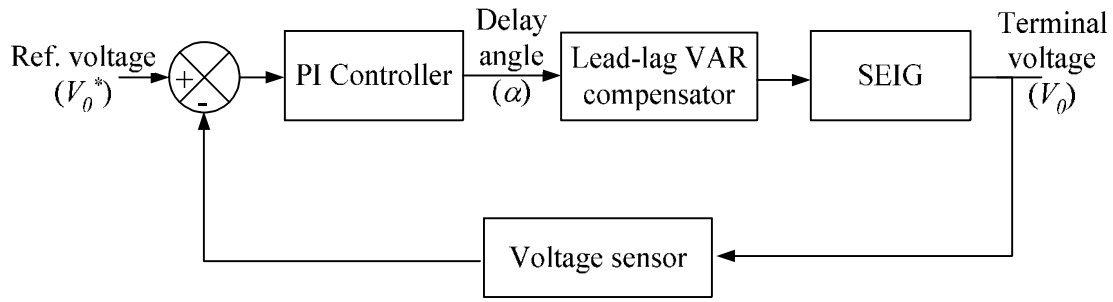


***Fig. 3.17 Closed loop control of VAR compensator***

### 3.4.4 Classical Series Compensation Schemes

The schemes based on a constant voltage transformer (CVT) and series compensated SEIG configurations are briefed herewith.

#### *3.4.4.1 Constant Voltage Transformer Based Scheme*

In this scheme, the CVT is connected between the SEIG and the load [137]. The shunt capacitance is selected to provide the rated voltage at the full load. At light load, the excess VARs are absorbed by the CVT while operating in deep saturation region. This VR scheme results in fair voltage regulation but causes additional losses in CVT.

#### *3.4.4.2 Series Capacitors Based Scheme*

In series compensated SEIG configurations, the suitable series capacitors are inserted into the line, which provides additional VARS during loading. Two configurations of series compensated SEIGs namely a short shunt SEIG and a long shunt

SEIG are possible and are shown in Fig. 3.18 and Fig. 3.19 respectively. With suitable series and shunt capacitances, it is possible to obtain almost flat load voltage profile in both these configurations. However, higher values of shunt and series capacitances are required for long shunt SEIG [122-130]. These configurations of VR schemes of SEIGs are simple and cost effective but cause unstable behavior with dynamic (induction motor) loads.

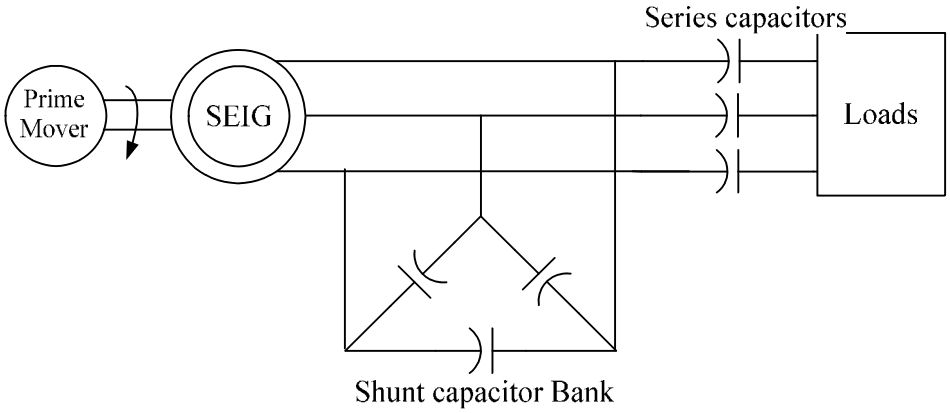


***Fig. 3.18 Short shunt SEIG***

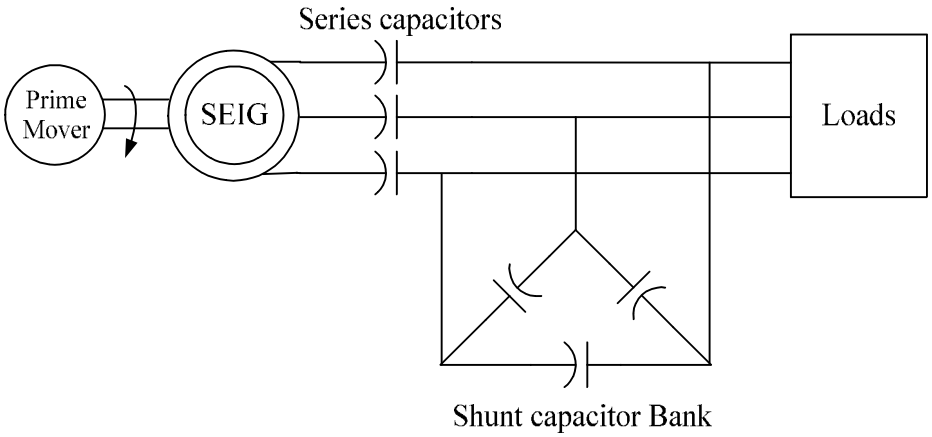


***Fig. 3.19 Long shunt SEIG***

### 3.4.5 Switching Device Based Series Compensation Scheme

This scheme introduces variable reactive impedance in series with the line [146], thus provides the variable reactive power to control the terminal voltage. As shown in Fig. 3.20, the series reactance is comprised of a fixed capacitor (FC) in parallel with a thyristor controlled reactor (TCR). Under varying loads, the series reactance is varied to obtain the rated load terminal voltage. With this arrangement, the variable series reactance can be obtained, which is not possible with classical series schemes.

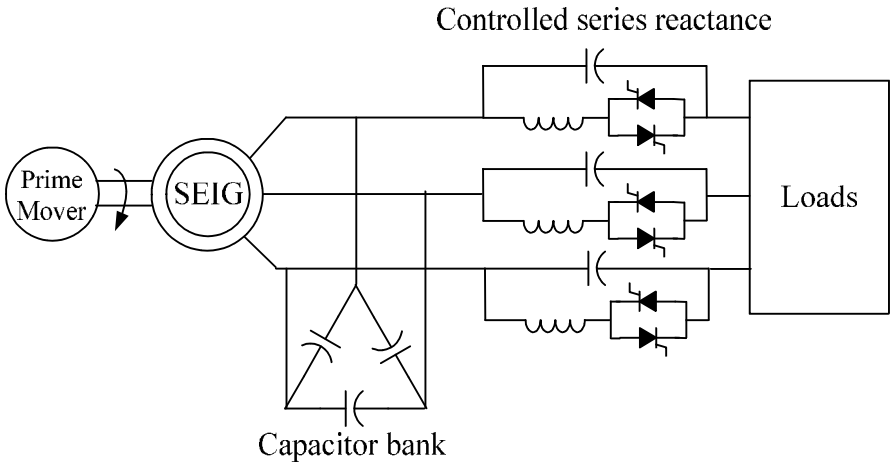


***Fig. 3.20 TCR-FC based series compensation scheme***

### 3.4.6 Converter Based Series Compensation Scheme

The schematic of SSSC (static synchronous series compensator) based VR scheme for the voltage control of the SEIG and associated control strategy are shown in Fig. 3.21. The SSSC consists of a three-phase IGBT based PWM (pulse width modulated), current controlled, voltage source converter (CC-VSC) with a suitable sized energy source at DC link. In self supporting DC bus configuration, a suitable size DC capacitor is connected [249-251]. It is connected in series with the line through an insertion transformer.

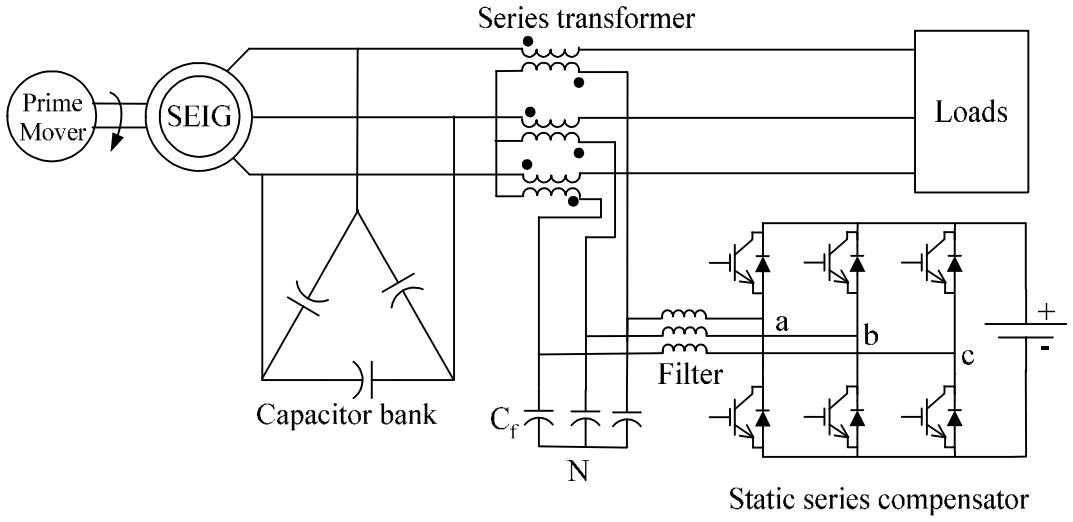


***Fig. 3.21 SSSC in operation with SEIG***

The SSSC efficiently modulates the effective impedance of the line by injecting a controllable voltage maintaining appropriate phase angle with the line current. Further, it can exchange both real and reactive power with energy storage system on the DC bus of

VSC. When the injected voltage is in the quadrature leading to the line current, the SSSC emulates an inductor and a capacitor when the injected voltage is in the quadrature lagging to the line current.

## 3.5 FREQUENCY REGULATING SCHEMES FOR SEIG

The frequency of SEIG also decreases due to the increase in the loads when it is driven by constant speed prime mover. The constant frequency is desired as the operation of some converter based loads is sensitive to supply frequency and the frequency deviation from nominal value may cause malfunctioning. The frequency of SEIG can be controlled by mechanical governor control by controlling the input to the turbine using speed governor. The frequency of SEIG system can also be controlled by electronic load controller (ELC) in which the total active power seen by SEIG remains constant [167-174]. In SEIG based stand alone schemes, the mechanical speed governing control causes the complexity of the operation and results into high system cost.

### 3.5.1 Chopper Based Electronic Load Controller Scheme

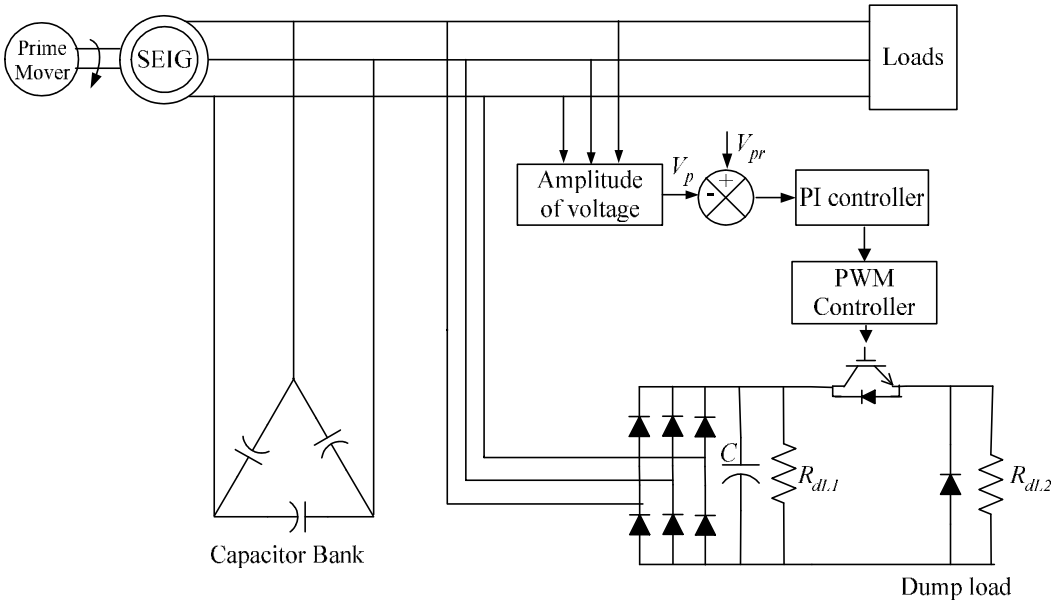


***Fig. 3.22 Electronic load controller scheme realization through chopper***

The SEIG with ELC is used in stand-alone micro and pico-hydro power generation employing uncontrolled turbines where input turbine power and total electrical output power remain constant. The power exceeding the requirement of loads is dumped in a resistive dump load to keep frequency constant under steady state condition. As shown in Fig. 3.22, the ELC scheme consists of an uncontrolled rectifier in series with an

IGBT based chopper and a dump load resistor [168-173]. The duty cycle of the chopper is decided through closed loop control of SEIG terminal voltage. The error between actual voltage ($V_p$) and reference voltage ($V_{pr}$) is processed in a PI controller and its output is used to generate pulse width modulated gating signal for IGBT.

### 3.5.2 Anti-Parallel Switch Based Electronic Load Controller Scheme

The anti-parallel switch based ELC [174], as shown in Fig. 3.23, employs anti-parallel IGBTs ($S_a$, $S_b$, $S_c$) to control the effective dump load resistance. The PI controller is employed over the reference ($V_{tr}$) and actual ($V_t$) terminal voltage. The PWM current controller is applied to generate the six gating signals to IGBTs, and set the firing angle to dump the excess power required for maintaining the terminal voltage. The SEIG with unregulated turbine has been attractive due to low cost, ruggedness, high reliability and low inertia. However, ELC injects the harmonic current into the stator and wastes significant electrical power in dump resistor.

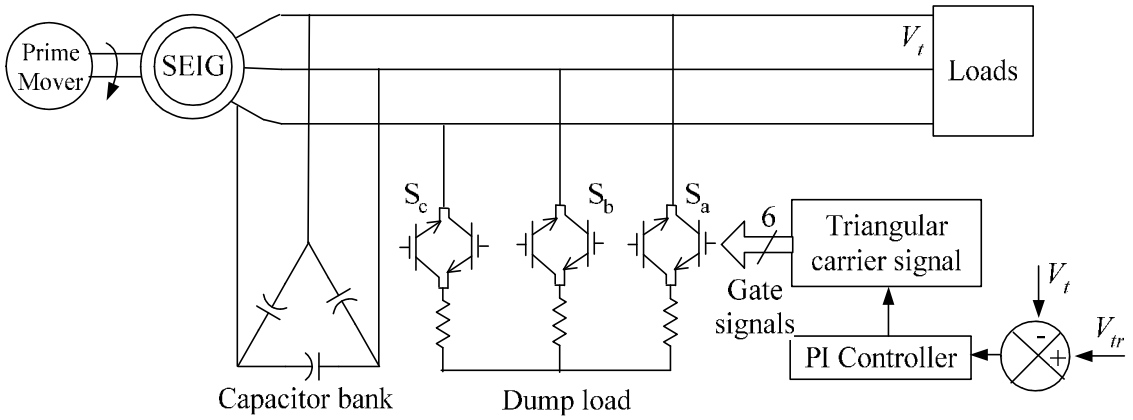


***Fig. 3.23 Electronic load controller scheme realization through anti-parallel switch***

## 3.6 VOLTAGE-FREQUENCY REGULATING SCHEMES FOR SEIG

The voltage and frequency can be controlled by controlling reactive and active power respectively. Such voltage-frequency regulating schemes applied for three-phase three-wire and three-phase four-wire configurations of SEIG are presented herewith.

### 3.6.1 STATCOM with Chopper Based Scheme

The voltage and frequency control using STATCOM with dc side chopper [189] is shown in Fig. 3.24. The objective of this control scheme is to maintain the dc voltage $V_{dc}$

constant by changing the effective value of dump resistance $R_{dc}$ to consume the excessive generated power. The total power supplied by the generator is matched with the power consumed by the loads and controlled dump resistance at all loading conditions. The constant $V_{dc}$ is reflecting the balance between the generated and consumed power. A decrease in $V_{dc}$ indicates deficit in generated power, whereas an increase in $V_{dc}$ indicates surplus generated power. The ac voltage can be kept constant by operating STATCOM at constant modulation index. Both these controls help to maintain the constant load voltage and frequency. The voltage and frequency control employing STATCOM without dc side chopper is achieved by regulating the ac voltage by changing the modulation index with unregulated dc link voltage.

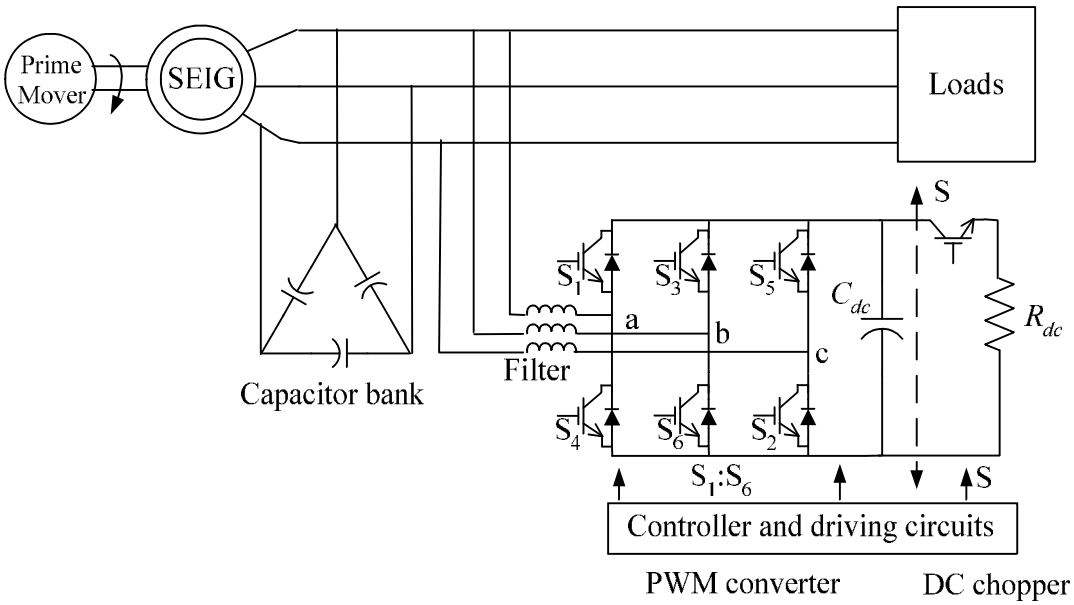


***Fig. 3.24 Voltage-frequency regulating scheme using STATCOM with DC side chopper***

### 3.6.2 STATCOM with Speed Governor Based Scheme

The scheme of voltage-frequency control by STATCOM and speed governor [180] is shown in Fig. 3.25. The control block is sensing load voltage ($v_l$), compensation current ($i_e$), dc link voltage ($V_{dc}$) and servo motor speed ($\omega_r$) and generating the switching signals for IGBTs of advanced STATCOM. This technique is based on relative rotation speed theory, which is estimating the frequency deviation and assisting the STATCOM in synchronism with system frequency by controlling the speed governor. The dc capacitor voltage is indicative of system power balance and is used as a control variable for the

speed governor in the isolated system. This scheme is suitable for IC engine driven SEIG system.

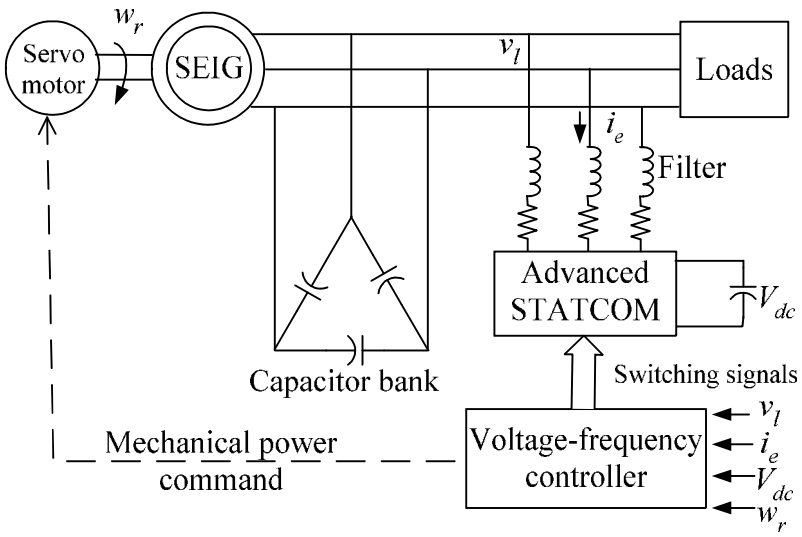


***Fig. 3.25 Voltage-frequency regulating scheme using STATCOM and speed governor***

### 3.6.3 Generalized Impedance Controller Based Scheme

The generalized impedance controller (GIC), an operational modification of STATCOM [183-187] as shown in Fig. 3.26, is a voltage source pulse width modulated bidirectional inverter with dc link battery, capable of providing bidirectional flow of both active and reactive power. The proper selection of modulation index ($m$) and phase angle $\delta$ (between the PWM voltage and SEIG voltages) enables the GIC to operate in any quadrant of the active power-reactive power ($P$-$Q$) diagram.

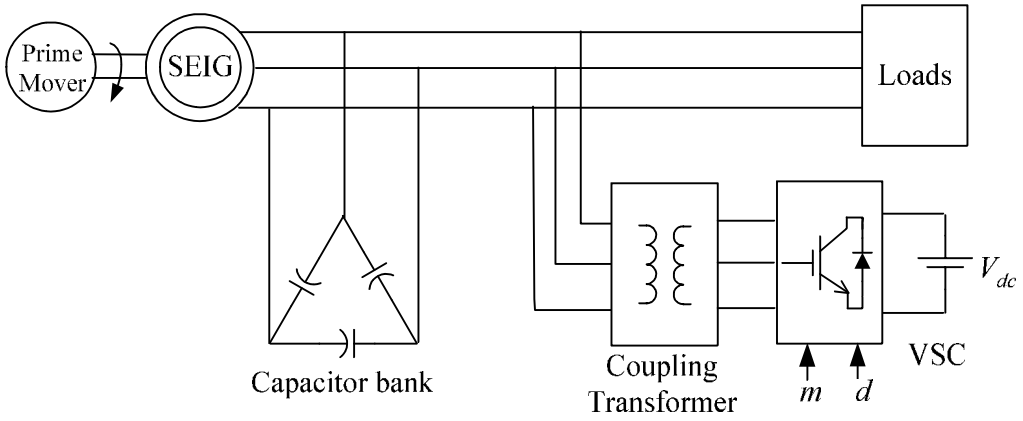


***Fig. 3.26 Voltage-frequency regulating scheme using GIC***

The operational aspect of it is explained in Fig.3.27. As the load is decreased, the excess power is used to charge the battery, whereas the GIC provides the shortfall during

the increase in the load demand. Depending upon the SEIG condition and load, the GIC can supply or absorb *P* and *Q*.

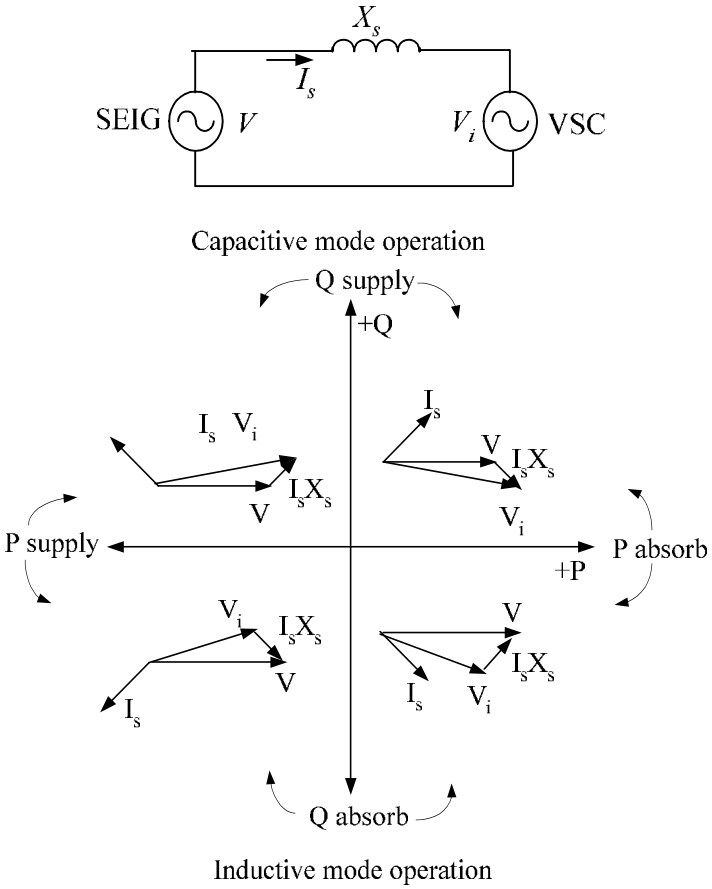


***Fig. 3.27 Equivalent circuit and mode of operation of GIC in P-Q plane***

### 3.6.4 Matrix Converter Based Scheme

The schematic diagram of a matrix converter based scheme [190] is shown in Fig. 3.28. The matrix converter, a three-phase ac-ac converter, is a modified version of forced commutated cyclo-converter (FCC). The matrix converter is capable of generating three-phase ac sinusoidal voltage of desired frequency and voltage without any energy storage element. Unlike two stage PWM voltage source rectifier-inverter circuit (back to back converter), matrix converter is a single stage converter circuit with nine bi-directional IGBT switch. It has bidirectional power flow capability, compact design due to absence of DC link energy storage component and controllable input power factor. The matrix converter finds applications usually in wind power conversion through induction generation and doubly fed induction generator.

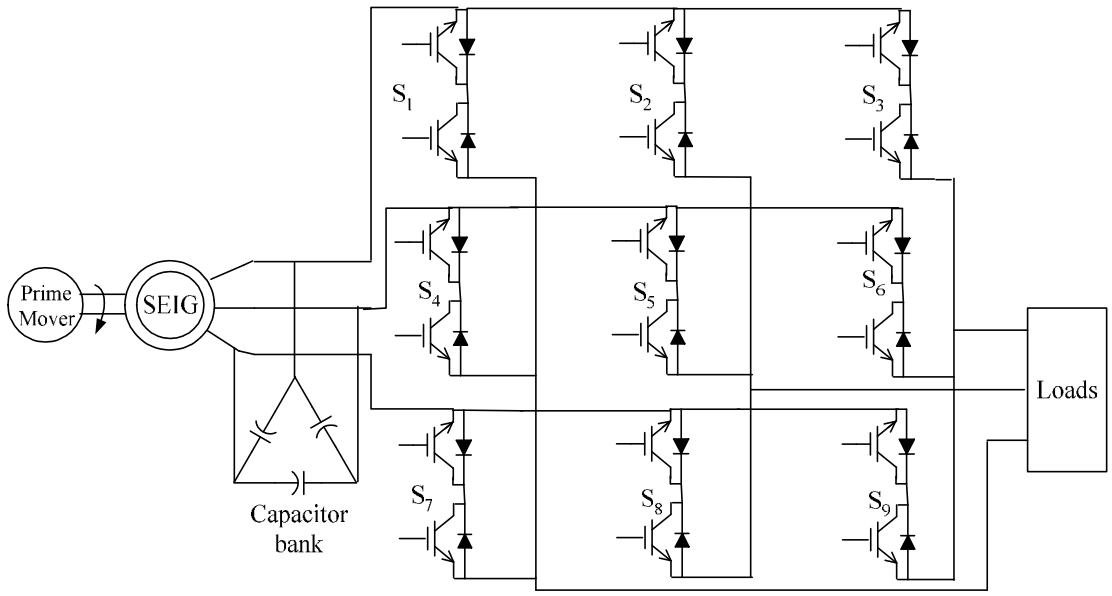


***Fig. 3.28 Voltage-frequency regulating scheme using Matrix converter***

The main disadvantages of matrix converter based scheme include limitation on voltage transfer ratio, complex control circuit and non availability of controlled bidirectional high frequency, high power integrated static switch. The control scheme consists of two PI controllers, one for controlling the active power and other for controlling the stator flux. The carrier based constant frequency PWM modulation or space vector pulse width modulation (SVPWM) based technique can be used to generate output voltage of MC.

### 3.6.5 Voltage-Frequency Regulating Schemes for Three-Phase Four-Wire System

The schematic diagram of decoupled voltage and frequency control (DVFC) is shown in Fig.3.29, which is a combination of electronic load controller (ELC) and STATCOM [191]. This scheme is suitable for isolated application such as pico-hydro uncontrolled turbine driven SEIG. The ELC is applied for consuming the excess generated active power by the SEIG keeping active load seen by the generator constant to obtain constant frequency operation. The STATCOM provides variable reactive power as required by the various single phase balanced/ unbalanced linear/non-linear load for constant terminal voltage, load balancing, neutral current compensation and harmonic elimination. Therefore, the STATCOM work as a voltage regulator, a load balancer, a neutral current compensator and a harmonic eliminator.

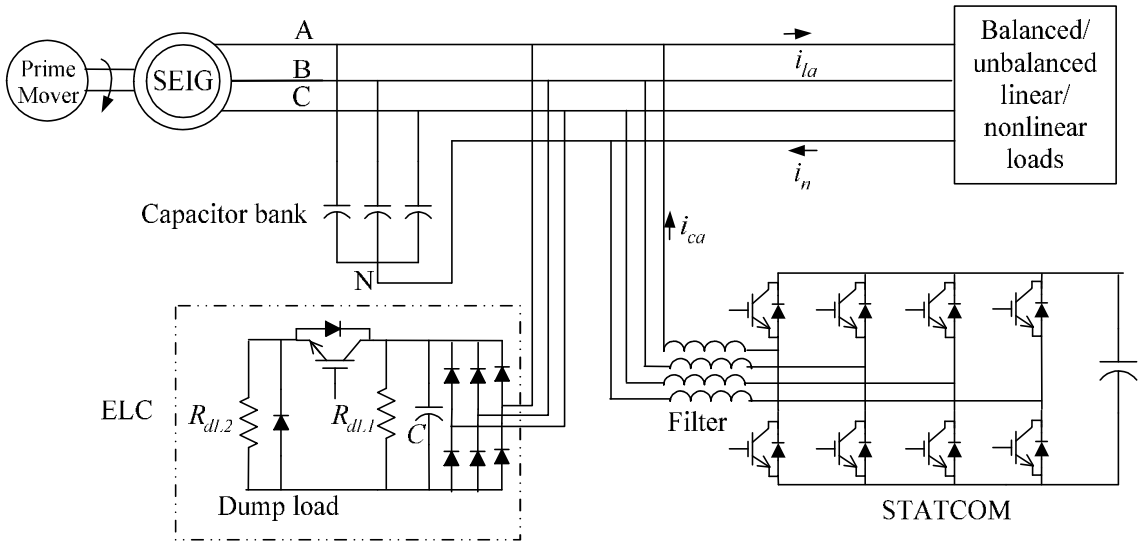


***Fig. 3.29 Schematic of DVFC for feeding three-phase four-wire load***

The schematic diagram of another electronic converter applied for three-phase four wire isolated system is depicted in Fig. 3.30. The scheme is a combination of shunt active filter (AF), bidirectional current battery converter (BC) and electronic load controller (ELC) [192]. The AF is made of a four leg voltage source inverter with a split capacitor and two dc-dc converters. The one dc converter works as a BC, which acts as a buck converter in the charging mode and as a boost converter in the discharging mode. The other dc converter is ELC made of a chopper connected to a resistive load.

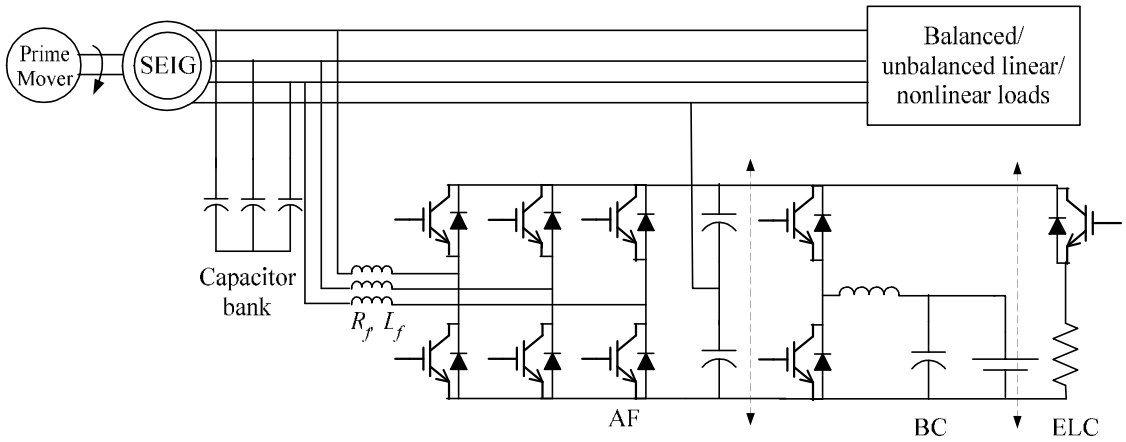


***Fig. 3.30 AF-BC-ELC based regulating scheme for three-phase four-wire load***

## 3.7 CONCLUSIONS

Different regulating schemes of the SEIG to obtain the improved voltage and frequency profile for feeding various loads have been classified in detail. These schemes are primarily classified as voltage, frequency and voltage-frequency regulating schemes.

Depending upon the shunt or series connections, voltage regulating schemes have been classified as classical, switching device based and converter based VR schemes. The schemes resulting improved frequency profile through effective active power control have been discussed in brief. The schemes capable of resulting voltage and frequency control have also been detailed for three phase four wire or during unbalanced conditions. The changes in the configurations from classical to latest converter based VR schemes are also highlighted. Following conclusions are drawn from this study.

- The saturable core reactor is the best among the classical shunt scheme from view point of the stability, the reliability and the cost for feeding linear loads.

- Among solid state switching device based shunt compensation schemes, the SVC based VR scheme is suited to supply sensitive loads. In this VR scheme, the TCR branch can be eliminated and an effective control can be achieved with only TSC.

- Among the converter based shunt compensation VR schemes, the voltage source converter based STATCOM is best suited due to the fast and an effective control. It can also supply the nonlinear unbalanced loads. The STATCOM acts as a voltage regulator, a harmonic eliminator, a load balancer and a neutral current compensator.

- For the effective series compensation, the short shunt SEIG is good option to supply static loads whereas the SSSC based scheme is effective to supply sensitive loads.

- Scheme employing shunt active filter (AF), bidirectional current battery converter (BC) and electronic load controller (ELC) is the most generalized arrangement for voltage-frequency control.

It is hoped that this study is helpful in developing the regulating schemes suited for various industrial applications of the SEIG feeding dynamic and non-linear loads.

# CHAPTER-IV

# STEADY STATE AND TRANSIENT ANALYSIS OF THREE-PHASE SEIG

## 4.1 GENERAL

The performance of SEIG is studied for supplying various linear and non-linear loads. This study helps to understand SEIG behavior and strengthen the concepts needed for the work on the static controllers for SEIG. The steady state analysis [16-42] is useful for estimating the performance indices, ensuring good quality power and identifying the suitable configuration for a particular application. The over-current, over-voltage, large electromagnetic torque etc. resulted in under various transient conditions during balanced and unbalanced operation can be accurately estimated by transient analysis [53-62]. The transient state analysis helps in assessing the suitability of winding, insulation level and capacitor rating etc.

This chapter presents the steady state and transient state analysis of SEIG feeding various types of loads. The steady state equivalent circuit of SEIG is used to formulate the voltage regulation as an optimization problem. The genetic algorithm, a global search and optimization method is used to obtain the optimum combination of capacitance and speed for optimum voltage regulation. The performance is studied for feeding resistive and resistive-inductive loads for optimum voltage regulation. The simulated results are validated experimentally for rated synchronous speed. The steady state performance of SEIG feeding an induction motor load is also analyzed through simulation and experimental investigations.

The transient performance of SEIG is investigated for feeding linear (static and induction motor) and non-linear (uncontrolled rectifier fed resistive and resistive-capacitive) loads. The SEIG is modeled in q-d axis with currents and voltages as state variables in stationary reference frame, considering the effects of main and cross flux saturation. The linear loads are represented in q-d variables, whereas the non-linear loads are modeled in phase variables. The transient performance is studied for various loading conditions for both linear and non-linear loads. The THD and harmonic spectrum are used for assessing the quality of voltage and current of generator and load.

## 4.2 STEADY STATE ANALYSIS OF SEIG FEEDING STATIC LOADS

The following assumptions are made to develop steady state equivalent circuit to analyze the steady state performance of SEIG feeding static and induction motor loads.

- The core loss of the machine is neglected.
- The magnetic saturation affects only the magnetizing reactance.
- The effect of frequency and temperature on the resistance is ignored.
- The effect of MMF space and time harmonics in induced voltage is neglected.

The steady state equivalent circuit of SEIG with static load is shown in Fig. 4.1. This equivalent circuit is used to obtain the speed ($v$) and the shunt capacitance ($C_{sh}$) for optimum voltage regulation.

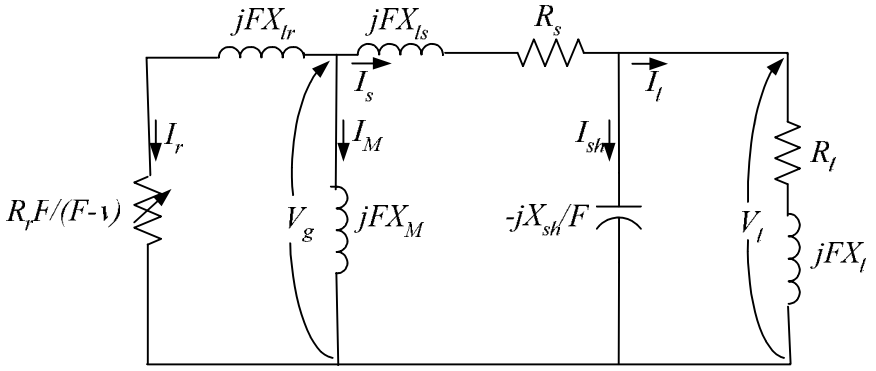


***Fig. 4.1 Equivalent circuit of SEIG with resistive-inductive load***

In the equivalent circuit, only the magnetizing reactance $X_M$ and frequency $F$ are unknown. After calculating the $X_m$ and $F$, the performance parameters like stator current $I_s$, load voltage $V_l$ (also equals to SEIG terminal voltage $V_s$) and load current $I_l$ are obtained as,

$$I_s = \frac{V_g}{(Z_s + Z_{hl})} \tag{4.1}$$

$$V_s = V_l = V_g - Z_s I_s \tag{4.2}$$

$$I_l = \frac{Z_{sh}}{(Z_{sh} + Z_l)} I_s \tag{4.3}$$

where, the $Z_r$, $Z_m$, $Z_s$, $Z_{sh}$, $Z_l$ and $Z_{hl}$ are expressed as,

$$Z_r = \frac{R_r F}{(F - \nu)} + jFX_{lr} \tag{4.4}$$

$$Z_M = jFX_M \tag{4.5}$$

$$Z_s = R_s + jFX_{ls} \tag{4.6}$$

$$Z_{sh} = -j\frac{X_{sh}}{F} \tag{4.7}$$

$$Z_l = R_l + jFX_l \tag{4.8}$$

$$Z_{hl} = \frac{Z_{sh} Z_l}{(Z_{sh} + Z_l)} \tag{4.9}$$

## 4.3 VOLTAGE REGULATION OPTIMIZATION FOR SEIG FED STATIC LOADS USING GENETIC ALGORITHM

The voltage regulation optimization for SEIG feeding static loads using GA is attempted to obtain the shunt capacitance and speed and is explained briefly from the following stages,

- Problem formulation
- Genetic algorithm approach
- Voltage regulation optimization algorithm

The algorithm to evaluate steady state performance for given shunt capacitance and speed is discussed separately in this section.

### 4.3.1 Problem Formulation

The formulation of voltage regulation optimization problem is detailed herewith using objective function defining the voltage regulation characteristic, equality and inequality constraints, bound on variables as follows,

#### *4.3.1.1 Objective Function*

The rated output of SEIG is represented into number of load points *npr*. The SEIG is loaded in steps. Therefore, *n*=0 corresponds to no load and *n*=*npr* corresponds to rated

load. The objective function is defined as the summation of squares of mismatch between load voltage and rated voltage for all the load points *npr* and written as,

$$f_{obj}(C_{sh},\nu)=\sum_{n=1}^{npr}\left(\frac{V_{l_n}(C_{sh},\nu)-V_r}{V_r}\right)^2 \tag{4.10}$$

The objective function is subjected to following bound on variables, equality and inequality constraints

### *4.3.1.2 Equality constraints*

Under the self-excitation in the steady state equivalent circuit, the loop impedance must be equal to zero. The real and imaginary part of loop impedance $Z_{LS}$ for all feasible load points in the loading range form the equality constraints for the problem and are expressed as,

$$Z_{LS}=\frac{Z_rZ_M}{(Z_r+Z_M)}+Z_s+\frac{Z_{sh}Z_l}{(Z_{sh}+Z_l)}=0 \tag{4.11}$$

where,

$$Z_{LSn}=G_{Sn}(C_{sh},\nu)+jH_{Sn}(C_{sh},\nu)$$

The eqn. (4.11) results into,

$$\left.\begin{aligned}G_{Sn}&=0\\H_{Sn}&=0\end{aligned}\right\}\quad \text{for } n=1:npr \tag{4.12}$$

The coefficients of polynomial $G_S$ and $H_S$ are expressed in Appendix-C.

### *4.3.1.3 Inequality constraints*

The inequality constraints are related to performance constraint and at $n^{th}$ load point, these are expressed as,

$$\left.\begin{aligned}X_M^{mn}&\le X_{M_n}\le X_M^{mx}\\F^{mn}&\le F_n\le F^{mx}\\V_s^{mn}&\le V_{s_n}\le V_s^{mx}\\I_{s_n}&\le I_s^{mx}\end{aligned}\right\}\quad \text{for } n=1:npr \tag{4.13}$$

#### *4.3.1.4 Bound on variables*

The self excitation in SEIG is possible for a limited range of $C_{sh}$ at a given prime mover speed ν. The $C_{sh}^{mn}$ is the minimum capacitance required to have rated terminal voltage at no load for $v^{mx}$, whereas the $C_{sh}^{mx}$ is the maximum capacitance required for rated terminal voltage at full load for $v^{mn}$. The $v^{mn}$ and $v^{mx}$ are considered as 0.8 pu and 1.2 pu respectively.

$$\begin{aligned} C_{sh}^{mn} \le C_{sh} \le C_{sh}^{mx} \\ v^{mn} \le \nu \le v^{mx} \end{aligned} \tag{4.14}$$

### 4.3.2 Genetic Algorithm Approach

The genetic algorithm (GA) mimics the principle of natural selection and natural genetics to constitute the search and optimization [270-273]. The GA is fundamentally different from classical optimization approach and is effective parallel global search method, which does not require good initial estimate of variables. The binary formulation of GAs is popular which works on the binary strings of variables. Normally, the GAs consists of following stages,

- Generation of initial population randomly
- Probabilistically selection of solution strings for mating pool
- Manipulation of strings on probability basis using
  - Crossover
  - Mutation
- Fitness calculation
- Termination criterion and
- Updating the mating pool for next generation

The description of theses stages is briefed herewith.

***(a) Initial Population***

The population of binary strings of specified length is generated randomly. When string has all values as 0, it corresponds to minimum value of the variable. Whereas, when string has all values as 1, it corresponds to maximum value of the variable. Therefore, the population will always have variable values between respective minimum and maximum values.

Corresponding to each population string, the objective function and fitness is evaluated.

***(b) Selection***

The function of reproduction operator is to select strings from generation probabilistically to form mating pools to be used by subsequent crossover and mutation operators. The roulette-wheel, Boltzmann and Tournament selection are the common reproduction operator [273]. Elitism can improve the performance of GA rapidly and prevents loosing the best solution [273]. In the elitism process, few best chromosomes are copied to the mating pool.

***(c) Crossover and crossover probability***

After the selection, the population is enriched with better individuals. The crossover operator is applied to generate the better strings. The objective of this operator is to create new strings randomly in search for good solution. The crossover operators can be realized using single, two and multi point crossover; in turn a single point recombination operator is implemented with three steps detailed as follows,

- Two strings are selected randomly from the mating pool.
- Crossover site is selected randomly along the string length.
- Position values are interchanged between two strings after the crossover site.

The crossover rate is the probability of crossover. The crossover rate is calculated by finding out the ratio of the number of pairs to be crossed to fixed population size.

***(d) Mutation and mutation probability***

The mutation operator flips a bit randomly with small mutation probability. The genetic algorithm treats the mutation operator as a secondary search operator after the crossover to further search new string for fine solution. Because of this reason, the mutation probability is kept low.

***(e) Fitness***

The genetic algorithm works on the fitness value of solution string. The selection, rejection of strings for the mating pool, termination criteria etc. are mainly fitness dependent.

***(f) Termination criteria***

A number of criteria are available in the literature for the termination of GA such as fixed number of generation, fixed percentage of stings in the population becoming same, no improvement in the fitness of best individual etc.

***(g) Updating of Mating Pool***

During crossover and mutation, a large number of new offspring are generated. These offspring are added with the existing mating pool, thus resulting into increased size of the population through which the mating pool is created by the *selection* for the next generation.

### 4.3.3 Voltage Regulation Optimization Algorithm

The formulation of voltage regulation optimization as a constraint optimization problem is explained through eqns. (4.10) to (4.14). The GA is used to obtain the optimum values of $C_{sh}$ and ν. The associated equality constraints are solved with Newton-Raphson (NR) method. The GA works with fitness, which is defines as,

$$f = \frac{1}{\left(1 + f_{obj}\right)} \tag{4.15}$$

The main steps of the optimization algorithm are as-

1. Read the SEIG and load parameters; specify GA parameters such as population size *ps*, maximum iterations $itr_{mx}$, maximum iterations for which fitness is not changing $itr_{ncm}$, crossover probability $P_c$ and mutation probability $P_m$, string lengths of each variable $C_{sh}$ and *v*.

2. Specify the limiting values of inequality constraints and the limiting values of variables $C_{sh}$, and ν.

3. Randomly generate the binary strings to form initial population. For each binary string decode the values of $C_{sh}$ and *v*.

4. Set the iteration $itr$=1, $itr_{nc}$=0.

5. Check the feasibility of each string against equality and inequality constraints and evaluate the fitness value for each feasible string using eqn. (4.15) and assign $bestfit = fit^{max}$.

6. Perform selection operation through Roulette-wheel method. Also retain the best fit solution *bestfit* to preserve the elitism.

7. Randomly select the two strings, randomly select the crossover site and perform single point crossover operation by comparing a random number with $P_c$.

8. Perform the mutation operation on each bit of each variable string by comparing a random number with $P_m$.

9. Decoding of the variables string to compute $C_{sh}$ and ν.

10. Check the feasibility of each string against equality and inequality constraints and evaluate the fitness of the newly generated offspring and obtain the best fit.

11. If ($fit^{max} = bestfit$) than $itr_{nc}=itr_{nc}$+1, else $bestfit=fit^{max}$, $itr_{nc}$=0.

12. Check for termination i.e. if ($itr<itr_{mx}$ or $itr_{nc}<itr_{ncm}$) $itr=itr$+1 and go to step 6.

13. Print the optimum solution.

The flow chart depicting the major steps of GA based voltage regulation optimization is shown in Fig. 4.2.

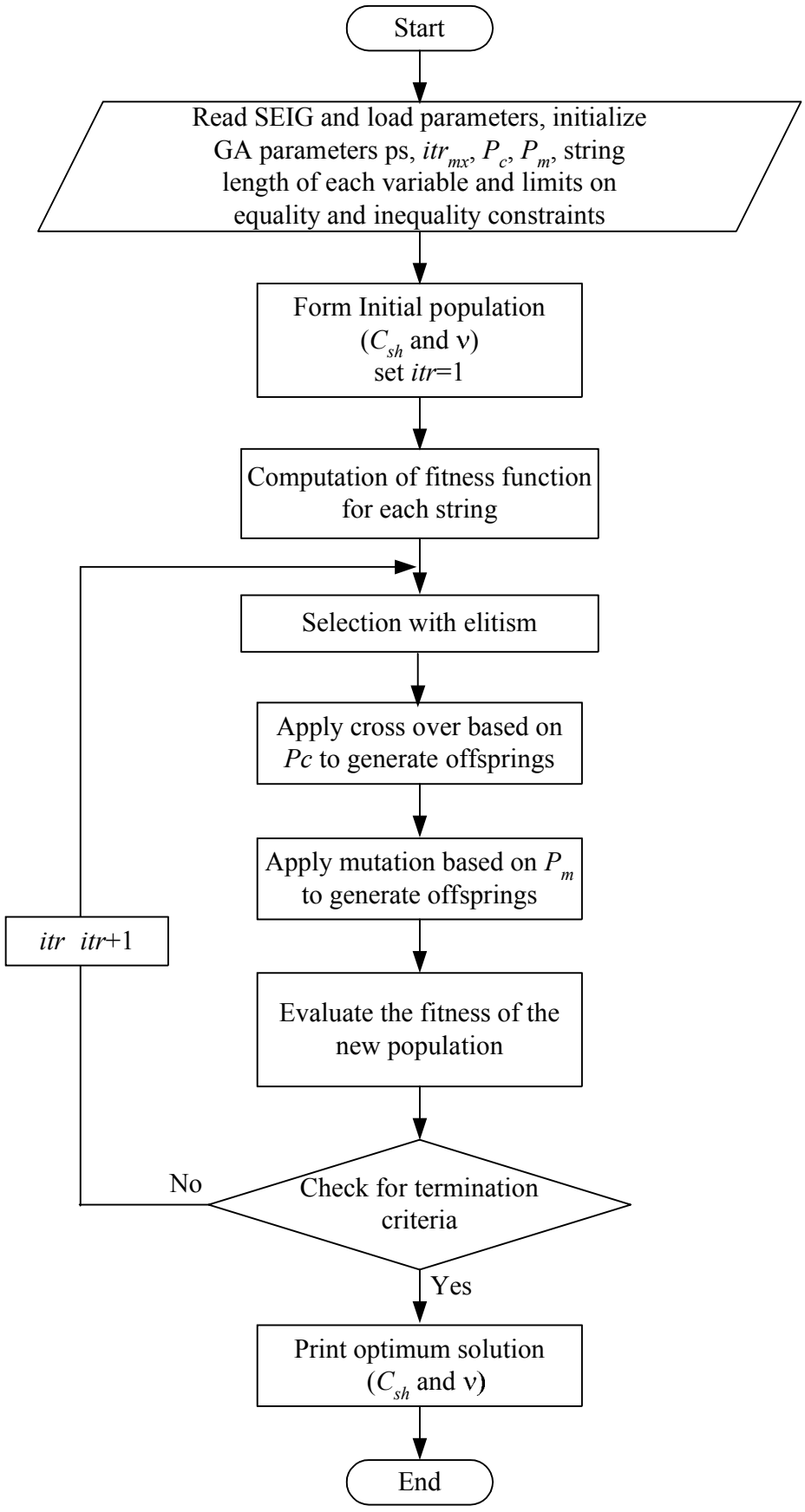


***Fig. 4.2 Flow chart for the GA based voltage regulation optimization algorithm***

### 4.3.4 Algorithm for Simulating Steady State Performance

The main steps of the algorithm for evaluating the steady state performance of SEIG feeding static loads are summarized as follows,

1. Read the SEIG parameters and its magnetizing characteristic, prime mover speed ($v$), shunt capacitance ($C_{sh}$), number of load points to represent rated machine capacity ($npr$).

2. Assign $F_0 = v$, $X_{M0} = X_M^{uns}$ and set convergence limit ($eps$).

3. Initialize the load point counter ($P_l$=1).

4. Compute load resistance and reactance $R_l$ and $X_l$ for given $P_l$.

5. Evaluate polynomial $G_S$ and $H_S$ from the equality constraints of SEIG-static load.

6. Compute $X_M$ and $F$ using NR method.

7. If $(X_M - X_{M0}) > eps$ or $(F - F_0) > eps$ than $F_0 = F$, $X_{M0} = X_M$ and go to step 5.

8. If the limits on $X_M$ and $F$ are violated d than go to step 12.

9. Compute the air gap voltage ($V_g$) and obtain the performance parameter $V_s$, $I_s$, $I_l$ and store them in a data file.

10. If the limits on $V_s$, $I_s$ violated than go to step 12.

11. If $(P_l < npr)$ than $P_l = P_l + 1$ and go to step 4.

12. Plot the required performance parameters from the data file.

The flow chart to simulate the steady state performance of SEIG feeding static load is depicted in Fig. 4.3,

## 4.4 STEADY STATE ANALYSIS OF SEIG FEEDING INDUCTION MOTOR LOAD

For the steady state analysis of SEIG feeding induction motor load, the equivalent circuit of SEIG with induction motor load is developed. Subsequently, the algorithm for simulating the steady state performance is presented.

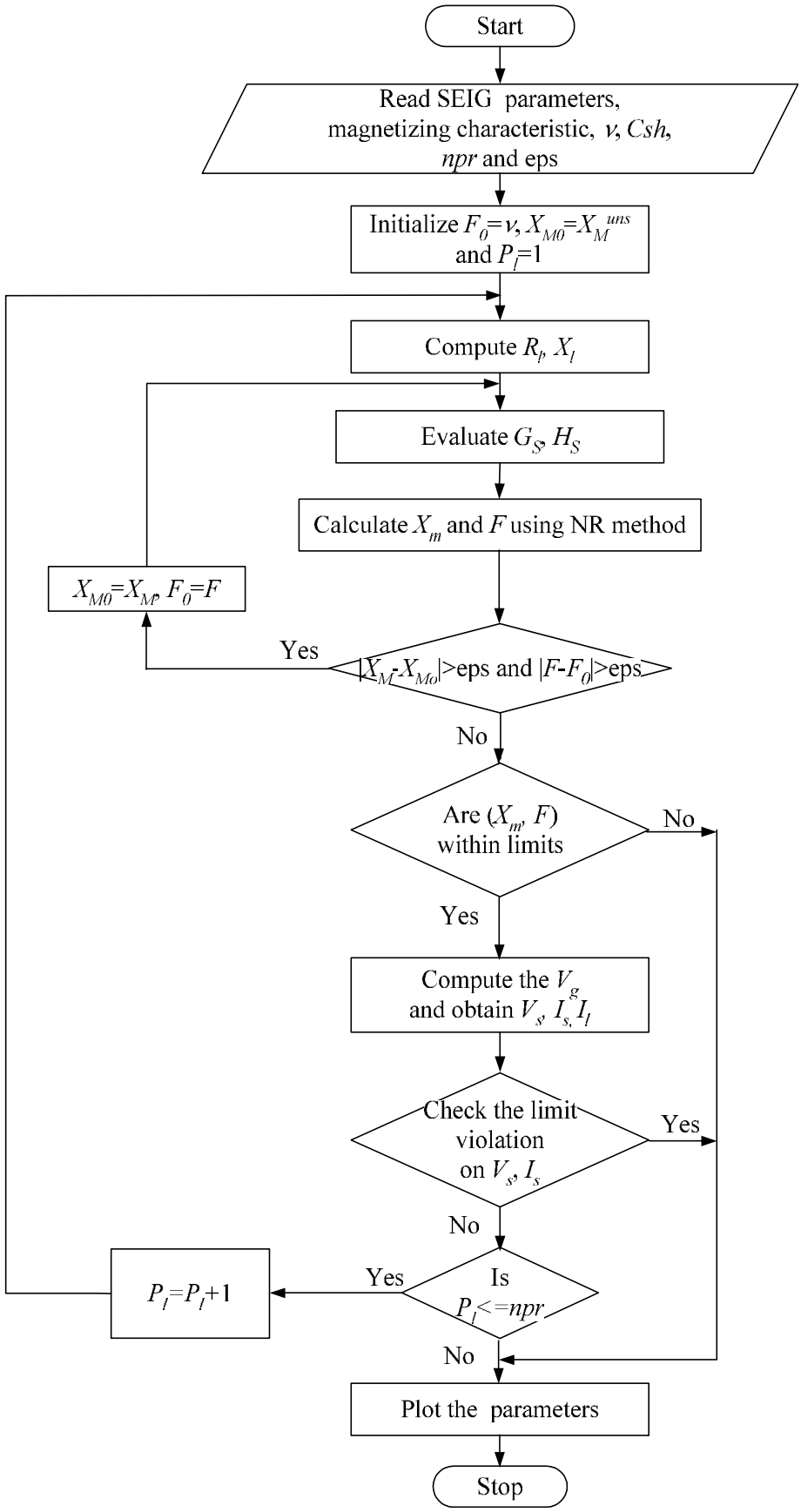


***Fig. 4.3 Flow chart for steady state performance of SEIG feeding static load***

### 4.4.1 Equivalent Circuit of SEIG with Induction Motor Load

With the assumptions stated in section 4.2, the equivalent circuit of SEIG with induction motor (IM) load, as shown in Fig. 4.4, is used for estimating the steady state performance of SEIG-IM load system.

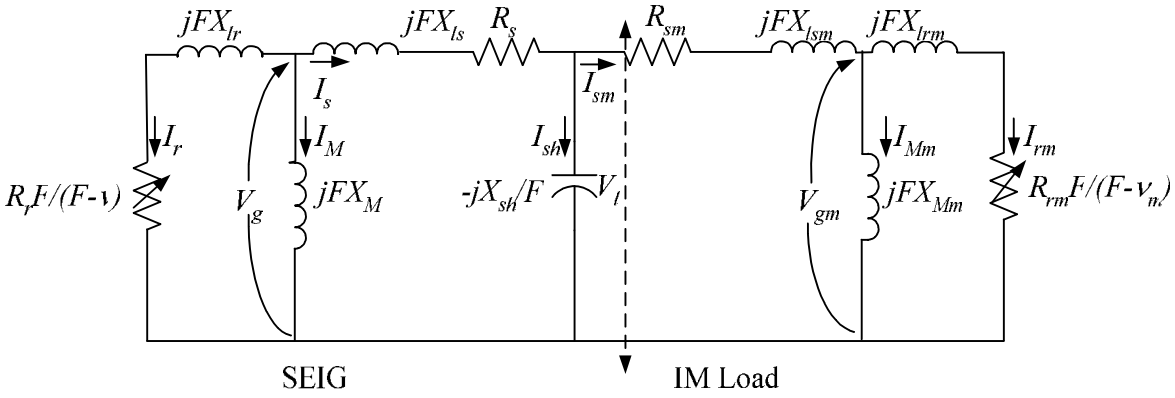


***Fig. 4.4 Equivalent circuit of SEIG with motor load***

The performance of SEIG-motor system is computed using the two steps as,

- Calculation of motor speed $\nu_m$ for given output power.
- Representation of the induction motor equivalent by R-L equivalent.

#### *4.4.1.1 Calculation of motor speed for specified output power and input voltage*

For a specified output power $P_0$, the speed can be calculated by converting the SEIG-motor circuit into the Thevenin equivalent across the load resistance, as shown in Fig. 4.5.

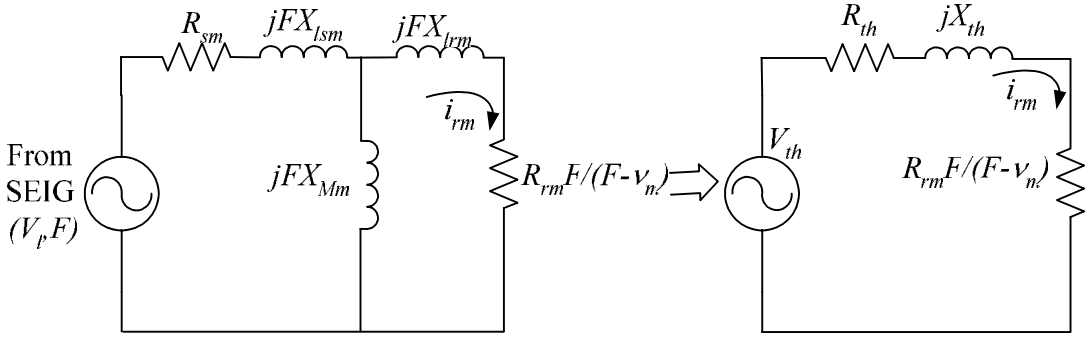


***Fig. 4.5 Thevenin equivalent across load resistance***

$$i_{rm} = \frac{V_{th}}{\left(R_{th} + \frac{R_{rm}F}{(F - \nu_m)}\right) + jX_{th}} \tag{4.16}$$

$$P_0 = i_{rm}^2 R_{rm} \frac{\nu_m}{\left(F - \nu_m\right)} \tag{4.17}$$

$$A\nu_m^2 + B\nu_m + C = 0 \tag{4.18}$$

where, $A$, $B$ and $C$ are expressed as,

$$\begin{aligned} A &= R_{th}^2 + X_{th}^2 + \frac{V_{th}^2 R_{rm}}{P_0} \\ B &= -\left\{2\left(R_{th} + R_{rm}\right)R_{th} + 2X_{th}^2 + \frac{V_{th}^2 R_{rm}}{P_0}\right\}F \\ C &= \left(R_{th} + R_{rm}\right)^2 F^2 + X_{th}^2 F^2 \end{aligned} \tag{4.19}$$

The solution of quadratic eqn. (4.18) gives two values of motor speed. The appropriate feasible value of the motor speed is selected for motoring mode operation.

#### *4.4.1.2 Representing induction motor as a R-L equivalent*

The total impedance offered by induction motor load has equivalent resistance and reactance ($R_{le}$, $X_{le}$), as shown in Fig. 4.6. After transforming the motor equivalent circuit, the overall SEIG-motor equivalent circuit is identical to SEIG-static R-L load equivalent circuit.

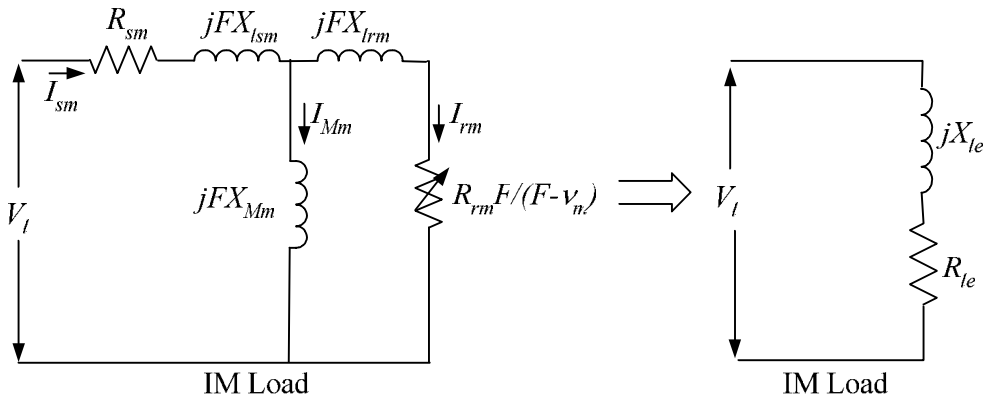


***Fig. 4.6 Transformation of steady state equivalent circuit of induction motor load to equivalent R-L load***

The induction motor rotor, magnetizing and stator impedances are $Z_{rm}$, $Z_{Mm}$ and $Z_{sm}$ respectively and expressed as,

$$Z_{rm} = \frac{R_{rm}F}{(F - \nu_m)} + jFX_{lrm} \tag{4.20}$$

$$Z_{Mm} = jFX_{Mm} \tag{4.21}$$

$$Z_{sm} = R_{sm} + jFX_{lsm} \tag{4.22}$$

The total impedance offered by induction motor load is calculated as,

$$Z_{lm} = Z_{sm} + \frac{Z_{Mm}Z_{rm}}{Z_{Mm} + Z_{rm}} \tag{4.23}$$

The generator current, motor terminal voltage ($V_l$) and current ($I_{sm}$) are obtained using eqn. (4.1) to eqn. (4.3).

### 4.4.2 Algorithm for Steady State Performance of SEIG Feeding Induction Motor Load

The main steps of the algorithm to simulate the steady state SEIG performance feeding IM load are described as follows. Correspondingly, the flow chart is depicted in Fig. 4.7.

1. Read the SEIG and induction motor parameters and their magnetizing characteristics, prime mover speed ($v$), shunt capacitance ($C_{sh}$), number of load points in the rated machine capacity ($npr$). Also transform the motor load parameter to the SEIG base value.

2. Assign $F_0 = v$, $X_{M0} = X_M^{uns}$, $X_{Mm0} = X_{Mm}^{uns}$, $V_{l0} = V_l = 1.0$ pu, and set convergence limit ($eps$).

3. Initialize the load point counter ($P_l$=1).

4. Compute the motor speed ($v_m$) for given output power.

5. Obtain $V_{gm}$ from the induction motor equivalent circuit.

6. Compute $X_{Mm}$ from the motor magnetizing characteristic.

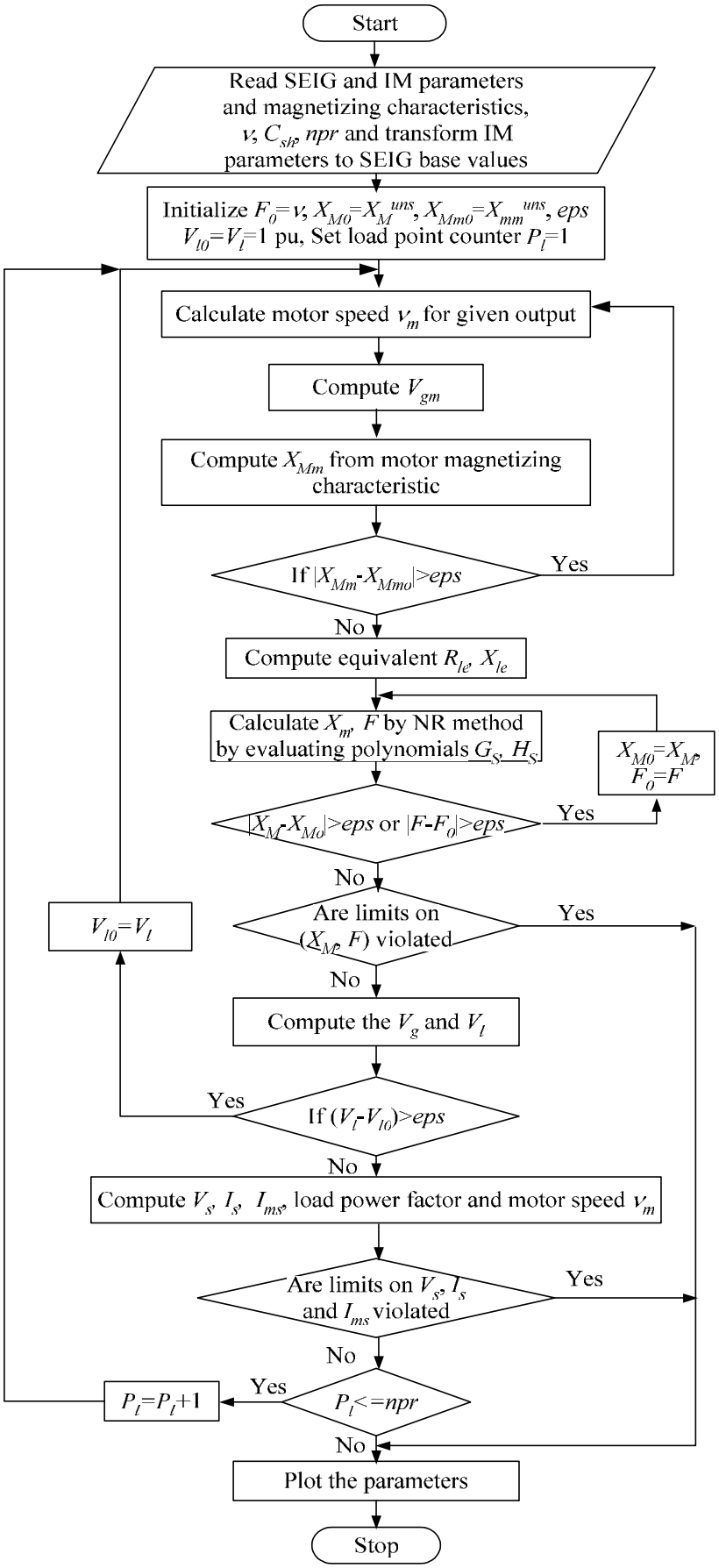


***Fig. 4.7 Flow chart for simulating steady state performance of SEIG with IM load***

7. If ($X_{Mm}$-$X_{Mm0}$) >*eps*, than go to step 4.

8. Compute equivalent resistance and reactance $R_{le}$ and $X_{le}$ from motor equivalent circuit.

9. Evaluate polynomial $G_S$ and $H_S$ from the equality constraints of SEIG-induction motor circuit and calculate $X_M$ and $F$ using NR method.

10. If ($X_M$-$X_{m0}$) <*eps* or ($F$-$F_0$) <*eps*, than $X_{M0}$=$X_M$ and $F_0$=$F$ and go to step 9.

11. If the limits on $X_M$ and $F$ violated, than go to step 17.

12. Compute the air gap voltage $V_g$ and $V_l$.

13. If ($V_l$-$V_{l0}$) >*eps* than $V_{l0}$=$V_l$ and go to step 4.

14. Obtain the performance parameter $V_s$, $I_s$, $I_{sm}$, $v_m$, motor power factor (*pf*) and store them in a data file.

15. If the limits on $V_s$, $I_s$, $I_{sm}$ violated than go to step 17.

16. If ($P_l$ <*npr*) than $P_l$=$P_l$+1 and go to step 4.

17. Plot the parameters.

## 4.5 TRANSIENT PERFORMANCE OF SEIG WITH LINEAR AND NON-LINEAR LOADS

The star connected induction machine driven by constant speed prime mover with suitable star connected capacitor bank is operated as a self-excited induction generator. Correspondingly, the schematic of SEIG feeding linear and non-linear load is shown in Fig. 4.8. The transient performance is studied for SEIG feeding linear static R-L and induction motor loads. The transient performance is also studied for SEIG feeding various non-linear loads.

Fig. 4.9 shows the SEIG-IM equivalent circuit representation for q and d axis in stationary reference frame. The stator and rotor side circuits for both SEIG and IM are represented separately for q-axis and d-axis with SEIG stator voltage $\left[v_s\right]=\left[v_{qs} \quad v_{ds}\right]^T$,

SEIG stator current $[i_s]=[i_{qs} \quad i_{ds}]^T$, motor stator current $[i_{sm}]=[i_{qsm} \quad i_{dsm}]^T$, shorted SEIG rotor current $[i_r]=[i_{qr} \quad i_{dr}]^T$ and shorted motor rotor current $[i_{rm}]=[i_{qrm} \quad i_{drm}]^T$. Various three-wire and four-wire non-linear loads such as three-wire uncontrolled rectifier fed resistive load, three-wire uncontrolled rectifier fed resistive-capacitive load and four-wire uncontrolled rectifier fed resistive-capacitive load are considered for transient performance analysis. These non-linear loads are shown in Fig. 4.10.

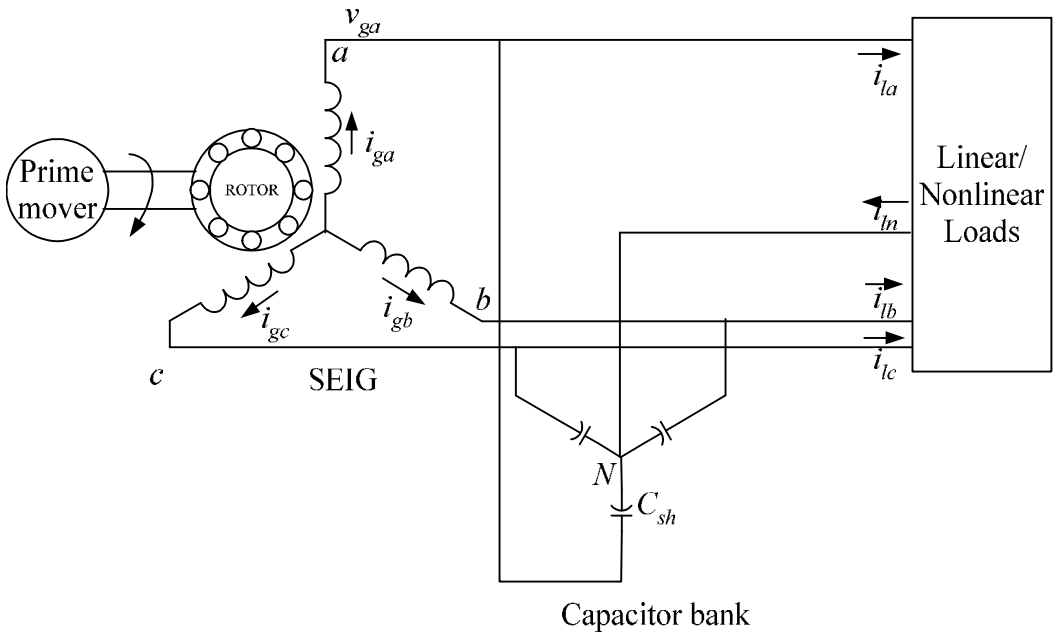


***Fig. 4.8 Schematic of SEIG feeding linear and non-linear loads***

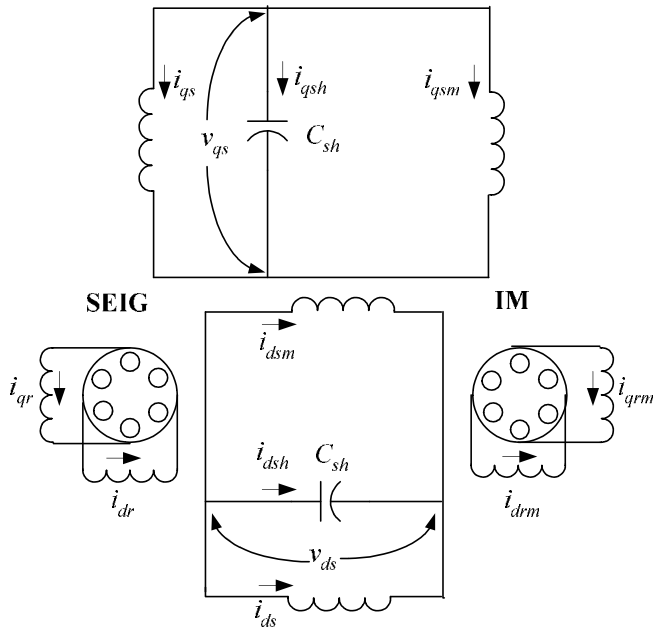


***Fig. 4.9 SEIG-induction motor representation in q-d axis stationary reference frame***

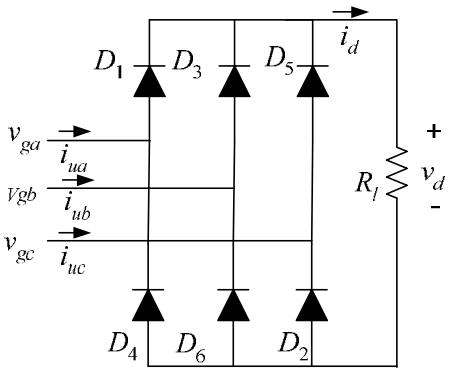


*Fig. 4.10a Three-wire uncontrolled rectifier fed resistive load*

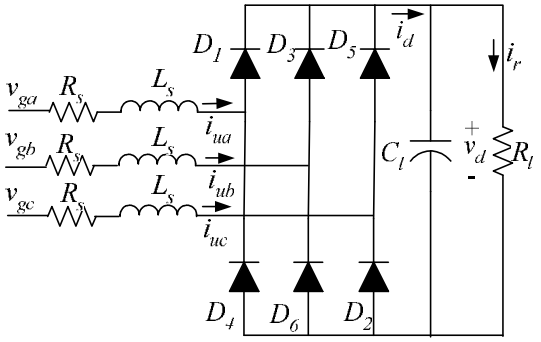


*Fig. 4.10b Three-wire uncontrolled rectifier fed resistive-capacitive load*

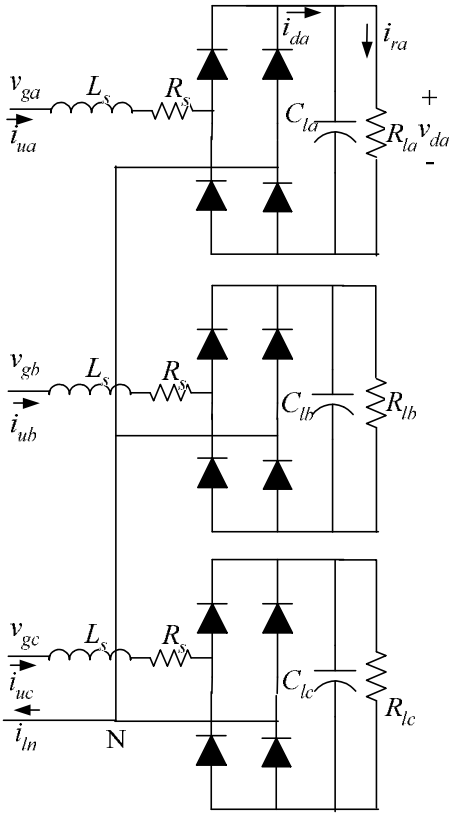


*Fig. 4.10c Four wire uncontrolled rectifier fed resistive-capacitive load*

***Fig. 4.10 Various loads on studied three-phase four-wire SEIG system***

The transient performance of SEIG feeding linear and non-linear loads is studied by developing the dynamic model of the system. The induction generator model is developed in q-d variables in stationary reference frame with currents and voltages as state variables, considering the effect of main and cross flux saturation. The linear loads are modeled in q-d variables, whereas the non-linear loads are modeled in phase variables. The dynamic model of system consists of differential equations for induction machine operated as SEIG, shunt capacitance and linear and non-linear load equations.

### 4.5.1 SEIG Model

The dynamic model of 3-ϕ SEIG is developed is stationary q-d reference frame. The q-d axis voltage equations of induction machine are expressed as,

$$[\mathbf{v}] = [\mathbf{R}][\mathbf{i}] + [\mathbf{L}]p[\mathbf{i}] + [\mathbf{G}][\mathbf{i}] \tag{4.24}$$

where, $[\mathbf{v}]$, $[\mathbf{i}]$ are expressed as,

$$[\mathbf{v}] = \begin{bmatrix} v_{qs} & v_{ds} & v_{qr} & v_{dr} \end{bmatrix}^T$$

$$[\mathbf{i}] = \begin{bmatrix} i_{qs} & i_{ds} & i_{qr} & i_{dr} \end{bmatrix}^T$$

The matrix $[\mathbf{R}]$, $[\mathbf{L}]$ and $[\mathbf{G}]$ are defined in Appendix-B.

The prime mover torque ($T_P$) is related to electromagnetic torque ($T_{em}$) as follows,

$$T_P = T_{em} + \frac{2J}{P} p\omega_r \tag{4.25}$$

where,

$$T_{em} = \frac{3P}{4} L_M \left( i_{qs} i_{dr} - i_{ds} i_{qr} \right) \tag{4.26}$$

The eqn. (4.24) and eqn. (4.25) while written in state space form results a set of five differential equations corresponding to variables $i_{qs}$, $i_{ds}$, $i_{qr}$, $i_{dr}$ and $\omega_r$ as,

$$p[\mathbf{i}] = [\mathbf{L}]^{-1} \left( [\mathbf{v}] - [\mathbf{R}][\mathbf{i}] - [\mathbf{G}][\mathbf{i}] \right) \tag{4.27}$$

$$p\omega_r = \frac{P}{2J} \left( T_P - T_{em} \right) \tag{4.28}$$

For SEIG, the air gap voltage does not remain constant and therefore the magnetizing reactance also varies accordingly. For the purpose, the magnetizing current is calculated as,

$$I_M = \sqrt{\left(i_{qs} + i_{qr}\right)^2 + \left(i_{ds} + i_{dr}\right)^2} \tag{4.29}$$

where, $i_{qs}$, $i_{qr}$ and $i_{ds}$, $i_{dr}$ are stator, rotor q and d axis currents respectively.

The current $\left[\mathbf{i}_{sh}\right]$ through the shunt capacitance $C_{sh}$ governs the generated voltage of SEIG. The current through the shunt capacitance is written as,

$$\left[\mathbf{i}_{sh}\right] = -\left[\mathbf{i}_s\right] - \left[\mathbf{i}_l\right] \tag{4.30}$$

The shunt capacitance voltage equations in state space form are expressed as,

$$p\left[\mathbf{v}_s\right] = \frac{\left[\mathbf{i}_{sh}\right]}{C_{sh}} \tag{4.31}$$

where, $\left[\mathbf{v}_s\right] = \begin{bmatrix} v_{qs} & v_{ds} \end{bmatrix}^T$, $\left[\mathbf{i}_s\right] = \begin{bmatrix} i_{qs} & i_{ds} \end{bmatrix}^T$, $\left[\mathbf{i}_{sh}\right] = \begin{bmatrix} i_{qsh} & i_{dsh} \end{bmatrix}^T$

For motor load, $\left[\mathbf{i}_l\right] = \begin{bmatrix} i_{qsm} & i_{dsm} \end{bmatrix}^T$

### 4.5.2 Linear Load Model

The SEIG performance is studied for static R-L load and induction motor load. The dynamic equations for these loads are obtained in q-d axis with currents as variables.

#### *4.5.2.1 Static R-L Load*

The dynamic model equations for static R-L load is governed by two differential equations corresponding to inductor current as,

$$p\left[\mathbf{i}_l\right] = \frac{1}{L_l}\left(\left[\mathbf{v}_s\right] - R_l\left[\mathbf{i}_l\right]\right) \tag{4.32}$$

#### *4.5.2.2 Induction Motor Load*

The 3-ϕ cage induction motor is considered as the dynamic load. The equations of induction motor load in stationary q-d reference frame are similar to induction generator

discussed in the section 4.5.1 and described by five differential equations with parameters pertaining to induction motor load. These equations are rewritten in state space form as,

$$p[\mathbf{i}_m] = [\mathbf{L}_m]^{-1}\left([\mathbf{v}_m] - [\mathbf{r}_m][\mathbf{i}_m] - [\mathbf{G}_m][\mathbf{i}_m]\right) \tag{4.33}$$

$$p\omega_{rm} = \frac{P_m}{2J_m}\left(T_{emm} - T_L\right) \tag{4.34}$$

The load current $[i_l]$ for motor load is expressed as,

$$[i_l] = \begin{bmatrix} i_{qsm} & i_{dsm} \end{bmatrix}^T$$

### 4.5.3 Non-linear load Model

As mentioned, the study has been carried out for the following non-linear loads,

- Three-wire uncontrolled rectifier feeding resistive load
- Three-wire uncontrolled rectifier feeding resistive-capacitive load
- Four-wire uncontrolled rectifier feeding resistive-capacitive load

The dynamic equations for these loads are deduced as follows,

#### *4.5.3.1 Three-Phase Uncontrolled Rectifier Fed Resistive Load*

The schematic of the three-wire uncontrolled rectifier feeding resistive load is shown in Fig. 4.10(a). In the three-wire uncontrolled rectifiers, the maximum line to line voltage is applied to the load resistance $R_l$ at all time instant.

Let $s_1$ and $s_{11}$ are the conducting function of '*a*' phase. The $s_1$ can have value either 1, when $v_{ga}$ is maximum of ($v_{ga}$, $v_{gb}$, $v_{gc}$), or 0. Similarly, $s_{11}$ can have the value either -1, when $v_{ga}$ is minimum of ($v_{ga}$, $v_{gb}$, $v_{gc}$), or 0. Similarly ($s_2$, $s_{22}$) and ($s_3$, $s_{33}$), the conducting functions for '*b*' and '*c*' phase are obtained.

$$\begin{aligned} v_{s1} &= s_1 v_{ga} + s_2 v_{gb} + s_3 v_{gc} \\ v_{s2} &= s_{11} v_{ga} + s_{22} v_{gb} + s_{33} v_{gc} \end{aligned} \tag{4.35}$$

The load voltage $v_s$ is calculated as,

$$v_s = v_{s1} - v_{s2} \tag{4.36}$$

For this load, $v_s$ is always be equal to $v_d$ and the DC side current is expressed as,

$$i_d = \frac{v_d}{R_l} \tag{4.37}$$

The AC side currents ($i_{ua}$, $i_{ub}$, $i_{uc}$) of uncontrolled rectifier are expressed as,

$$\begin{aligned} i_{ua} &= (s_1 + s_{11}) i_d \\ i_{ub} &= (s_2 + s_{22}) i_d \\ i_{uc} &= (s_3 + s_{33}) i_d \end{aligned} \tag{4.38}$$

### *4.5.3.2 Three-Wire Uncontrolled Rectifier Fed R-C Load*

The three-wire uncontrolled rectifier feeding resistive-capacitive load, as shown in Fig. 4.10 (b), is a commonly used practical non-linear load. The capacitor on DC side works as a filter capacitor. The load consists of very small supply resistance and inductance ($R_s$ and $L_s$) on each line, 3-ϕ uncontrolled bridge rectifier, DC side capacitor $C_l$ and resistor $R_l$. The load is operating in two modes; conducting (a segment of maximum line to line voltage is applied to load) and non conducting mode (DC side capacitor discharge).

In conducting mode, the DC side current $i_d$ of the 3-wire uncontrolled rectifier can be written in state space form as,

$$p i_d = \frac{\left(v_s - v_d - 2 i_d R_s\right)}{2 L_s} \tag{4.39}$$

Charging and discharging of capacitor is governed by following equation in conduction mode as,

$$p v_d = \frac{\left(i_d - i_r\right)}{C_l} \tag{4.40}$$

where, $i_r = \frac{v_d}{R_l}$

During non conducting mode, the $i_d$=0, and the eqns. (4.39) and (4.40) are modified accordingly.

The ac side currents ($i_{ua}$, $i_{ub}$, $i_{uc}$) can be calculated from $i_d$ and conducting functions as calculated in eqn. (4.38).

### *4.5.3.3 Four-Wire Uncontrolled Rectifier Fed R-C Load*

The modeling of four-wire uncontrolled rectifier feeding resistive-capacitive load, as shown in Fig. 4.10 (c), is carried out on single phase basis. The $S_a$, $S_b$, $S_c$ are the conducting function of '*a*', '*b*' and '*c*' phase. The model equations governing the behavior for phase '*a*' are explained. Let $v_{sa}$ is the positive value of segment ($v_{ga}$, $-v_{ga}$) and is impressed on the DC side of uncontrolled rectifier. Depends upon conducting segment, $S_a$ has the value 1 or -1.

The DC side current $i_d$ equation in state space form can be written as,

$$pi_{da} = \frac{\left(v_{sa} - v_{da} - R_s i_{da}\right)}{L_s} \tag{4.41}$$

The charging and discharging of load capacitor $C_{la}$ is governed by following equation as,

$$pv_{da} = \frac{\left(i_{da} - i_{ra}\right)}{C_{la}} \tag{4.42}$$

where, $i_{ra} = \frac{v_{da}}{R_{la}}$

During non conducting mode, the $i_{da}$=0, and the eqns. (4.41) and (4.42) are modified accordingly.

The ac side current of uncontrolled rectifier for phase '*a*' can be obtained as,

$$i_{ua} = S_a i_{da} \tag{4.43}$$

Depending upon conducting functions $S_b$, $i_{db}$ and $S_c$, $i_{dc}$ for 'b' and 'c' phase respectively, the $i_{ub}$ and $i_{uc}$ can be obtained as,

$$i_{ub} = S_b i_d \tag{4.44}$$

$$i_{uc} = S_c i_d \tag{4.45}$$

The transient model of SEIG feeding linear and non-linear loads is therefore represented by the state space equations along with important equations from eqn. (4.24) to eqn. (4.45). These equations of system model are solved by fourth order Runge-Kutta

integration method in MATLAB environment. The algorithmic steps are summarized in the following section 4.5.4.

### 4.5.4 Algorithm for Simulating Transient Performance

The flow chart for simulating transient performance of SEIG feeding induction motor load is shown in Fig. 4.11. The main steps of algorithm are as follows,

1. Read the SEIG and induction motor parameters and their magnetizing characteristics, prime mover speed ($v$) and shunt capacitance ($C_{sh}$).
2. Set the various time settings such as incremental step ($\Delta t$), time for motor load connection ($t_{ms}$), time for mechanical loading on motor ($t_{ml}$), total simulation time ($t_T$), load resistance for no load voltage buildup ($R_L$), [$i_{qr}$; $i_{dr}$]=[0.0001;0.0001] for residual magnetism.
3. Calculate $i_M$, $L_M$ and compute matrix [**L**] and [**G**] accounting main and cross flux saturation.
4. If($t<t_{ms}$) than obtain seven derivatives $p$[**i**], $p\omega_r$, $p$[$\mathbf{v}_s$] for no load voltage buildup and go to step 8.
5. Compute $i_{Mm}$, $L_{Mm}$ and Compute matrix [$\mathbf{L}_m$] and [$\mathbf{G}_m$].
6. If ($t<t_{ml}$) than set $T_L$=0 else set value of $T_L$ equals to rated mechanical load.
7. Evaluate twelve derivatives $p$[**i**], $p\omega_r$, $p$[$\mathbf{v}_s$], $p$[$\mathbf{i}_m$], $p\omega_{rm}$ for SEIG feeding motor load.
8. Obtain the instantaneous values of variables $i_{qs}$, $i_{qr}$, $i_{ds}$, $i_{dr}$, $\omega_r$, $v_{sqs}$, $v_{sds}$, $i_{qsm}$, $i_{dsm}$, $i_{qrm}$, $i_{drm}$, and $\omega_{rm}$ from the Runge-Kutta method of integration and transform the required q-d variables into phase variables and store them.
9. If ($t<t_T$) than $t=t+\Delta t$ and go to step 3.
10. Draw the required waveforms from the data file.

The simulation algorithm is modified accordingly for SEIG feeding static or non-linear load.

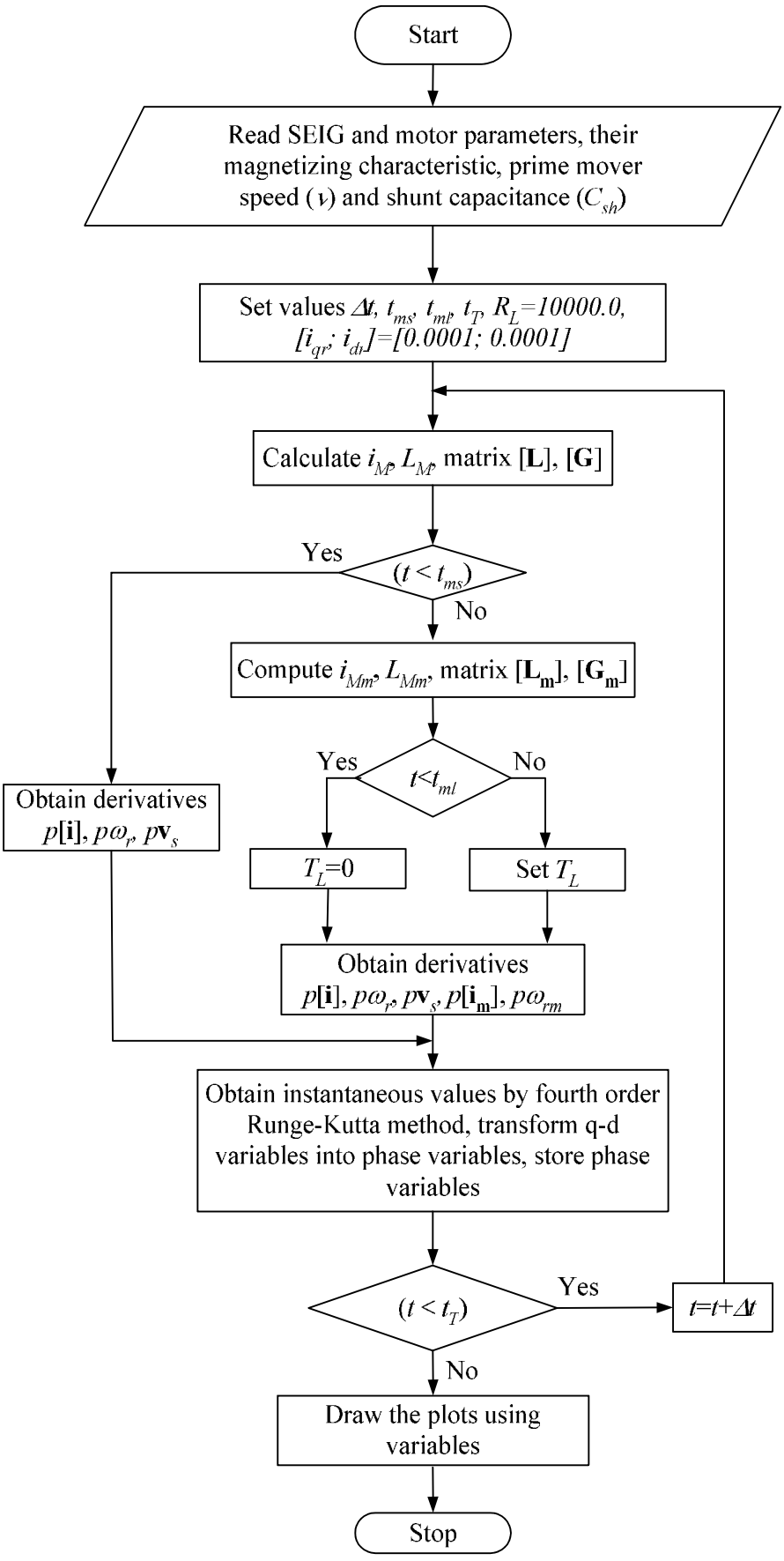


***Fig. 4.11 Flow chart for simulating transient performance of SEIG feeding motor load***

## 4.6 RESULTS AND DISCUSSION

The simulated and experimental steady state performance is investigated on 415V, 5.5 kW, 10.1 A, squirrel cage induction machine, operated as a SEIG. The parameters of induction machine along with magnetizing characteristic are given in Appendix-A. The SEIG is driven by 3-ϕ, 415V, 10 kVA, 0.8 pf, 1500 rpm synchronous motor. The limits on various inequality parameters are summarized in Table 4.1. The lower and upper limits on terminal voltage are relaxed compared to respective limits for resistive load to ensure sufficient loading of SEIG for resistive-inductive load.

***Table 4.1 Limits on various parameters for SEIG fed static loads***

| Parameters | Resistive Load | 0.9 pf, R-L Load |
|---|---|---|
| $X_M$ (pu) | $0.1 < X_M < X_M^{uns}$ | $0.1 < X_M < X_M^{uns}$ |
| $F$ (pu) | $0.95\ v < F < v$ | $0.95\ v < F < v$ |
| $V_s$ (pu) | $0.92 < V_s < 1.08$ | $0.85 < V_s < 1.15$ |
| $I_s$ (pu) | $I_s < 1.1$ | $I_s < 1.1$ |

### 4.6.1 Steady State Performance of SEIG with Static Load

The summary of optimum voltage regulation for feeding resistive load, using GA is shown in Table 4.2. The parameters of GA are summarized in Appendix-D. During the optimization, a large number of solution strings are generated. The solution strings (speed and shunt capacitance) which are having at least 0.5 pu output power are considered for fitness calculation. The results for SEIG fed resistive load are summarized in Table 4.2. The best fitness is achieved at 0.964 pu speed with 21.64 μF shunt capacitance. Whereas, the maximum loading of 0.656 pu is obtained with reduced fitness value for higher shunt capacitance of 35 μF and higher speed of 0.978 pu as compared to best fitness string. The results corresponding to 1.0 pu speed are experimentally validated.

***Table 4.2 Summary of optimum voltage regulation for SEIG fed resistive load***

| $f_1$ | $C_{sh}$ (μF) | $v$ (pu) | $P_l$ (pu) | Remark |
|---|---|---|---|---|
| 0.981582 | 21.64 | 0.964 | 0.513582 | Best Fitness |
| 0.966228 | 35.0 | 0.978 | 0.655953 | Maximum loading |
| 0.958907 | 20.2 | 1.0 | 0.582679 | Experimentally verified |

The steady state performance for optimum voltage regulation of SEIG feeding resistive load is shown in Fig. 4.12 using SEIG stator voltage and current ($V_s$, $I_s$) and load current $I_l$ for $C_{sh}$ as 20.2 μF and $v$ as 1.0 pu speed. At no load condition, the $V_s$ is around 1.08 pu, which gradually decreases with increase in load. At the same time, $I_s$ and $I_l$ are increasing up to 0.58 pu load, beyond which, minimum constraint on $V_l$ is violated.

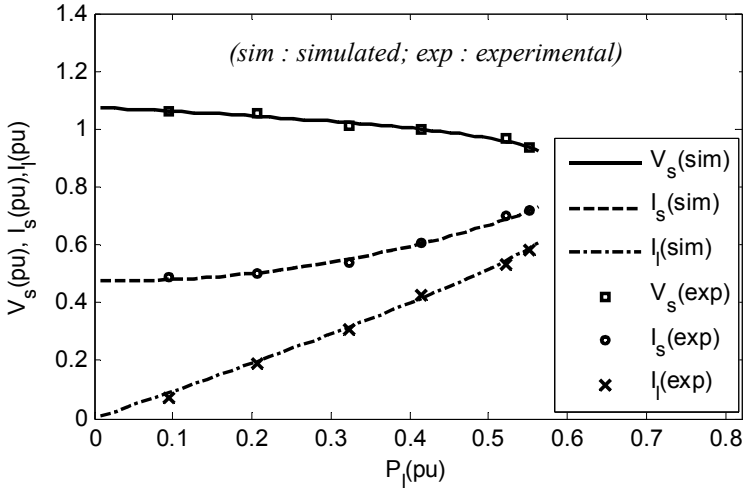


***Fig. 4.12 Steady state performance characteristics for optimum voltage regulation of SEIG feeding resistive load***

The summary of optimum voltage regulation for 0.9 pf resistive-inductive load is shown in Table 4.3. The strings that are resulting atleast 0.3 pu output are considered for optimum voltage regulation. The best fitness is obtained at $C_{sh}$ as 27.5 μF and $v$ as 0.947 pu. The maximum loading occurs with $C_{sh}$ of 33.9 μF and higher $v$ of 0.966 pu with lower fitness value as compared to fittest solution. The results corresponding to 1.0 pu speed are experimentally verified.

***Table 4.3 Summary of optimum voltage regulation for SEIG fed 0.9 pf R-L load***

| $f_1$ | $C_{sh}$ (μF) | $v$ (pu) | $P_l$ (pu) | Remark |
|---|---|---|---|---|
| 0.964994 | 27.50 | 0.947 | 0.300243 | Best fitness |
| 0.88121 | 33.90 | 0.966 | 0.482808 | Maximum loading |
| 0.916426 | 25.4 | 1.0 | 0.327944 | Experimentally verified |

Fig. 4.13 shows the steady state performance for optimum voltage regulation of SEIG feeding 0.9 pf resistive-inductive load for $C_{sh}$ as 25.4 μF and $v$ as 1.0 pu. At no load, $V_s$ is very high and quickly decreasing with increase in load. The current $I_s$ is not

changing much and $I_l$ gradually increasing with increase in load. The lower limit of $V_s$ is violated first, as the load is increasing beyond 0.32 pu. The reduced loading capacity for R-L load is achieved compared to the loading capacity for resistive load.

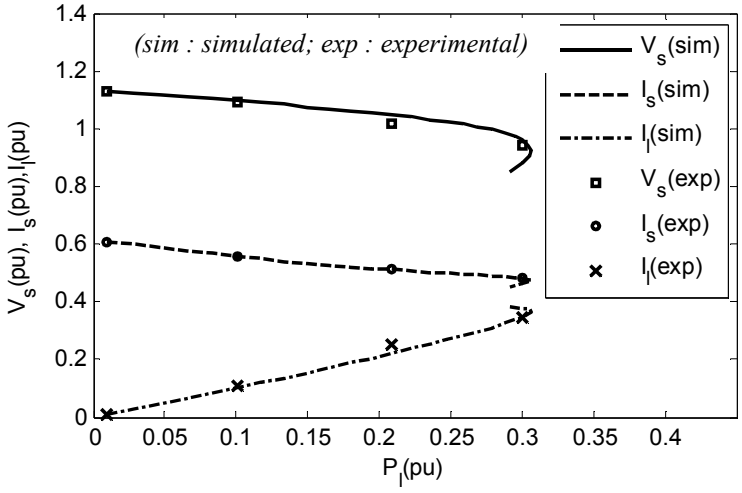


***Fig. 4.13 Steady state performance characteristics for optimum voltage regulation of SEIG feeding 0.9 pf R-L load***

### 4.6.2 Steady State Performance of SEIG with Motor Load

The simulated and experimental steady state performance of SEIG with motor load is investigated on Δ-connected, 415V, 2.2 kW, 4.8A, squirrel cage induction machine operated as a motor load. The parameters of motor load are summarized in Appendix-A. The steady state performance of SEIG feeding induction motor load is studied for two different values of shunt capacitances at $v$ as 1.0 pu. The realistic limits on various parameters, as shown in Table 4.4 are considered for satisfactory SEIG operation.

***Table 4.4 Limits on various parameters for SEIG fed induction motor load***

| Parameters | Motor Load |
|---|---|
| $X_M$ (pu) | $0.1 < X_M < X_M^{uns}$ |
| $F$ (pu) | $0.95\ v < F < v$ |
| $V_s$ (pu) | $0.85 < V_s < 1.15$ |
| $I_s$ (pu) | $I_s < 1.1$ & $I_{sm} < 1.1$ |
| $X_{Mm}$(pu) | $0.1 < X_{Mm} < X_{Mm}^{uns}$ |

The performance of SEIG feeding induction motor load corresponding to $C_{sh}$ as 47 μF is studied using SEIG terminal voltage and current ($V_s$ and $I_s$), induction motor

current $I_{sm}$, induction motor speed $v_m$ and power factor *pf* of induction motor load and shown in Fig. 4.14.

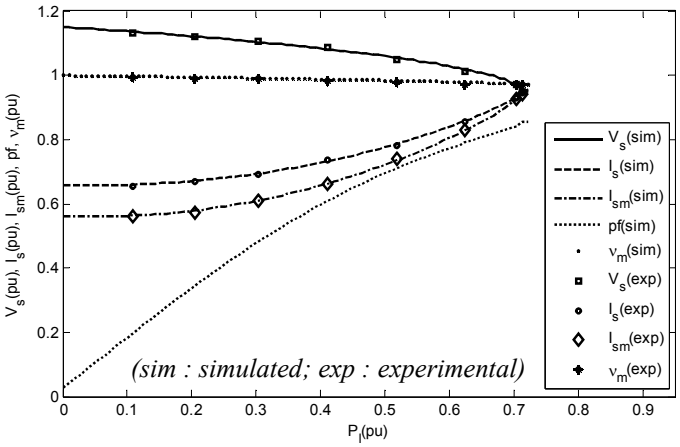


***Fig. 4.14 Steady state performance characteristics of SEIG feeding induction motor load for shunt capacitance of 47 µF***

The motor is suitably loaded with an induction motor-DC generator set. As the loading on motor increases, $V_s$ decreases from limiting 1.15 pu, $I_s$ and $I_{sm}$ increases, speed $v_m$ slowly decreases. The *pf* of an induction motor improves with increase in the load on induction motor. The lower limit on $V_s$ is violated first with increase in loading beyond 0.72 pu.

The performance corresponding to $C_{sh}$ as 39 µF is shown in Fig. 4.15. Due to low value of $C_{sh}$, the $V_s$ at no load is 1.02 pu. As the load on the induction motor is increasing, the $V_s$ decreases and reaches minimum limiting value of 0.85 around 0.35 pu output power. The decrease in the speed is marginal with an increase in loading.

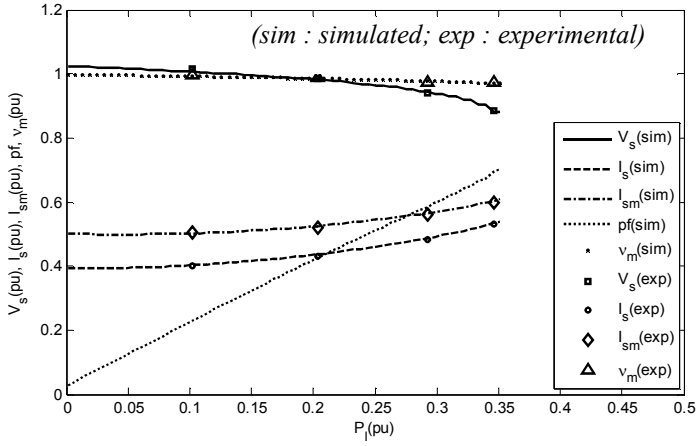


***Fig. 4.15 Steady state performance characteristics of SEIG feeding induction motor load for shunt capacitance of 39 µF***

### 4.6.3 Transient Performance of SEIG with R-L load

The investigations for transient performance are carried out on a 415V, 3.7 kW, 7.6 A, Y-connected squirrel cage induction machine, operating as a SEIG, driven by prime-mover with prime mover torque as $T_P = 6200 - 20\omega_r$ and excited by star connected capacitor bank. The machine parameter are summarized in Appendix-A. The capacitance of 48.3 μF/phase is required to obtain rated no load phase voltage of 239 V (peak phase voltage $V_{pl}$ is 338 V) and line voltage of 415V.

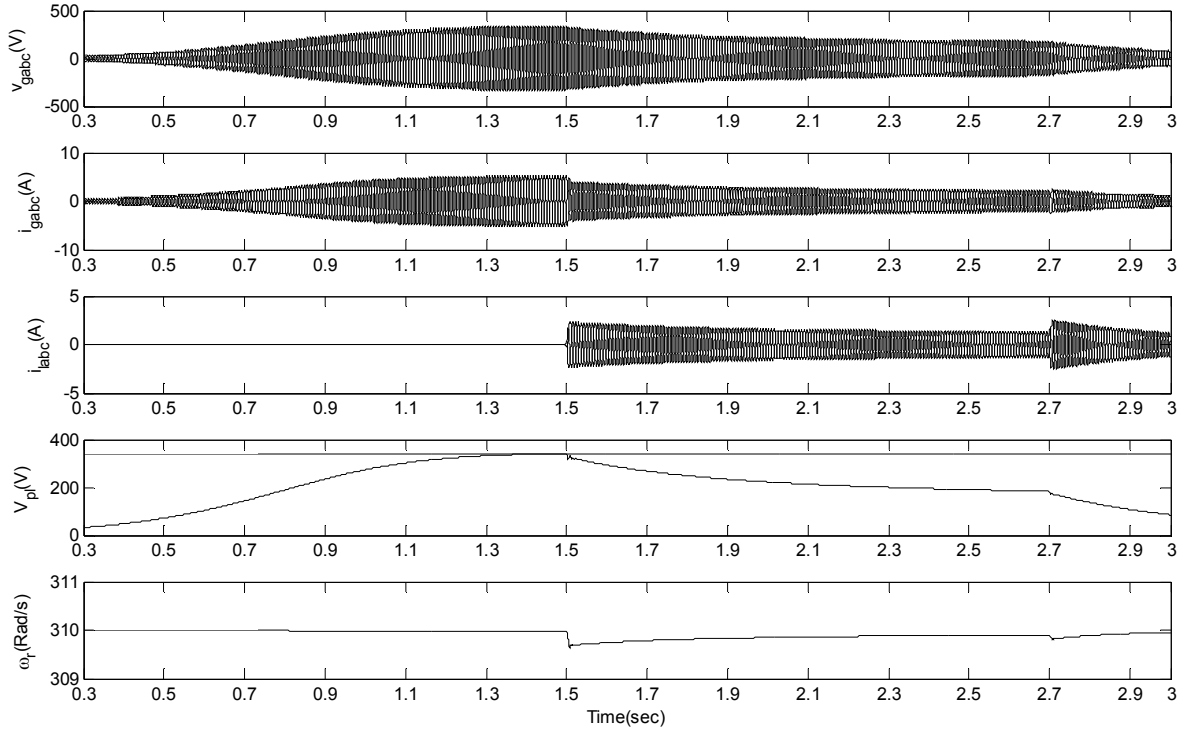


***Fig. 4.16 Transient performance characteristics of SEIG feeding 0.8 pf R-L load (Load conditions : 1.0 kW at 1.5 sec. and 2.0 kW at 2.7 sec.)***

The transient performance characteristics of SEIG feeding 0.8 pf resistive-inductive load are shown in Fig. 4.16 for generator voltages $v_{gabc}$, generator currents $i_{gabc}$, load current $i_{labc}$ and peak load voltage $V_{pl}$, prime mover speed $\omega_r$. The SEIG is suddenly loaded by application of 1 kW, 0.8 pf, load at 1.5 sec., which is resulting into decrease in $v_{gabc}$, $i_{gabc}$, $\omega_r$ and increase in $i_{labc}$. The $V_{pl}$ decreases gradually to around 192 V. With the application of 2.0 kW at 2.7 sec., the generator voltage gradually collapses owing to shortage of VARs for its operation. It is evident that controlled VARs are required to be injected to stabilize the terminal voltage and to maintain good voltage regulation.

### 4.6.4 Transient Performance of SEIG with Motor Load

The transient performance of SEIG feeding motor load is carried out on Δ-connected, 415 V, 1.5 kW, 3.2 A, squirrel cage induction machine operating as a motor load. The parameters of motor load are summarized in Appendix-A. The transient performance of SEIG feeding motor load is explained using generator voltages $v_{gabc}$, generator currents $i_{gabc}$, motor currents $i_{mabc}$, motor electromagnetic torque $T_{emm}$, induction motor speed $\omega_{rm}$, peak load voltage $V_{ps}$ and prime mover speed $\omega_r$. With the connection of load at 1.5 sec., voltage collapses, owing to insufficient reactive VARs provided by the capacitor bank.

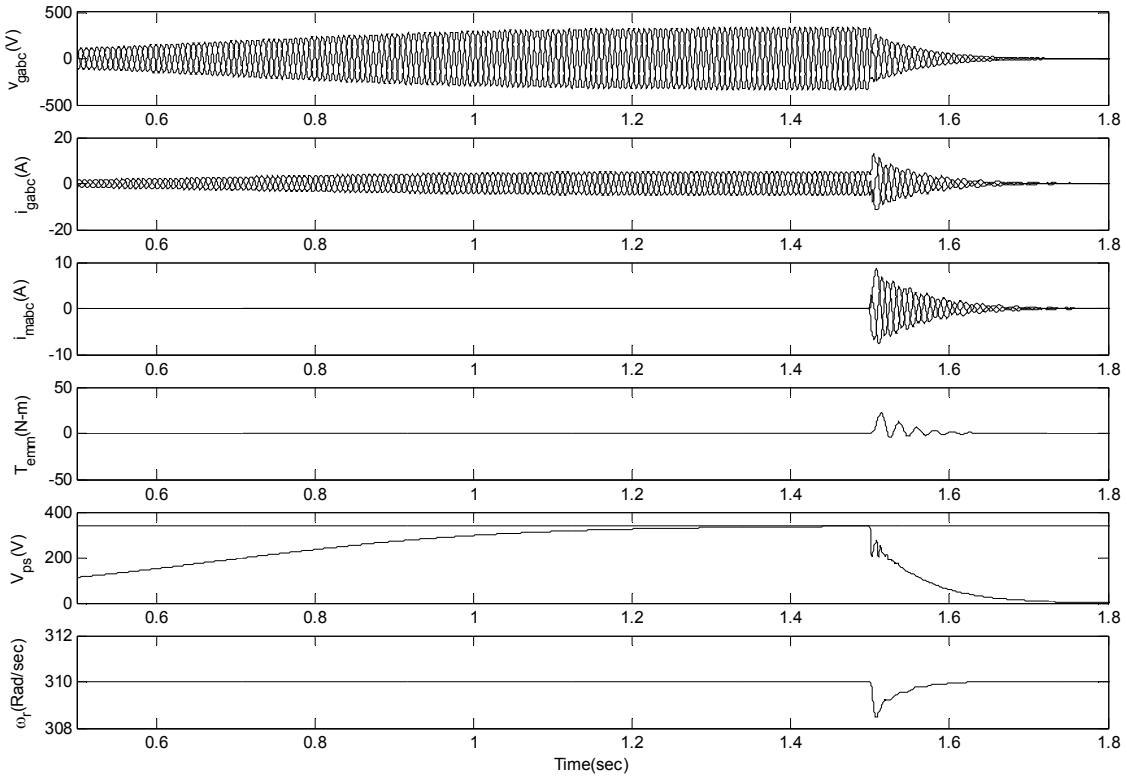


***Fig. 4.17 Transient performance characteristics of SEIG for unsuccessful starting of motor load with shunt capacitance needed for rated no load voltage***

The successful starting of motor load at 0.5 sec. is shown in Fig. 4.18 with shunt capacitance of 109 μF. During starting, the motor draws more than twice of the rated current and appreciable transients are observed in $v_{gabc}$, $i_{gabc}$, $T_{emm}$ and in $\omega_r$. The starting of induction motor load is achieved in around 0.7 sec with dip in $V_{ps}$ to 180 V. The $\omega_{rm}$ gradually increases to no load speed with decrease in $\omega_r$. The full mechanical load on induction motor is applied at 1.3 sec., which is resulting into slight increase in $i_{gabc}$, $i_{mabc}$, $T_{emm}$ and decrease in $\omega_{rm}$, $\omega_r$. Finally, the SEIG is unloaded by disconnecting the

induction motor load, which is causing large increase in $i_{gabc}$, gradually decrease of motor speed to zero due to rotor inertia effect and slight increase in $\omega_r$. The SEIG should not be operated for long duration under no load condition due to large generator voltage and current and capacitance should either be reduced or disconnected.

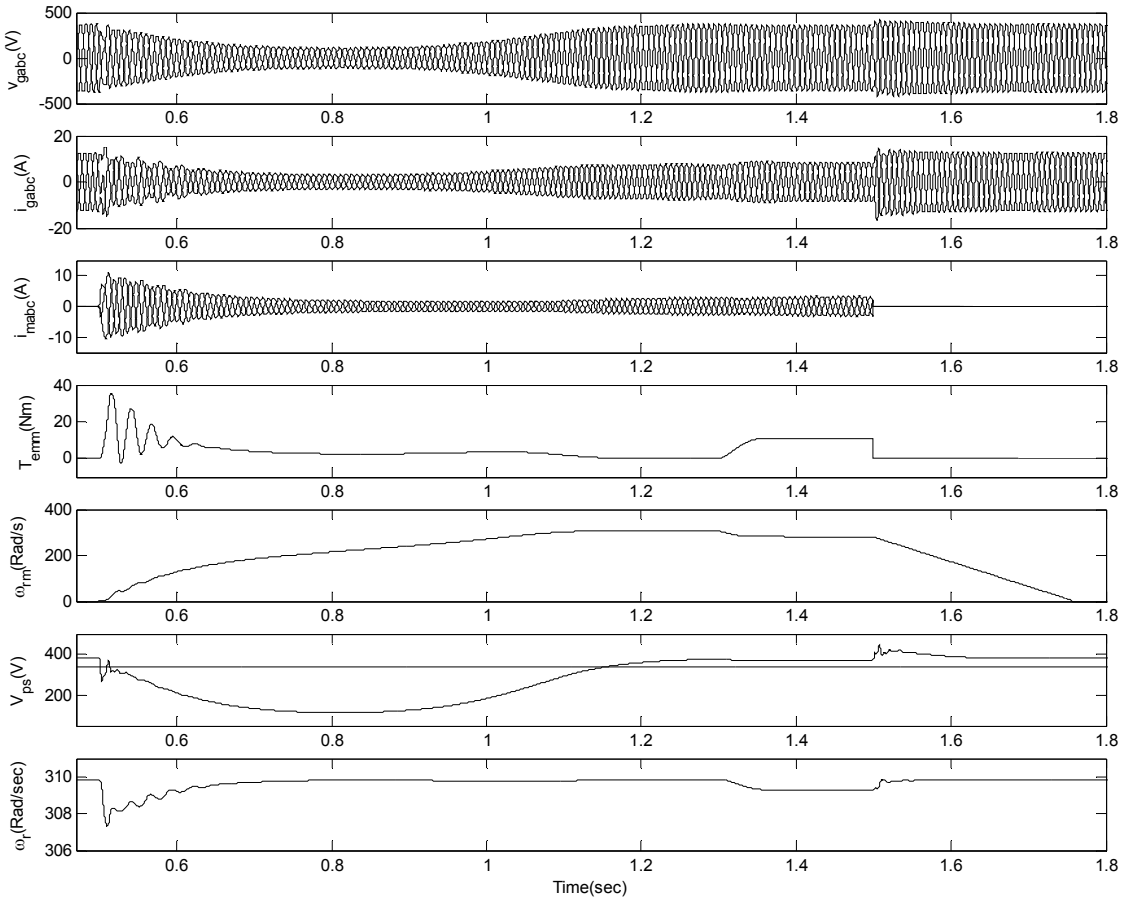


***Fig. 4.18 Transient performance characteristics of SEIG feeding motor load for successful starting with high shunt capacitance of 109 µF***

***(Load conditions : motor start with $T_L$ =0 at 0.5 sec., $T_L$ = rated at 1.3 sec.)***

### 4.6.5 Transient Performance of SEIG with Three-wire Uncontrolled Rectifier Fed Resistive Load

The transient performance characteristics of SEIG feeding three-wire uncontrolled rectifier fed resistive load, as shown in Fig. 4.19, are studied with shunt capacitance of 48.3 µF using generator voltages $v_{gabc}$, generator currents $i_{gabc}$, load currents $i_{ua}$, $i_{ub}$ $i_{uc}$, prime mover speed $\omega_r$ and peak load voltage $V_{ps}$. Due to connection of 1.0 kW load at 1.4 sec., generator currents slightly increase and become non-sinusoidal, load currents increase, $\omega_r$ decreases correspondingly and $V_{ps}$ slight decreases. The load is increased to 2.0 kW at 1.6 sec., causing further increase and distorted in generator current, increase in

load currents, further decrease in $\omega_r$ and $V_{ps}$. The load is reduced to 1.0 kW at 1.8 sec. and is disconnected at 2.0 sec. This causes the system dynamics to change accordingly.

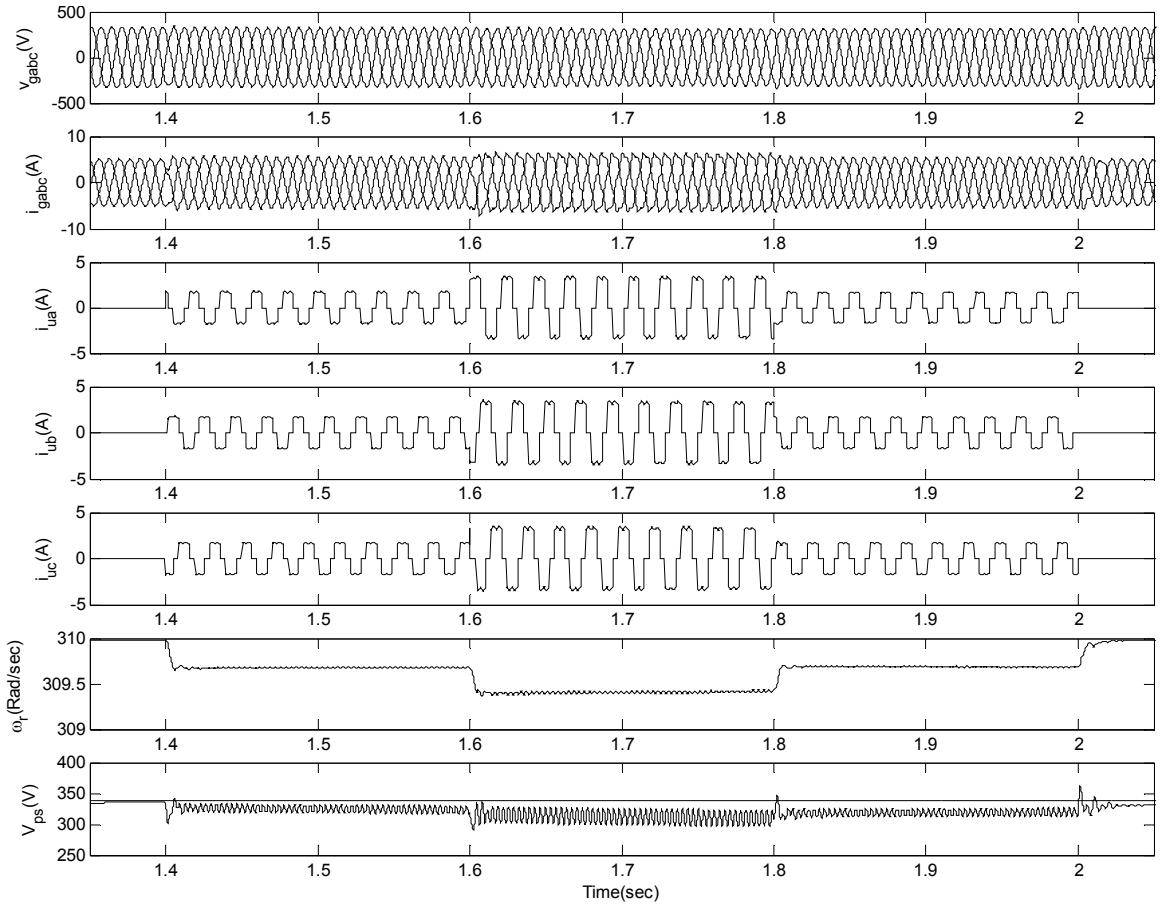


***Fig. 4.19 Transient performance characteristics of SEIG feeding three-wire uncontrolled rectifier fed resistive load***

***(Load conditions : 1.0 kW at 1.4 sec., 2.0 kW at 1.6 and 1.0 kW at 1.8 sec.)***

### 4.6.6 Transient Performance of SEIG with Three-Wire Uncontrolled Rectifier Fed R-C Load

The transient performance characteristics of SEIG feeding three-wire uncontrolled rectifier fed resistive-capacitive load are shown in Fig. 4.20 with shunt capacitance of 48.3 µF. Due to connection of 1.0 kW load at 1.4 sec., the appreciable transients are observed. The $v_{gabc}$ decreases, $i_{gabc}$ increases and $\omega_r$ decreases momentarily. After the initial transients, the steady state is achieved and the generator and load currents increase, $\omega_r$ decreases and $V_{ps}$ hovers around initial. As expected, the generator current becomes non-sinusoidal. The load is increased to 2.0 kW at 1.6 sec., resulting into increase in generator current, which becomes more distorted and decrease in $\omega_r$. The load is decreased to 1.0 kW at 1.8 sec., which changes the dynamics of system accordingly.

Finally, the load is disconnecting at 2.0 sec., with results into sinusoidal generator voltage and current and $V_{ps}$ also becomes steady at rated voltage mark of 338 V.

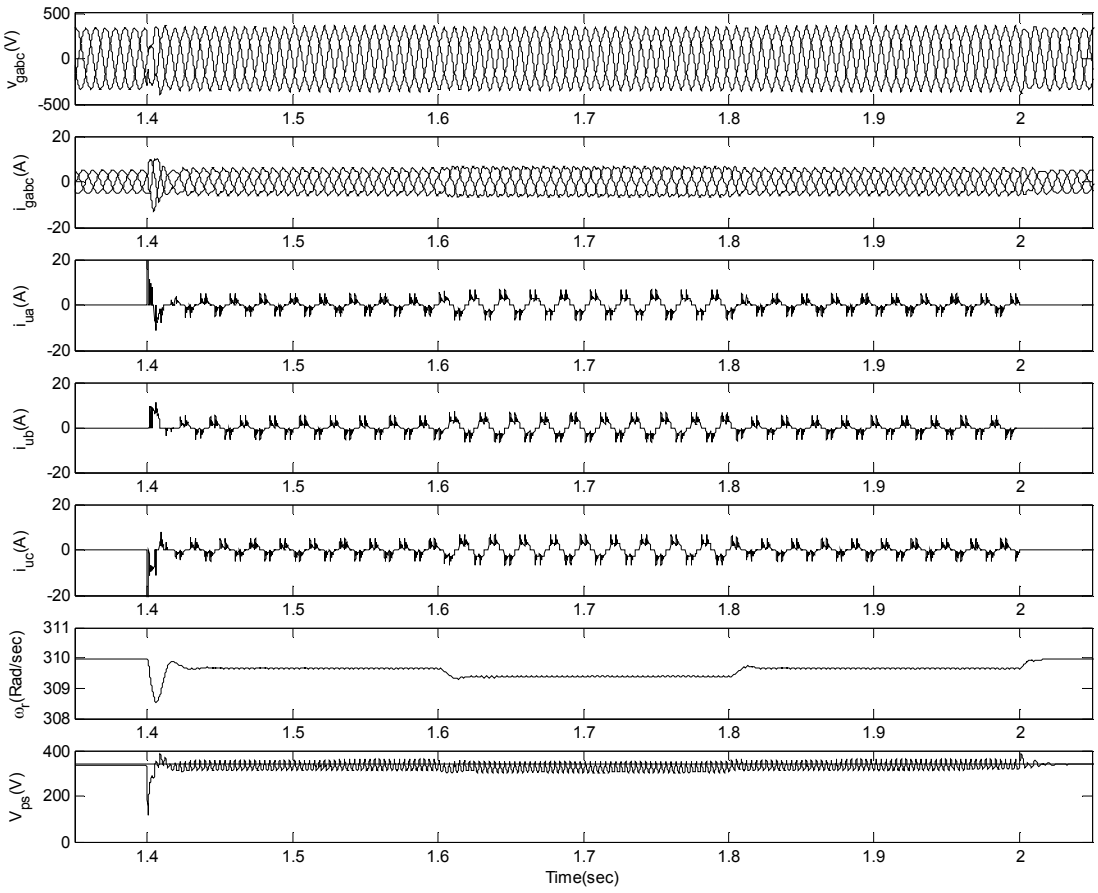


***Fig. 4.20 Transient performance characteristics of SEIG feeding three-wire uncontrolled rectifier fed R-C load***

***(Load conditions : 1.0 kW at 1.4 sec., 2.0 kW at 1.6 and 1.0 kW at 1.8 sec.)***

### 4.6.7 Transient Performance of SEIG with Four-Wire Uncontrolled Rectifier Fed R-C Load

The transient performance of SEIG feeding four-wire uncontrolled rectifier fed resistive-capacitive load is shown in Fig. 4.21 with shunt capacitance of 48.3 μF. The balanced load of 0.5 kW/phase is connected at 1.3 sec., resulting into increase in $i_{gabc}$, increase in load neutral current $i_{ln}$, and decrease in $\omega_r$. As the load is drawing non-linear current, $v_{gabc}$ and $i_{gabc}$ become non-sinusoidal. The load is increased to 1.0 kW/phase at 1.4 sec., which is resulting into increase in $i_{gabc}$ and $i_{ln}$, decrease in $\omega_r$ and increased distortion in $i_{gabc}$.

The unbalance has been created by changing the balanced load of 1.0 kW/phase to a load of 0.75 kW, 1.0 kW and 1.5 kW to a, b and c phase respectively at 1.5 sec. This

results into unbalanced generator voltages $v_{gabc}$ and currents $i_{gabc}$. The $\omega_r$ also becomes oscillating. Further unbalance has been created by disconnecting phase c at 1.6 sec., which is causing $v_{gabc}$ and $i_{gabc}$ unequal and distorting as evident from the waveforms. The $\omega_r$ also experience large magnitude oscillations. The balanced load of 1.0 kW/phase is connected at 1.7 sec. and accordingly system dynamics changes. The SEIG is unloaded by disconnecting the non-linear load at 1.8 sec. The system returns to stable state after some transients.

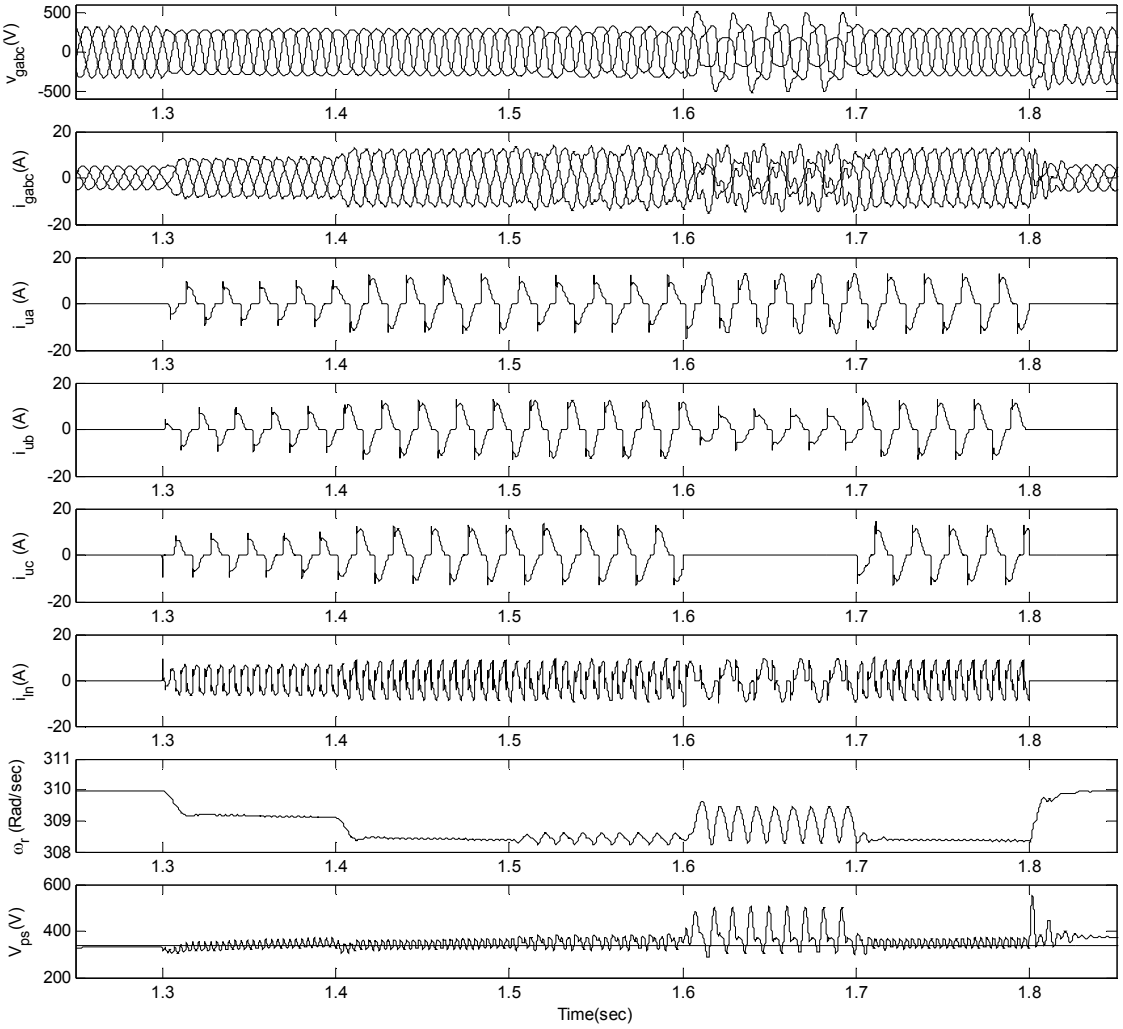


***Fig. 4.21 Transient performance characteristics of SEIG feeding four-wire uncontrolled rectifier fed R-C load***

### 4.6.8 Power Quality Performance

The quality of voltage and current at generator and load terminal is assessed on the basis of harmonic spectra and total harmonic distortion (THD) of the waveform, which are obtained using fast Fourier transform (FFT) of the waveforms in steady state

condition. A discrete Fourier transform (DFT) algorithm of MATLAB is used for this purpose.

#### *4.6.8.1 Harmonic spectra for SEIG with three-wire uncontrolled rectifier fed resistive load*

The steady state waveforms along with harmonic spectrum of $v_{ga}$, $i_{ga}$ and $i_{ua}$ for uncontrolled rectifier fed resistive load of 2.0 kW is shown in Fig. 4.22. The THD in generator voltage and current is obtained as 5.57% and 8.5%, whereas load current THD is 21.02%. The THD on generator side is more than the permissible IEEE-519 standard limit.

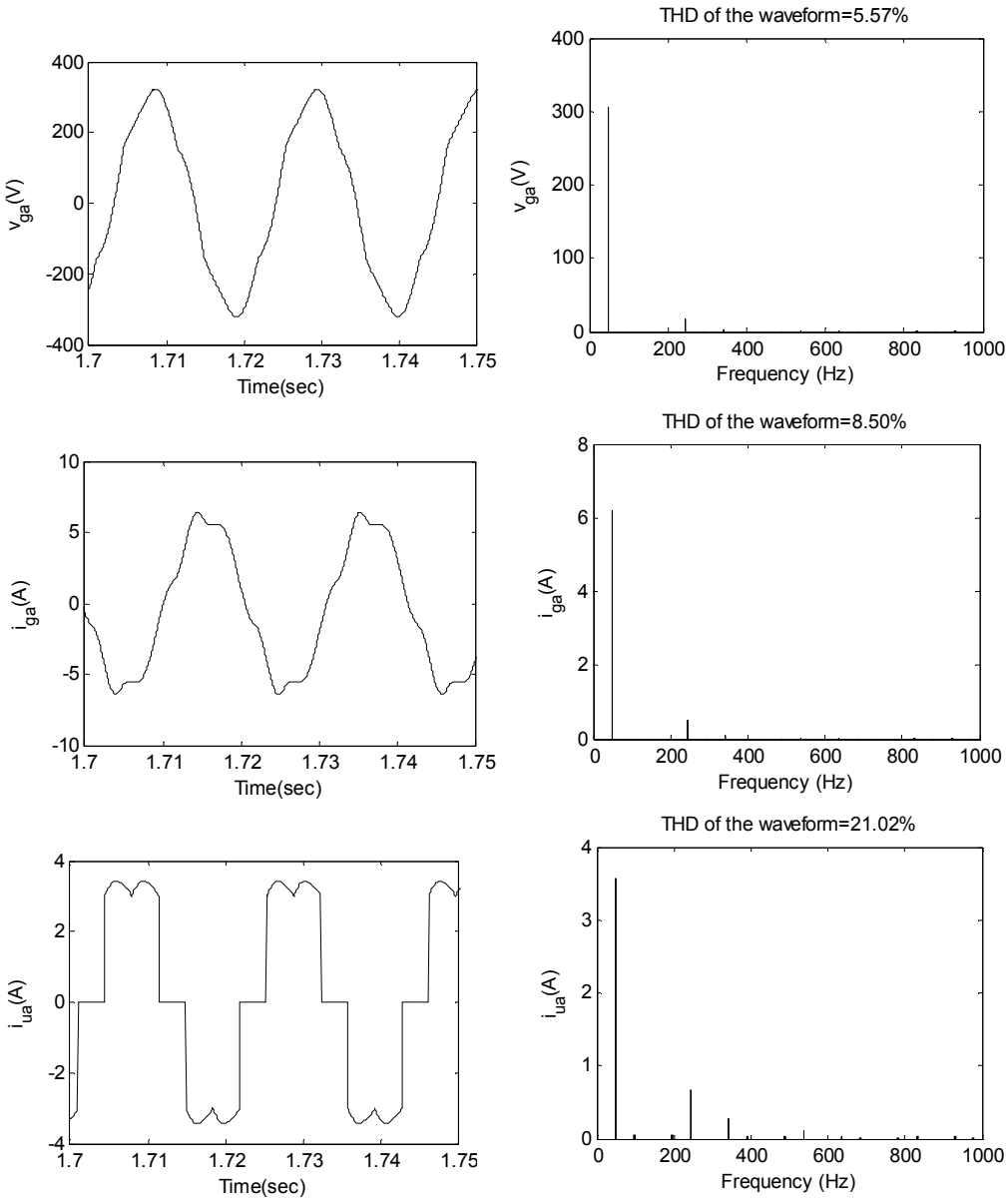


***Fig. 4.22 Harmonic spectra during steady state for SEIG with 2.0 kW three-wire uncontrolled rectifier fed resistive load***

### *4.6.8.2 Harmonic spectra for SEIG with three-wire uncontrolled rectifier fed R-C load*

The steady state waveforms along with harmonic spectrum of $v_{ga}$, $i_{ga}$ and $i_{ua}$ for uncontrolled rectifier fed resistive-capacitive load of 2.0 kW is shown in Fig. 4.23. The generator voltage and current are having THD of 6.58% and 10.06%, whereas load current THD is having 26.78%. The THD on generator side is more than the IEEE-519 standard limit of 5%.

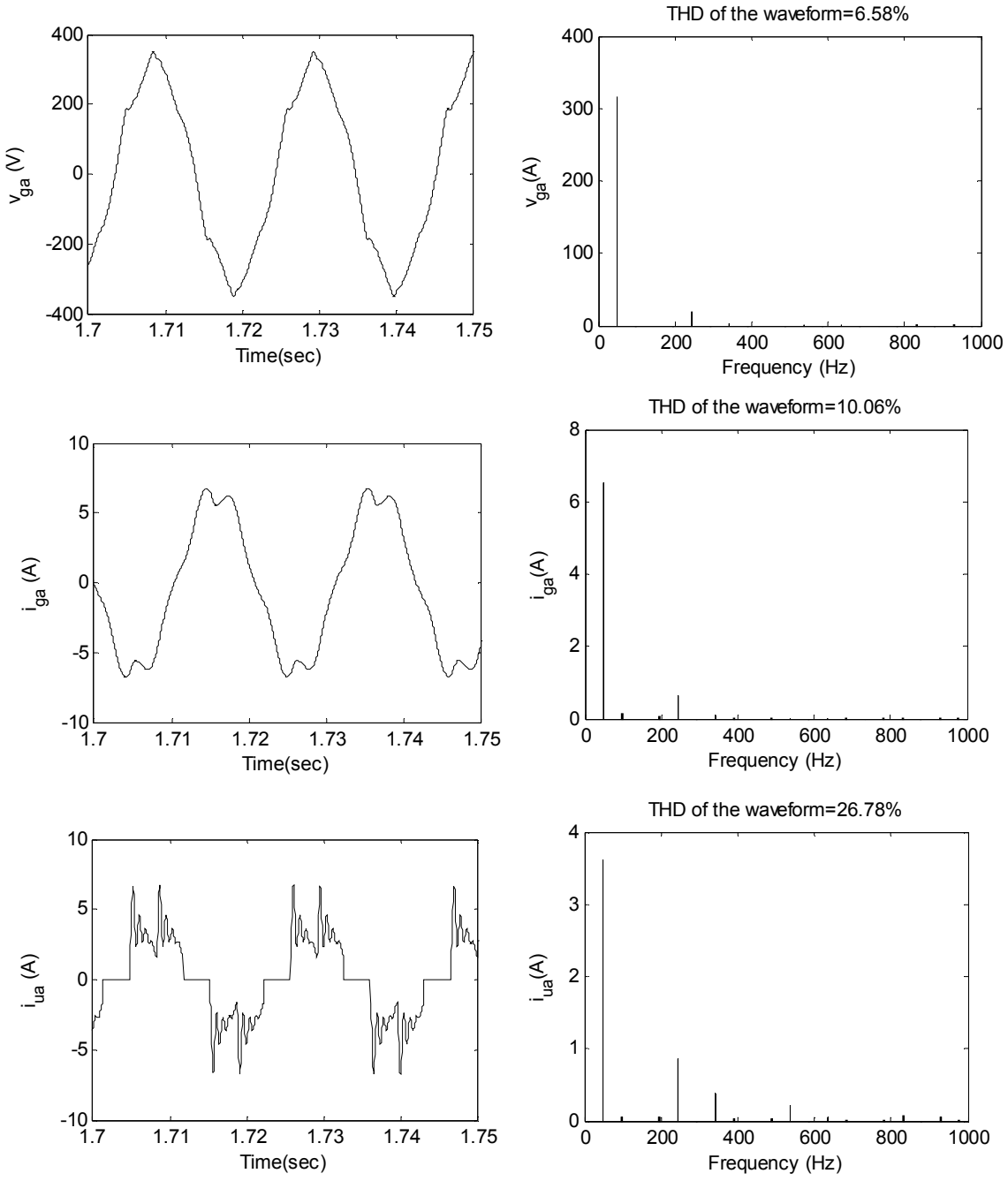


***Fig. 4.23 Harmonic spectra during steady state for SEIG with 2.0 kW three-wire uncontrolled rectifier fed R-C load***

### *4.6.8.3 Harmonic spectra for SEIG with four-wire uncontrolled rectifier fed R-C load*

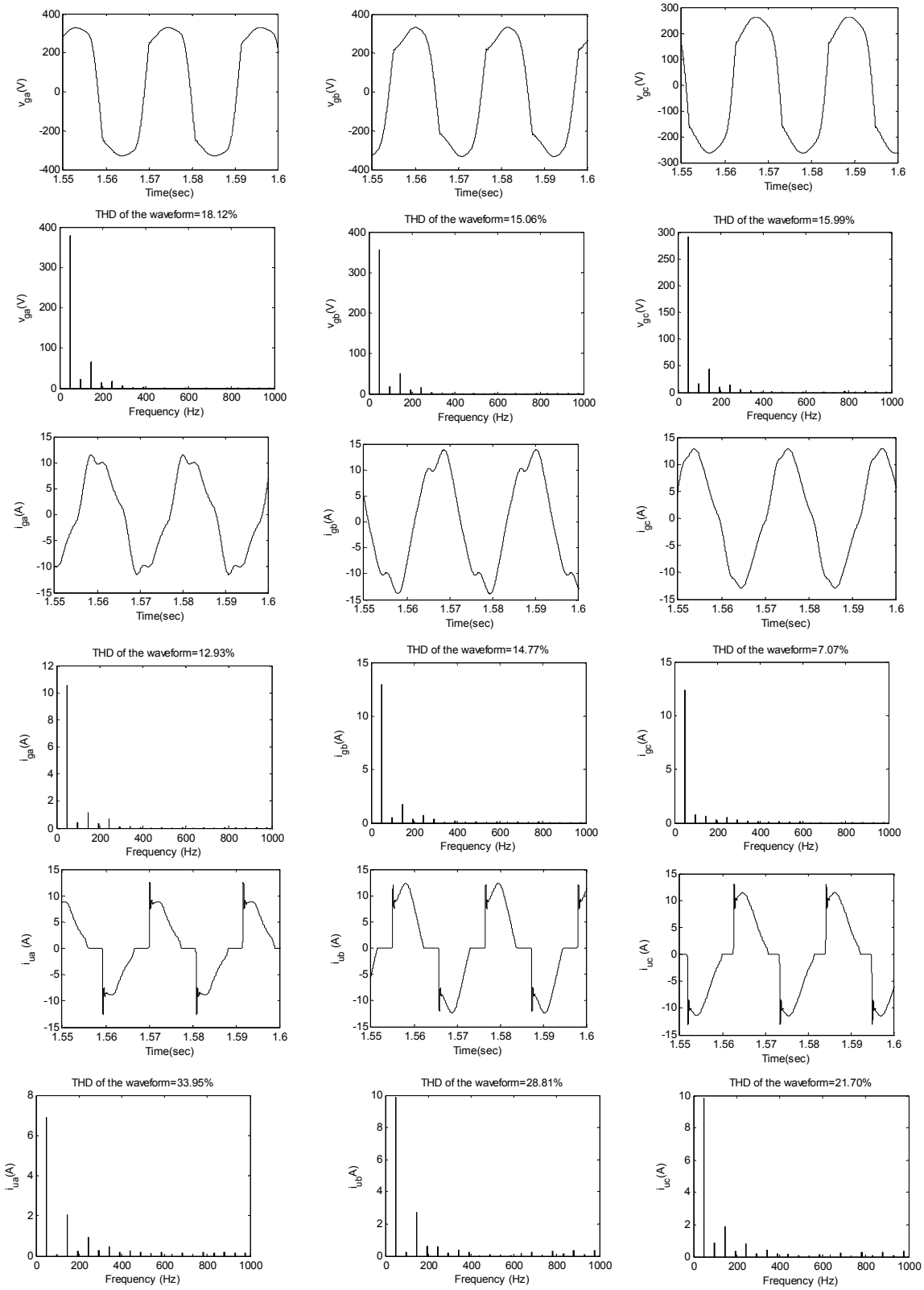


***Fig. 4.24 Harmonic spectra during steady state for SEIG with unbalanced four-wire uncontrolled rectifier fed R-C load***

The harmonic spectrum along with the steady state waveform of generator voltages ($v_{ga}$, $v_{gb}$, $v_{gc}$), generator currents ($i_{ga}$, $i_{gb}$, $i_{gc}$) and load currents ($i_{ua}$, $i_{ub}$, $i_{uc}$) are shown in Fig. 4.24 for unbalanced (0.75 kW, 1.0 kW and 1.5 kW on a, b and c phases) load. The THD in the generator voltages of a, b and c phases are 18.12%, 15.06% and 15.99% respectively, and in the generator currents in a, b and c phase are 12.93%, 14.77% and 7.07% respectively, whereas in the load currents in a, b and c phases are 33.95%, 28.81% and 21.70%. The large and unequal value of THD on generator side, as shown in Table 4.5 suggests the SEIG can not be run for prolong duration without necessary balancing and harmonic elimination arrangement.

***Table 4.5 THD values for SEIG fed non-linear loads***

| **Load** | **THD in generator voltage (%)** | **THD in generator current (%)** | **THD in load current (%)** |
|---|---|---|---|
| Three-wire uncontrolled rectifier fed 2.0 kW resistive load | 5.57 | 8.50 | 21.02 |
| Three-wire uncontrolled rectifier fed 2.0 kW R-C load | 6.58 | 10.06 | 26.78 |
| Four-wire uncontrolled rectifier fed R-C load (0.75 kW, 1.0 kW and 1.5 kW on a, b and c phases) | 18.21 ($v_{ga}$)<br>15.06 ($v_{gb}$)<br>15.99 ($v_{gc}$) | 12.93 ($i_{ga}$)<br>14.77 ($i_{gb}$)<br>7.07 ($i_{gc}$) | 33.95 ($i_{ua}$)<br>28.81 ($i_{ub}$)<br>21.70 ($i_{uc}$) |

## 4.7 CONCLUSIONS

The steady state and transient state performance of SEIG for feeding various types of loads has been investigated in this chapter. An optimization problem for voltage regulation has been formulated for static loads, subjected to various equality and inequality constraints to obtain optimum shunt capacitance and speed using steady state equivalent circuit. The genetic algorithm, a global search and optimization approach, has been used to obtain the combination of speed and shunt capacitance for optimum voltage regulation. The results corresponding to rated speed have been experimentally verified for static loads. The steady state performance of SEIG fed induction motor load is also studied and verified experimentally.

The transient performance of SEIG feeding linear and non-linear loads has also been analyzed in this chapter. The SEIG model in q-d variables with currents as a state space variable in stationary reference frame has been developed for the transient analysis. The linear loads are modeled in q-d variables, whereas the non-linear loads have been modeled in phase variables. The effect of non-linear loads on SEIG performance has been estimated using THD and harmonic spectrum. From the study carried out in this chapter, following conclusions are drawn.

- The developed algorithm employing GA has been found effective in providing the optimum values of shunt capacitance and speed.
- In spite of optimum capacitance selection, the SEIG exhibits drooping terminal voltage with the load.
- Improved voltage regulation with increased loading capacity has been obtained with resistive loads as compared to resistive-inductive loads.
- The voltage collapse is resulted with lower shunt capacitance during starting of induction motor load. However, successful starting is resulted when capacitance is increased to sufficiently high value.
- The large voltage drop and large starting time are serious power quality problems for the SEIG feeding an induction motor load, which suggests the use of static controllers for supplying the reactive power.
- The THD on generator side due to non linear loads is resulted in higher than specified IEEE 519 standard. The high content of harmonics on generator side causes more losses, temperature rise, insulation stress and poor efficiency. Therefore, the SEIG should not be run for prolong time to avoid any damage.

# CHAPTER-V

# SEIG OPERATION WITH STATCOM FEEDING STATIC AND DYNAMIC LOADS

## 5.1 GENERAL

In the previous chapter, the performance of SEIG has been studied for feeding linear and non-linear loads. It has been shown that the terminal voltage of SEIG is governed by several parameters such as a capacitance, the prime mover speed, the nature of speed torque characteristic and the loads. As the generator is loaded from no load to full load, the difference between the VAR supplied by the capacitor bank and VAR demanded by the generator and loads widen, causing poor voltage regulation. To keep the terminal voltage within the permissible limit, various schemes have been devised and discussed in the literature [122-192]. These schemes have been detailed in Chapter-3. These schemes include classical schemes such as series capacitors, switching device based schemes like switching shunt capacitors and converter based scheme such as static VAR compensator (STATCOM).

Recently, the voltage source converters (VSC) are being used in flexible AC transmission system (FACTS) devices because of their fast response, better switching features and the low cost [250]. The STATCOM consisting of insulated gate bipolar transistors (IGBTs) based CC-VSC (Current Controlled-Voltage Source Converter), is an important FACTS device and is connected as a shunt element [231-248]. The STATCOM is normally a pulse width modulated (PWM) Current Controlled–Voltage Source Converter (CC-VSC) with self supporting DC bus. The main advantages of CC-VSC based STATCOM are fast response, ability to operate at high switching frequency and operated in almost identical capacitive and inductive range as shown in Fig. 5.1. The STATCOM has been used for various applications in the power system such as harmonic elimination, reactive power compensation and load balancing. The STATCOM can also be used to supply lagging (or leading) reactive VAR to the SEIG to regulate the load voltage. Furthermore, the design of STATCOM is also important to meet the specific load requirement.

The use of AC motor drives is continuously increasing nowadays. Traditionally, DC motor drives have been used for position and speed control applications because of their excellent performance and still continue to be used in many applications [231]. Therefore, it is worth to investigate the performance of SEIG with AC motor and rectifier controlled DC motor loads apart from the static resistive-inductive loads.

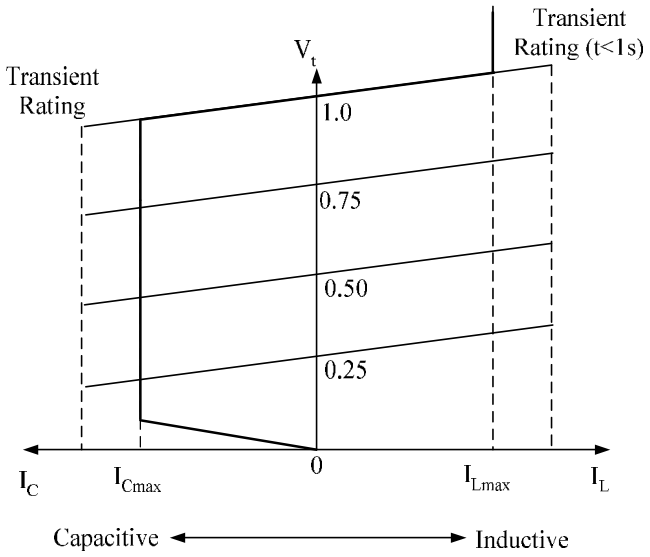


***Fig. 5.1 Operational capability limits of STATCOM***

The complete SEIG system comprising of 3-ϕ self-excited induction generator, STATCOM and various 3-ϕ loads is shown in Fig. 5.2. The performance of system is studied for static resistive-inductive (R-L), squirrel cage induction motor (IM) and controlled bridge rectifier fed DC motor loads. The schematics of these loads are shown in Fig. 5.3. The modeling and transient analysis of 3-$\phi$ SEIG is carried out for feeding static resistive-inductive loads, induction motor loads and rectifier controlled DC motor loads with STATCOM. This chapter also deals with the necessary steps and guidelines to decide the parameters of STATCOM for these loads. The full rating STATCOM and reduced rating STATCOM design are presented and the transient performance is studied for these loads. The reduced rating STATCOM design is considered to provide the cost effective design for remote applications. The STATCOM provides the additional VAR required by the loads and thus results in good voltage regulation. With consideration of designed static VAR compensator parameters, the system is studied for switching of the static compensator, loading of static resistive-inductive loads, starting and loading of both inductions motor and DC motor loads.

## 5.2 DESCRIPTION AND CONTROL OF SEIG-STATCOM SYSTEM

The description of system components and associated control strategy is discussed in this section.

### 5.2.1 System Description

The schematic of the complete system is shown in Fig. 5.2. A suitable capacitor bank is connected to generate the rated terminal voltage at no load. The STATCOM consists of the IGBTs based 3-ϕ current controlled-voltage source converter, AC side filter inductors and a capacitor on DC side for self supporting DC bus. The STATCOM injects leading (or lagging) current into the AC system at quadrature to the supply voltage which thereby adjusts the VAR requirement of the loads and the generator to maintain the load voltage. The system effectiveness is studied for static resistive-inductive loads, 3-ϕ induction motor and controlled rectifier fed DC motor loads. The induction motor requires excessive reactive power during its starting and additional VARs are to be supplied by the STATCOM to avoid voltage collapse and unsuccessful starting.

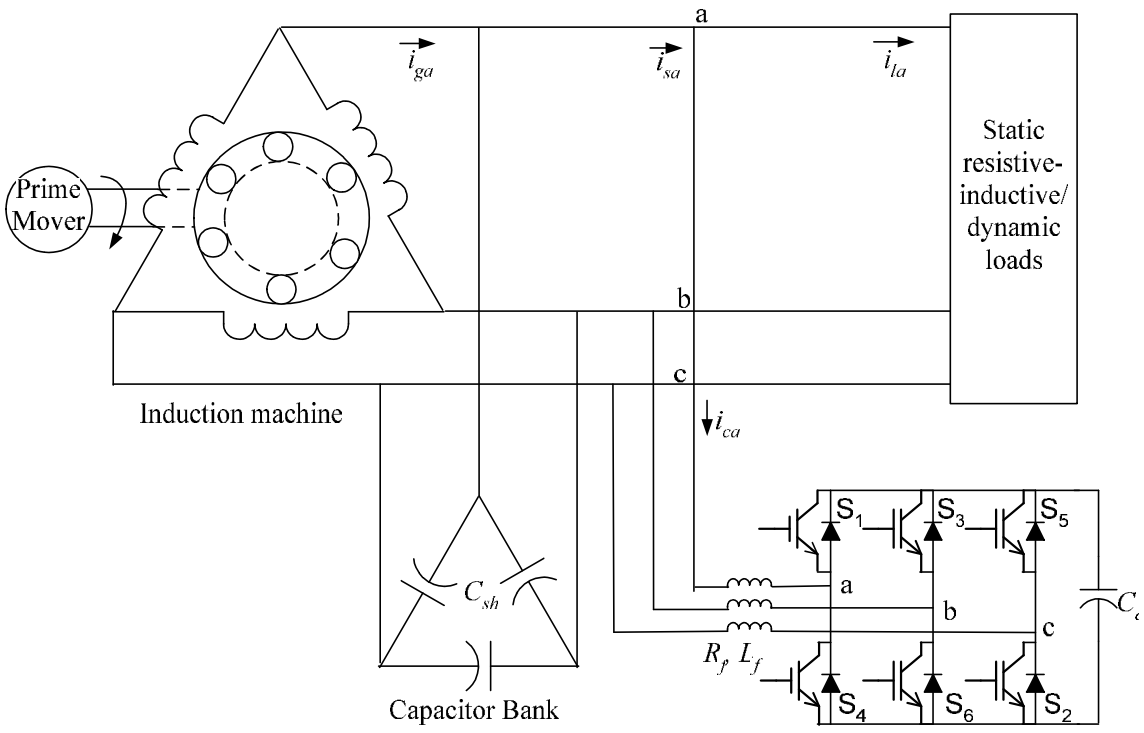


***Fig. 5.2 SEIG-STATCOM system feeding three-phase load***

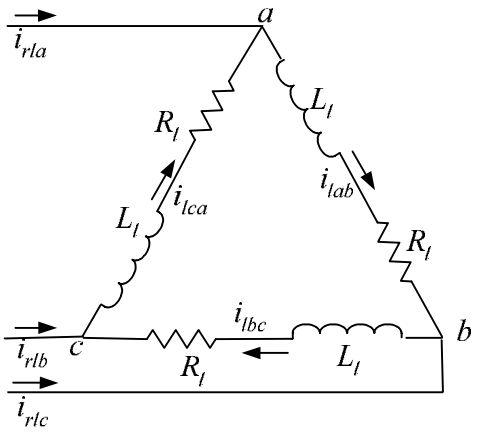


***Fig. 5.3a Delta connected static resistive-inductive load***

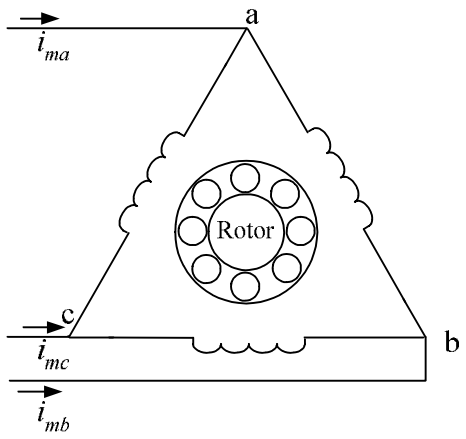


***Fig. 5.3b Squirrel cage induction motor load***

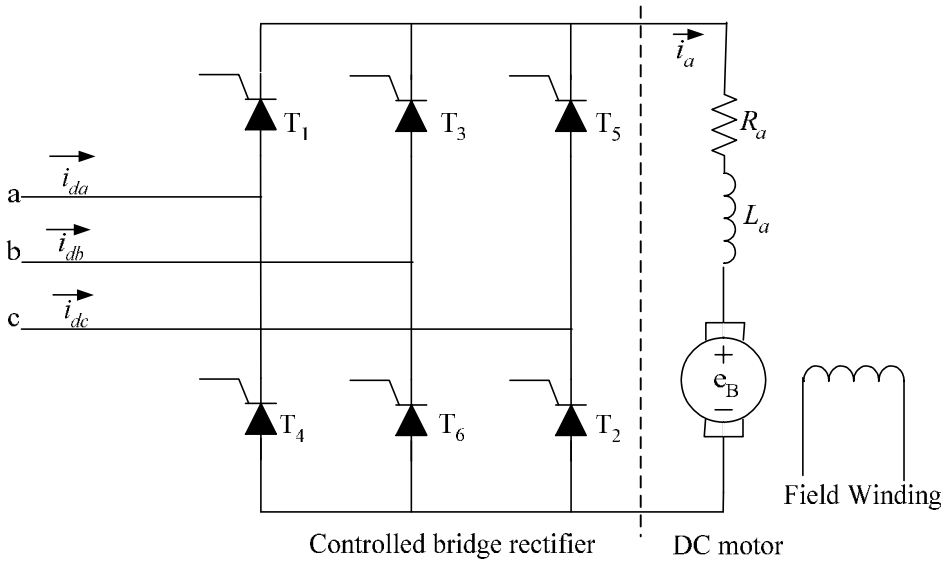


***Fig 5.3c Three-phase controlled bridge rectifier fed DC motor load***

***Fig. 5.3 Various loads on SEIG-STATCOM system***

### 5.2.2 Control Strategy

The flow diagram of control strategy is shown in Fig. 5.4. In this scheme, two control loops are employed; one for regulating the terminal voltage of SEIG and other for regulating the DC bus voltage of STATCOM. The proportional-integral (PI) controllers are used with both the control loops.

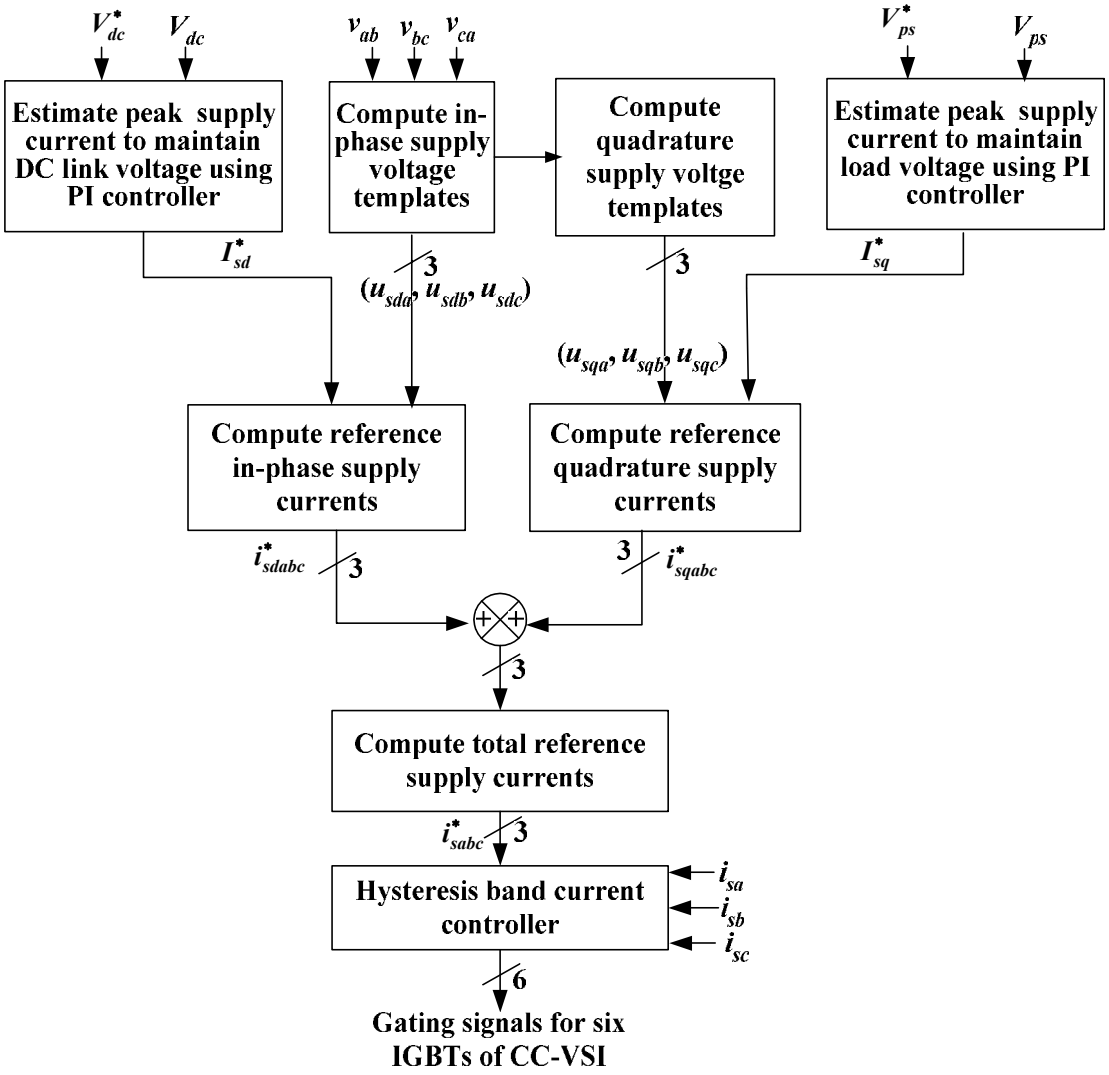


***Fig. 5.4 Control scheme for STATCOM***

The control scheme is based on direct control of the *supply current* [244], which consists of in-phase supply current and quadrature supply current components. The in-phase supply current component is the active current drawn from SEIG to maintain the DC bus voltage of STATCOM by charging (or discharging) the DC bus capacitor. The quadrature supply current component is the reactive current required to maintain the

voltage. For the control loop employed to maintain the DC bus voltage, the DC bus voltage $V_{dc}$ is sensed and compared with the reference DC bus voltage $V_{dc}^{*}$. The voltage error is processed in PI controller and the controller output is taken as the reference peak in-phase supply current $I_{sd}^{*}$. The 3-ϕ reference in-phase supply currents are obtained by multiplying $I_{sd}^{*}$ to the in-phase voltage templates.

The voltage error signal for another PI controller, used for regulating SEIG terminal voltage, is obtained from actual peak supply voltage $V_{ps}$ and reference peak supply voltage $V_{ps}^{*}$. The output of the controller is taken as the reference peak quadrature supply current $I_{sq}^{*}$. The 3-$\phi$ reference quadrature supply currents are obtained by multiplying $I_{sq}^{*}$ by quadrature voltage templates. The total reference supply currents are taken as the sum of reference in-phase and quadrature currents. The sensed supply currents and reference supply currents are processed in rule based carrier less Hysteresis band current controller to derive gating signals for IGBTs of CC-VSC of STATCOM.

## 5.3 DESIGN METHODOLOGY

The design of STATCOM briefed herewith, is based on the following assumptions,

- The maximum reactive VAR capacity of STATCOM is fixed.
- The source voltages are sinusoidal.
- The PWM voltage source converter operates in linear amplitude modulation mode ($m=1$).

The VAR rating of STATCOM is estimated using the line voltage $V_s$, capacitance needed for providing rated voltage at no load ($C_{NL}$) and the capacitance needed for stable operation while feeding full load ($C_{FL}$).

$$(VAR)_{STATCOM} = 3V_s^2\left[\frac{1}{X_{C_{FL}}} - \frac{1}{X_{C_{NL}}}\right] \tag{5.1}$$

The STATCOM current $I_{st}$ is calculated as,

$$I_{st} = \frac{(VAR)_{STATCOM}}{\sqrt{3}V_s} \tag{5.2}$$

The STATCOM adjusts the currents to compensate the reactive power, for which the reference DC bus voltage is an important parameter. The low value of $V_{dcr}$ is not sufficient to inject the compensation currents during transient condition. Whereas, the high value of $V_{dcr}$ results more stresses on the devices of the STATCOM. Therefore, $V_{dcr}$ is calculated using peak supply line voltage $V_m$ [245, 246] as,

$$V_{dcr} = (1.2\text{-}2.0)\ V_m, \qquad V_{dcr} > V_m \tag{5.3}$$

The DC bus capacitor works as an energy storage element to supply the real power difference between the loads and the source during the transients and maintains the DC bus voltage with small ripple in steady state conditions. With a large capacitance, the compensation capability is improved and the ripples in $V_{dc}$ are reduced but at the cost of large size capacitor.

The DC bus capacitor sizing is based on the energy balance equation characterized by actual DC bus voltage $V_{dc}$ and appropriate response time $t$ (normally in between 250μs to 350 μs) [233]. The DC bus capacitor is obtained as,

$$C_{dc} = \frac{\sqrt{3}V_s I_{st} t}{\left(V_{dcr}^2 - V_{dc}^2\right)} \tag{5.4}$$

The sizing of AC filter inductor is based on the allowable ripples in the compensation current. By considering operation in linear modulation mode i.e. modulation index $m$=1, maximum switching frequency $f_s$ is taken as 10 kHz. The large inductor size results in the sluggish STATCOM response. The filter inductance [156, 231] is calculated as,

$$L_f = \frac{\left(\frac{\sqrt{3}}{2}\right)V_{dc}}{6af_s K_{rp} i_{rpp}} \tag{5.5}$$

where, range of factor $a$ (due to transient current) =1.2 to 2.0 and ripple factor ($K_{rp}$) as 0.05 to 0.1 for the peak to peak ripple current $i_{rpp}$ in the filter inductor.

The IGBTs are considered for STATCOM because of their good performance for medium rating and high frequency operation.

$$\text{Device voltage rating} = V_{dev} = (1 + K_L + K_t)V_m \tag{5.6}$$

$$\text{Device current rating} = I_{dev} = \sqrt{2}K_s(K_{rp} + 1)I_{st} \tag{5.7}$$

where, the range of $K_L$ (factor for filter inductor drop) = 0.05 to 0.1, the range of $K_t$ (factor for transient voltage) = 0.5 to 0.75, and the range of $K_s$ (factor of safety) = 1.25 to 2.0. The slightly higher value of $K_s$ is taken for dynamic loads. For reduced rating STATCOM, the transient current due to additional capacitor connection is considered to decide the device current rating of STATCOM.

### 5.3.1 VAR Requirement of Controlled Rectifier Fed DC Motor

The reactive power requirement by the controlled rectifier fed DC motor load is calculated on the basis of assumption of continuous conduction and with constant current consideration [278].

The back emf $e_B$ developed in the DC motor depends upon the angular DC motor speed $\omega_{rd}$ and is given as,

$$e_B = k_a * \omega_{rd} \tag{5.8}$$

The developed electromagnetic torque $T_{emd}$ depends upon the armature current $i_a$ and is calculated as,

$$T_{emd} = k_a * i_a \tag{5.9}$$

For a given speed, the armature applied voltage $v_a$ can be find out as,

$$v_a = e_B + i_a R_a \tag{5.10}$$

The operating firing angle of the controlled rectifier, as shown in Fig. 5.3c, can be evaluated from the known value of the peak supply voltage ($V_{ps}$) as,

$$\cos\alpha = \frac{\pi v_a}{3V_{ps}} \tag{5.11}$$

The rms supply current ($i_{da}$) for given value of armature current $i_a$ is calculated as,

$$i_{da} = \sqrt{\frac{2}{3}} i_a \tag{5.12}$$

Neglecting associated rectifier losses, equating DC side power and AC side power with line voltage $v_{ab}$, the power factor ($\cos\phi$) can be evaluated as,

$$\cos\phi = \frac{v_a i_a}{\sqrt{3} v_{ab} i_{da}} \tag{5.13}$$

The VAR requirement is computed as,

$$Q_{dc} = \sqrt{3} v_{ab} i_{da} \sin\phi \tag{5.14}$$

After calculating the VAR requirement of the controlled rectifier fed DC motor, the STATCOM parameters can be calculated using eqns. (5.2)-(5.7).

### 5.3.2 Full Rating STATCOM Design

The ability of STATCOM to supply the reactive VARs also depends on DC bus capacitance $C_{dc}$ under dynamic conditions. Therefore, the $C_{dc}$ must be selected while considering the VAR requirement of the configuration carefully. The SEIG has inherent poor voltage regulation because it requires additional capacitive VAR when loaded to maintain the terminal voltage. The VAR requirement increases further when the load becomes inductive. The design of the STATCOM for feeding various loads is carried out while calculating the capacitance required to maintain the rated voltage using the steady state equivalent circuit. The sequential unconstraint minimization technique (SUMT) in conjunction with direct search Rosenbroack method of rotating coordinate optimization method is applied for the purpose and brief algorithm is explained in Appendix-G.

For a 2.2 kW R-L load of 0.8 power factor, 30.4 μF is resulted and therefore the full rating STATCOM design is carried out using $C_{NL}$ =16.1 μF and $C_{FL}$ as 30.4 μF. The full rating STATCOM parameters for this case are summarized in Table 5.1.

The values of capacitance calculated for SEIG with an IM load configuration under no load and rated load on the motor are $C_{NL}$ =16.1 μF and $C_{FL}$ =26.5 μF respectively. The ratings and parameters of IM load are given in Appendix-A. It is found that the motor (IM) is unable to starting even with $C_{FL}$, which is the capacitance corresponding to the rated motor load under steady state, and results into voltage collapse. This is because the

capacitor bank, which is only the source of the reactive power, unable to meet the excessive VAR requirements of SEIG and a motor load during starting transient. The successful starting of the motor load is resulted in while capacitance is equal or more than 36.3 μF, which is more than twice the $C_{NL}$. The STATCOM is designed for the $C_{NL}$ as 16.1 μF and other value as 36.3 μF. The full rating STATCOM design parameter for an induction motor load is also summarized in Table 5.1.

***Table 5.1 Full rating STATCOM parameters for various loads***

| Parameter | 2.2 kW, 0.8 pf R-L load | 1.5 kW AC motor load | Controlled rectifier fed DC motor load |
|---|---|---|---|
| STATCOM rating | 2.42 kVAR | 3.23 kVAR | 3.96 kVAR |
| Current supplied by STATCOM | 3.37 A | 4.6 A | 5.5 A |
| Reference DC bus voltage | 700 V | 700 V | 700 V |
| DC bus capacitance | 172.6 $\mu$F | 236.3 $\mu$F | 282.6 $\mu$F |
| AC Filter inductance | 5.58 mH | 4.08 mH | 3.42 mH |
| Device selection | IGBT | IGBT | IGBT |
| Device voltage rating | 1094 V | 1094 V | 1094 V |
| Device current rating | 11.0 A | 15.0 A | 18.0 A |

The STATCOM design is carried out with a 1.5 kW DC motor load supplied by 3-ϕ fully controlled thyristor rectifier. For achieving the rated voltage across the DC motor, the firing angle of a converter should be kept around 70°. With the assumption of continuous conduction and constant current, the DC motor along with the rectifier requires 3.6 kVAR. Therefore the STATCOM rating is decided by taking a margin of 10%. The rating of STATCOM parameters are also depicted in Table 5.1.

### 5.3.3 Reduced Rating STATCOM Design

Keeping in view of SEIG utility for the remote application, the reduced rating STATCOM may be a cost effective solution. Therefore, the analysis is also carried for reduced rating STATCOM. The STATCOM design parameters for reduced rating STATCOM for above loads are given in Table 5.2.

The value of capacitance $C_{FL}$ considered for full rating STATCOM design, which is 30.4 μF and 36.3 μF for static R-L load of 2.2 kW, 0.8 pf and an induction motor load

are taken as reference even for reduced rating STATCOM design. The design is carried out using limiting capacitance of $C_{NL}$ and $C_{NL}$ + ($C_{FL}$-$C_{NL}$)/2 while an additional shunt capacitance ($C_{FL}$-$C_{NL}$)/2 is switched on with the load.

***Table 5.2 Reduced rating STATCOM parameters for various loads***

| Parameter | For 2.2 kW, 0.8 pf static load | For 1.5 kW induction motor load | For controlled rectifier fed DC motor load |
|---|---|---|---|
| STATCOM rating | 1.21 kVAR | 1.615 kVAR | 1.98 kVAR |
| Current supplied by STATCOM | 1.68 A | 2.25 A | 2.75 A |
| Reference DC bus voltage | 700 V | 700 V | 700 V |
| DC bus capacitance | 86.3 $\mu$F | 118.1 $\mu$F | 141.3 $\mu$F |
| AC Filter inductance | 11.16 mH | 8.16 mH | 6.84 mH |
| Device selection | IGBT | IGBT | IGBT |
| Device voltage rating | 1094 V | 1094 V | 1094 V |
| Device current rating | 6.5 A | 11.0A | 12.0 A |

For controlled rectifier fed DC motor load, the STATCOM is designed for half of the VAR required for full rating STATCOM. Correspondingly, the additional capacitance of 12.3 μF is connected with the load, which is equivalent to half of the VAR required.

For the reduced rating STATCOM, DC bus capacitance and the current rating of IGBTs are reduced. Therefore, the reduced rating STATCOM operation with SEIG can be a cost effective solution where the strict power quality is not a concern.

## 5.4 MODELING OF SEIG-STATCOM SYSTEM

The complete SEIG system, as shown in Fig. 5.2, consists of a SEIG, a STATCOM with associated control scheme and dynamic loads. The dynamic model of each component is presented herewith.

### 5.4.1 SEIG Model

The dynamic model of 3-ϕ SEIG has been developed in stationary q-d reference frame in previous chapter. The model in state space form is reproduced herewith for ready reference.

$$p[\mathbf{i}] = [\mathbf{L}]^{-1}\left([\mathbf{v}] - [\mathbf{R}][\mathbf{i}] - [\mathbf{G}][\mathbf{i}]\right) \tag{5.15}$$

$$p\omega_r = \frac{P}{2J}\left(T_P - T_{em}\right) \tag{5.16}$$

where, $[\mathbf{v}]$, $[\mathbf{i}]$, $[\mathbf{R}]$, $[\mathbf{L}]$, $[\mathbf{G}]$ and $T_{em}$ are defined in Appendix-B.

For SEIG, the air gap voltage does not remain constant and therefore the magnetizing reactance also varies accordingly. For the purpose, the magnetizing current is calculated from the stator and rotor q-d axis currents.

The q-d axis stator currents $i_{qs}$ and $i_{ds}$ of SEIG are converted into 3-$\phi$ stator currents $i_{ga}$, $i_{gb}$ and $i_{gc}$ using 2-axis to 3-axis phase transformation. The capacitor equations governing the AC terminal voltage of SEIG are written by applying KCL as,

$$\begin{aligned} pv_{ab} &= \frac{\left\{\left(i_{ga} - i_{la} - i_{ca}\right) - \left(i_{gb} - i_{lb} - i_{cb}\right)\right\}}{3C_{sh}} \\ pv_{bc} &= \frac{\left\{\left(i_{ga} - i_{la} - i_{ca}\right) + 2\left(i_{gb} - i_{lb} - i_{cb}\right)\right\}}{3C_{sh}} \end{aligned} \tag{5.17}$$

and $\quad v_{ab} + v_{bc} + v_{ca} = 0$

where, $i_{ga}$, $i_{la}$ and $i_{ca}$ are the line 'a' currents of SEIG, load and STATCOM respectively. The q-d axis terminal voltages $v_{qs}$ and $v_{ds}$ are obtained from phase voltages $v_{ab}$, $v_{bc}$ and $v_{ca}$ using transformation.

### 5.4.2 STATCOM Control Model

The 3-ϕ reference supply currents are computed based on peak supply voltages and DC bus voltage of the STATCOM. The reference supply current consists of in-phase and quadrature components. The modeling of STATCOM is explained in the following sub sections.

#### *5.4.2.1 In-phase Current Component*

The reference peak in-phase supply current $I_{sd}^{*}$ is taken as the output $y_{vdc}$ of PI controller while processing the voltage error $e_{vdc}$ computed over DC bus voltage $V_{dc}$ and

its reference DC bus voltage $V_{dc}^{*}$. The discrete PI controller equation as shown in eqn. (5.18) is derived in Appendix-E. The voltage error at $n^{th}$ sampling instant is,

$$\begin{aligned} e_{vdc}(n) &= V_{dc}^{*}(n) - V_{dc}(n) \\ y_{vdc}(n) &= y_{vdc}(n-1) + K_{pvdc}(e_{vdc}(n) - e_{vdc}(n-1)) + K_{ivdc}e_{vdc}(n) \\ &= I_{sd}^{*} \end{aligned} \tag{5.18}$$

The reference in-phase supply currents are expressed using in-phase voltage templates $u_{sda}, u_{sdb}, u_{sdc}$ as,

$$\begin{aligned} i_{sda}^{*} &= I_{sd}^{*} u_{sda} \\ i_{sdb}^{*} &= I_{sd}^{*} u_{sdb} \\ i_{sdc}^{*} &= I_{sd}^{*} u_{sdc} \end{aligned} \tag{5.19}$$

where $u_{sda}$, $u_{sdb}$ and $u_{sdc}$ are derived as,

$$\begin{aligned} u_{sda} &= \frac{v_{ab}}{V_{ps}} \\ u_{sdb} &= \frac{v_{bc}}{V_{ps}} \\ u_{sdc} &= \frac{v_{ca}}{V_{ps}} \end{aligned} \tag{5.20}$$

$V_{ps}$, the peak supply voltage is computed as,

$$V_{ps} = \left\{ \frac{2}{3}\left( v_{ab}^{2} + v_{bc}^{2} + v_{ca}^{2} \right) \right\}^{1/2} \tag{5.21}$$

### *5.4.2.2 Quadrature Current Component*

The reference peak quadrature supply current $I_{sq}^{*}$ is taken as the output $y_{vsm}$ of PI controller resulted in while processing the error $e_{vsm}$ over the actual $V_{ps}$ and its reference peak supply voltage $V_{ps}^{*}$. The voltage error at $n^{th}$ sampling instant for PI controller is as,

$$\begin{aligned} e_{vsm}(n) &= V_{ps}^{*}(n) - V_{ps}(n) \\ y_{vsm}(n) &= y_{vsm}(n-1) + K_{pvps}\left(e_{vsm}(n) - e_{vsm}(n-1)\right) + K_{ivps}e_{vsm}(n) \\ &= I_{sq}^{*} \end{aligned} \tag{5.22}$$

The quadrature components of the reference supply current are computed using $I_{sq}^{*}$ and quadrature templates $u_{sqa}, u_{sqb}$ and $u_{sqc}$ as,

$$\begin{aligned} i_{sqa}^{*} &= I_{sq}^{*} u_{sqa} \\ i_{sqb}^{*} &= I_{sq}^{*} u_{sqb} \\ i_{sqc}^{*} &= I_{sq}^{*} u_{sqc} \end{aligned} \tag{5.23}$$

The quadrature templates from in-phase templates are derived in Appendix-F. The quadrature and in-phase templates are related as,

$$\begin{bmatrix} u_{sqa} \\ u_{sqb} \\ u_{sqc} \end{bmatrix} = \begin{bmatrix} 0 & -1/\sqrt{3} & 1/\sqrt{3} \\ \sqrt{3}/2 & 1/2\sqrt{3} & -1/2\sqrt{3} \\ -\sqrt{3}/2 & 1/2\sqrt{3} & -1/2\sqrt{3} \end{bmatrix} \begin{bmatrix} u_{sda} \\ u_{sdb} \\ u_{sdc} \end{bmatrix} \tag{5.24}$$

The 3-ϕ reference supply currents are obtained by adding respective in-phase and quadrature components as,

$$\begin{bmatrix} i_{sa}^{*} \\ i_{sb}^{*} \\ i_{sc}^{*} \end{bmatrix} = \begin{bmatrix} i_{sda}^{*} \\ i_{sdb}^{*} \\ i_{sdc}^{*} \end{bmatrix} + \begin{bmatrix} i_{sqa}^{*} \\ i_{sqb}^{*} \\ i_{sqc}^{*} \end{bmatrix} \tag{5.25}$$

### *5.4.2.3 Hysteresis Band Current Controller*

The ON/OFF switching functions to obtain gating signals for IGBTs of the CC-VSC, as shown in Fig. 5.2, are derived from the carrier less Hysteresis controller. The switching function $S_a$ for phase 'a' is expressed as,

$$\begin{aligned} &\text{If } i_{sa} < \left(i_{sa}^{*} - HB\right) \;\; S_1 \text{ OFF}, \; S_4 \text{ ON} \Rightarrow S_a = 0 \\ &\text{If } i_{sa} > \left(i_{sa}^{*} + HB\right) \;\; S_1 \text{ ON}, \; S_4 \text{ OFF} \Rightarrow S_a = 1 \end{aligned} \tag{5.26}$$

where, $HB$ is the current band of controller.

Similarly, switching functions $S_b$ and $S_c$ can be derived for phase '*b*' and phase '*c*' respectively.

### *5.4.2.4 DC Bus Capacitor and Filter*

The STATCOM is a 3-ϕ CC-VSC with self-supporting DC bus employing suitable valued capacitor. The charging/discharging of DC bus capacitor is governed by,

$$pV_{dc} = \frac{\left(i_{ca}S_a + i_{cb}S_b + i_{cc}S_c\right)}{C_{dc}} \tag{5.27}$$

The DC bus voltage reflects on the AC side of the PWM converter in the form of voltages $e_a$, $e_b$ and $e_c$, which are expressed as,

$$\begin{bmatrix} e_a \\ e_b \\ e_c \end{bmatrix} = \frac{V_{dc}}{3}\begin{bmatrix} 2 & -1 & -1 \\ -1 & 2 & -1 \\ -1 & -1 & 2 \end{bmatrix}\begin{bmatrix} S_a \\ S_b \\ S_c \end{bmatrix} \tag{5.28}$$

The KVL equations for the AC side inductor filter are as,

$$\begin{aligned} v_{ab} &= R_f i_{ca} + L_f pi_{ca} + e_a - e_b - R_f i_{cb} - L_f pi_{cb} \\ v_{bc} &= R_f i_{cb} + L_f pi_{cb} + e_b - e_c - R_f i_{cc} - L_f pi_{cc} \end{aligned} \tag{5.29}$$

And $\quad i_{ca} + i_{cb} + i_{cc} = 0$

The eqn. (5.29) can be written in state space form as,

$$\begin{aligned} pi_{ca} &= \frac{\left\{\left(v_{bc} + 2v_{ab}\right) - \left(e_{bc} + 2e_{ab}\right) - 3R_f i_{ca}\right\}}{3L_f} \\ pi_{cb} &= \frac{\left\{\left(v_{bc} - v_{ab}\right) - \left(e_{bc} - e_{ab}\right) - 3R_f i_{cb}\right\}}{3L_f} \end{aligned} \tag{5.30}$$

where $e_{ab} = e_a - e_b$ and $e_{bc} = e_b - e_c$

### 5.4.3 Static R-L Load Model

The static load is expressed as delta connected load as shown in Fig. 5.3a and dynamic equations are as,

$$\begin{aligned} pi_{lab} &= (v_{ab} - R_l i_{lab})/L_l \\ pi_{lbc} &= (v_{bc} - R_l i_{lbc})/L_l \end{aligned} \tag{5.31}$$

and, $i_{lab}+i_{lbc}+i_{lca}=0$

where, $i_{lab}$, $i_{lbc}$ and $i_{lca}$ are the phase currents. The line currents $i_{rla}$, $i_{rlb}$ and $i_{rlc}$ are related with phase currents as,

$$\begin{aligned} i_{rla} &= i_{lab} - i_{lca} \\ i_{rlb} &= i_{lbc} - i_{lab} \\ i_{rlc} &= i_{lca} - i_{lbc} \end{aligned} \tag{5.32}$$

### 5.4.4 AC Dynamic Motor Load Model

The equations of the induction motor load in stationary q-d reference frame are similar to the induction generator discussed in the section 5.4.1 with parameters pertaining to an induction motor load. These equations, while written in state space form are as,

$$p[\mathbf{i}_m] = [\mathbf{L}_m]^{-1}\left([\mathbf{v}_m] - [\mathbf{r}_m][\mathbf{i}_m] - [\mathbf{G}_m][\mathbf{i}_m]\right) \tag{5.33}$$

$$p\omega_{rm} = \frac{P_m}{2J_m}\left(T_{emm} - T_L\right) \tag{5.34}$$

### 5.4.5 Controlled Rectifier Fed DC Dynamic Motor Load Model

The model equations for DC motor load and controlled rectifier are briefed in this section.

#### *5.4.5.1 DC Motor Load*

If $v_a$ is applied voltage to the armature terminals of the separately excited DC motor, the armature current $i_a$ is determined by $v_a$, the induced back-emf $e_B$, the armature winding resistance $R_a$ and armature winding inductance $L_a$. The governing equation in state space form is as,

$$pi_a = \frac{1}{L_a}\left(v_a - e_B - i_a R_a\right) \tag{5.35}$$

The motor speed is build up by interaction of electromagnetic torque $T_{emd}$ and output load torque $T_L$ as,

$$p\omega_{rd} = \frac{P_d}{2J_d}\left(T_{emd} - T_L\right) \tag{5.36}$$

where, $J_d$ is the total equivalent inertia of the DC motor-load combination.

#### *5.4.5.2 Controlled bridge rectifier*

The controllable DC voltage, obtained from controlled rectifier is applied to DC motor. Such type of arrangement is used in the industry and the two quadrant operation of drive is achieved with this type of configuration.

- *Phase angle of generated voltage of SEIG*

The generated terminal voltage of SEIG $v_{sabc} = [v_{ab} \quad v_{bc} \quad v_{ca}]^T$ from eqn. (5.17) is transformed in to q-d axis variables ($v_{qs}$, $v_{ds}$) in stationary reference frame and the phase angle of voltage is calculated as,

$$\theta = \tan^{-1}\left(v_{ds}/v_{qs}\right) \tag{5.37}$$

The angle $\theta$ is essential for generating switching functions for thyristors of the controlled rectifier feeding a DC motor load.

- *Switching functions of bridge rectifier*

The thyristors in a controlled rectifier are divided in two groups namely odd group thyristors ($T_1$, $T_3$ & $T_5$) and even group thyristors ($T_2$, $T_4$ & $T_6$) are marked. The conduction angle of thyristors ($T_1$ to$T_6$) are governed by firing angle α and illustrated for α=60° in Table 5.3.

***Table 5.3 Conduction sequence of thyristors in controlled rectifier***

| | | | | | | | | | | | | |
|---|---|---|---|---|---|---|---|---|---|---|---|---|
| Odd group Thyristor conduction region | $T_5$ | | | | $T_1$ | | | | $T_3$ | | | |
| Even group Thyristor conduction region | $T_4$ | | $T_6$ | | | | $T_2$ | | | | $T_4$ | |
| Angle ($\theta$) | 0 | $\pi/3$ | | $2\pi/3$ | | $\pi$ | | $4\pi/3$ | | $5\pi/3$ | | $2\pi$ |

Depending upon the switching states of different thyristors on particular moment, $v_a$ can be easily calculated as:

$T1$ is 'ON' and $T6$ is 'ON', $v_a = v_{ab}$ (5.38)

The AC side currents of fully controlled rectifier fed DC motor are as,

$$\begin{aligned} i_{da} &= \left(T_1 + T_4\right) i_a \\ i_{db} &= \left(T_3 + T_6\right) i_a \\ i_{dc} &= \left(T_5 + T_2\right) i_a \end{aligned} \tag{5.39}$$

where, $i_a$ is the armature current of DC motor.

The complete SEIG system model is therefore represented by the state space equations along with the other important expressions from eqns. (5.15) to (5.39). These equations are solved by fourth order Runge-Kutta integration method in MATLAB environment.

## 5.5 ALGORITHM FOR SIMULATING SEIG-STATCOM PERFORMANCE

The algorithm for simulating the transient performance of SEIG-STATCOM system feeding static R-L load is briefly explained.

1. Read the SEIG parameters, its magnetizing characteristic, shunt capacitance $C_{sh}$, Static load resistance and reactance, time for connecting the STATCOM ($t_{STC}$), time for load connection ($t_{RL}$), time for load changing ($t_{RLC}$), total simulation time ($t_T$), time step ($\Delta t$). Also read the STATCOM parameters, DC voltage PI controller gains ($K_{pvdc}$, $K_{ivdc}$) terminal voltage PI controller gains ($K_{pvps}$, $K_{ivps}$).

2. Set $t$=0, $[i_{qs} \quad i_{ds}]^T = [0.0001 \quad 0.0001]^T$ to account residual magnetism, voltage buildup resistance ($R_{lvb}$)=20000.0.

3. Compute $i_M$, $L_M$ and obtain $[\mathbf{L}]$ and $[\mathbf{G}]$ accounting the effect of saturation.

4. If $t < t_{STC}$, evaluate seven derivatives as $p[\mathbf{i}]$, $p\omega_r$, $pv_{ab}$, $pv_{bc}$ for no load voltage buildup and go to step 9.

5. Detect the zero crossing instant and sense the $V_{dc}$, $v_{ab}$ $v_{bc}$ and $v_{ca}$ and calculate the peak terminal voltage ($V_{ps}$) using eqn. (5.21) from sensed terminal voltages $v_{ab}$, $v_{bc}$ and $v_{ca}$.

6. Generate the gating signals for the six IGBTs of STATCOM from the control scheme depicted in Fig. 5.4.

7. If $t<t_{RL}$, evaluate ten derivatives as $p[\mathbf{i}]$, $p\omega_r$, $pv_{ab}$, $pv_{bc}$, $pV_{dc}$, $pi_{ca}$, $pi_{cb}$ for switching of STATCOM in the system,

   else evaluate twelve derivatives as $p[\mathbf{i}]$, $p\omega_r$, $pv_{ab}$, $pv_{bc}$, $pV_{dc}$, $pi_{ca}$, $pi_{cb}$, $pi_{lab}$, $pi_{lbc}$ for connection of load to the SEIG-STATCOM system.

8. If $t>t_{RLC}$, change the load parameters $R_l$ and $L_l$.

9. Compute the instantaneous values by fourth order Runge-Kutta method.

10. Express generator currents into phase variables and evaluate line currents, store the necessary variables.

11. If $t<t_T$, than $t=t+\Delta t$, and go to step 3.

12. Plot the required waveforms.

The simulation algorithm is modified accordingly for dynamic IM load and controlled rectifier fed DC motor load.

## 5.6 RESULTS AND DISCUSSION

The investigations have been carried out on 3.7 kW induction machine operated as SEIG, driven by prime-mover with $T_P = 6200 - 20\omega_r$. The parameters of SEIG, IM load and DC motor load are given in Appendix-A. The results of the system dynamics are being discussed with AC motor load and controlled rectifier fed DC motor load in following sub sections.

### 5.6.1 System Performance with Full Rating STATCOM

The full rating STATCOM parameters for R-L load of 2.2 kW, 0.8 pf, 1.5 kW induction motor load and controlled rectifier fed 1.5 kW DC motor load are given in Table 5.1.

#### *5.6.1.1 Voltage Buildup and Switching of STATCOM*

The no load voltage buildup with the capacitance $C_{NL}$, i.e. 16.1 μF, and subsequent application of STATCOM is shown in Fig. 5.5. During the voltage build-up, the DC bus capacitor $C_{dc}$ is also charged and the voltage across $C_{dc}$ increases but attains value lower than the reference DC bus voltage $V_{dc}^*$ kept as 700 V. The charging of $C_{dc}$ is due to $i_{sa}$, which is the current at the point of common coupling, during the build up process. When the STATCOM is switched into the system at 2.0 sec., the $V_{dc}$ reaches its reference value after momentary transients. Once the capacitor is charged to reference level, the magnitude of current $i_{sa}$, which is the sum of the load and compensation currents, reduces considerably.

### *5.6.1.2 Performance with Static Resistive-Inductive Load*

The value of $C_{dc}$ taken for simulation is slightly higher than maximum designed value among considered loads, which ensures some safety margins for successful operation during transient operation. The performance characteristic of SEIG-full rating STATCOM for application and rejection of 0.8 pf static R-L load is shown in Fig. 5.6.

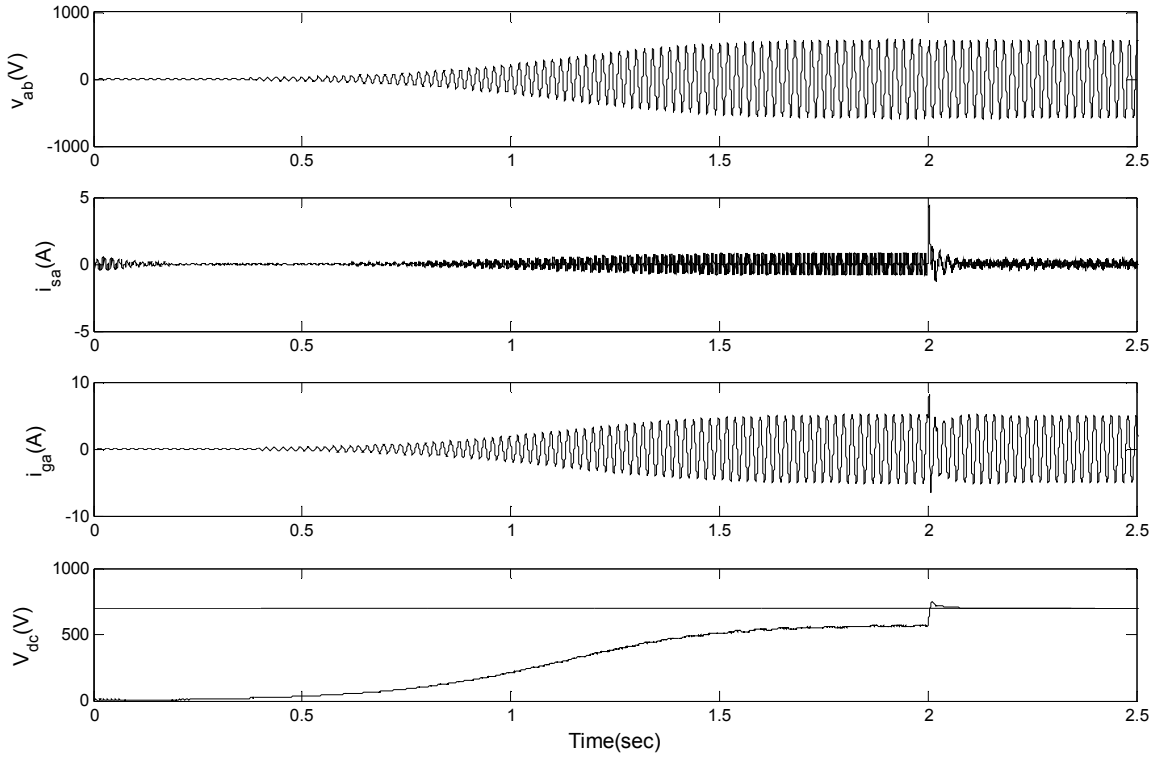


***Fig. 5.5 Performance characteristics during voltage buildup and the switching of full rating STATCOM***

The static 0.8 pf R-L load of 2.2 kW at 2.5 sec., 3.0 kW at 3.0 sec. and 2.2 kW at 3.5 sec. is applied to SEIG-full rating STATCOM system. Due to the sudden application of 2.2 kW load at 2.5 sec., transients are observed in the generator current $i_{ga}$, compensation current $i_{ca}$ and DC bus voltage $V_{dc}$, which are settled down after 5-6 cycles. The DC bus voltage decreases to 500 V momentarily and after some transients gradually increases to the reference level. The load is increased to 3.0 kW at 3.0 sec., which is taken care without any appreciably transients owing to incremental safety margin considered in $C_{dc}$ for providing required reactive power. The currents $i_{ga}$, $i_{rla}$, $i_{ca}$ are increased correspondingly, however $V_{dc}$ reduces momentarily to 630 V due to increase of load and returns to reference value with the PI controller action. The load is reduced to 2.2 kW at

3.5 sec., which is successfully taken care by the system without any noticeable transients but the $V_{dc}$ momentarily rises to 760 V and returns to reference mark.

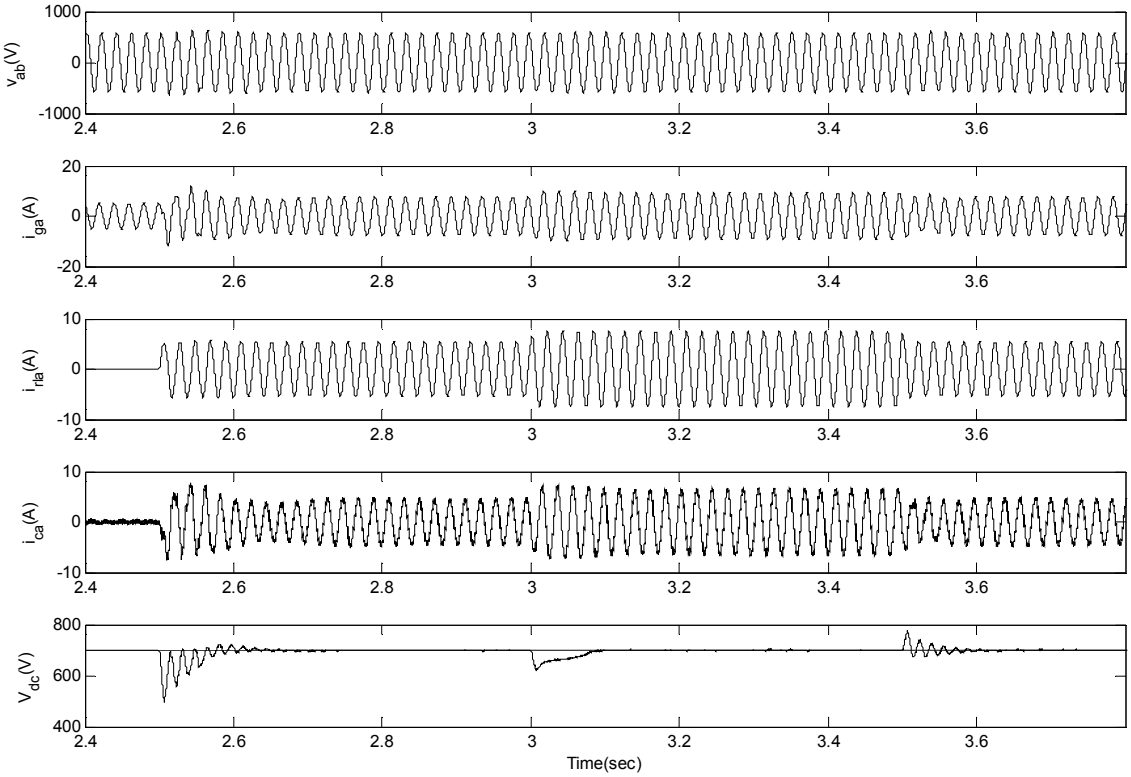


***Fig. 5.6 Performance characteristics of SEIG-full rating STATCOM with 0.8 pf R-L load***

***(Load conditions : 2.2 kW at 2.5 sec., 3.0 kW at 3.0 sec., and 2.2 kW at 3.5 sec.)***

### *5.6.1.3 Performance with AC Dynamic Motor load*

A 1.5 kW induction machine is operated as a motor load and its parameters are given in Appendix-A. The values of capacitance calculated for SEIG-IM configuration under no load and rated load on the motor are $C_{NL}$ =16.1 μF and $C_{FL}$ =26.5 μF respectively. The characteristics showing the voltage buildup with $C_{FL}$ and consequently the switching on of an induction motor is shown in Fig. 5.7. The motor is unable to starting even with $C_{FL}$, which is the capacitance corresponding to the rated motor load under steady state, and results into a voltage collapse. This is because the capacitor bank, which is only the source of the reactive power, unable to meet the excessive VAR requirements of the SEIG and the motor load during starting transient. The successful starting of the motor load is resulted in when capacitance is more than 36.3 $\mu F$, which is more than twice the $C_{NL}$.

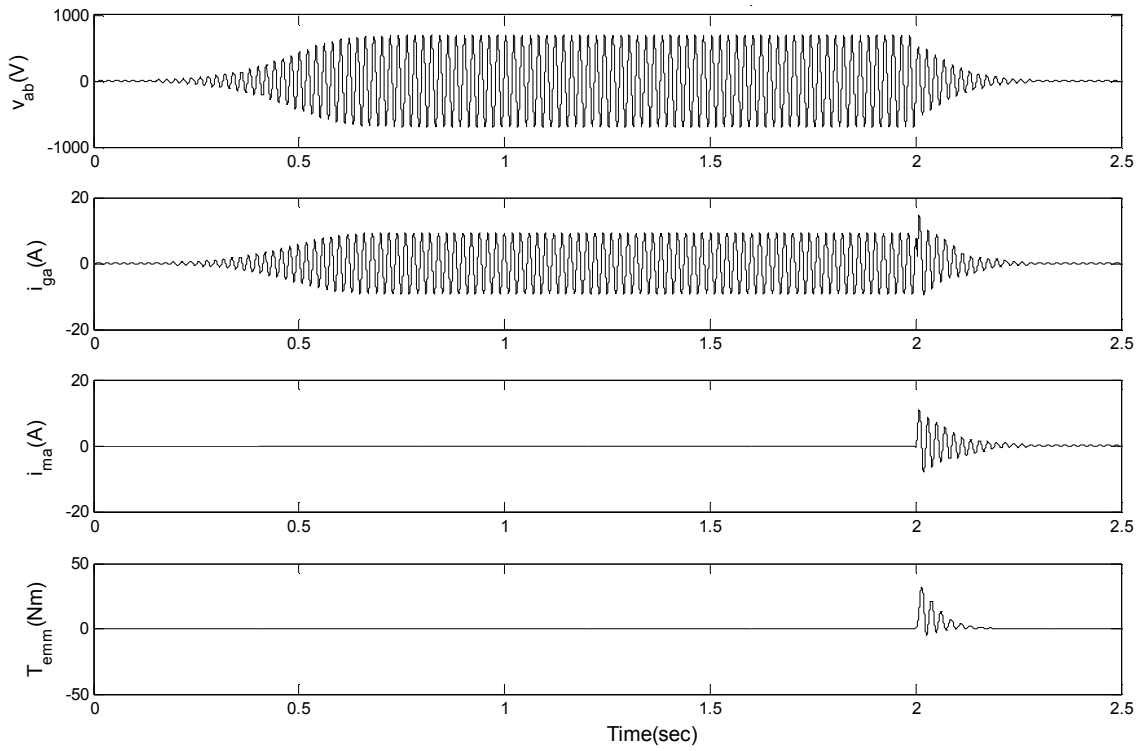


***Fig. 5.7 Performance characteristics of SEIG feeding 1.5 kW induction motor load with unsuccessful starting***

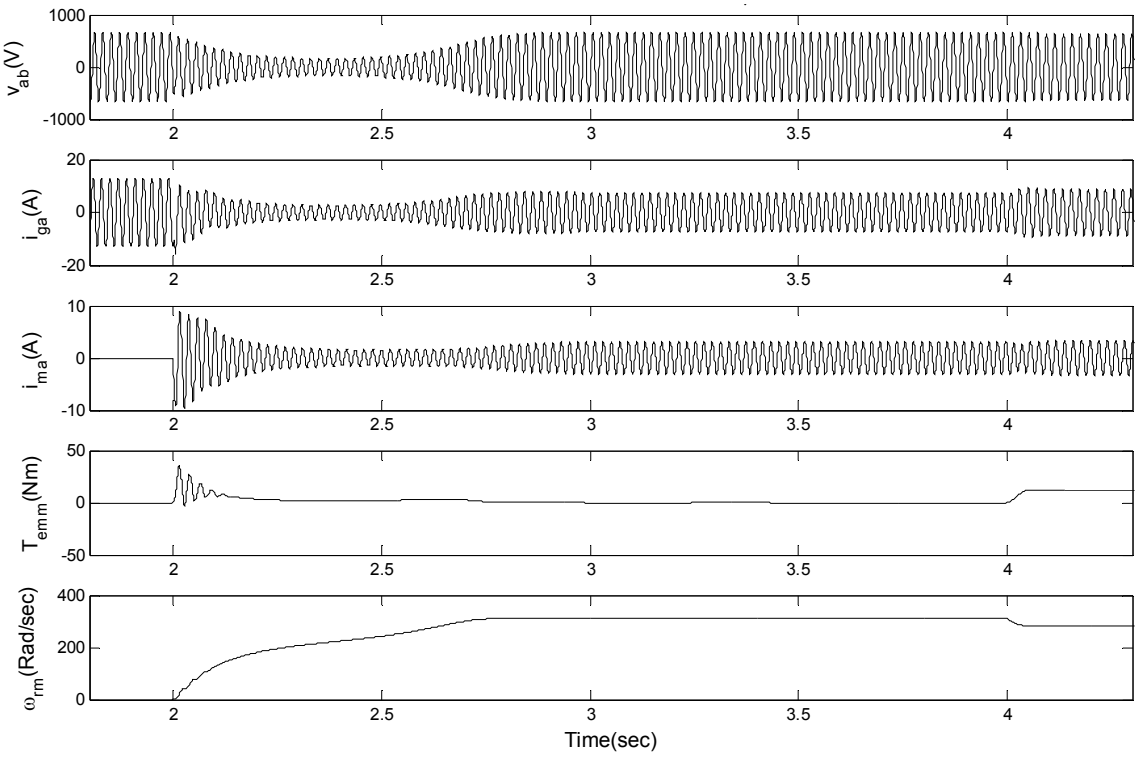


***Fig. 5.8 Performance characteristics of SEIG feeding 1.5 kW motor load with successful starting and full mechanical loading***

***(Load conditions : $T_L$=0 at 2.0 sec. and $T_L$=rated torque at 4.0 sec.)***

The successful starting and subsequent mechanical loading on an induction motor corresponding to 36.3 μF is shown in Fig. 5.8. Although the successful starting is resulted in, the terminal voltage reduces to about 0.25 pu. and the induction motor takes about 0.7 second to stabilize the starting transients. This excessive dip in the voltage level and longer time duration for the starting are the serious quality concerns, which are taken care of using the developed strategy for the STATCOM based voltage regulator. Due to the dynamic nature of the induction motor load, high inductive current results into significant supply voltage dip. This increases the loading on SEIG and reduces the VARs that can be supplied by the shunt capacitor, therefore high reactive VARs to be supplied for successful operation.

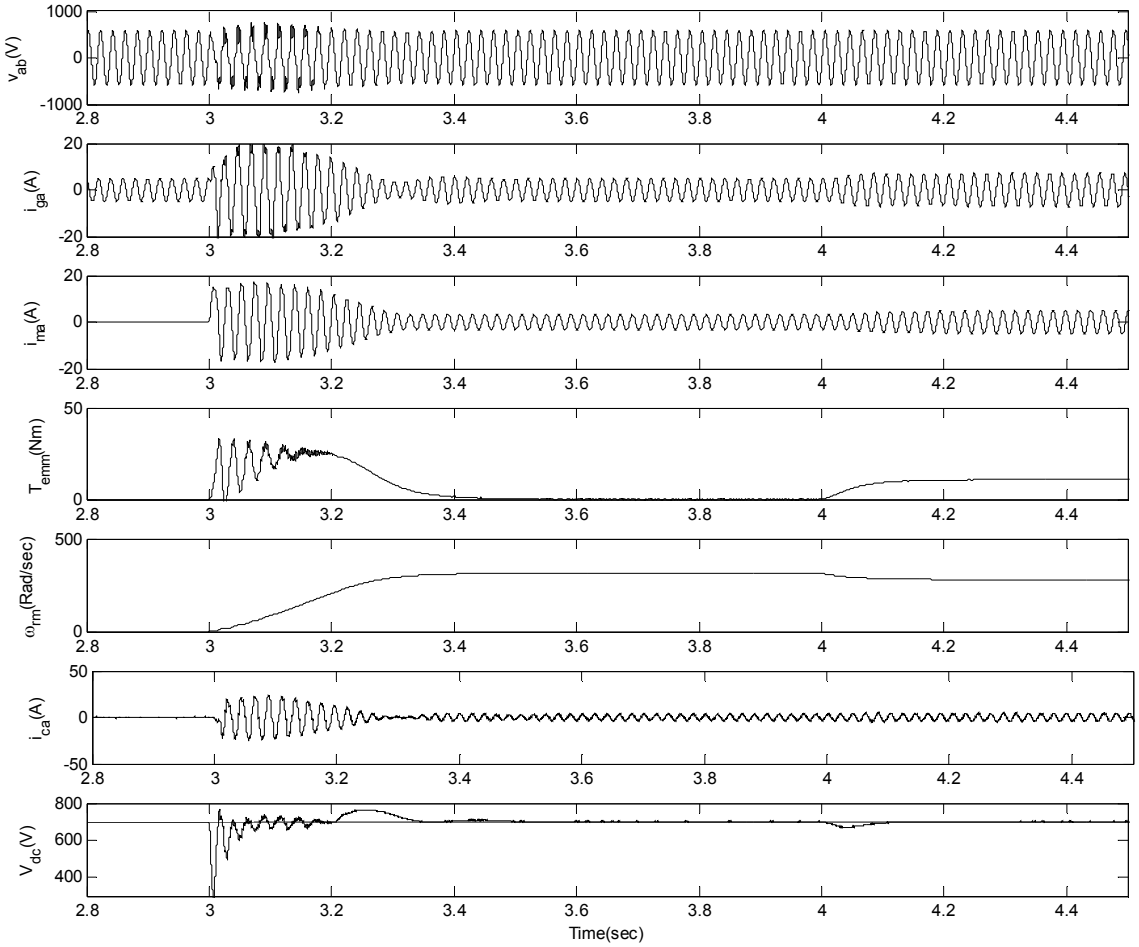


***Fig. 5.9 Performance characteristics of SEIG-full rating STATCOM with induction motor load***

***(Load conditions : $T_L$=0 at 3.0 sec. and $T_L$=rated torque at 4.0 sec.)***

The performance characteristics during the starting of an induction motor load and sudden mechanical loading on the motor on SEIG-STATCOM system are shown in Fig.

5.9. The motor load is applied at 3.0 sec. The application of the motor load results into few cycles of obvious transient disturbance however system returns to steady state after replenishing the charge on DC bus capacitor. During the starting of the motor, excessive reactive VARs are drawn, which results into reduction of $V_{dc}$ to 300 V level, than quickly rises to 760 V before returns back to reference level.

The starting of the motor is attained in 0.40 sec. with only 6% decrease in SEIG voltage which decreases to 30% level without STATCOM. The SEIG is now loaded with a rated motor load at 4.0 sec., which results into increase in the motor current, a decrease in the speed and increase in electromagnetic torque correspondingly without any significant transients. The $V_{dc}$ momentarily decreases to 670 V, which quickly returns to reference value under the control action. The performance of SEIG-IM configuration is compared with and without STATCOM for the AC dynamic motor load and the quality parameters are summarized in Table 5.4.

### *5.6.1.4 Performance with Controlled Rectifier Fed DC Dynamic Motor Load*

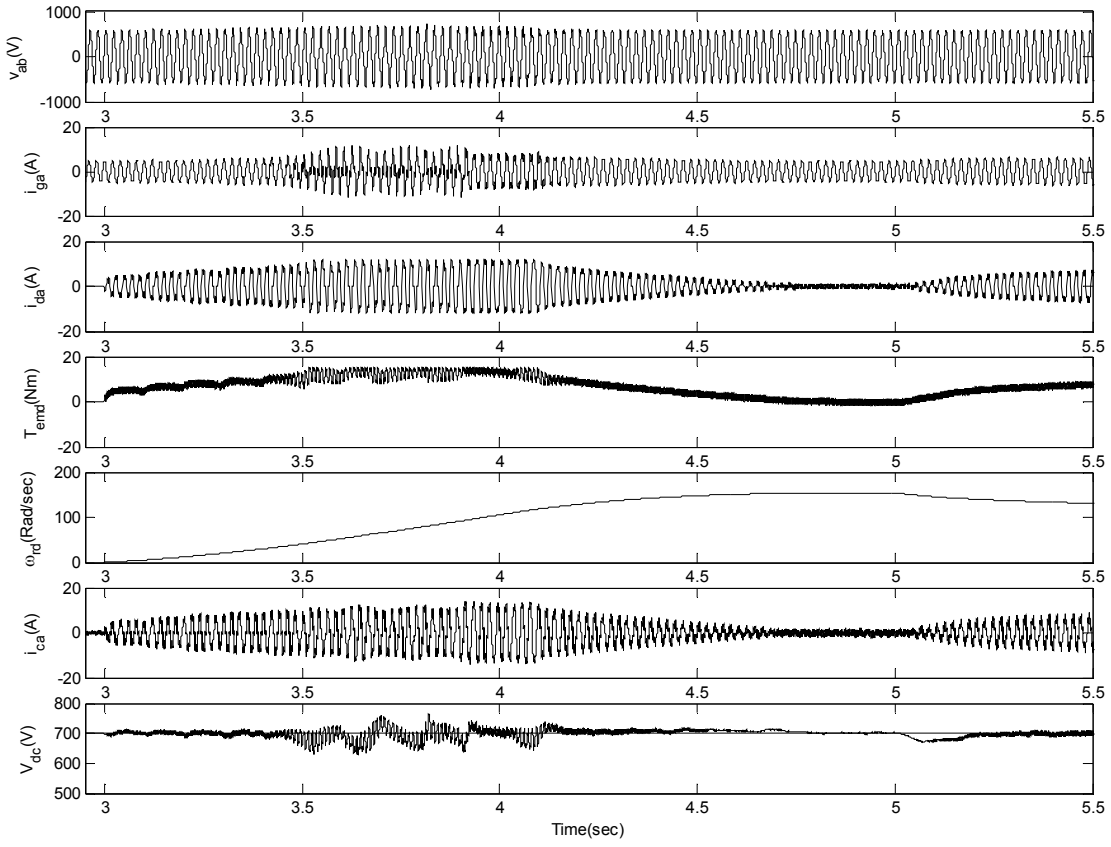


***Fig. 5.10 Performance characteristics of SEIG-full rating STATCOM with controlled rectifier fed DC motor load***

***(Load conditions : $T_L$=0 at 3.0 sec. and $T_L$=rated torque at 5.0 sec.)***

The performance characteristics of SEIG-full rating STATCOM feeding a controlled rectifier fed DC motor are shown in Fig. 5.10. The DC motor load is connected at 3.0 sec, and the soft starting is performed by gradual change of firing angle from 90° to 70° in 1.2 sec. Due to soft starting, the armature current is not surging to very high value and therefore the electromagnetic torque developed remains within limits. After the application of a motor load, observable transients are experienced in the generator current $i_{ga}$ due to rise in load current $i_{da}$, but DC bus voltage $V_{dc}$ is not decreased appreciably owing to soft starting of the DC motor and remains within 640V-740V. The speed of the motor gradually increases and the starting is achieved in 1.6 sec. The SEIG is now loaded by loading the DC motor with mechanical load of 10 Nm at 5.0 sec., which results into correspondingly increase in the motor current, an increase in compensation current, the decrease in DC motor speed and an increase in electromagnetic torque of the DC motor without much significant transients. The DC bus voltage shortly falls to 680V due to loading but gradually returns back to reference value.

### 5.6.2 System Performance with Reduced Rating STATCOM

The performance of SEIG with a reduced rating STATCOM is studied for static resistive-inductive, an induction motor and a controlled rectifier fed DC motor loads. The half of the VAR requirement is supplied by STATCOM and additional capacitance corresponding to half of the VAR requirement is connected across the load. The design parameters of reduced rating STATCOM for 2.2 kW, 0.8 pf R-L load, an induction motor load and an uncontrolled rectifier fed DC motor loads are summarized in Table 5.2.

#### *5.6.2.1 Performance with Static Resistive-Inductive Load*

The performance of SEIG-reduced rating STATCOM for feeding static 0.8 pf resistive-inductive load of 2.2 kW at 2.5 sec., 3.0 kW at 3.0 sec., and 2.2 kW at 3.5 sec. is shown in Fig. 5.11. The application of 2.2 kW load at 2.5 sec. is causing visible transients in $v_{ab}$, $i_{ga}$ and $V_{dc}$. The $V_{dc}$ changes in between 480 V-800 V and later returns to reference value with the DC bus PI controller action. The steady state condition is reached around 0.25 sec. as compared to 0.12 sec. with SEIG-full rating STATCOM system. The static load is increased to 3.0 kW at 3.0 sec., and taken care by STATCOM without any major disturbance owing to margin taken in $C_{dc}$, to provide a reactive power during transient conditions. The currents $i_{ga}$, $i_{rla}$ and $i_{ca}$ are increased correspondingly, whereas $V_{dc}$ decreases to 630 V at once and gradually returns to reference value. The load is reduced

to 2.2 kW at 3.5 sec., which changes the dynamics of system correspondingly after a small transient period and afterward the system attains steady state condition.

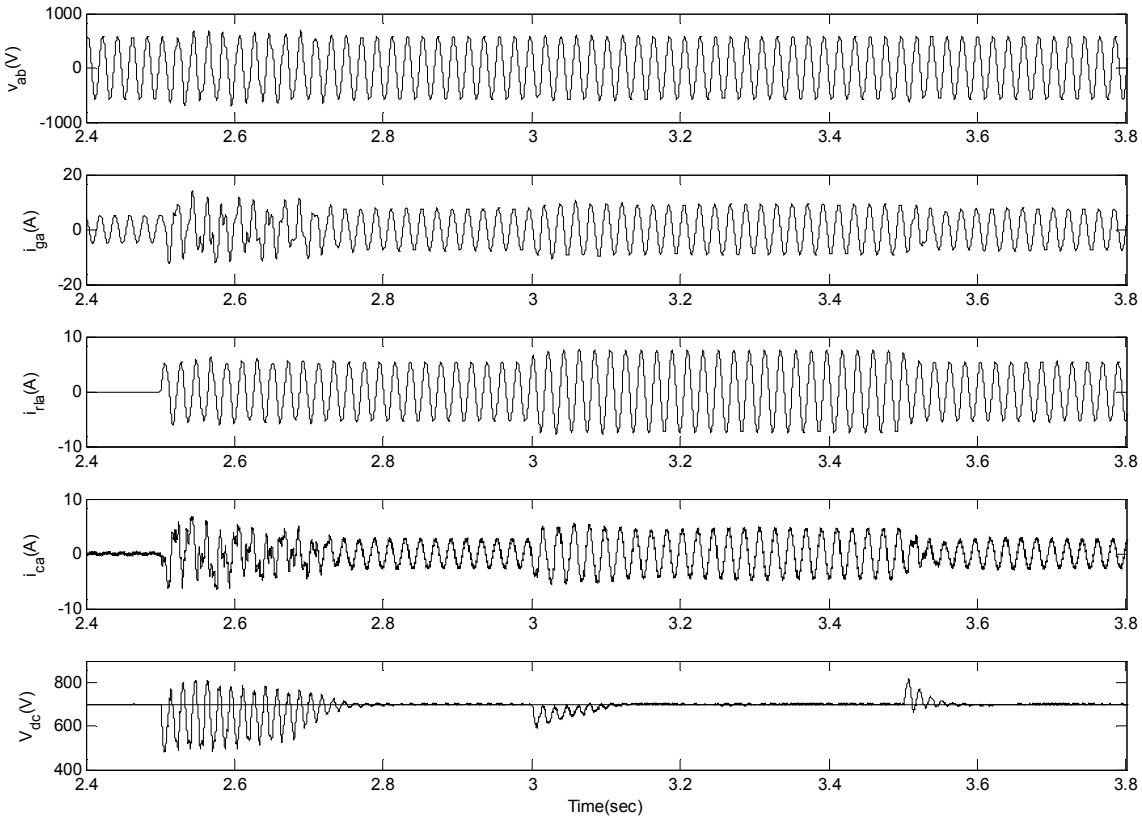


***Fig. 5.11 Performance characteristics of SEIG-reduced rating STATCOM with 0.8 pf static R-L load***

***(Load conditions : 2.2 kW at 2.5 sec., 3.0 kW at 3.0 sec. and 2.2 kW at 3.5 sec.)***

### *5.6.2.2 Performance with AC Dynamic Motor Load*

The performance of SEIG-reduced rating STATCOM for feeding an induction motor load is shown in Fig. 5.12. The sudden application of an induction motor load at 3.0 sec. is causing significant transients in $v_{ab}$, $i_{ga}$, $i_{ma}$, $T_{emm}$ and $V_{dc}$, owing to half rating of STATCOM and additional uncharged capacitor connected across the load terminals. With reduced rating STATCOM system, the generator voltage dip is around 10% and the transients are settled in around 0.5 sec. as compared to 0.4 sec. for full rating STATCOM system. Because of lower compensation level, the $i_{ca}$ in steady state is lesser as compared to full rating STATCOM system. The $V_{dc}$ decreases to 300 V and later returns to reference value of 700 V. The induction motor is loaded with full mechanical load at 4.0 sec. After small transients, the system response changes accordingly, as $i_{ga}$, $i_{ma}$, $T_{emm}$ are

increased, $\omega_{rm}$ decreases and $V_{dc}$ decreases to 670 V before returns to steady state condition.

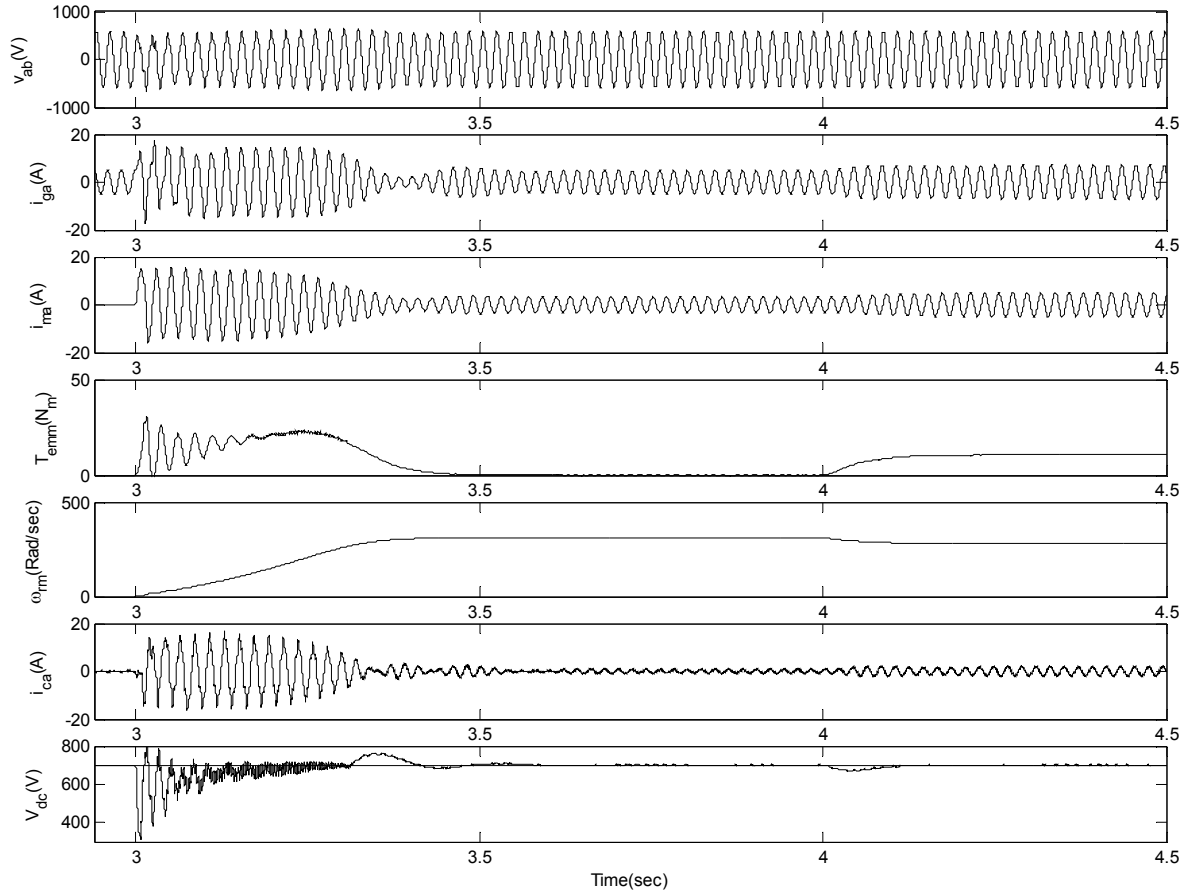


***Fig. 5.12 Performance characteristics of SEIG-reduced rating STATCOM with induction motor load***

***(Load conditions : $T_L$=0 at 3.0 sec. and $T_L$=rated torque at 4.0 sec.)***

***Table 5.4 Key parameters comparison for AC motor load***

| Performance index | Without STATCOM | With full rating STATCOM | With reduced rating STATCOM |
|---|---|---|---|
| Line voltage dip at starting | 70% | 6% | 10% |
| Starting time | 0.7 sec. | 0.4 sec. | 0.5 |
| Supply current THD at full motor load | NA | < 0.3% | < 0.3% |

### *5.6.2.3 Performance with Controlled Rectifier Fed DC Dynamic Motor Load*

The performance of SEIG-reduced rating STATCOM feeding controlled rectifier fed DC motor is shown in Fig. 5.13. With the application of load, the $V_{dc}$ rises to 760 V

and showing large variation over the reference DC bus voltage. The mechanical load of 10 Nm is connected at 5.0 sec., which is causing a dip in $V_{dc}$ to 670 V. The harmonics in generator voltage and current are higher owing to limited capacity of STATCOM. The system performance with reduced rating STATCOM has also found satisfactory under non-linear load.

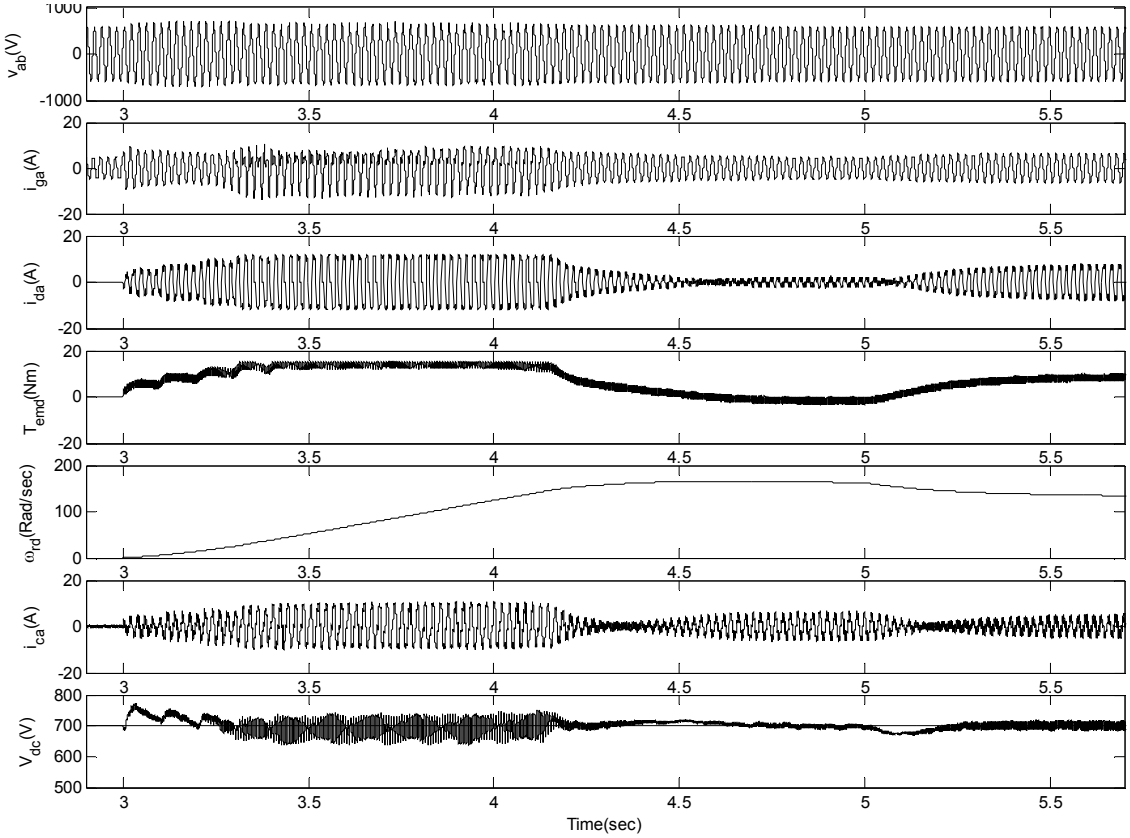


***Fig. 5.13 Performance characteristics of SEIG-reduced rating STATCOM with controlled rectifier fed DC motor load***

***(Load conditions : $T_L$=0 at 3.0 sec. and $T_L$=rated torque at 5.0 sec.)***

### 5.6.3 Power Quality Performance

The quality of voltage and current at the generator and the loads is assessed using harmonic spectra and total harmonic distortion (THD), obtained through fast Fourier transform (FFT) of the relevant waveforms. A MATLAB discrete Fourier transform (DFT) algorithm is used to estimate harmonics component under steady state condition.

#### *5.6.3.1 Harmonic spectra for SEIG-STATCOM fed 0.8 pf R-L load*

The steady state waveforms and harmonic spectra of generator voltage $v_{ab}$ and generator current $i_{ga}$ are shown in Fig. 5.14 and Fig. 5.15 for SEIG-full rating STATCOM

and SEIG-reduced rating STATCOM feeding static 0.8 pf resistive-inductive load respectively. The harmonic spectra consist of mainly fundamental component and negligible harmonic components. The THD in $v_{ab}$, $i_{ga}$ for the full rating STATCOM system and the reduced rating STATCOM system are 0.85%, 0.68% and 1.04%, 1.45% respectively. The THD in the generator quantities is on slightly higher side because the designed parameters of STATCOM are corresponding to 2.2 kW, 0.8 pf static R-L loads.

### *5.6.3.2 Harmonic spectra for SEIG-STATCOM fed induction motor load*

The steady state waveforms and harmonic spectra of $v_{ab}$ and $i_{ga}$ are shown in Fig. 5.16 and Fig. 5.17 for SEIG-full rating STATCOM and SEIG-reduced rating STATCOM feeding induction motor load respectively. The THD in $v_{ab}$, $i_{ga}$ for the full rating STATCOM system and the reduced rating STATCOM system are 0.26%, 0.27% and 0.33%, 0.35% respectively.

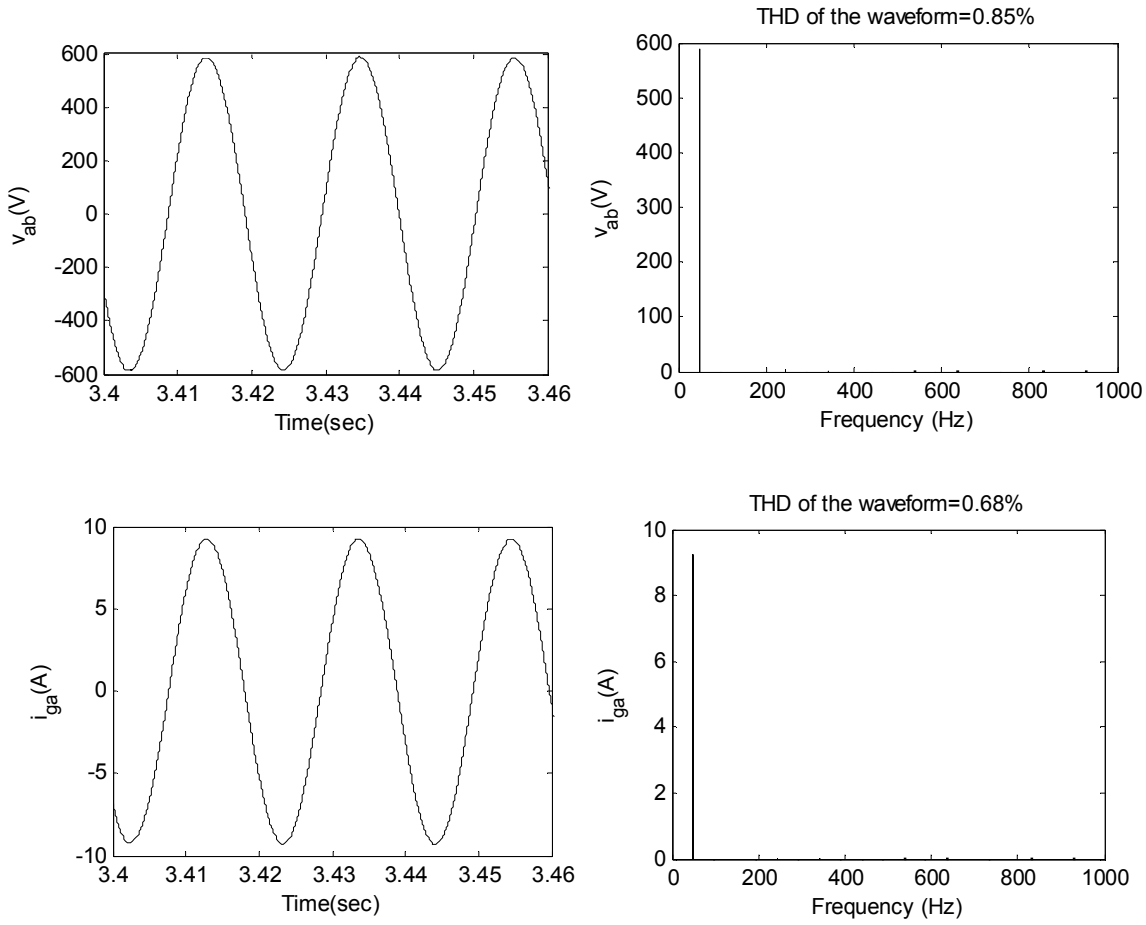


***Fig. 5.14 Harmonic spectra of generator voltage and current during steady state for SEIG-full rating STATCOM fed 3.0 kW static R-L load***

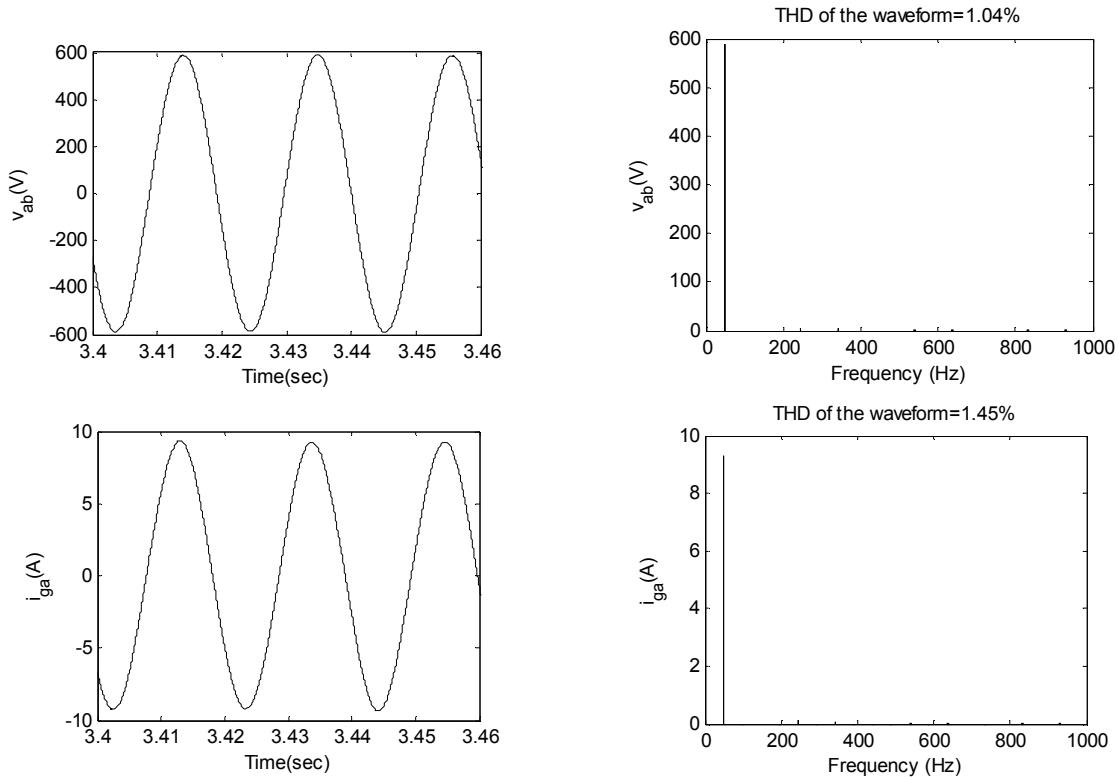


***Fig. 5.15 Harmonic spectra of generator voltage and current during steady state for SEIG- reduced rating STATCOM fed 3.0 kW static R-L load***

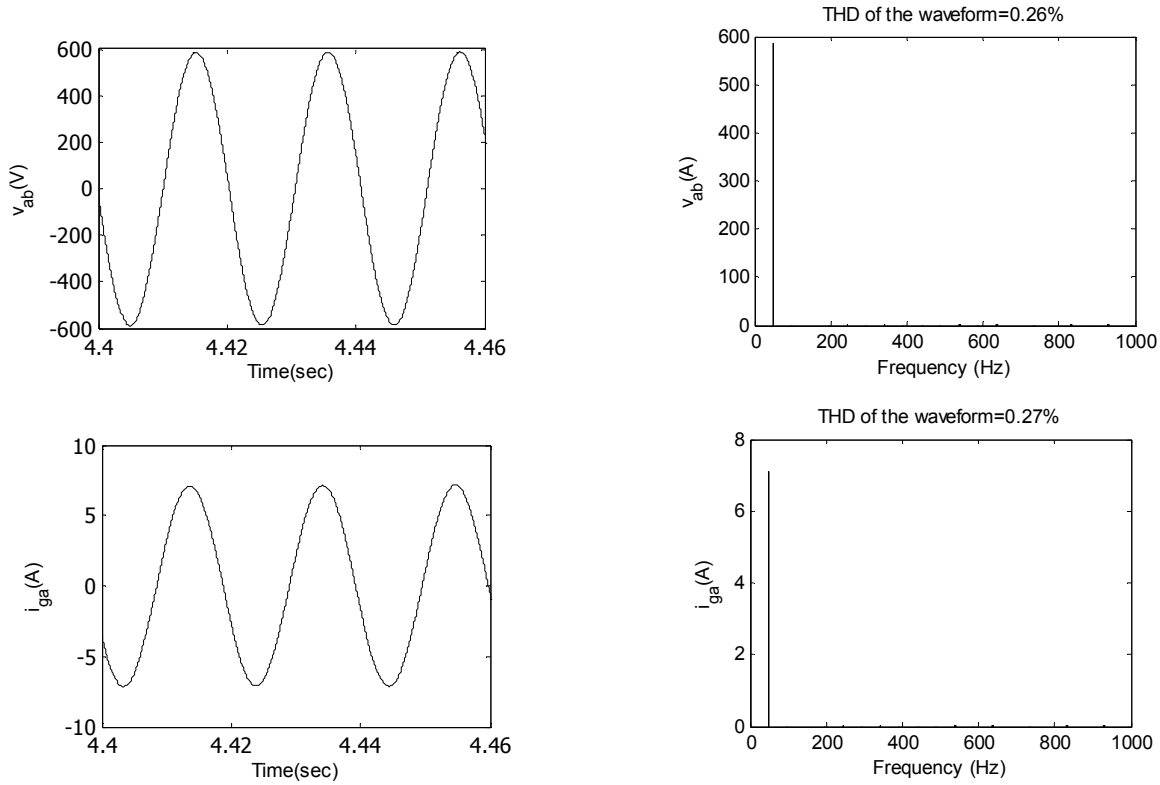


***Fig. 5.16 Harmonic spectra of generator voltage and current during steady state for SEIG- full rating STATCOM fed induction motor load***

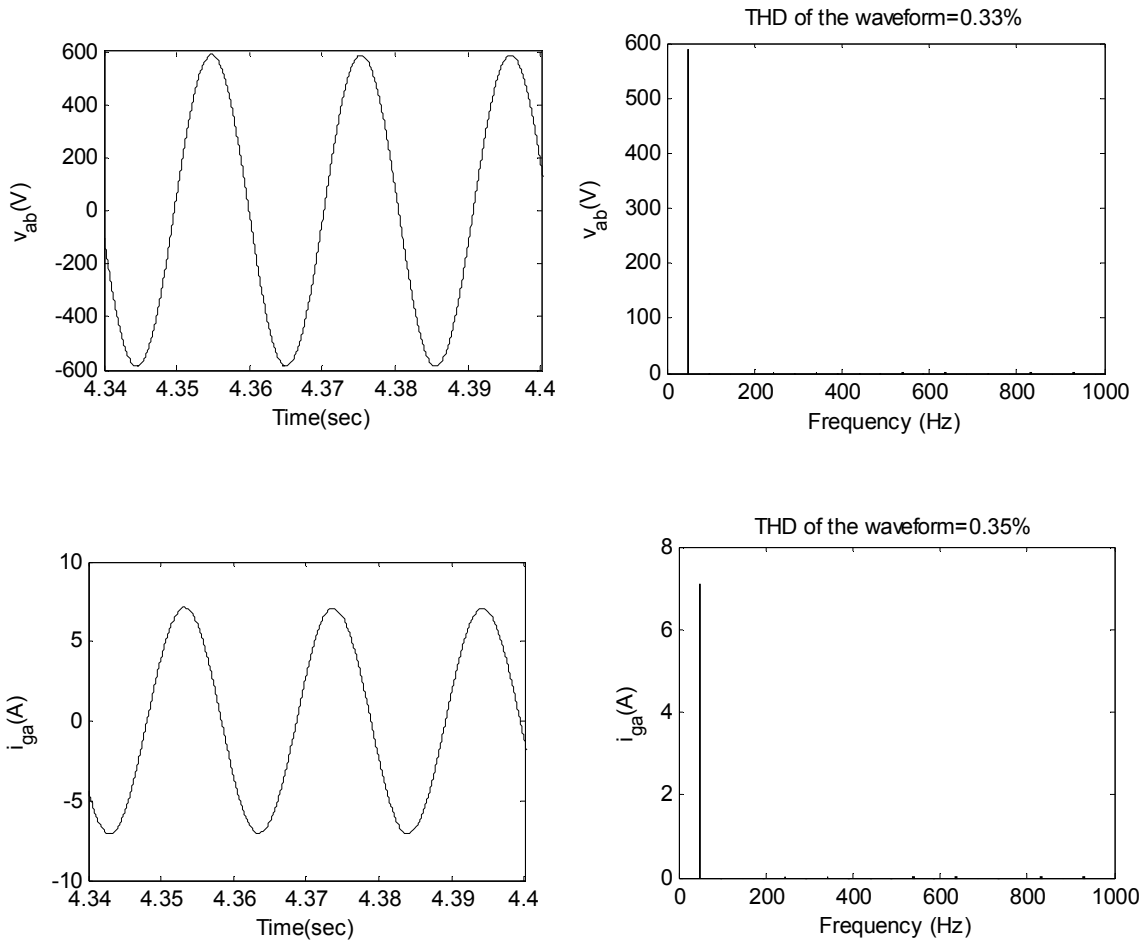


***Fig. 5.17 Harmonic spectra of generator voltage and current during steady state for SEIG- reduced rating STATCOM fed induction motor load***

### *5.6.3.3 Harmonic spectra for SEIG-STATCOM with controlled rectifier fed DC motor load*

The steady state waveforms along with harmonic spectra of $i_{da}$, $v_{ab}$ and $i_{ga}$ for the full rating STATCOM and reduced rating STATCOM with controlled rectifier fed DC motor load are shown in Fig. 5.18 and Fig. 5.19 respectively. The THD in the $i_{da}$ comes out to be 37.36%, while $v_{ab}$ and $i_{ga}$ are having 0.97% and 1.13% under no load condition of the DC motor with full rating STATCOM. The THD in $i_{da}$, $v_{ab}$ and $i_{ga}$ for reduced rating STATCOM are 38.97%, 1.62% and 3.02% respectively. The THD level in the generator quantities under mechanical loading of DC motor is also calculated and comes out to be less than 5%, which is clearly showing the distortion level in the generator line current and voltage are well within permissible level.

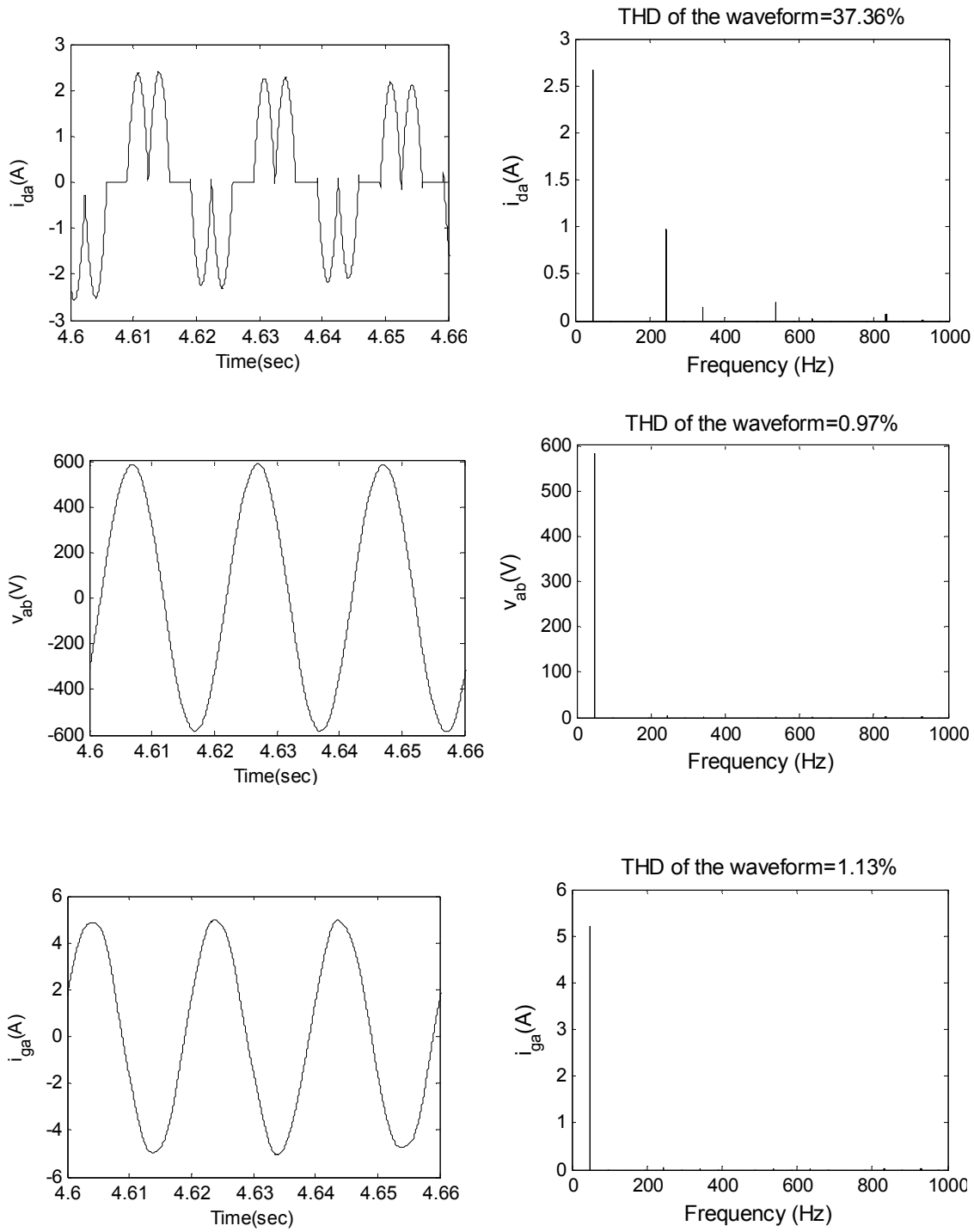


***Fig. 5.18 Harmonic spectra during steady state for SEIG- full rating STATCOM with controlled rectifier fed DC motor load***

The THD values for SEIG system with full rating and reduced rating STATCOM feeding various loads are summarized in Table 5.5. The generator side THD values are within the permissible level, which demonstrates the overall system performance is satisfactory.

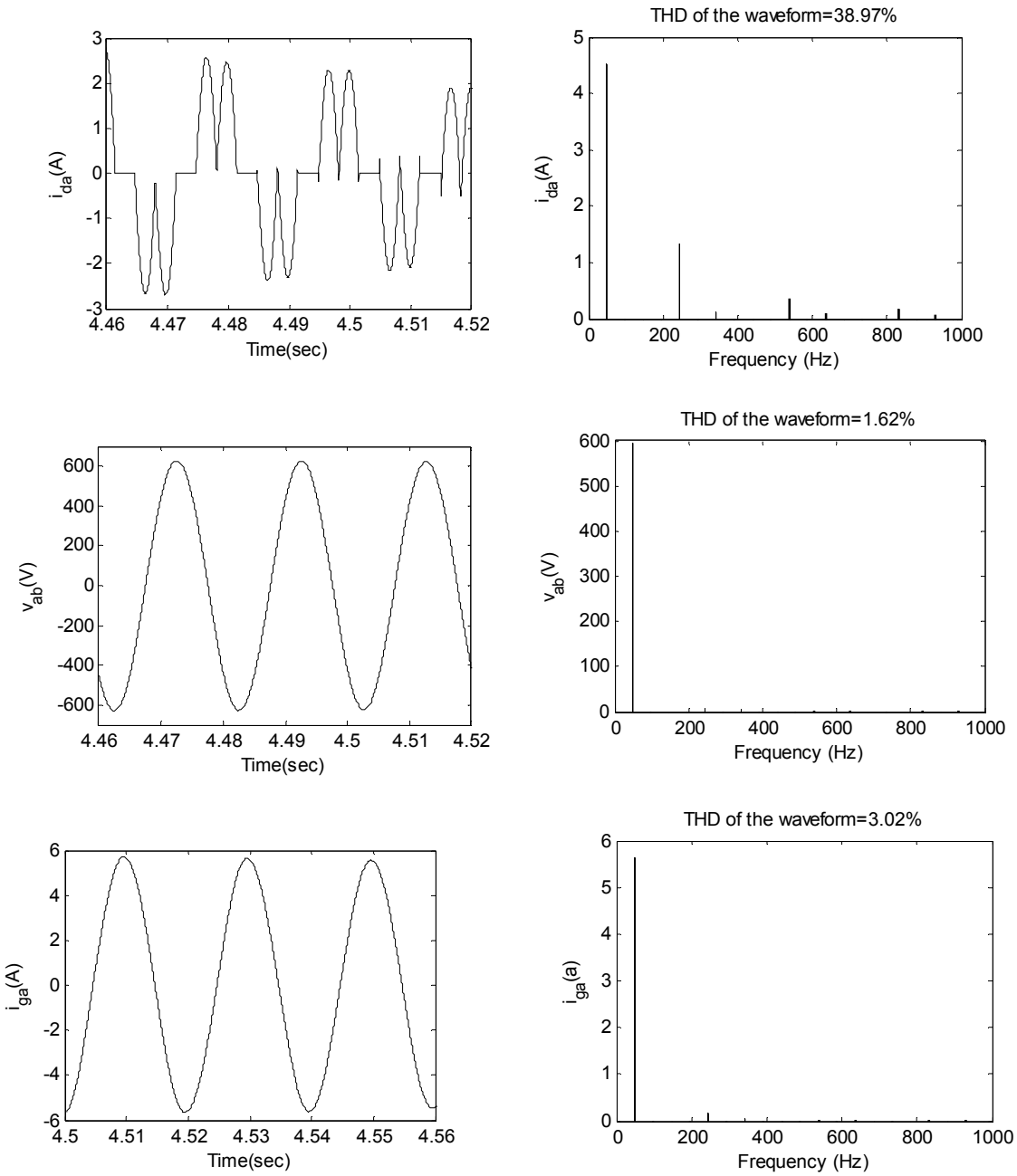


***Fig. 5.19 Harmonic spectra during steady state for SEIG- reduced rating STATCOM with controlled rectifier fed DC motor load***

***Table 5.5 THD values for various loads on SEIG- STATCOM system***

| Type of system | 3.0 kW, 0.8 pf, R-L load (%THD) | Induction motor load (%THD) | Controlled rectifier fed DC motor load (%THD) |
|---|---|---|---|
| **SEIG system with full rating STATCOM** | 0.85 ($v_{ab}$)<br>0.68 ($i_{ga}$) | 0.26 ($v_{ab}$)<br>0.27 ($i_{ga}$) | 37.36 ($i_{da}$)<br>0.97 ($v_{ab}$)<br>1.13 ($i_{ga}$) |
| **SEIG system with reduced rating STATCOM** | 1.04 ($v_{ab}$)<br>1.45 ($i_{ga}$) | 0.33 ($v_{ab}$)<br>0.35 ($i_{ga}$) | 38.97 ($i_{da}$)<br>1.62 ($v_{ab}$)<br>3.02 ($i_{ga}$) |

## 5.7 CONCLUSIONS

In this chapter, the analysis, design and control of SEIG feeding static resistive-inductive load, an induction motor load and fully controlled rectifier fed DC motor load have been discussed with reactive power controlled by STATCOM. The simplified modeling of the each system component and the methodology to decide the STATCOM rating and its parameters have been explained in detail. The STATCOM has been designed for two cases, namely full rating SATACOM and reduced rating SATACOM. A simplified control technique has been proposed for obtaining the gating signals of STATCOM. Two PI controllers are used in the control technique, one for regulating the DC bus voltage and other for regulating the SEIG terminal voltage. The transient performance characteristics of the complete system have been studied with both the cases of STATCOM design parameters. Various studies such as voltage buildup, switching of STATCOM into the system, sudden application of load and change of load have been carried out on SEIG-STATCOM system. The power quality of the SEIG supply is assessed with harmonic spectrum and THD. The following conclusions are deduced from the study carried out in this chapter.

- The starting time and the voltage dip during the starting of induction motor on SEIG-STATCOM system are reduced in comparison to the respective quantities obtained during the application of induction motor on SEIG system.

- The SEIG-STATCOM system is able to supply controlled rectifier fed DC motor load with soft starting arrangement and restricting the generator current, DC motor current and developed electromagnetic torque from attaining excessive high value.

- The developed control technique has been found effective in regulating the terminal voltage. The harmonic content and THD of generator voltage and current are lower than the standard IEEE-519 limits.

- The reduced rating STATCOM results into lower current rating of device, lower DC bus capacitance but higher value of filter inductor. As expected, reduced rating of STATCOM results into lower value of current that can be supplied by STATCOM.

- The performance of both full rating and reduced rating STATCOM are found commendable as far as starting, voltage dip during transient period and THD components under steady state condition are concerned.

# CHAPTER-VI

# SEIG-STATCOM OPERATION AS THREE-PHASE FOUR-WIRE ISOLATED SYSTEM

## 6.1 GENERAL

The poor voltage regulation of self-excited induction generator (SEIG) restricts its adoption as an isolated electric supply for commercial and industrial applications. To keep the voltage regulation within the permissible limit, various schemes have been investigated [132-153]. The fast response, better switching characteristics and the low cost of the power electronics converters have attracted the researchers to use static compensator (STATCOM), a proven technology for power system applications, for small capacity applications also. Various authors have investigated the operation of STATCOM with SEIG for three-phase, three-wire system [154-165], but the problems associated with isolated three-phase, four-wire systems [166] such as load unbalancing and the neutral current have not been dealt commonly.

The previous chapter has summarized the studies for the balanced operation of SEIG with STATCOM feeding static resistive-inductive, AC and DC dynamic motor loads. The STATCOM has been used as a voltage regulator, which regulates the SEIG voltage close to rated voltage. The performance of SEIG-STATCOM system has been studied for sudden application and change of loads. In the present chapter, the transient performance of three-phase SEIG is discussed with three-phase, four-wire STATCOM feeding various types of balance/unbalance linear and non-linear loads. The applied STATCOM is an insulated gate bipolar transistor (IGBT) based, pulse width modulation (PWM) operated, four-leg voltage source converter (VSC), with suitable DC bus capacitor for self supporting DC bus. The proportional-integral (PI) controller based control technique is used for generating the gating signals. Various transient studies are carried out on three-phase, four-wire stand alone induction generator system to address the problems of voltage regulation, unbalanced operation, harmonic compensation and neutral current compensation feeding static linear and non-linear loads. The quality of supply for non-linear loads is assessed through harmonic spectrum and total harmonic distortion (THD).

## 6.2 DESCRIPTION AND CONTROL OF FOUR-WIRE SEIG-STATCOM SYSTEM

The four-wire SEIG-STATCOM system along with the various loads and the control strategy are presented in this section.

### 6.2.1 System Description

The complete system is shown in the Fig. 6.1. The system comprises of following components:

- Three-phase star connected SEIG
- Three-phase, four-wire configuration of STATCOM
- Load comprises of either four wire static resistive inductive (R-L) load, three-wire uncontrolled rectifier fed resistive and resistive-capacitive (R-C) load and four-wire uncontrolled rectifier fed R-C load

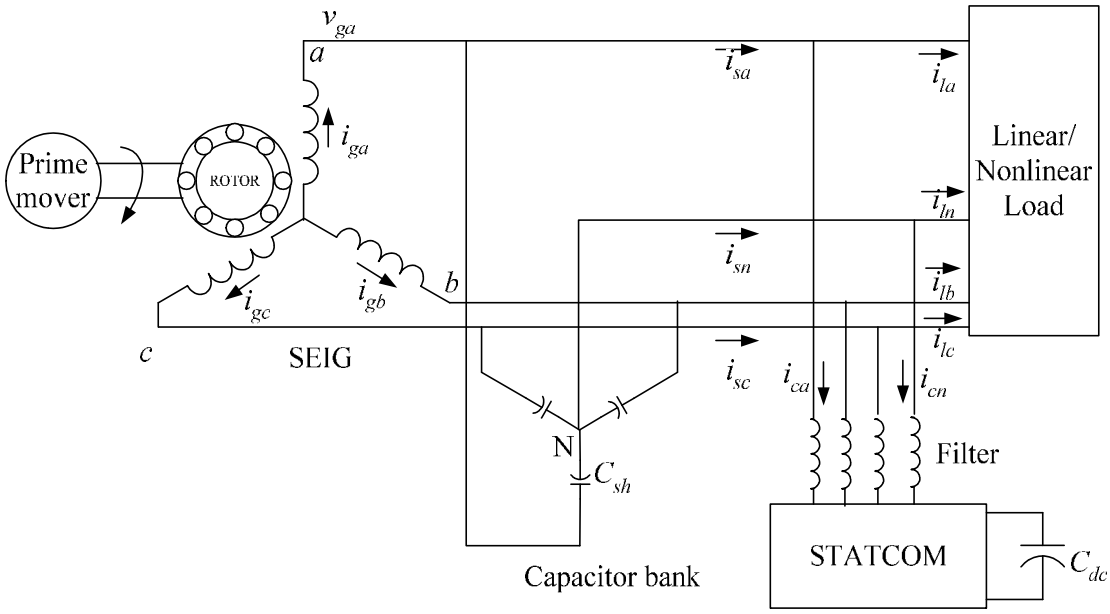


***Fig. 6.1 Schematic of SEIG-STATCOM as three-phase four-wire isolated system***

Three-phase star connected squirrel cage induction machine with suitable size capacitor bank operates as a self-excited induction generator with a prime-mover such as a diesel engine. The SEIG is intended to supply different types of loads, which are shown in Fig. 6.2. The load of different natures such as linear (static R-L) and non-linear (uncontrolled rectifier fed) loads are considered for the analysis.

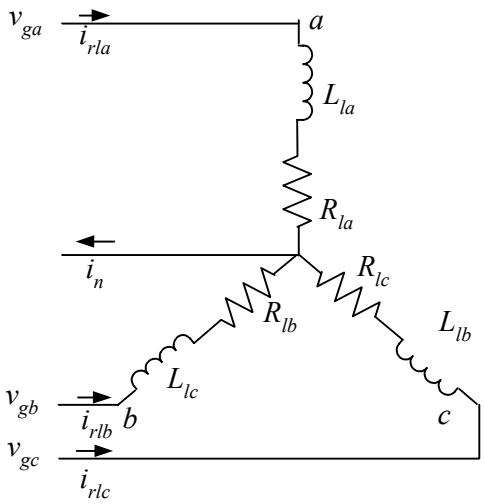


*Fig. 6.2a Four-wire linear (static R-L) Load*

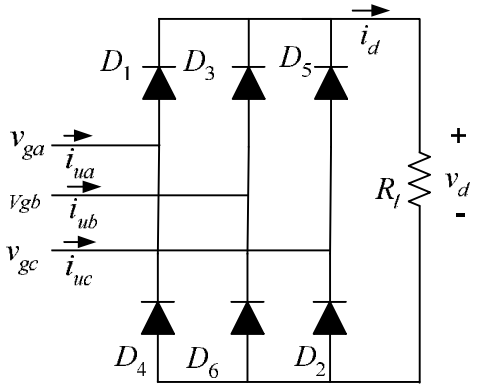


*Fig. 6.2b Three-wire uncontrolled rectifier fed resistive load*

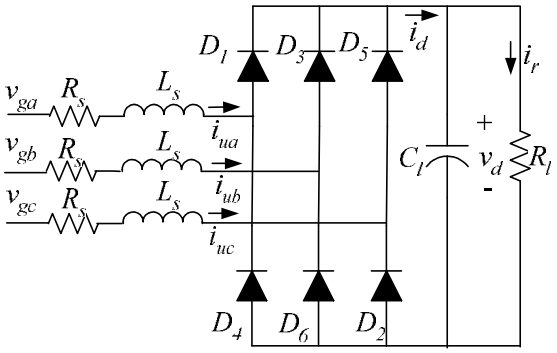


*Fig. 6.2c Three-wire uncontrolled rectifier fed resistive-capacitive load*

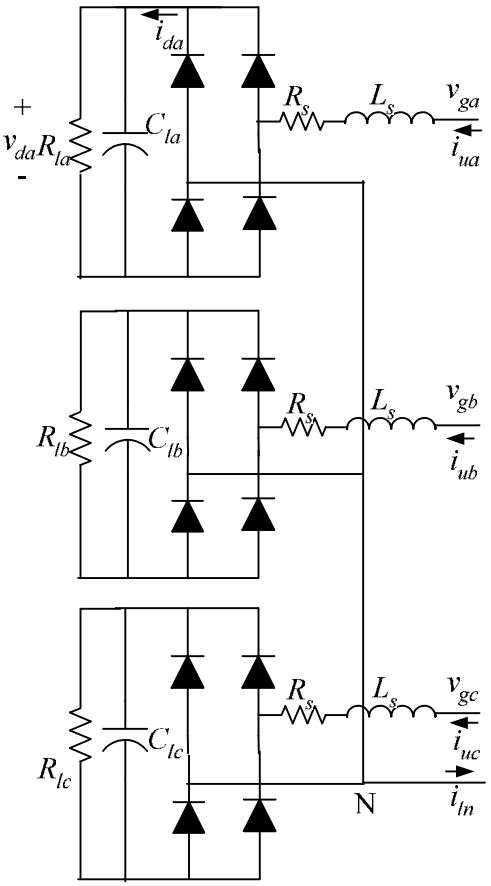


*Fig. 6.2d Four wire uncontrolled rectifier fed resistive-capacitive load*

***Fig. 6.2 Various loads on studied three-phase four-wire SEIG-STATCOM system***

The employed three-phase, four-wire STATCOM is an IGBT based pulse width modulated CC-VSC with suitable size capacitor for self supporting DC bus. With this configuration, the STATCOM can generate or absorb controllable reactive power by internally generating a set of controllable compensating currents and should inject them into respective lines at the point of common coupling. Apart from reactive power exchange for voltage regulation, it should have the capability to balance the load by compensating the neutral current.

### 6.2.2 Control Strategy

The block diagram of control scheme for generating reference current signals and subsequent gating signals for IGBTs of three-phase, four-wire STATCOM are depicted in Fig. 6.3. The proposed control strategy, which is based on *supply current control*, is simple and elegant and deploys two control loops for generating reference supply currents. One PI controller is employed on sensed DC bus voltage $V_{dc}$ and reference DC bus voltage $V_{dc}^{*}$. The output of this PI controller is taken as reference peak in-phase supply current component $I_{sd}^{*}$. This current component is responsible of charging (or discharging) of DC bus capacitor to regulate DC bus voltage and supplying losses in devices of the voltage source converter. The other PI controller is employed on peak source voltage $V_{ps}$ and corresponding reference voltage $V_{ps}^{*}$. The output of this PI controller is taken as peak of reactive component of current $I_{sq}^{*}$. This component is responsible of regulating load voltage by compensating the reactive power. In-phase current templates ($u_{sda}$, $u_{sdb}$, $u_{sdc}$) are generated from supply voltages ($v_{ga}$, $v_{gb}$, $v_{gc}$). Three-phase reference in-phase supply currents are obtained by multiplying in-phase current templates by $I_{sd}^{*}$. The quadrature current templates ($u_{sqa}$, $u_{sqb}$, $u_{sqc}$) are obtained from in-phase current templates and after multiplying it by $I_{sq}^{*}$ to get three-phase reference quadrature supply currents. The three-phase reference supply currents are obtained by adding three-phase reference in-phase and quadrature supply current components. The reference neutral current is taken as zero. The eight gating signals for IGBTs of STATCOM are obtained by comparing sensed and reference supply currents through carrier-less hysteresis current controller.

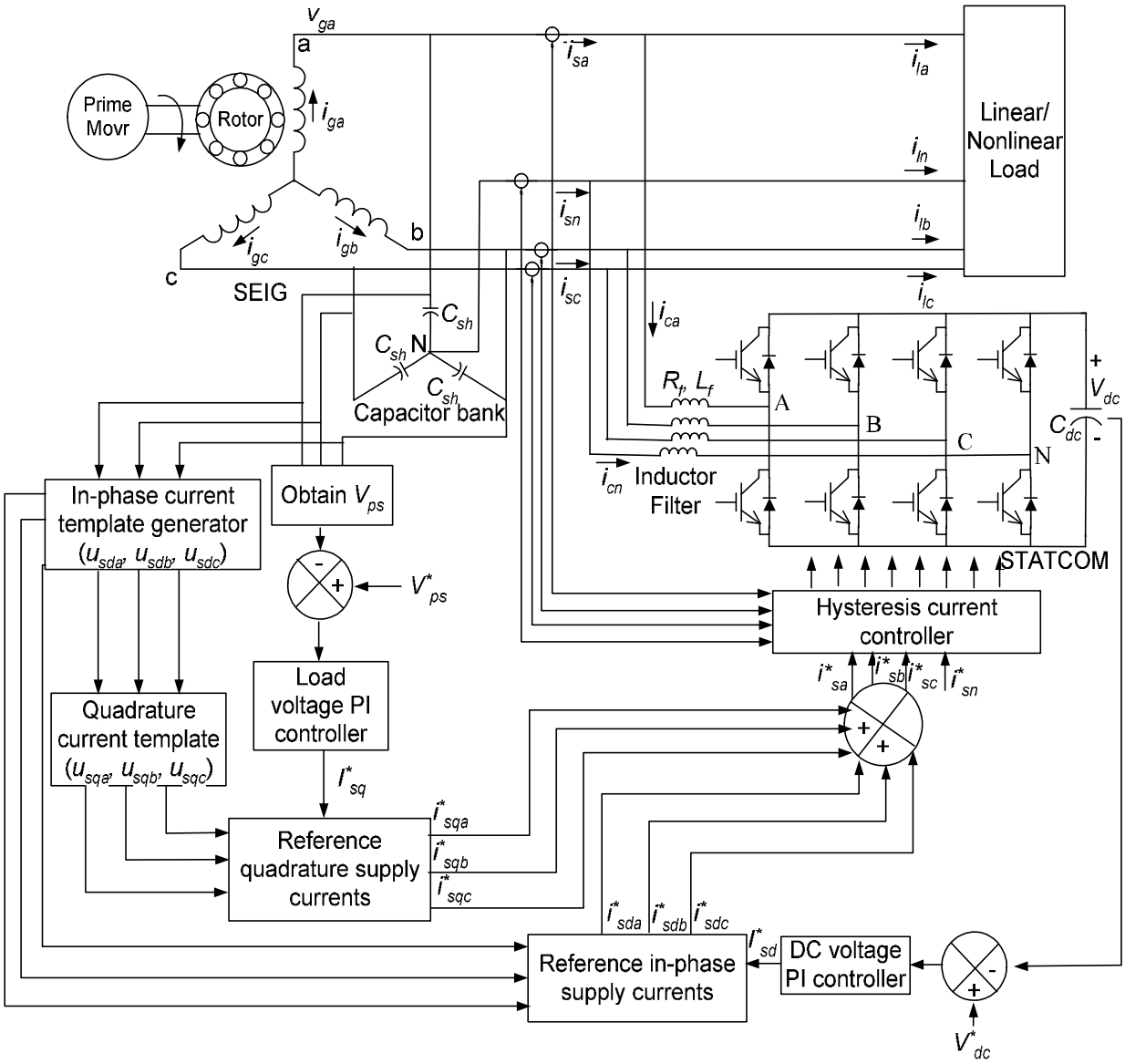


***Fig. 6.3 Control scheme for four wire STATCOM***

## 6.3 MODELING OF FOUR-WIRE SEIG-STATCOM SYSTEM

The system is shown in Fig. 6.3. The system model is derived by relating the equations of the following,

- SEIG model
- STATCOM model
- Reference signals generation
- Load model

### 6.3.1 SEIG Model

The dynamic model of an induction generator has been developed in stationary q-d reference frame and discussed in previous chapter. The state space equations of the model are reproduced here for ready reference as,

$$p[\mathbf{i}] = [\mathbf{L}]^{-1}\left([\mathbf{v}] - [\mathbf{r}][\mathbf{i}] - [\mathbf{G}][\mathbf{i}]\right) \tag{6.1}$$

$$p\omega_r = \frac{P}{2J}\left(T_P - T_{em}\right) \tag{6.2}$$

where, $[\mathbf{v}]$, $[\mathbf{i}]$, $[\mathbf{r}]$, $[\mathbf{L}]$, $[\mathbf{G}]$ and $T_{em}$ are defined in Appendix-B.

Star connected shunt capacitor bank equations at SEIG terminal in state space form are as,

$$\begin{aligned} pv_{ga} &= \frac{(i_{ga} - i_{la} - i_{ca})}{C_{sh}} \\ pv_{gb} &= \frac{(i_{gb} - i_{lb} - i_{cb})}{C_{sh}} \\ pv_{gc} &= \frac{(i_{gc} - i_{lc} - i_{cc})}{C_{sh}} \end{aligned} \tag{6.3}$$

where, $i_{ga}$, $i_{gb}$, $i_{gc}$ are SEIG line currents, $i_{la}$, $i_{lb}$, $i_{lc}$ are load currents, and $i_{ca}$, $i_{cb}$, $i_{cc}$ are compensation currents of STATCOM.

### 6.3.2 STATCOM Model

The STATCOM used for the analysis is a three-phase, four-wire configuration of CC-VSC with self supporting DC bus. The behavior of STATCOM is governed by the model equations of the following subcomponents.

- AC side filter
- DC bus capacitor

#### *6.3.2.1 AC Side Filter*

The filter current ($i_{ca}$, $i_{cb}$, $i_{cc}$) equations in state space form are written as,

$$
\begin{aligned}
pi_{ca} &= \frac{1}{L_f}\left(v_{ga} - e_a - R_f i_{ca}\right) \\
pi_{cb} &= \frac{1}{L_f}\left(v_{gb} - e_b - R_f i_{cb}\right) \\
pi_{cc} &= \frac{1}{L_f}\left(v_{gc} - e_c - R_f i_{cc}\right) \\
pi_{cn} &= \frac{1}{L_f}\left(-e_n - R_f i_{cn}\right)
\end{aligned}
\tag{6.4}
$$

where, $e_a$, $e_b$, $e_c$, $e_n$ are the instantaneous ac side voltage of CC-VSC, $v_{ga}$, $v_{gb}$, $v_{gc}$ are the SEIG phase voltages.

### *6.3.2.2 DC Bus Capacitor*

The charging or discharging currents $i_{cad}$, $i_{cbd}$, $i_{ccd}$, $i_{cnd}$ to the DC bus from each leg of the converter can be written as,

$$
\begin{aligned}
i_{cad} &= i_{ca}(S_{a1} - S_{a2}) \\
i_{cbd} &= i_{cb}(S_{b1} - S_{b2}) \\
i_{ccd} &= i_{cc}(S_{c1} - S_{c2}) \\
i_{cnd} &= i_{cn}(S_{n1} - S_{n2})
\end{aligned}
\tag{6.5}
$$

The DC bus voltage is obtained from $i_{cad}$, $i_{cbd}$, $i_{ccd}$ and $i_{cnd}$ and expressed in state space from as,

$$
pV_{dc} = \frac{1}{C_{dc}}\left(i_{cad} + i_{cbd} + i_{ccd} + i_{cnd}\right) \tag{6.6}
$$

The DC bus voltage is reflected on the ac side of the PWM converter in the form of voltages $e_a$, $e_b$, $e_c$ and $e_n$ which are expressed as,

$$
\begin{aligned}
e_a &= \frac{V_{dc}}{2}(S_{a1} - S_{a2}) \\
e_b &= \frac{V_{dc}}{2}(S_{b1} - S_{b2}) \\
e_c &= \frac{V_{dc}}{2}(S_{c1} - S_{c2}) \\
e_n &= \frac{V_{dc}}{2}(S_{n1} - S_{n2})
\end{aligned}
\tag{6.7}
$$

where, $S_{a1}$, $S_{a2}$ are switching functions corresponding to 'a' leg of CC-VSC decided by carrier-less hysteresis current controller.

### 6.3.3 Reference Signals Generation

The control strategy for generating reference supply currents is shown in block diagram depicted in Fig. 6.3. The reference signal generation is explained through the model equations of following subcomponents.

- PI controllers
- Reference supply currents
- Hysteresis current controllers

#### *6.3.3.1 PI Controller*

The voltage error at n$^{th}$ sampling instant is difference between reference voltage signal ($V^*$) and actual voltage ($V$) signal at $n^{th}$ sampling instant is

$$\begin{aligned} e(n) &= V^*(n) - V(n) \\ y(n) &= y(n-1) + K_p\left(e(n) - e(n-1)\right) + K_i e(n) \end{aligned} \tag{6.8}$$

The output at n$^{th}$ sampling instant is given by eqn. (6.8), where $y(n\text{-}1)$ and $e(n\text{-}1)$ are values of output and error at $(n\text{-}1)^{th}$ sampling instant. The PI controller equation as shown in eqn. (6.8) is derived in Appendix-E.

#### *6.3.3.2 Reference Supply Currents*

The control technique for the generation of reference supply currents ($i_{sa}^*$ $i_{sb}^*$ $i_{sc}^*$) is depicted in Fig. 6.3. In-phase current templates and quadrature currents template are derived as,

$$\begin{bmatrix} u_{sda} & u_{sdb} & u_{sdc} \end{bmatrix}^T = \begin{bmatrix} \dfrac{v_{ga}}{V_{ps}} & \dfrac{v_{gb}}{V_{ps}} & \dfrac{v_{gc}}{V_{ps}} \end{bmatrix}^T \tag{6.9}$$

$$\text{where, } V_{ps} = \sqrt{\frac{2}{3}\left(v_{ga}^2 + v_{gb}^2 + v_{gc}^2\right)} \tag{6.10}$$

The quadrature current templates are obtained from in-phase current template as briefed in Appendix-F and are related as,

$$\begin{bmatrix} u_{sqa} \\ u_{sqb} \\ u_{sqc} \end{bmatrix} = \begin{bmatrix} 0 & -1/\sqrt{3} & 1/\sqrt{3} \\ \sqrt{3}/2 & 1/2\sqrt{3} & -1/2\sqrt{3} \\ -\sqrt{3}/2 & 1/2\sqrt{3} & -1/2\sqrt{3} \end{bmatrix} \begin{bmatrix} u_{sda} \\ u_{sdb} \\ u_{sdc} \end{bmatrix} \tag{6.11}$$

The reference supply currents are obtained by summing up of reference in-phase supply current component and reference quadrature supply current components. The output of PI controller over actual DC bus voltage and reference DC bus voltage gives reference peak of in-phase supply current. After multiplying it with in-phase current templates ($u_{sda}$, $u_{sdb}$, $u_{sdc}$), gives reference in-phase supply current components ($i^*_{sda}, i^*_{sdb}, i^*_{sdc}$). Another PI controller over peak source voltage ($V_{ps}$) and reference peak source voltage ($V^*_{ps}$) gives reference peak of quadrature supply currents. When this peak component is multiplied by quadrature current templates ($u_{sqa}$, $u_{sqb}$, $u_{sqc}$), gives reference quadrature supply current ($i^*_{sqa}$, $i^*_{sqb}$, $i^*_{sqc}$).

$$\begin{bmatrix} i^*_{sda} & i^*_{sdb} & i^*_{sdb} \end{bmatrix}^T = I^*_{sd} \begin{bmatrix} u_{sda} & u_{sdb} & u_{sdc} \end{bmatrix}^T \tag{6.12}$$

$$\begin{bmatrix} i^*_{sqa} & i^*_{sqb} & i^*_{sqb} \end{bmatrix}^T = I^*_{sq} \begin{bmatrix} u_{sqa} & u_{sqb} & u_{sqc} \end{bmatrix}^T \tag{6.13}$$

The total reference supply currents are obtained by adding corresponding reference in-phase and quadrature components. The reference neutral current is taken as zero.

$$\begin{bmatrix} i^*_{sa} & i^*_{sb} & i^*_{sc} \end{bmatrix}^T = \begin{bmatrix} i^*_{sda} & i^*_{sdb} & i^*_{sdc} \end{bmatrix}^T + \begin{bmatrix} i^*_{sqa} & i^*_{sqb} & i^*_{sqc} \end{bmatrix}^T \tag{6.14}$$

#### *6.3.3.3 Hysteresis Current Controller*

The ON/OFF switching functions to obtain gating signals for IGBTs of the CC-VSC, as shown in Fig. 6.1, are derived from the carrier-less hysteresis current controller. The switching function $S_{a1}$ and $S_{a2}$ for phase 'a' is expressed as,

$$\begin{aligned} &\text{if } i_{sa} < (i^*_{sa} - HB) \;\; S_1 \text{ OFF}, S_4 \text{ ON} \Rightarrow S_{a1} = 0, S_{a2} = 1 \\ &\text{if } i_{sa} > (i^*_{sa} + HB) \;\; S_1 \text{ ON}, S_4 \text{ OFF} \Rightarrow S_{a1} = 1, S_{a2} = 0 \end{aligned} \tag{6.15}$$

where, $HB$ is the current band of controller.

Similarly, switching functions for other legs of CC-VSC can be derived.

### 6.3.4 Load Model

Various linear and non-linear loads have been considered for simulation and analysis. The model equations of following loads are summarized herewith.

- Four-wire static resistive-inductive load
- Three-wire uncontrolled rectifier feeding resistive load
- Three-wire uncontrolled rectifier feeding resistive-capacitive load
- Four-wire uncontrolled rectifier feeding resistive-capacitive load

### *6.3.4.1 Four-Wire Static R-L Load*

The static R-L load considered as a Y-connected load. The dynamic equations for load currents $i_{rla}$, $i_{rlb}$, $i_{rlc}$ are written in state space form as,

$$\begin{aligned} pi_{rla} &= \frac{1}{L_{la}}\left(v_{ga} - R_{la}i_{rla}\right) \\ pi_{rlb} &= \frac{1}{L_{lb}}\left(v_{gb} - R_{lb}i_{rlb}\right) \\ pi_{rlc} &= \frac{1}{L_{lc}}\left(v_{gc} - R_{lc}i_{rlc}\right) \end{aligned} \tag{6.16}$$

The load neutral current, $i_{\ln} = -\left(i_{rla} + i_{rlb} + i_{rlc}\right)$ (6.17)

### *6.3.4.2 Three-Wire Uncontrolled Rectifier Fed Resistive Load*

The modeling equations of these non-linear loads have been explained in previous chapter. The main equations are replicated herewith for ready reference.

In the three-wire uncontrolled rectifiers, the maximum line to line voltage $v_s$ (equals to $v_d$) is applied to the load resistance $R_l$ at all time instant. The DC side current is expressed as,

$$i_d = \frac{v_d}{R_L} \tag{6.18}$$

The AC side currents ($i_{ua}$, $i_{ub}$, $i_{uc}$) of uncontrolled rectifier are expressed in terms of conducting functions, say $s_1$, $s_{11}$ for a phase and $i_d$ as,

$$\begin{aligned} i_{ua} &= (s_1 + s_{11})i_d \\ i_{ub} &= (s_2 + s_{22})i_d \\ i_{uc} &= (s_3 + s_{33})i_d \end{aligned} \tag{6.19}$$

### *6.3.4.3 Three-Wire Uncontrolled Rectifier Fed R-C Load*

This type of load operates in two modes; conducting (a segment of maximum line to line voltage is applied to load) and non conducting mode (DC side capacitor discharge).

In conducting mode, the DC side current $i_d$ of the three-wire uncontrolled rectifier is written in state space form as,

$$pi_d = \frac{\left(v_s - v_d - 2i_d R_s\right)}{2L_s} \tag{6.20}$$

Charging and discharging of capacitor are governed by following equation in conduction mode as,

$$pv_d = \frac{\left(i_d - i_r\right)}{C_l} \tag{6.21}$$

where, $i_r = \frac{v_d}{R_l}$

During non conducting mode, the $i_d$=0, and the eqn. (6.20) and (6.21) are modified accordingly.

The ac side currents ($i_{ua}$, $i_{ub}$, $i_{uc}$) can be calculated from $i_d$ and conducting functions as calculated in eqn. (6.19).

### *6.3.4.4 Four-Wire Uncontrolled Rectifier Fed R-C Load*

Let $S_a$, $S_b$, $S_c$ is the conducting function of 'a', 'b' and 'c' phase. The modeling equations governing the behavior for phase 'a' are explained. Let $v_{sa}$ is the positive value of segment ($v_{ga}$, -$v_{ga}$) and is impressed on the DC side of uncontrolled rectifier. Depends upon conducting segment, $S_a$ has the value 1 or -1.

For resistive-capacitive (R-C) on DC side, the capacitor works as a filter capacitor. The DC side current $i_{da}$ in state space form can be written as,

$$pi_{da} = \frac{\left(v_{sa} - v_d - R_s i_{da}\right)}{L_s} \tag{6.22}$$

The ac side current of uncontrolled rectifier for phase 'a' can be obtained as,

$$i_{ua} = S_a i_{da} \tag{6.23}$$

The charging and discharging of load capacitor $C_{la}$ is governed by eqn. (6.21). Depending upon conducting function $S_b$, $i_{db}$ and $S_c$, $i_{dc}$ for 'b' and 'c' phase respective, the $i_{ub}$ and $i_{uc}$ can be determined.

The complete system model is therefore represented by the state space equations along with important equations from eqn. (6.1) to eqn. (6.23). These equations of complete system model are solved by fourth order Runge-Kutta integration method in MATLAB environment.

## 6.4 ALGORITHM FOR SIMULATING FOUR-WIRE SEIG-STATCOM SYSTEM PERFORMANCE

The simulation algorithm is briefly explained for the transient analysis of four-wire SEIG-STATCOM system feeding static R-L load.

1. Read the SEIG parameter, its magnetizing characteristic, shunt capacitance $C_{sh}$, Static load parameter, time for connecting the STATCOM ($t_{STC}$), time for load connection ($t_{RL}$), time for load changing ($t_{RLC}$), time for load unbalancing ($t_{RLU1}$, $t_{RLU2}$), total simulation time ($t_T$), time step ($\Delta$t). Also read the STATCOM parameters, DC voltage and terminal voltage PI controller gains.
2. Set $t$=0, $[i_{qs} \quad i_{ds}]^T = [0.0001 \quad 0.0001]^T$ to account residual magnetism, voltage buildup resistance ($R_{lvb}$)=20000.
3. Compute $i_M$, $L_M$ and obtain $[\mathbf{L}]$ and $[\mathbf{G}]$.
4. Detect the zero crossing instant and sense the $V_{dc}$, $v_{ga}$, $v_{gb}$, $v_{gc}$ and calculate the peak terminal voltage ($V_{ps}$) using eqn. (6.10) from sensed terminal voltages $v_{ga}$, $v_{gb}$, $v_{gc}$.
5. Generate the gating signals for the eight IGBTs of STATCOM from the control scheme depicted in Fig. 6.3.
6. If $t<t_{STC}$, than evaluate eight derivatives as $p[\mathbf{i}]$, $p\omega_r$, $pv_{ga}$, $pv_{gb}$, $pv_{gc}$ for no load voltage buildup and go to step 11.

7. If $t<t_{RL}$, than evaluate twelve derivatives as $p[\mathbf{i}]$, $p\omega_r$, $pv_{ga}$, $pv_{gb}$, $pv_{gc}$, $pV_{dc}$, $pi_{ca}$, $pi_{cb}$, $pi_{cc}$ for switching of STATCOM in the system,

   else evaluate fifteen derivatives as $p[\mathbf{i}]$, $p\omega_r$, $pv_{ga}$, $pv_{gb}$, $pv_{gc}$, $pV_{dc}$, $pi_{ca}$, $pi_{cb}$, $pi_{cc}$ $pi_{rla}$ $pi_{rlb}$, $pi_{rlc}$ for connection of R-L load to the SEIG-STATCOM system.

8. If $t>t_{RLC}$, change the load parameters $R_l$ and $L_l$.

9. If $t>t_{RLU1}$, create unbalance by making $i_{rlc}$ equals to zero.

10. If $t>t_{RLU2}$, create single-phasing by making $i_{rlb}$ and $i_{rlc}$ equal to zero.

11. Compute the instantaneous values by fourth order Runge-Kutta method.

12. Express generator currents into phase variables and evaluate line currents. Store the necessary variables.

13. If $t<t_T$, than $t=t+\Delta t$ and go to step 3.

14. Plot the required waveforms.

The simulation algorithm is modified accordingly for three-wire uncontrolled rectifier fed resistive and resistive-capacitive load and four wire uncontrolled rectifier fed resistive-capacitive load.

## 6.5 RESULTS AND DISCUSSION

The detailed investigation has been carried out on 3.7 kW, 415 V, 7.5 A, Y-connected squirrel cage induction machine operated as SEIG, driven by prime-mover with prime mover torque as $T_P = 6200 - 20\omega_r$ with 48.3 μF/phase shunt capacitance at its terminals. The parameters of the machine are given in Appendix-A and the parameters of STATCOM are summarized in Appendix-H. The voltage buildup of SEIG, switching in of STATCOM, load changing, load unbalancing are the various studies carried out on SEIG-STATCOM system. The quality of generator voltage and current is estimated through harmonic spectrum and THD. The performance of SEIG in conjunction with three-phase, four-wire STATCOM is studied for the following cases.

- System performance with four-wire resistive load
- System performance with four-wire resistive-inductive (R-L) load
- System performance with three-wire uncontrolled rectifier fed resistive load

- System performance with three-wire uncontrolled rectifier fed resistive-capacitive (R-C) load
- System performance with four-wire uncontrolled rectifier fed resistive-capacitive (R-C) load

### 6.5.1 System Performance with Four-Wire Resistive Load

The transient performance characteristics of four wire SEIG-STATCOM system feeding balanced and unbalanced resistive loads is shown in Fig. 6.4. The behavior during voltage buildup and switching of STATCOM in the system is also shown. The system has been studied for application of load, load changing, load unbalancing and load rejection using generator voltages $v_{gabc}$, generator currents $i_{gabc}$, supply side neutral current $i_{sn}$ at the point of common coupling, load currents $i_{ra}$, $i_{rb}$, $i_{rc}$, load side neutral current $i_{ln}$, compensation currents $i_{ca}$, $i_{cb}$, $i_{cc}$, $i_{cn}$, prime mover speed $\omega_r$, peak source voltage $V_{ps}$, DC bus voltage $V_{dc}$ waveforms.

The voltage buildup process of SEIG is completed in approximately 1.2 sec. The voltage buildup up to the rated voltage requires 48.3 μF/phase capacitor at the SEIG terminal. In the mean time, DC bus capacitor of STATCOM is started charging and $V_{dc}$ level is gradually increasing and settling below the reference voltage mark of 700 V. During this interval, the STATCOM draws small amount of current from supply lines. At 1.2 sec., STATCOM control algorithm is switched in to the action which results in visible transient in the various currents and voltages. These transients could last only in two cycles owing to the controller action and $V_{dc}$ and $V_{ps}$ reach their reference mark after a little disturbance.

The SEIG-STATCOM system is loaded with 1.5 kW balanced resistive load at 1.3 sec., resulting into increase in load currents and compensation currents, decrease in $\omega_r$. Due to this loading, $V_{dc}$ momentarily decreases. At 1.4 sec., the load on SEIG is changed to 3.0 kW balanced resistive load. This increased loading results into corresponding change in $i_{gabc}$, $i_{rabc}$, $i_{ca}$, $i_{cb}$, $i_{cc}$, and $\omega_r$ with almost constant $V_{ps}$, which hovers around reference value of 340V.

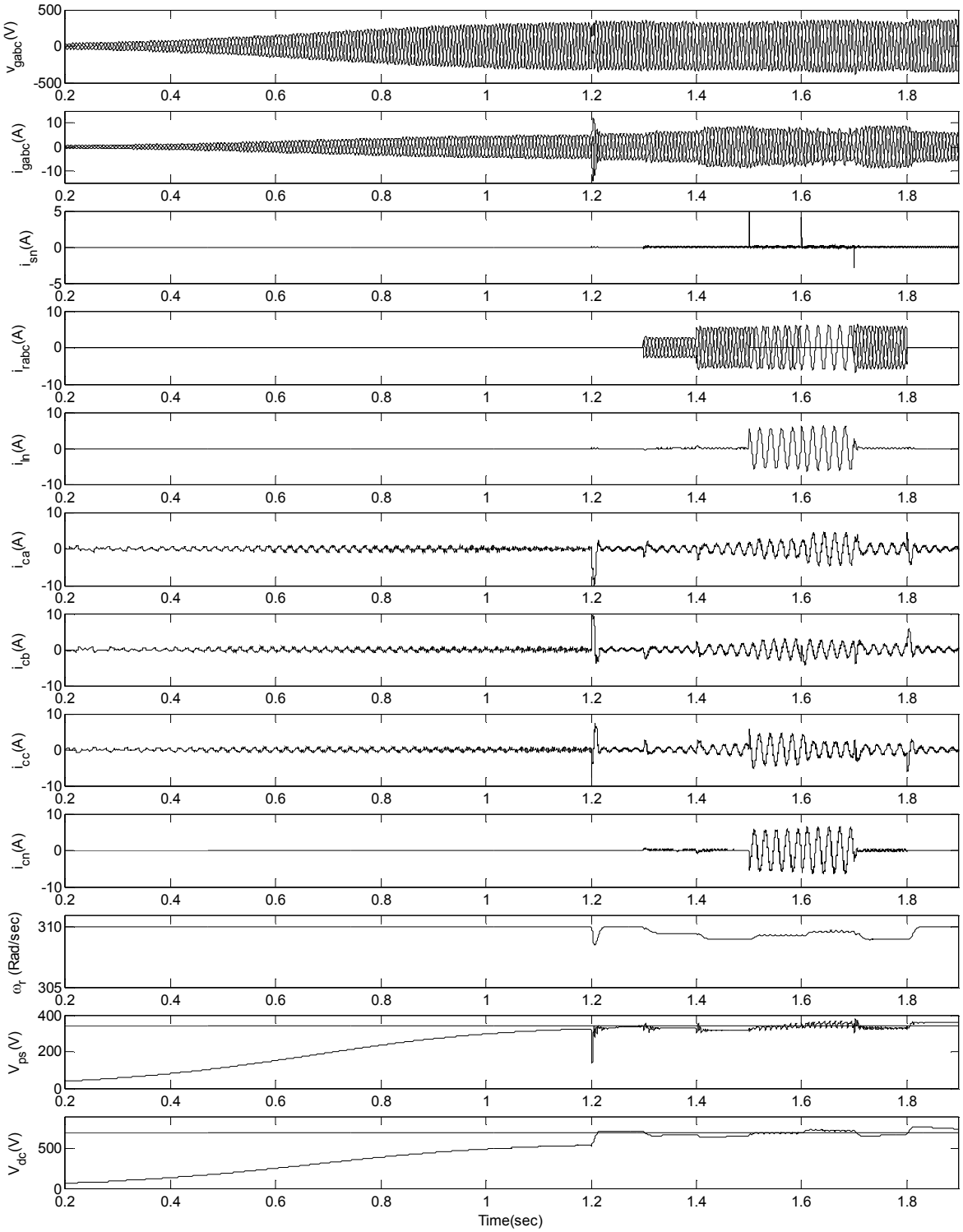


***Fig. 6.4 Transient performance characteristics of four- wire SEIG-STATCOM with resistive load***

***(Load conditions : 1.5 kW at 1.3 sec., 3.0 kW at 1.4 sec., disconnection of 'c' phase at 1.5 sec., single phasing at 1.6 sec. and 3.0 kW at 1.7 sec.)***

The unbalance in the load is created by disconnecting 'c' phase at 1.5 sec. Further, single phasing is imposed in the load by disconnecting phase 'b' also at 1.6 sec. For both

these cases of unbalance, the STATCOM regulates good supply balance and voltage regulation. Moreover due to the effectiveness of STATCOM, the supply side neural current reduces to almost zero. At 1.7 sec., both 'b' and 'c' phases are loaded to bring back the system to balanced 3.0 kW load. This results into momentarily voltage dip in DC bus voltage to 660 V and slight fluctuation in terminal voltage around reference value of 340V. At 1.8 sec., the generator is unloaded and system dynamic changes accordingly with $V_{dc}$ momentarily increasing to 770 V and returns to reference value of 700 V. This study demonstrates that the STATCOM operates as a voltage regulator, a load balancer and a neutral current compensator.

### 6.5.2 System Performance with Four-Wire R-L Load

The transient performance of SEIG-STATCOM with balanced and unbalanced four-wire 0.8 pf static R-L load is shown in Fig. 6.5 using various waveforms such as $v_{gabc}$, $i_{gabc}$, $i_{sn}$, $i_{rla}$, $i_{rlb}$, $i_{rlc}$, $i_{ln}$, $i_{ca}$, $i_{cb}$, $i_{cc}$, $i_{cn}$, $\omega_r$, $V_{ps}$, $V_{dc}$. The SEIG is loaded with 1.0 kW, balanced static R-L load at 1.3 sec., which results into increase in load currents, compensation currents with little transient in $v_{gabc}$ and $i_{gabc.}$ Due to this loading, $V_{dc}$ momentarily decreases to 670 V, but quickly returns to reference value. At 1.4 sec., the load on SEIG is increased to 2.2 kW, which results additional reactive power loading on STATCOM and momentarily $V_{dc}$ dip slightly to the reference value. This increased loading results corresponding increase in generator, load and compensation currents with almost constant $V_{ps}$, which hovers around reference value of 340V.

The unbalance in the load is created by disconnecting 'c' phase, which reduces total load on system to 1.47 kW at 1.5 sec. Further, single phasing is created in the system by disconnecting phase 'b' at 1.6 sec. which thereby reduces the load to 0.73 kW. For both these cases of unbalance, the STATCOM still regulates good voltage regulation and also reduces the supply side neural current to almost zero value. At 1.7 sec., both 'b' and 'c' phases are loaded to have 2.2 kW balanced load condition. But, resulting momentarily voltage dip to 670 V and voltage fluctuates around reference value of 340V. Finally at 1.8 sec., the generator is unloaded by disconnecting R-L load and system dynamics change with $V_{dc}$ instantly increased to 750 V and quickly returns to reference value of 700 V.

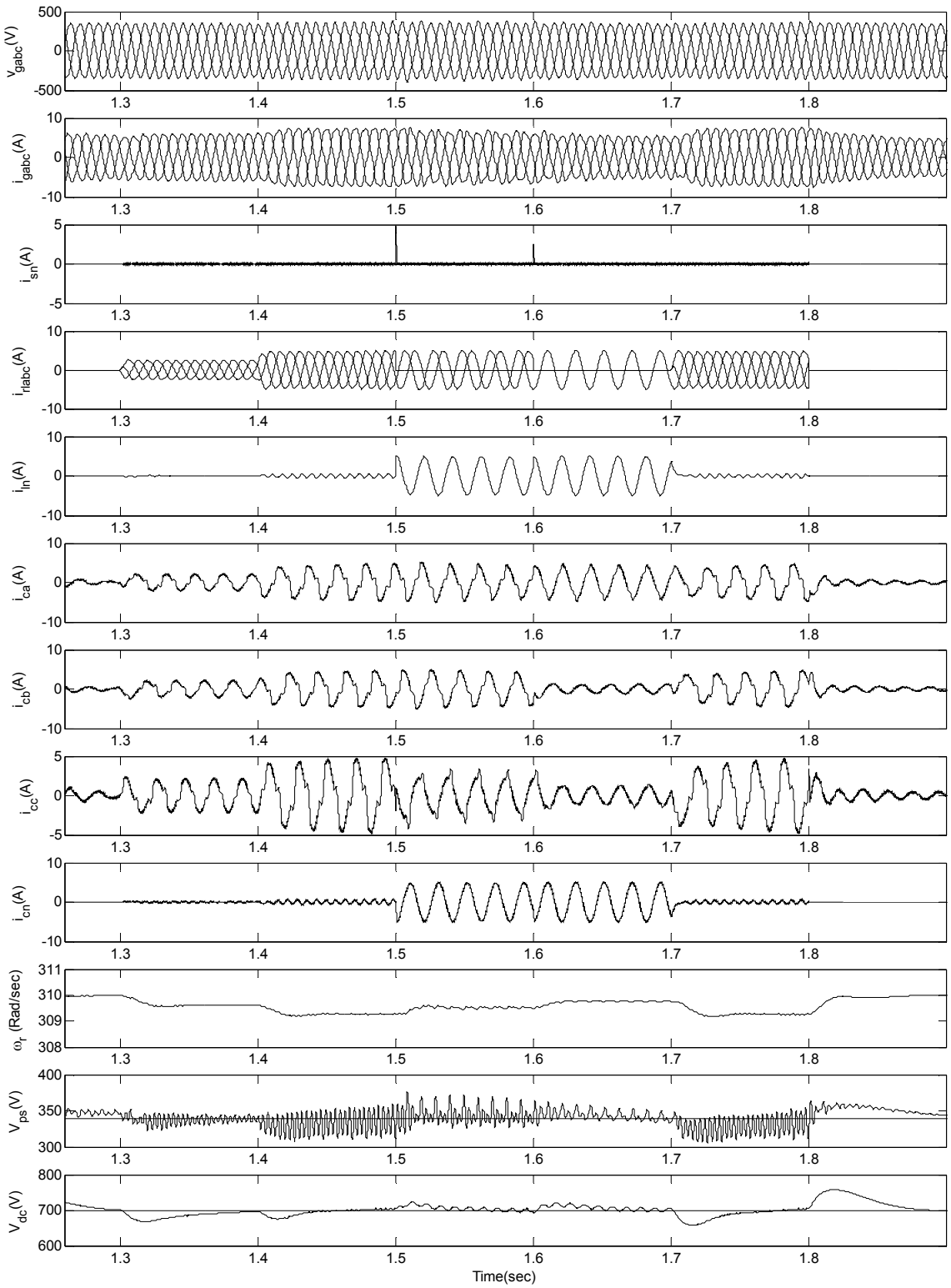


***Fig. 6.5 Transient performance characteristics of four- wire SEIG-STATCOM with static 0.8 pf R-L load***

***(Load conditions : 1.0 kW at 1.3 sec., 2.2 kW at 1.4 sec., disconnection of 'c' phase at 1.5 sec., single phasing at 1.6 sec. and 2.2 kW at 1.7 sec.)***

### 6.5.3 System Performance with 3-wire Uncontrolled Rectifier Fed Resistive Load

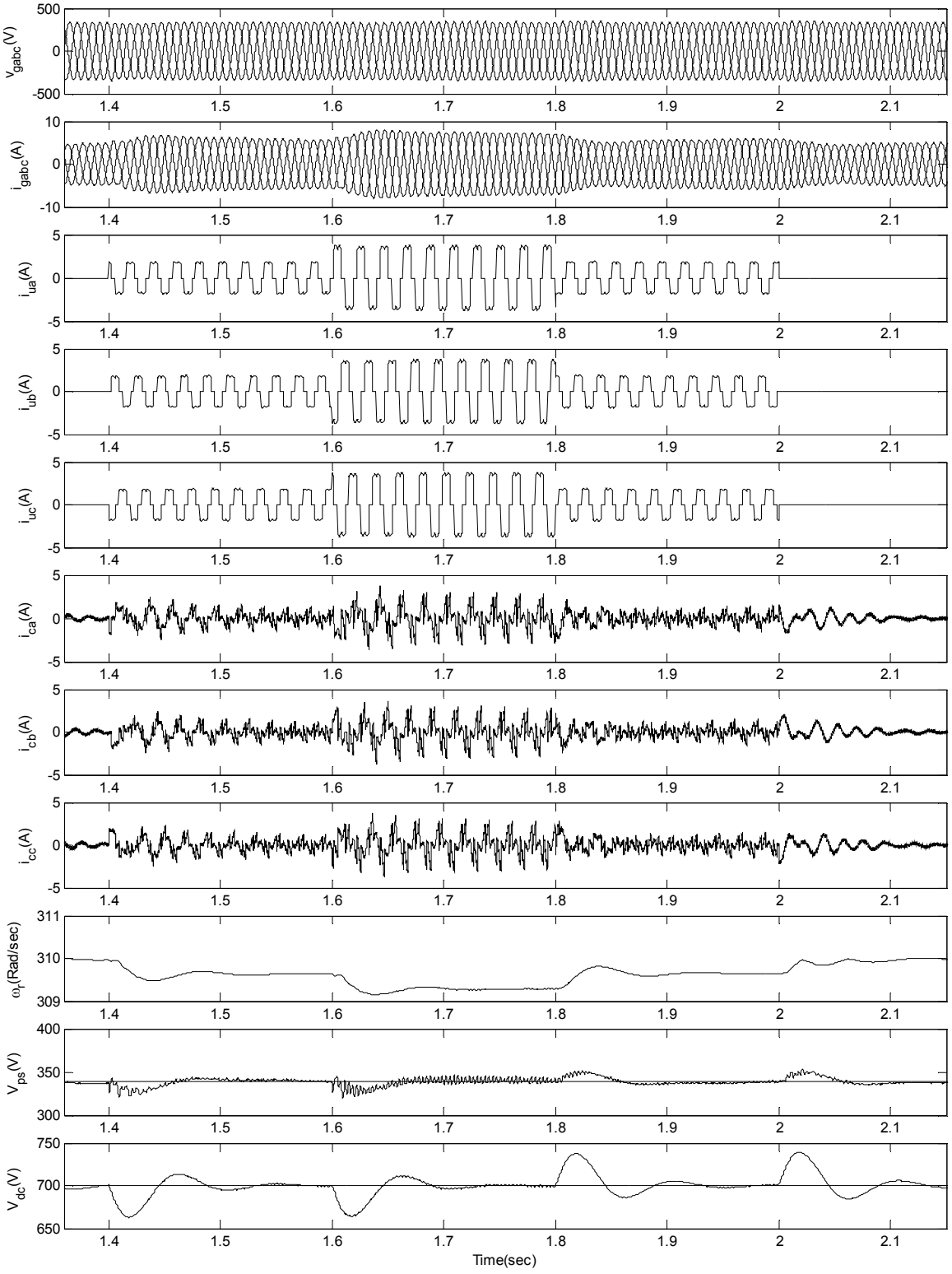


***Fig. 6.6 Transient performance characteristics of four- wire SEIG-STATCOM with three-wire uncontrolled rectifier fed resistive load***

***(Load conditions : 1.0 kW at 1.4 sec., 2.0 kW at 1.6 sec. and 1.0 kW at 1.8 sec.)***

The transient performance characteristics of SEIG-STATCOM with balanced three-wire uncontrolled rectifier fed resistive load for $v_{gabc}$, $i_{gabc}$, $i_{la}$, $i_{lb}$, $i_{lc}$, $i_{ca}$, $i_{cb}$, $i_{cc}$, $\omega_r$, $V_{ps}$, $V_{dc}$ are shown in Fig. 6.6. The SEIG is loaded with 1 kW uncontrolled rectifier fed resistive load at 1.4 sec., which results in an increase in $i_{gabc}$, decrease in $\omega_r$, and momentarily voltage dip in $V_{dc}$ from reference 700 V to 670V. The $V_{dc}$ returns back to reference value due to action of the DC bus PI controller. No significant transients are observed in generator $v_{gabc}$ and $i_{gabc}$ on account of this loading. The load on SEIG is changed to 2 kW at 1.6 sec., which causes additional reactive power burden on STATCOM and momentarily voltage drop in $V_{dc}$ to 660V. Due to this load change, the $i_{gabc}$, $i_{ua}$, $i_{ub}$, $i_{uc}$, $i_{ca}$, $i_{cb}$, $i_{cc}$ increase while $\omega_r$ decreases correspondingly. Momentarily, the $V_{ps}$ and $V_{dc}$ decrease and later attain their reference value. At 1.8 sec., load is shed to 1 kW and system responds accordingly and achieves its steady state after couple of cycles with corresponding change in system quantities. The total load on SEIG is rejected at 2.0 sec., which results small decrease in $i_{gabc}$, slightly increase in $\omega_r$, and little overshoot in $V_{dc}$ to 740 V, a minute increase in $V_{ps}$ to balance the active and reactive powers. The system returns to steady state corresponding to no load condition. In this case, STATCOM operates as a voltage regulator, a load balancer and a neutral current compensator.

### 6.5.4 System Performance with Three-Wire Uncontrolled Rectifier Fed R-C Load

The system performance is studied to feed three-phase uncontrolled rectifier fed resistive-capacitive load, a common non-linear load. The performance characteristics are shown in Fig. 6.7. The system is studied for application of load, load changing and load rejection for such harmonics rich load. The uncontrolled rectifier fed R-C load, which is absorbing 1 kW power is connected at 1.4 sec. The system is experiencing transients for the connection of such non-linear load due to load side capacitor. The sudden connection of load results into an increase in $i_{gabc}$, $i_{ua}$, $i_{ub}$, $i_{uc}$, $i_{ca}$, $i_{cb}$, $i_{cc}$, decrease in $\omega_r$, instantly decrease in $V_{dc}$ to 615V. The system regains steady state after couple of cycles. The load is increased to 2.0 kW at 1.6 sec., which is resulting additional burden of reactive power and harmonic power on STATCOM. The increased load causes further increase in $i_{gabc}$, load currents and compensation currents, decrease in $\omega_r$ and sudden dip in $V_{dc}$ to 675V. The $V_{ps}$ is also hovering around reference mark with some oscillations. The $v_{gabc}$ and $i_{gabc}$ are not experiencing any noticeable transients with this increase in the load.

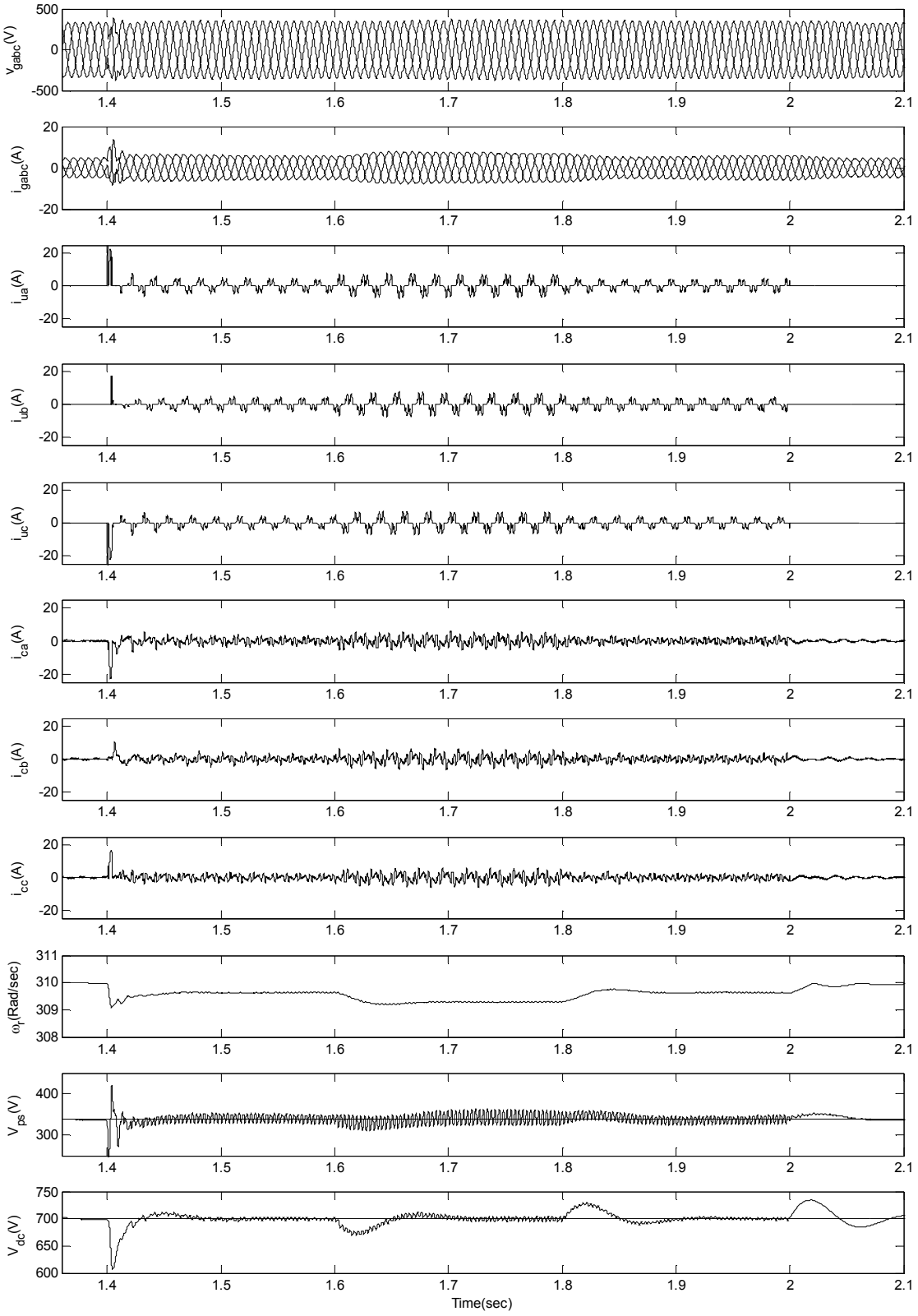


***Fig. 6.7 Transient performance characteristics of four- wire SEIG-STATCOM with three-wire uncontrolled rectifier fed R-C load***

***(Load conditions : 1.0 kW at 1.4 sec., 2.0 kW at 1.6 sec. and 1.0 kW at 1.8 sec.)***

At 1.8 sec., the load is decreased to 1.0 kW, showing corresponding decrease in generator currents, load currents, compensation currents and increase in $\omega_r$. The $V_{dc}$ shortly increases and returns to reference mark. Furthermore, the load is disconnected at 2.0 sec., and after few cycle with corresponding change in system dynamics, the system attains normal state with steady $V_{dc}$ and $V_{ps}$. Here, the STATCOM operates as a voltage regulator and a harmonic compensator.

### 6.5.5 System Performance with Four-Wire Uncontrolled Rectifier Fed R-C Load

The transient performance for feeding four-wire balanced and unbalanced uncontrolled rectifier fed resistive-capacitive (R-C) load is shown in Fig. 6.8 using generator voltages $v_{gabc}$, generator currents $i_{gabc}$, AC side current of uncontrolled rectifier $i_{uabc}$, compensation currents $i_{cabc}$, neutral currents at supply $i_{sn}$ and load $i_{ln}$ side and compensator $i_{cn}$, prime mover speed $\omega_r$, peak source voltage $V_{ps}$, DC bus voltage $V_{dc}$ waveforms.

The SEIG is loaded with single-phase uncontrolled rectifier fed R-C loads in all the phases at 1.3 sec. consuming total 1.5 kW. The currents $i_{gabc}$, $i_{uabc}$, and $i_{cabc}$ increase, whereas $\omega_r$ decreases. At loading, the $V_{dc}$ gradually falls to 637 V and returns to reference value due to PI controller action. The load is increased to 3.0 kW at 1.4 sec. which is resulting corresponding change in the system quantities without appreciable transients. The increase in $i_{sn}$ is very small compared to $i_{ln}$ due to the compensation provided by $i_{cn}$.

The performance during unbalance in the load is studied by loading 0.75 kW, 1.0 kW and 1.25 kW load on ‘a’, ‘b’ and ‘c’ phases respectively at 1.5 sec. The generator voltages and currents are found balanced due to the effective STATCOM control. At 1.6 sec., the balanced load of 3.0 kW is connected and load is rejected at 1.7 sec. After a transients of 2 to 3 cycles, the system returns to steady state. Due to sudden rejection of large load, $V_{ps}$ rises to 390 V from the reference 340 V and $V_{dc}$ jumps to 830 V before settling at reference 700 V. In this case, STATCOM operates as a voltage regulator, a harmonics compensator, a load balancer and a neutral current compensator.

### 6.5.6 Power Quality Performance

The FFT is carried out using standard DFT algorithm of MATLAB to evaluate the harmonic spectra and total harmonic distortion (THD) of various waveforms of interest.

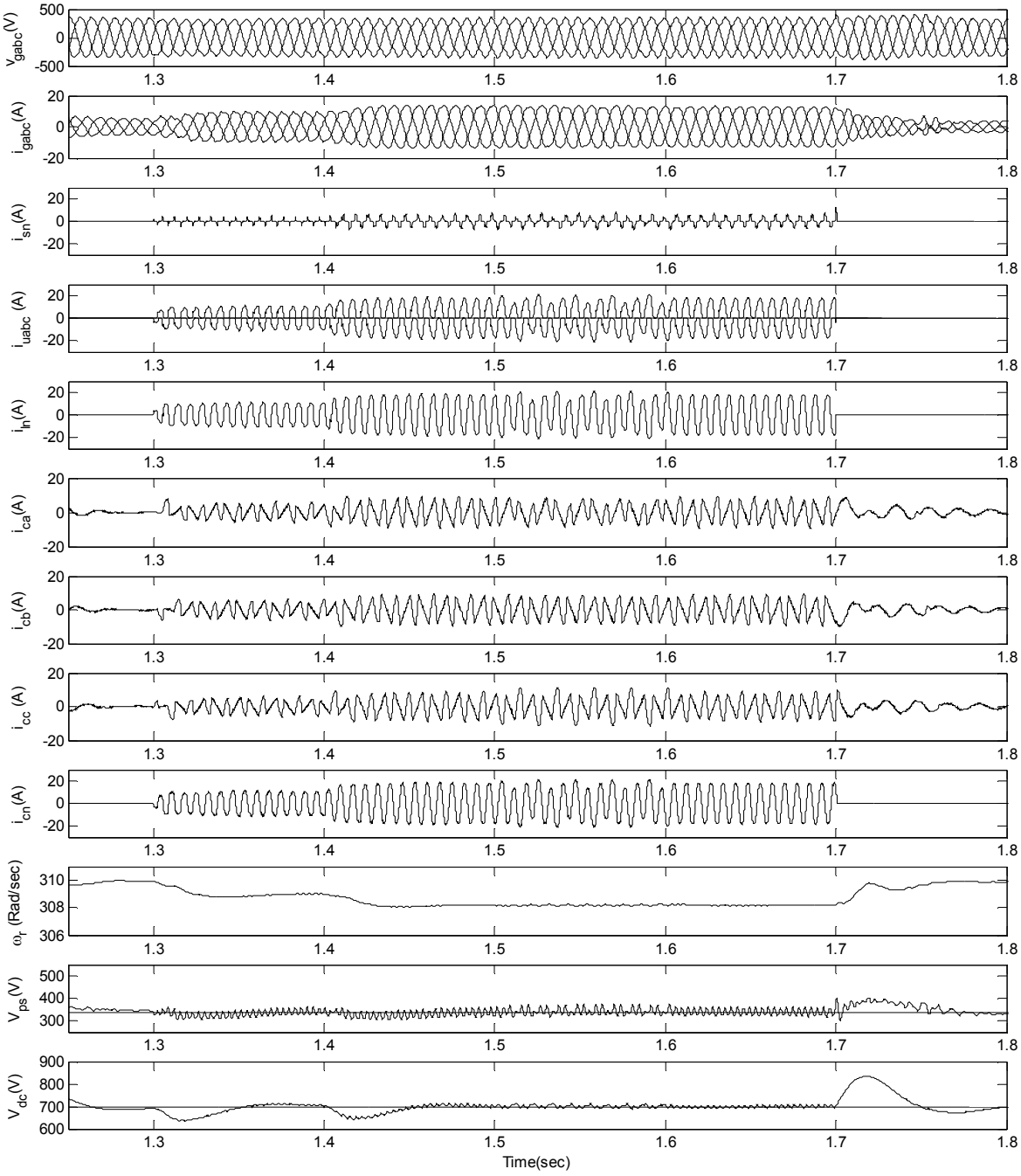


***Fig. 6.8 Transient performance characteristics of four- wire SEIG-STATCOM with four-wire uncontrolled rectifier fed R-C load***

***(Load conditions : Balanced 1.5 kW at 1.3 sec., 3.0 kW at 1.4 sec., unbalanced (0.75 kW, 1.0 kW, 1.25 kW on 'a', 'b', 'c' phases at 1.5 sec.) and balanced 3.0 kW at 1.6 sec.)***

### *6.5.6.1 Harmonic spectra for four-wire SEIG-STATCOM fed resistive load*

The spectrum analysis of steady state $v_{ga}$, $i_{ga}$ is shown in Fig. 6.9 during single-phase condition with 1.0 kW resistive load. The THD of $v_{ga}$ and $i_{ga}$ is calculated as 1.04 % and 1.62 % respectively.

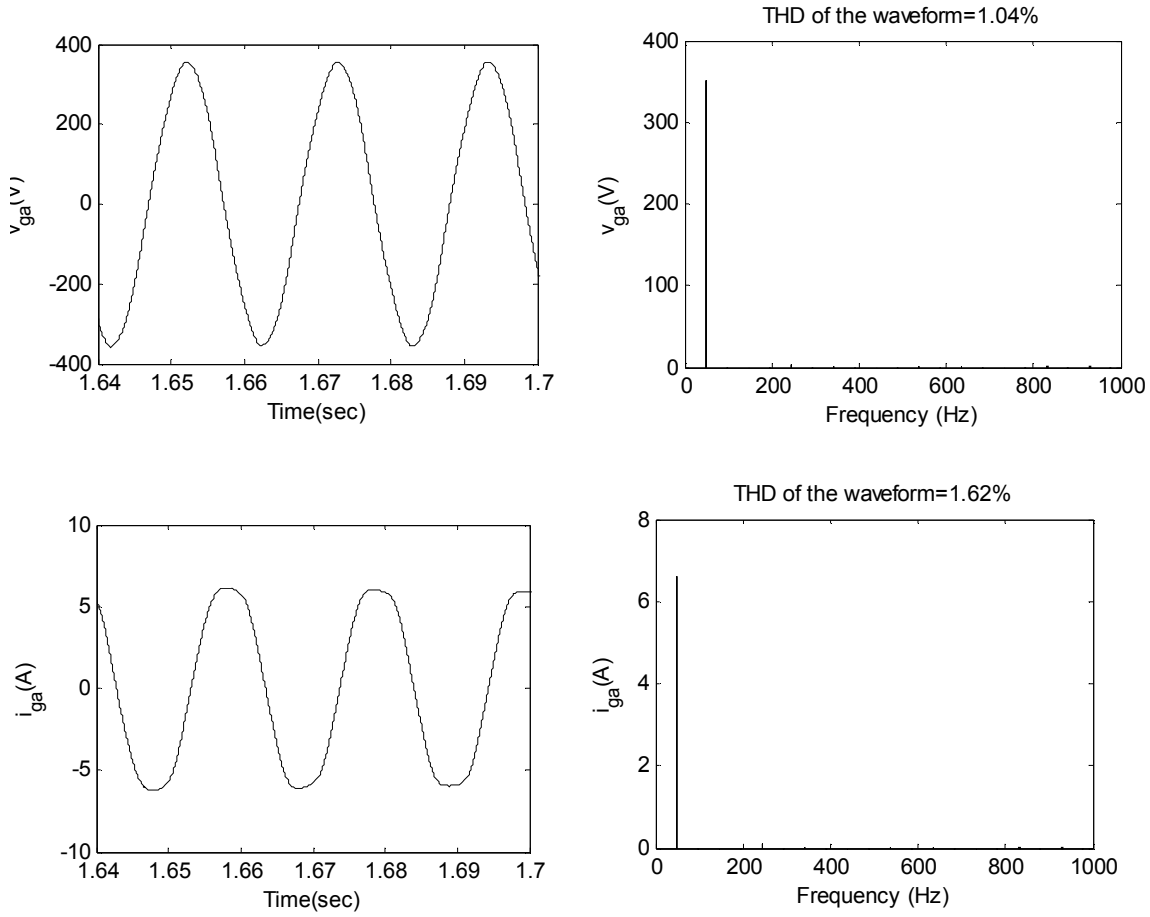


***Fig. 6.9 Harmonic spectra during steady state of four-wire SEIG-STATCOM with static resistive load during single-phase condition***

### *6.5.6.2 Harmonic spectra for four-wire SEIG-STATCOM fed R-L load*

With the spectrum analysis of steady state $v_{ga}$, $i_{ga}$, as shown in Fig. 6.10 during single-phase condition of resistive-inductive load with 0.8 pf, 0.733 kW load. The Total harmonic distortion (THD) of $v_{ga}$ and $i_{ga}$ is calculated as 1.05 % and 1.57 % respectively.

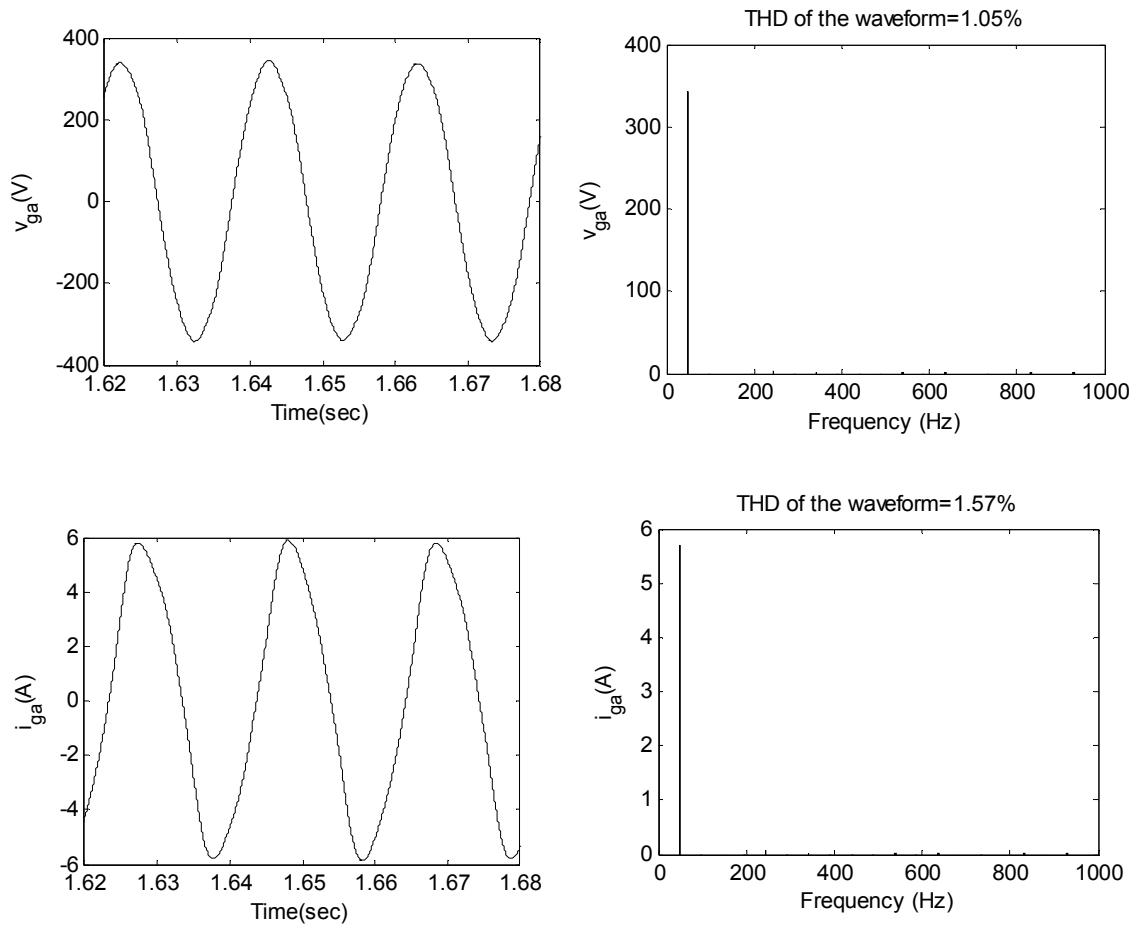


***Fig. 6.10 Harmonic spectra during steady state of four-wire SEIG-STATCOM with static R-L load during single-phase condition***

### *6.5.6.3 Harmonic spectra for four-wire SEIG-STATCOM with three-wire uncontrolled rectifier fed resistive load*

The spectrum analysis of steady state $v_{ga}$, $i_{ga}$ and $i_{ua}$ is shown in Fig. 6.11 for 3-wire uncontrolled rectifier fed resistive load of 1.0 kW. The total harmonic distortion (THD) of $v_{ga}$ and $i_{ga}$ is calculated as 2.46% and 3.03% respectively, which is well below the IEEE 519 harmonics standard, while the load current $i_{ua}$ is having THD of 28.05%.

### *6.5.6.4 Harmonic spectra for four-wire SEIG-STATCOM with three-wire uncontrolled rectifier fed R-C load*

The spectrum analysis of $v_{ga}$, $i_{ga}$ and $i_{ua}$ are shown in Fig. 6.12 for three-wire uncontrolled rectifier fed R-C load of 1.0 kW. The total harmonic distortion (THD) of $v_{ga}$ and $i_{ga}$ is obtained as 1.36% and 2.41% respectively, which is well below the IEEE 519 harmonic standard, whereas the load current is having THD of 64.48%.

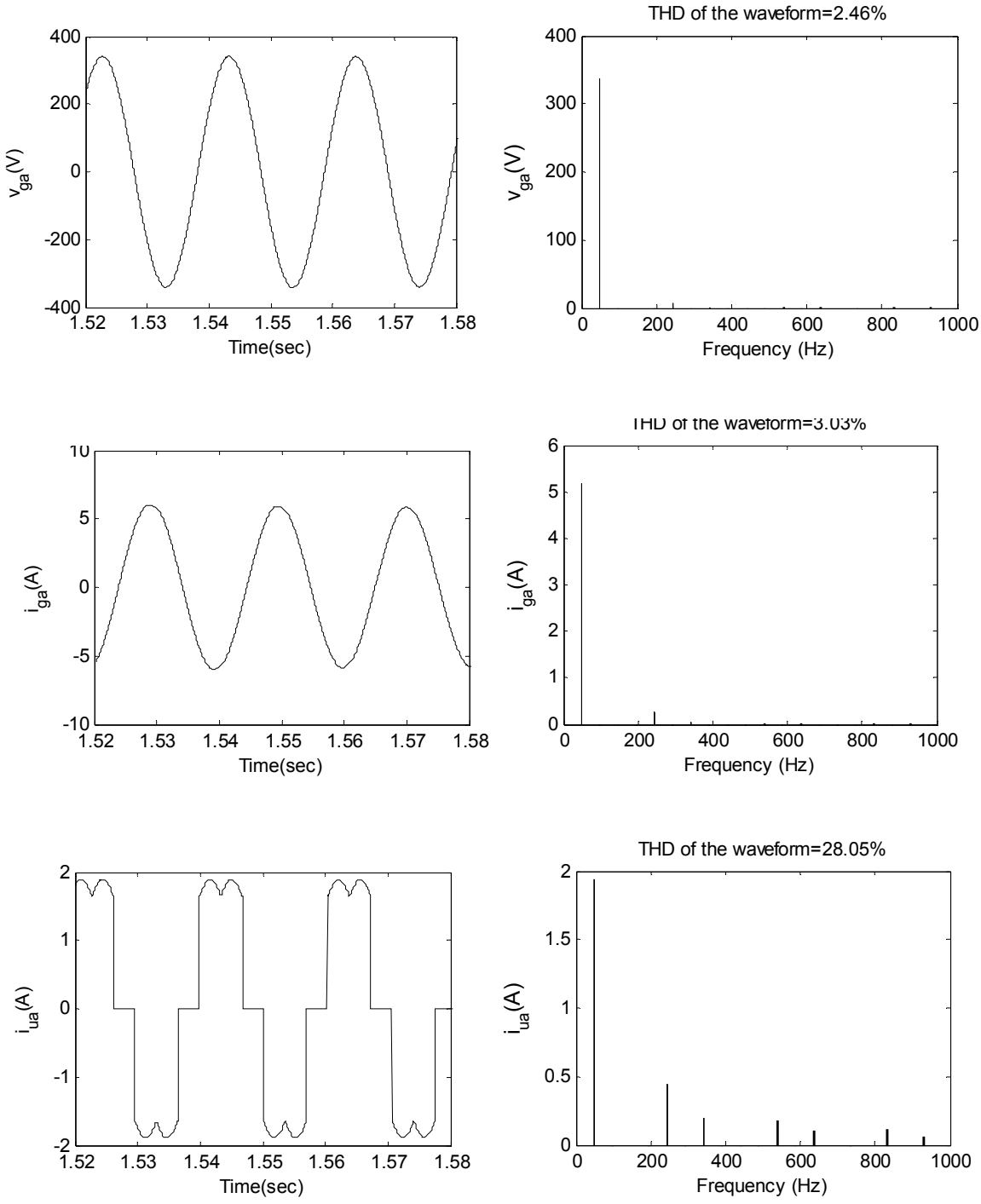


***Fig. 6.11 Harmonic spectra during steady state of four-wire SEIG-STATCOM with 1.0 kW 3-wire uncontrolled rectifier fed resistive load***

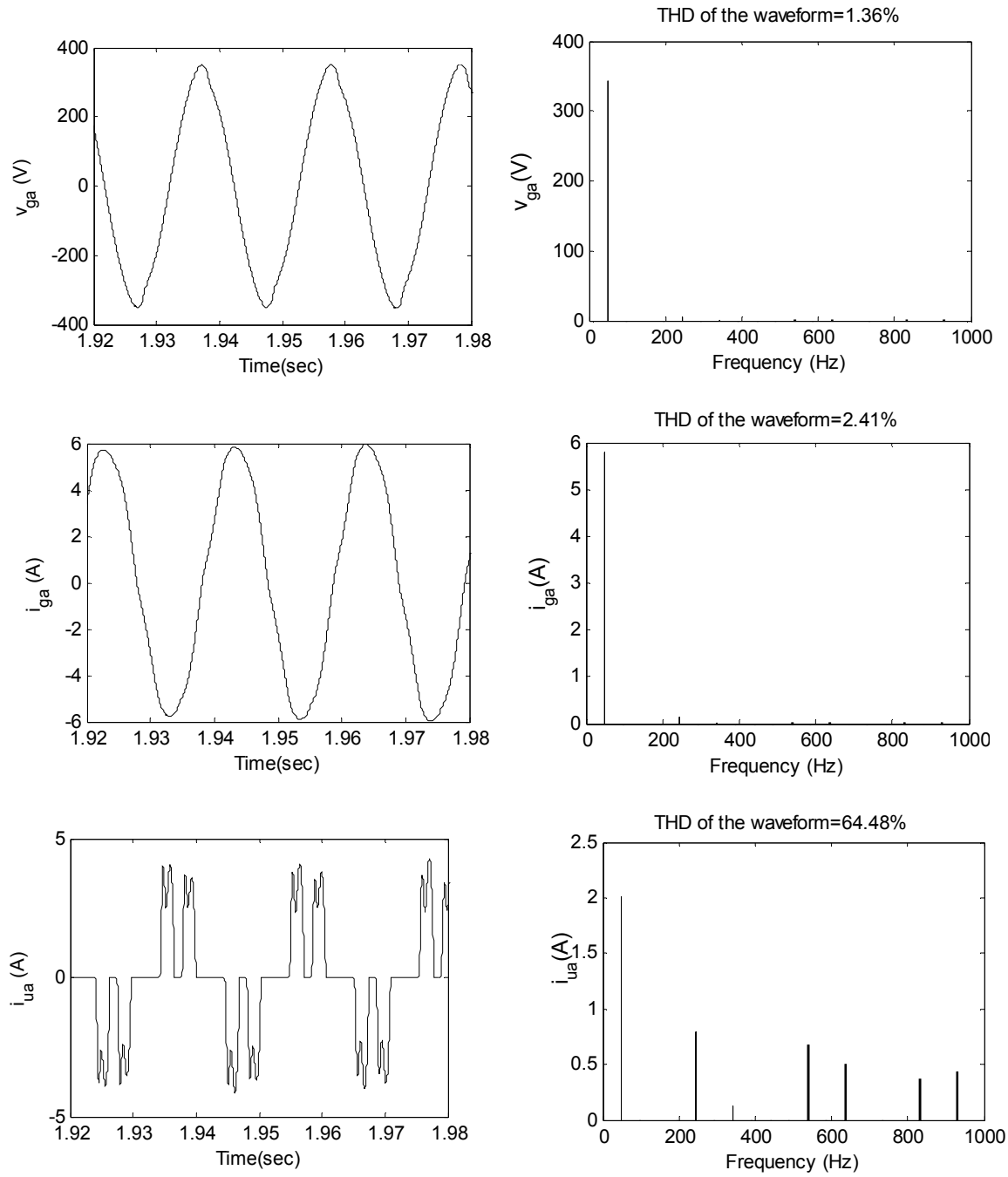


***Fig. 6.12 Harmonic spectra during steady state of four-wire SEIG-STATCOM with 1.0 kW 3-wire uncontrolled rectifier fed R-C load***

The total harmonic distortion (THD) values on generator and load terminals for four-wire uncontrolled rectifier fed R-C load are summarized in Table 6.1.

The THD value of generator $v_{ga}$ and $i_{ga}$ are within the acceptable range for linear as well as various non-linear loads, which demonstrates the effectiveness of control algorithm. Therefore, the performance of SEIG with STATCOM feeding three-wire and four-wire linear and non-linear loads is excellent as far as power quality aspects are considered.

***Table 6.1 THD values for four-wire SEIG-STATCOM with uncontrolled rectifier fed R-C load***

| Loading condition | THD of load current (%) | THD of generator voltage (%) | THD of generator current (%) |
|---|---|---|---|
| Balanced 3.0 kW | 65.52 | 4.48 | 3.85 |
| Unbalanced (0.75 kW, 1.0 kW, 1.25 kW on 'a', 'b', 'c' phases ) load | 68.62 ($i_{ua}$)<br>67.90 ($i_{ub}$)<br>65.45 ($i_{uc}$) | 4.98 ($v_{ga}$)<br>4.88 ($v_{gb}$)<br>4.09 ($v_{gc}$) | 3.69 ($i_{ga}$)<br>2.91 ($i_{gb}$)<br>4.06 ($i_{gc}$) |

## 6.6 CONCLUSIONS

In this chapter, the transient analysis of three-phase self-excited induction generator has been discussed with four-wire configuration of STATCOM feeding four-wire linear and non-linear loads. The proposed control strategy is simple and uses two PI controllers; one PI controller regulates the DC bus voltage and meets the device losses by drawing small active current component from the generator. Other PI controller regulates the load voltage by internally generating the reactive power. Carrier-less hysteresis current controller is used for obtaining the eight switching signals of IGBTs of STATCOM. The STATCOM injects the controllable compensation currents into the supply lines by effectively generating them using the proposed control algorithm. The control technique is tested for various loading conditions and the system is studied for application of load, change in load, load unbalance and rejection of load. The effect of load harmonics on the generator voltage and current is assessed by the harmonic spectrum and THD. The following conclusions are made from the study carried out in this chapter.

- The capability of the STATCOM has been demonstrated to operate as a voltage regulator, a load balancer, a harmonic eliminator and a neutral current compensator.

- The harmonics content and THD have been observed lower than the standard IEEE-519 limit for generator side, which validate the effectiveness of control technique.

- With the support of STATCOM, the SEIG system has been found to operate as an ideal four-wire isolated supply feeding linear and non-linear loads.

# CHAPTER-VII

# SEIG OPERATION WITH SSSC FEEDING STATIC LOADS

## 7.1 GENERAL

The investigations on performance of SEIG with STATCOM have been summarized in previous two chapters. Various aspects such as voltage regulation, harmonic compensation, load balancing etc. of SEIG- STATCOM have been investigated for linear and non-linear loads. Conventionally, series capacitors are used in power system to augment the power flow control and stability enhancement. The series capacitors in conjunction with shunt capacitors are used for the control of reactive power and voltage regulation of SEIG. Contrary to series capacitors, static synchronous series compensator (SSSC) with SEIG may offer several advantages including mitigation of resonance, reactive power control, voltage regulation etc. The investigations on the performance of SEIG employing series compensation through series capacitors and SSSC for static loads are summarized in this chapter.

The terminal voltage of SEIG is governed by the shunt capacitance, prime mover (PM) speed and the load. As the generator is loaded, the terminal voltage decreases due to the increasing difference between the VAR supplied by the capacitor bank and VAR demanded by the generator and the load. A number of researchers have discussed the different criteria for the selecting limiting value of capacitance and speed for successful SEIG operation under various loading conditions [70-78]. The various voltage regulating schemes have been discussed in the literature to obtain regulated voltage using SEIG. The additional series capacitances are used in short shunt and long shunt SEIG configurations [122-130]. Shridhar et al. [124] have deliberated on the selection of capacitances for short shunt SEIG configuration. The shunt capacitance is selected to give no load voltage and the series capacitance is selected for required voltage regulation at full load. The results of short shunt and long shunt SEIG configuration are compared by Wang and Su [127] for the given capacitances. The shunt and series capacitances are selected for optimum voltage regulation of short shunt SEIG feeding an induction motor load [129]. Anagreh and Al-Kofahi [40] have studied the performance of SEIG through genetic algorithm and

Joshi et al. [181] have selected the capacitance and speed using genetic algorithm to obtain constant voltage and frequency operation of SEIG. The development in solid state converter topologies has attracted researchers and various schemes [154-166] have been explored for obtaining improved voltage regulation. In spite of various advantages, the complexity in control and high cost offset the advantages of these schemes for SEIG.

The SSSC is a proven technology for transmission and distribution systems and is referred by various names such as dynamic voltage restorer, series active filter, series active line conditioner, static series compensator etc. [249-269]. The single line diagram of SSSC is shown in Fig. 7.1. The SSSC consists of a three-phase, insulated gate bipolar transistors (IGBTs) based pulse width modulated (PWM), current controlled-voltage source converter (CC-VSC) with a capacitor or battery on dc bus. It is connected in series with the line through an insertion transformer. It efficiently modulates the effective line impedance of the line by injecting a controllable voltage at appropriate phase angle with the line current. It can exchange both real and reactive powers with energy storage system on the dc bus. The SSSC emulates an inductor, when the injected voltage is quadrature leading to the line current, whereas it emulates a capacitor when the injected voltage is quadrature lagging to the line current.

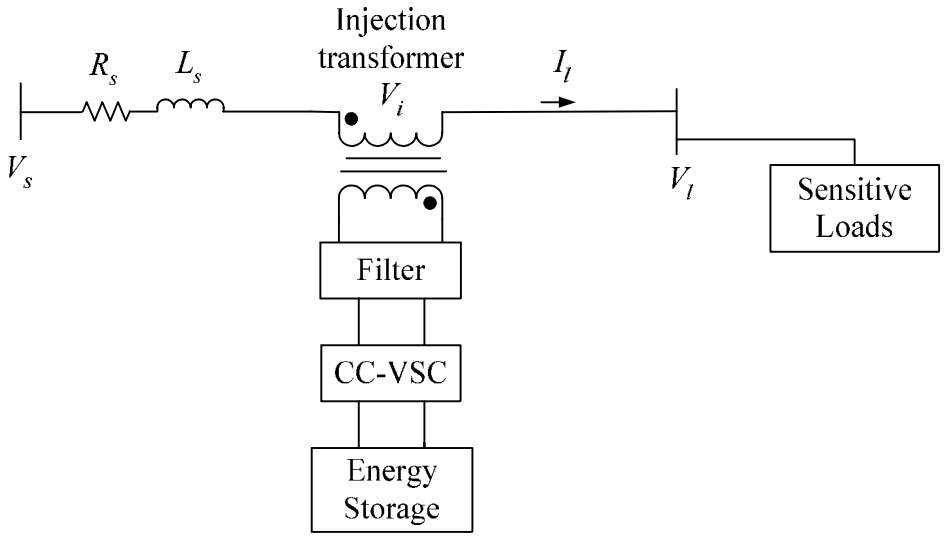


***Fig. 7.1 Representation of SSSC in circuit***

It is well known that three-phase self-excited induction generator shows drooping terminal voltage characteristic with the load and thus exhibits poor performance. The improved performance can be achieved through short shunt SEIG configuration, as shown

in Fig. 7.2. In the present chapter, the steady state performance analysis for short shunt SEIG is investigated in detail. The series and the shunt capacitances are selected for short shunt SEIG to provide optimum voltage regulation and to provide optimum performance, a combination of voltage regulation and loadability. Correspondingly, the optimization is attempted using genetic algorithm (GA) considering various equality and inequality constraints related to SEIG operation. The GA, a multidirectional global search and optimization method provides optimum values of series and shunt capacitances.

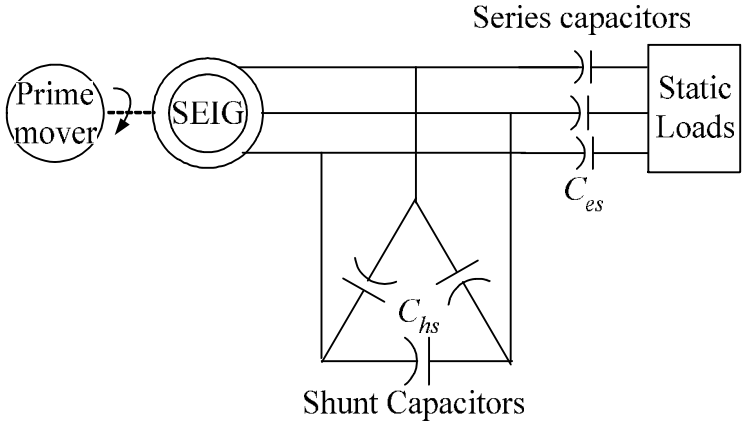


***Fig. 7.2 Schematic of short shunt self-excited induction generator***

The transient performance of three-phase SEIG-SSSC is also investigated to study its effectiveness in meeting the reactive power requirements for voltage regulation for feeding static loads. Two configurations of SSSC have been considered for the study. The SSSC with a battery on DC bus as energy storage is referred as *battery supported SSSC*, whereas the SSSC with capacitor on DC bus as energy storage is referred as *capacitor supported SSSC*. The SSSC parameters are designed by computing steady state voltage. The control technique using a proportional-integral (PI) controller is proposed to generate the reference signals. The performance of SEIG-battery supported SSSC system is studied for resistive, resistive-inductive and resistive-capacitive loads. Both the inductive and capacitive operating modes of SSSC are validated under different loading conditions. The performance of SEIG-capacitor supported SSSC system for feeding static resistive-inductive load is also studied.

## 7.2 DESCRIPTION AND CONTROL OF SEIG-SSSC SYSTEM

The configuration and control of SEIG-battery supported SSSC and SEIG-capacitor supported SSSC are described in this section.

### 7.2.1 SEIG-Battery Supported SSSC System

The schematic of SEIG-battery supported SSSC system with the associated control strategy are shown in Fig. 7.3. The system consists of a three-phase, star connected SEIG, star connected load, unity turn ratio voltage insertion transformer and the SSSC. The battery supported SSSC consists of current controlled-voltage source converter (CC-VSC), dc bus battery and a ripple LC filter. The proposed control strategy is based on *indirect current control* (ICC) and employs a PI controller in control loop for generating reference supply currents. In the ICC, the reference currents are indirectly controlled by controlling supply currents. The load voltage is required to be maintained within close tolerance to the nominal load voltage by injecting the compensating voltage at appropriate phase angle.

The PI controller is employed on peak load voltage $V_{pl}$ and corresponding reference peak voltage $V_{pl}^{*}$. The output of the controller is taken as reference peak current $I_{m}^{*}$, which is responsible for maintaining load voltages by adjusting the reactive power. In-phase current templates ($u_{sda}$, $u_{sdb}$, $u_{sdc}$) are generated from supply currents ($i_{sa}$, $i_{sb}$, $i_{sc}$) at the point of common coupling. The supply currents are equal to load currents ($i_{la}$, $i_{lb}$, $i_{lc}$) for series connected VSC. The quadrature current templates ($u_{sqa}$, $u_{sqb}$, $u_{sqc}$) are obtained from in-phase current templates and transformation matrix. The quadrature current templates are multiplied by $I_{m}^{*}$ to get three-phase reference supply currents. The six gating signals for IGBTs of VSC are obtained by passing sensed and reference supply currents through the hysteresis current controller.

### 7.2.2 SEIG-Capacitor Supported SSSC System

The schematic of SEIG-capacitor supported SSSC with associated control technique is shown in Fig. 7.4. The capacitor supported SSSC consists of current controlled voltage source converter with capacitor at DC bus.

The operating capability of capacitor supported SSSC can be explained with the phasor diagram shown in Fig. 7.5. The SSSC ensures the load voltage to be regulated to rated value during supply side disturbance and voltage dip ($V_g$). The injected voltage $V_i$ consists of two components; $V_{id}$, which is along the direction of current $I_l$, regulates the DC bus voltage and $V_{iq}$, which is in quadrature to the current, regulates the load voltage. During the voltage dip, $V_i$ is injected by SSSC, which thereby attains $V_L$ to rated value.

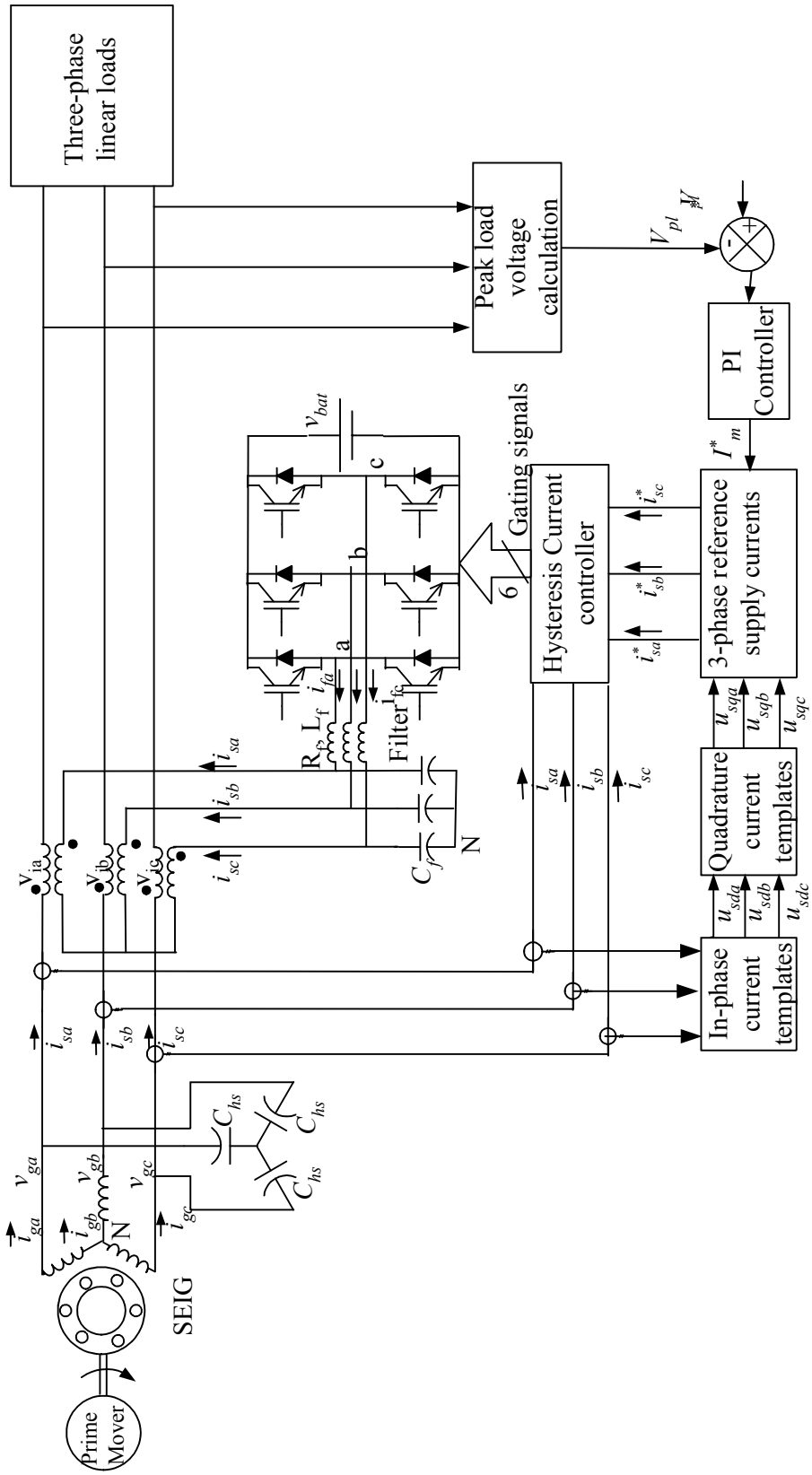


***Fig. 7.3 SEIG-battery supported SSSC system with associated control technique***

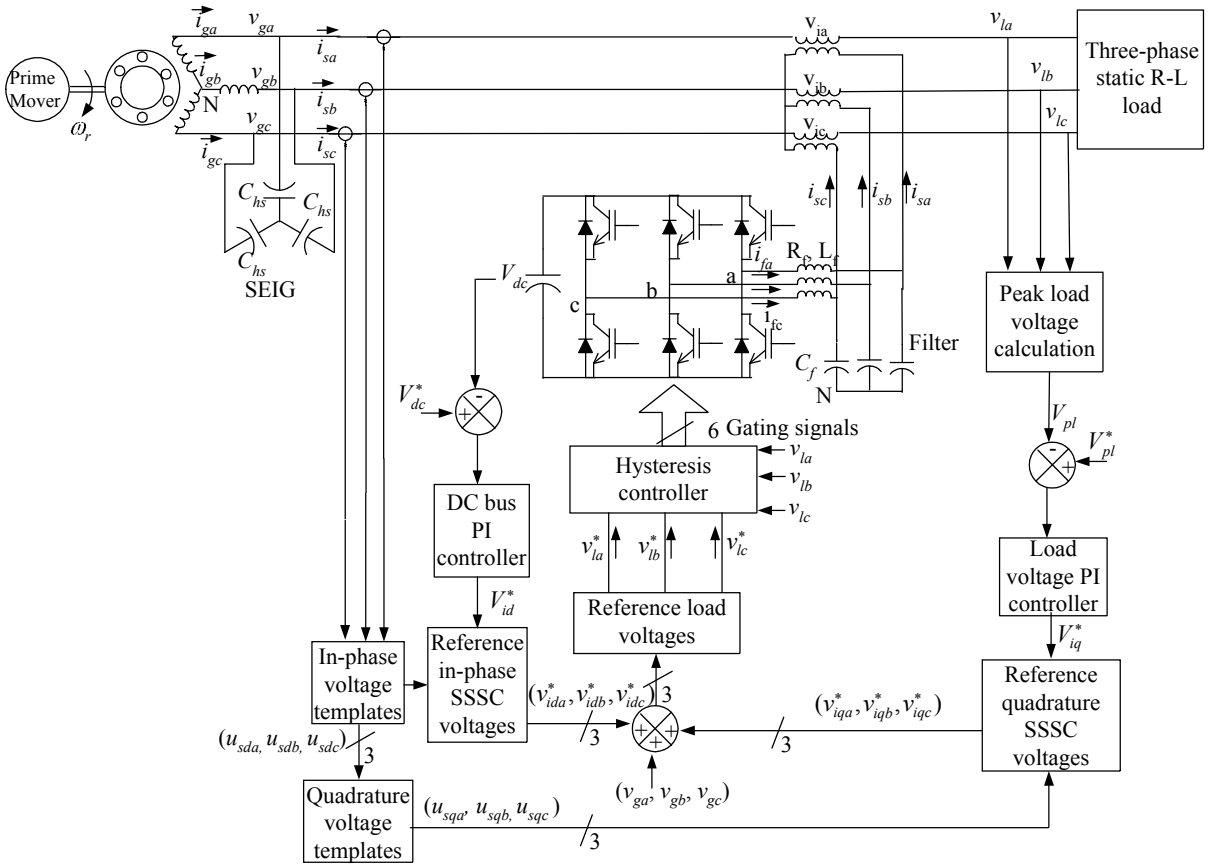


***Fig. 7.4 SEIG-capacitor supported SSSC system with the associated control technique***

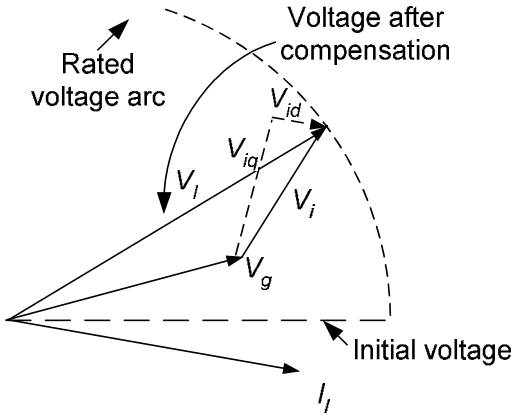


***Fig. 7.5 Phasor diagram of system under supply voltage dip***

The proposed control technique is based on current control mode and consists of two proportional-integral (PI) controllers. First PI control is employed on DC bus voltage ($V_{dc}$) and its reference value ($V^*_{dc}$), which maintains the DC bus voltage by charging and discharging the DC bus capacitor. The output of this PI controller is taken as peak in-

phase SSSC voltage ($V_{id}^{*}$). The in-phase voltage templates ($u_{sda}$, $u_{sdb}$, $u_{sdc}$) are obtained using sensed supply currents ($i_{sa}$, $i_{sb}$, $i_{sc}$) and quadrature current templates are derived using in-phase current templates. The reference in-phase SSSC voltages ($v_{ida}^{*}, v_{idc}^{*}, v_{idc}^{*}$) are obtained by multiplying peak in-phase SSSC voltage and in-phase voltage templates. The second PI controller is employed on peak load voltage ($V_{pl}$) and its reference value ($V_{pl}^{*}$), which maintains the load voltage by injecting the voltages in quadrature. The output of this PI controller is taken as peak quadrature SSSC voltage ($V_{iq}^{*}$). The reference quadrature SSSC voltages ($v_{iqa}^{*}, v_{iqb}^{*}, v_{iqc}^{*}$) are obtained by multiplying peak quadrature SSSC voltage with quadrature voltage templates. The reference load voltages ($v_{la}^{*}, v_{lb}^{*}, v_{lc}^{*}$) are obtained by summing up the generator voltages ($v_{ga}$, $v_{gb}$, $v_{gc}$), reference in-phase SSSC voltages and reference quadrature SSSC voltages. The hysteresis controller is used for generating the gating signals ($S_a$, $S_b$, $S_c$) for IGBTs of SSSC by comparing actual and reference load voltages. This scheme is similar to the control technique used for the STATCOM, is discussed in previous chapter.

## 7.3 DESIGN METHODOLOGY OF SSSC PARAMETERS

A general design methodology is proposed in this section for the selection of SSSC parameters for both battery and capacitor supported SSSC systems.

### 7.3.1 Battery Supported SSSC Parameters

- Volt-ampere (VA) rating of SSSC is equal to the product of maximum injection voltage and the current, which is taken as the supply current with an additional margin of 10%, to account for transient in supply current.

- Battery voltage $v_{bat}$ is decided by the depth of compensation desired from the SSSC. Smaller value of $v_{bat}$ results insufficient voltage injection. Here, $v_{bat}$ is taken with 10% higher over the maximum injection voltage, to account for the voltage drop in the ripple filter.

- The main aim of L-C filter is to remove the high frequency components from the output voltage of VSC. The sizing of filter inductor is governed by the allowable ripples in the compensation currents. Small inductor results in high ripple content

in the compensation voltage, and polluting the load voltage with high frequency switching harmonics. Whereas, the large inductor results in sluggish response of the compensator. An appropriate value of the inductor depends upon switching frequency $f_s$ and peak ripple current $i_{rpp}$ with associated ripple band $K_{rp}$. The inductor value [156, 231] is therefore expressed as,

$$L_f = \frac{\left(\frac{\sqrt{3}}{2}\right) v_{bat}}{6af_s K_{rp} i_{rpp}} \tag{7.1}$$

where, constant $a$ lies between 1.2-2.0 to account for transient current and ripple band ($K_{rp}$) =0.05-0.1.

- The sizing of ripple filter capacitor $C_f$ is decided on the basis of filtering requirement of compensation voltage. The lower capacitance offers large impedance to the fundamental frequency current component and therefore reasonable value is selected to obtain good compensation voltage at fundamental frequency. The natural frequency $f_n$ of L-C filter is selected as $K_{sf}$ times the switching frequency $f_s$ of VSC [267]. The switching frequency is varying in hysteresis current controller. The maximum switching frequency is assumed to be10 kHz. The natural frequency of L-C filter $f_n$ and switching frequency $f_s$ are related as,

$$f_n = \frac{1}{2\pi\sqrt{L_f C_f}} \tag{7.2}$$

$$f_n = K_{sf} f_s \tag{7.3}$$

The range of $K_{sf}$ is 0.05-0.2.

The $C_f$ can be obtained from eqn. (7.2) and eqn. (7.3) as,

$$C_f = \frac{1}{\left(2\pi K_{sf} f_s\right)^2 L_f} \tag{7.4}$$

- The performance of VSC depends on appropriate series injection transformer. The selection of injection transformer [265] is made, considering the following points.

  - It should possess low power loss, as the transformer is permanently connected in the lines.

- It should have small leakage reactance to result small non-sinusoidal voltage drop during the non-linear current flowing through the transformer.

- It should have high operating frequency, as it has to reproduce the pulsating high switching frequency voltage of VSC.

- It should have VA rating higher than SSSC rating, It although involves higher cost and larger size but the transformer of lower VA rating may lead to saturation, overheating and improper operation of VSC.

- The SSSC device ratings depend upon type of the transformer. For the step up series transformer (step up the injected voltage to the supply side), the current ratings of IGBTs and the ripple filter elements are to be high whereas voltage rating is small and vice versa for the step down series transformer.

- On the basis of above factors, the volt-ampere (VA) rating of unity turn ratio insertion transformer is selected 20% over the VA rating of SSSC for satisfactory performance.

- The IGBTs are selected to have good performance for moderate voltage/current ratings and high switching frequency operation. The device voltage and current ratings are selected on the basis of battery voltage and SSSC rating with a factor, which accounts transient conditions and safe operation of device.

The steady state load voltage drop under specified load condition gives a criterion about injected voltage. On the basis of above selection guidelines, the SSSC is designed for resistive, resistive-inductive and resistive-capacitive loads. Correspondingly, the designed parameters are summarized in Table 7.1.

### 7.3.2 Capacitor Supported SSSC Parameters

The methodology described in section 7.3.1 can be used to design various parameters of capacitor supported SSSC. In the capacitor supported SSSC, the sizing of DC bus capacitor is important because it acts as a DC source to provide real power exchange during transient conditions. The $C_{dc}$ is calculated on the basis of energy balance equation as,

$$C_{dc} = \frac{3V_l I_l t}{\left[V_{dcr}^2 - V_{dc}^2\right]} \tag{7.5}$$

where, $V_l$ and $I_l$ are the load voltage and current respectively, t is the response time of SSSC, $V_{dc}$ and $V_{dcr}$ are the actual and reference DC bus voltage.

The parameters of capacitor supported SSSC for feeding 0.8 pf static resistive-inductive load are summarized in Table 7.2.

***Table 7.1 Values of battery supported SSSC parameters for different loads***

| **SSSC Components** | **Resistive load (3 kW)** | **R-L Load (0.8 pf, 2.0 kW)** | **R-C load (0.8 pf, 3.0 kW)** |
|---|---|---|---|
| SSSC kVA rating | 1.247 | 2.426 | 0.612 |
| Battery voltage (V) | 99 | 231 | 38.5 |
| Filter inductor (mH) | 1.202 | 3.37 | 0.37 |
| Filter capacitor (μF) | 21.05 | 7.52 | 68.3 |
| Transformer kVA rating | 1.372 | 2.668 | 0.673 |
| Device selection | IGBT | IGBT | IGBT |
| Device voltage rating (V) | 119.0 | 277.0 | 46.0 |
| Device current rating (A) | 5.55 | 4.62 | 7.0 |

***Table 7.2 Values of capacitor supported SSSC parameters for static R-L load***

| **SSSC Components** | **R-L Load (0.8 pf, 2.0 kW)** |
|---|---|
| SSSC kVA rating | 2.426 |
| Reference DC bus voltage (V) | 350 |
| DC bus capacitor (μF) | 491.0 |
| Filter inductor (mH) | 7.73 |
| Filter capacitor (μF) | 3.27 |
| Transformer kVA rating | 2.668 |
| Device selection | IGBT |
| Device voltage rating (V) | 420 |
| Device current rating (A) | 4.62 |

## 7.4 STEADY STATE ANALYSIS OF SHORT SHUNT SEIG

The steady state analysis of short shunt SEIG feeding static resistive and resistive-inductive loads is carried out using steady state equivalent circuit as shown in Fig. 7.6. The optimum values of capacitances are selected using the algorithm, which is based on genetic algorithm, is described herewith.

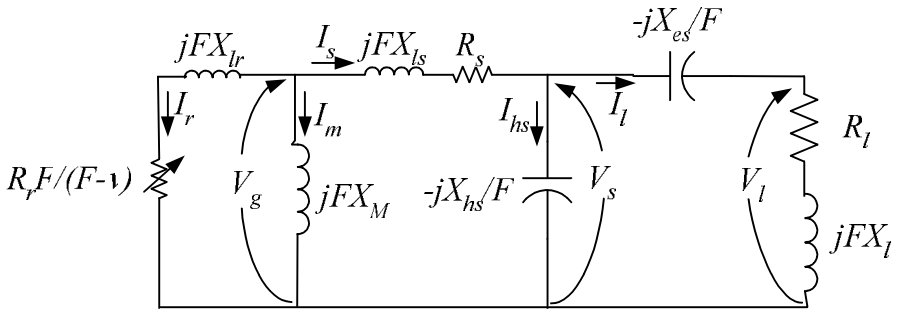


***Fig. 7.6 Steady state equivalent circuit of short shunt SEIG feeding R-L load***

### 7.4.1 Problem Statement

The shunt and series capacitances $C_{hs}$, $C_{es}$ are selected to provide the optimum performance for short shunt SEIG using steady state equivalent circuit, which is shown in Fig. 7.4. The parameters $C_{hs}$, $C_{es}$ at specified speed ν are computed for optimum voltage regulation for loading up to rated capacity at rated voltage and for optimum performance defined as a combination of loading capacity and voltage regulation characteristic. The problem formulation is explained through the following as,

- Fitness function
- Equality constraints
- Inequality constraints
- Bound on variables

#### *7.4.1.1 Fitness function*

The objective function '$f_{obj1}$' representing the voltage regulation characteristic, is defined as the minimization of the summation of squared mismatch between load voltage and rated voltage from no load ($n$=0) to *npr* point and is expressed as,

$$f_{obj1}(C_{hs}, C_{es}, \nu) = \sum_{n=0}^{npr} \left( \frac{V_{\ln}(C_{hs}, C_{es}) - V_r}{V_r} \right)^2 \tag{7.6}$$

Correspondingly, the fitness function $f_1$ is expressed as,

$$f_1 = \frac{1}{\left(1 + f_{obj1}\right)} \tag{7.7}$$

The optimum performance, defined as a combination of the of voltage regulation characteristic and loadability for *npm* points, correspondingly, the fitness function $f_2$ is expressed as,

$$f_2 = K_{vr} \frac{1}{\left(1 + f_{obj2}\right)} + K_{ld} \left( \frac{P_l}{P_r} \right) \tag{7.8}$$

where,

$$f_{obj2}(C_{hs}, C_{es}, \nu) = \sum_{n=0}^{npm} \left( \frac{V_{\ln}(C_{hs}, C_{es}) - V_r}{V_r} \right)^2 \tag{7.9}$$

The $K_{vr}$ and $K_{ld}$ are the weightage factor for voltage regulation and loadability respectively.

### *7.4.1.2 Equality Constraints*

The equality constraints are obtained from real and imaginary parts of loop impedance, derived as,

From Fig. 7.6, the loop impedance $Z_{LH}$ can be obtained as,

$$Z_{rM} = \frac{jX_M \left( \frac{R_r F}{(F - \nu)} + jFX_{lr} \right)}{\frac{R_r F}{(F - \nu)} + j(X_M + FX_{lr})} \tag{7.10}$$

$$Z_{hel} = \frac{-j \frac{X_{hs}}{F} \left\{ R_l + j \left( -\frac{X_{es}}{F} + FX_l \right) \right\}}{R_l + j \left( -\frac{X_{es}}{F} - \frac{X_{hs}}{F} + FX_l \right)} \tag{7.11}$$

$$Z_s = R_s + jFX_{ls} \tag{7.12}$$

The loop impedance $Z_{LS}$ can be obtained as,

$$Z_{LH} = Z_{rM} + Z_{hel} + Z_s \tag{7.13}$$

The voltage drop in the stator side loop should be zero. Due to self-excitation, $I_s$ can not be zero, the equality constraints are derived as,

$$Z_{LH} = 0 \tag{7.14}$$

where, $Z_{LH} = G_H(C_{hs}, C_{es}, \nu) + jH_H(C_{hs}, C_{es}, \nu) = 0$

The $G_H$ and $H_H$ at '$n^{th}$' load point are expressed as,

$$\begin{aligned} G_{Hn} &= \sum_{m=0}^{4}\left(C_n^{2m+1} + C_n^{2m+2}X_{Mn}\right)F_n^m = 0 \\ H_{Hn} &= \sum_{m=0}^{5}\left(D_n^{2m+1} + D_n^{2m+2}X_{Mn}\right)F_n^m = 0 \end{aligned} \tag{7.15}$$

The coefficients $C$ and $D$ are expressed in Appendix-I.

### *7.4.1.3 Inequality Constraints*

The limiting values of various performance parameters $I_s$, $V_s$ and $V_l$ are included as inequality constraint. These inequality constraints for $n^{\text{th}}$ load point are as,

$$\begin{aligned} X_M^{mn} &\le X_{Mn} \le X_M^{mx} \\ F^{mn} &\le F_n \le F^{mx} \\ I_{sn} &\le I_s^{mx} \\ V_{sn} &\le V_s^{mx} \\ V_l^{mn} &\le V_{l\text{n}} \le V_l^{mx} \end{aligned} \tag{7.16}$$

The minimum and maximum limiting value of $X_M$ is taken as 0.1 pu (representing SEIG operation in deep saturation) and $X_M^{uns}$ beyond which self-excitation is not possible. The maximum and minimum frequency is considered as ν pu to 0.95ν pu respectively. The current $I_s^{mx}$ and voltage $V_s^{mx}$ are taken as 1.1 pu, beyond which the machine is not allowed to operate continuously due to overheating and insulation stress. The voltages $V_l^{mn}$ and $V_l^{mx}$ are taken as 0.92 pu and 1.08 pu respectively. The more stringent limit on the load voltage results poor loading capacity of SEIG for inductive loads. It is also desired that the SEIG delivers at least 70% of rated power for the reasonable utilization of the machine.

#### *7.4.1.4 Bounds on variables*

The self-excitation in SEIG is possible for a limited range of $C_{hs}$ at a given prime mover speed ν. The capacitance $C_{hs}^{mn}$ is the minimum value required for rated terminal voltage at no load for $v^{mx}$, whereas the $C_{hs}^{mx}$ is the maximum capacitance required for rated terminal voltage at full load for $v^{mn}$ beyond which self-excitation is not possible.

$$\begin{aligned} C_{hs}^{mn} \le C_{hs} \le C_{hs}^{mx} \\ C_{es}^{mn} \le C_{es} \le C_{es}^{mx} \end{aligned} \tag{7.17}$$

The limiting values of $C_{es}$ are selected as $C_{hs}^{mn}$ and $2C_{hs}^{mx}$ to cover the possible optimum solution.

### 7.4.2 Optimization Algorithm

The genetic algorithms (GAs) are derived from natural phenomenon, which mimics the principle of natural selection to constitute the search and optimization technique. The formulation of optimum voltage regulation and optimum performance as constraint optimization problems consist of eqn. (7.6) to eqn. (7.17). These optimization problems are solved using GA. The applied binary GA consists of binary coding of variables, Roulette-wheel selection, single point random crossover and random mutation operator. The algorithm to select the optimum values of $C_{hs}$, $C_{es}$ for specified ν are described in brief as,

1. Initialize the parameters such as population size (*ps*), iteration *itr*=1, not changing fitness iteration ($i_{trnc}$) =0, maximum iteration $itr_{mx}$, maximum iteration for which fitness is not changing ($itr_{ncm}$). Moreover, choose the crossover ($P_c$) and mutation ($P_m$) probability, string length of each variable.
2. Specify the limiting values of inequality constraints and calculate the limiting values of $C_{hs}$, and $C_{es}$ for specified speed ν.
3. Randomly generate the population of binary strings and decode the $C_{hs}$, and $C_{es}$.
4. Check the feasibility and Evaluate the fitness value for each string using eqn. (7.7) and eqn. (7.8) and let $gbest = fit^{max}$.
5. Create the selection pool through Roulette-wheel selection and retain the best solution to preserve the elitism.

6. Randomly select the two strings from pool and the crossover site. Generate new solutions through crossover operation by comparing a random number with $P_c$.

7. Perform the mutation operation on each bit of offspring generated through crossover by comparing a random number with $P_m$.

8. Decode $C_{hs}$ and $C_{es}$, check the feasibility and evaluate the fitness of the newly generated offspring and $itr=itr+1$.

9. if $fit^{max}$ = gbest, $itr_{nc}=itr_{nc}+1$ otherwise $gbest = fit^{max}$, $itr_{nc}=0$.

10. If $itr<itr_{mx}$ or $itr_{nc}<itr_{ncm}$ then go to step 5, otherwise stop.

## 7.5 TRANSIENT PERFORMANCE ANALYSIS OF SEIG-SSSC SYSTEM

The dynamic model of SEIG-SSSC is obtained through the equations of the following,

- SEIG model
- Battery supported SSSC with associated control
- Capacitor supported SSSC with associated control
- Loads

### 7.5.1 SEIG Model

The dynamic model of an induction generator, in stationary q-d reference frame, considering the effect of both main and cross flux saturation is explained in previous chapter. The state space equations are expressed herewith for ready reference as,

$$p[\mathbf{i}] = [\mathbf{L}]^{-1}\left([\mathbf{v}] - [\mathbf{r}][\mathbf{i}] - [\mathbf{G}][\mathbf{i}]\right) \tag{7.18}$$

$$p\omega_r = \frac{P}{2J}\left(T_P - T_{em}\right) \tag{7.19}$$

where, $[\mathbf{v}]$, $[\mathbf{i}]$, $[\mathbf{r}]$, $[\mathbf{L}]$, $[\mathbf{G}]$ and $T_{em}$ are defined in Appendix-B.

The equations for star connected shunt capacitor at SEIG terminals in state space form are written as,

$$pv_{ga} = \frac{(i_{ga} - i_{sa})}{C_{sh}}$$
$$pv_{gb} = \frac{(i_{gb} - i_{sb})}{C_{sh}} \quad (7.20)$$
$$pv_{gc} = \frac{(i_{gc} - i_{sc})}{C_{sh}}$$

where, $i_{ga}$, $i_{gb}$, $i_{gc}$ are generator line currents and $i_{sa}$, $i_{sb}$, $i_{sc}$ are supply currents, which are equal to load currents.

### 7.5.2 Battery Supported SSSC Model and Control

The model equations of SSSC and associated control technique are comprised of the equations of the following components.

- Filter inductor currents
- AC side PWM voltages
- Filter capacitor
- PI controller
- Reference supply currents
- Hysteresis current controller
- Battery model

#### *7.5.2.1 Filter Inductor Currents*

The filter current equations in state space form are written as,

$$pi_{fa} = \frac{1}{L_f}\left(e_a - v_{ia} - R_f i_{fa}\right)$$
$$pi_{fb} = \frac{1}{L_f}\left(e_b - v_{ib} - R_f i_{fb}\right) \quad (7.21)$$
$$pi_{fc} = \frac{1}{L_f}\left(e_c - v_{ic} - R_f i_{fc}\right)$$

where, $e_a$, $e_b$, $e_c$ are the ac side voltage of VSC; and $v_{ia}$, $v_{ib}$, $v_{ic}$ are injected voltage into the supply lines.

### *7.5.2.2 AC Side PWM Voltages*

The dc bus voltage $v_{bat}$ is reflected on the ac side of the PWM inverter in the form of voltages $e_a$, $e_b$ and $e_c$, which are expressed as,

$$\begin{bmatrix} e_a \\ e_b \\ e_c \end{bmatrix} = \frac{v_{bat}}{3} \begin{bmatrix} 2 & -1 & -1 \\ -1 & 2 & -1 \\ -1 & -1 & 2 \end{bmatrix} \begin{bmatrix} S_a \\ S_b \\ S_c \end{bmatrix} \tag{7.22}$$

where, $S_a$, $S_b$ and $S_c$ are switching functions of VSC.

### *7.5.2.3 Filter Capacitor*

The equations of ripple filter capacitor in terms of compensation currents $i_{fa}$, $i_{fb}$, $i_{fc}$ and unity turn ratio injection transformer secondary currents, which are equal to supply currents $i_{sa}$, $i_{sb}$, $i_{sc}$, in state space form are written as,

$$\begin{aligned} pv_{ia} &= \frac{1}{C_c}\left(i_{fa} - i_{sa}\right) \\ pv_{ib} &= \frac{1}{C_c}\left(i_{fb} - i_{sb}\right) \\ pv_{ic} &= \frac{1}{C_c}\left(i_{fc} - i_{sc}\right) \end{aligned} \tag{7.23}$$

### *7.5.2.4 PI Controller*

The voltage error, $e$ is the difference between reference peak voltage $V_{pl}^*$ and actual peak voltage $V_{pl}$ sensed through load voltages. At n$^{th}$ sampling instant, the error $e(n)$ and output $y(n)$ are expressed as,

$$\begin{aligned} e(n) &= V_{pl}^*(n) - V_{pl}(n) \\ y(n) &= y(n-1) + K_p\{(e(n) - e(n-1))\} + K_i e(n) \\ &= I_{sm}^* \end{aligned} \tag{7.24}$$

where, $y(n-1)$ and $e(n-1)$ are values of output and error at $(n-1)^{th}$ sampling instant. The PI controller equation as shown in eqn. (7.24) is derived in Appendix-E.

### *7.5.2.5 Reference Supply Current*

The control technique for generating reference supply currents $\left(i_{sa}^*, i_{sb}^*, i_{sc}^*\right)$ is depicted in Fig. 7.3. In-phase current templates $\left(u_{sda}, u_{sdb}, u_{sdc}\right)$ are obtained as,

$$\begin{bmatrix} u_{sda} & u_{sdb} & u_{sdc} \end{bmatrix}^T = \begin{bmatrix} \frac{i_{sa}}{i_{sm}} & \frac{i_{sb}}{i_{sm}} & \frac{i_{sc}}{i_{sm}} \end{bmatrix}^T \tag{7.25}$$

where,

$$i_{sm} = \sqrt{\frac{2}{3}\left(i_{sa}^2 + i_{sb}^2 + i_{sc}^2\right)} \tag{7.26}$$

Quadrature current templates $\left(u_{sqa}, u_{sqb}, u_{sqc}\right)$ are obtained from in-phase current templates as,

$$\begin{bmatrix} u_{sqa} \\ u_{sqb} \\ u_{sqc} \end{bmatrix} = \begin{bmatrix} 0 & -1/\sqrt{3} & 1/\sqrt{3} \\ \sqrt{3}/2 & 1/2\sqrt{3} & -1/2\sqrt{3} \\ -\sqrt{3}/2 & 1/2\sqrt{3} & -1/2\sqrt{3} \end{bmatrix} \begin{bmatrix} u_{sda} \\ u_{sdb} \\ u_{sdc} \end{bmatrix} \tag{7.27}$$

The PI controller over peak load voltage ($V_{pl}$) and reference peak load voltage ($V_{pl}^*$) results in reference peak supply current $I_{sm}^*$, which when multiplied by quadrature current templates ($u_{sqa}$, $u_{sqb}$, $u_{sqc}$) gives reference supply currents $\left(i_{sa}^*, i_{sb}^*, i_{sc}^*\right)$ as,

$$\begin{bmatrix} i_{sa}^* \\ i_{sb}^* \\ i_{sc}^* \end{bmatrix} = I_{sm}^* \begin{bmatrix} u_{sqa} \\ u_{sqb} \\ u_{sqc} \end{bmatrix} \tag{7.28}$$

#### *7.5.2.6 Hysteresis Current Controller*

The switching functions to obtain gating signals for IGBTs of the CC-VSC are derived from the hysteresis controller having *HB* current band. The switching function $S_a$ for phase '*a*' is expressed as,

$$\text{If } i_{sa} < \left(i_{sa}^* - HB\right) \; S_1 \text{ OFF}, \; S_4 \text{ ON} \Rightarrow S_a = 0 \tag{7.29}$$

$$\text{If } i_{sa} > \left(i_{sa}^* + HB\right) \; S_1 \text{ ON}, \; S_4 \text{ OFF} \Rightarrow S_a = 1 \tag{7.30}$$

Similarly, switching functions $S_b$ and $S_c$ can be derived for phase '*b*' and phase '*c*' respectively.

#### *7.5.2.7 Battery Model*

The inductive loading of SEIG is associated with a dip in the generated voltage, therefore SSSC is always in operative mode and the battery is continuously in charging

and discharging modes. The Thevenin's discharge electrical model [263], as shown in Fig. 7.7, is used for this study.

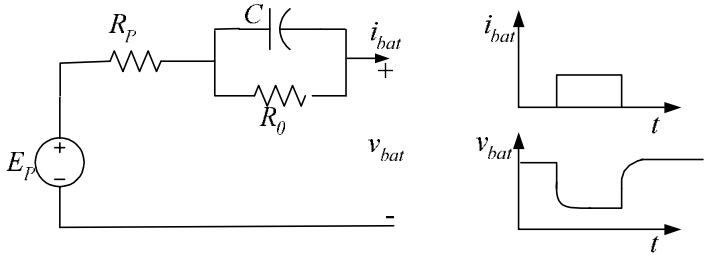


***Fig. 7.7 Thevenin's discharge battery model***

The battery parameters are as,

- $E_p$ signifies the equilibrium electromotive force of the battery under discharged condition.
- $R_P$ represents ohmic polarization.
- Resistance $R_0$ signifies charge transfer losses.
- Capacitance $C$ signifies the double layer effect dynamics.

These battery parameters are non-linear and assumed to be dependent mainly on battery discharge current. At the beginning of discharge, the battery voltage decreases sharply because of ohmic polarization resistance, followed by exponential slow decrease caused by chemical changes at the surface of the active materials, which can be better explained by RC discharge time coefficient ($\tau_0=R_0C$). The charging also follows the same sequence. During discharge, the $v_{bat}$ can be written [263] as,

$$v_{bat} = E_p - i_{bat}(R_p + R_0) + i_{bat}R_0 e^{(-t/\tau_0)} \tag{7.31}$$

### 7.5.3 Capacitor Supported SSSC Model and Control

The model of capacitor supported SSSC and associated control consists of equations for the following,

- In-phase SSSC voltages
- Quadrature SSSC voltages

- Reference load voltages
- Hysteresis controller
- DC bus capacitor and filter inductor current

### *7.5.3.1 In-Phase SSSC Voltages*

The reference peak in-phase SSSC voltage $V_{id}^{*}$ is taken as the output $y_{vdc}$ of PI controller while processing the voltage error $e_{vdc}$ computed over DC bus voltage $V_{dc}$ and its reference DC bus voltage $V_{dc}^{*}$. The voltage error $e_{vdc}(n)$ and output $y_{vdc}(n)$ at $n^{th}$ sampling instant are expressed as,

$$\begin{aligned} e_{vdc}(n) &= V_{dc}^{*}(n) - V_{dc}(n) \\ y_{vdc}(n) &= y_{vdc}(n-1) + K_{pvdc}(e_{vdc}(n) - e_{vdc}(n-1)) + K_{ivdc}e_{vdc}(n) \\ &= V_{id}^{*} \end{aligned} \tag{7.32}$$

where, $y_{vdc}(n\text{-}1)$ and $e_{vdc}(n\text{-}1)$ are the output of the PI controller and error at $(n\text{-}1)^{th}$ sampling instant respectively.

The reference in-phase SSSC voltages are expressed using in-phase voltage templates $u_{sda}, u_{sdb}, u_{sdc}$ as,

$$\begin{bmatrix} v_{ida}^{*} \\ v_{idb}^{*} \\ v_{idc}^{*} \end{bmatrix} = V_{id}^{*} \begin{bmatrix} u_{sda} \\ u_{sdb} \\ u_{sdc} \end{bmatrix} \tag{7.33}$$

where $u_{sda}$, $u_{sdb}$ and $u_{sdc}$ are derived as,

$$\begin{aligned} u_{sda} &= \frac{i_{sa}}{I_{sm}} \\ u_{sdb} &= \frac{i_{sb}}{I_{sm}} \\ u_{sdc} &= \frac{i_{sc}}{I_{sm}} \end{aligned} \tag{7.34}$$

$I_{sm}$, the peak supply current is computed as,

$$I_{sm} = \left\{ \frac{2}{3} \left( i_{sa}^{2} + i_{sb}^{2} + i_{sc}^{2} \right) \right\}^{1/2} \tag{7.35}$$

### *7.5.3.2 Quadrature SSSC Voltages*

The PI control is employed over reference peak load voltage $V_{pl}^{*}$ and actual peak load voltage $V_{pl}$ sensed through load voltages. The output of this PI controller is taken as reference peak quadrature SSSC voltage ($V_{iq}^{*}$). The voltage error $e_{vpl}(n)$ and output $y_{vpl}(n)$ at n$^{th}$ sampling instant are expressed as,

$$\begin{aligned} e_{vpl}(n) &= V_{pl}^{*}(n) - V_{pl}(n) \\ y_{vpl}(n) &= y_{vpl}(n-1) + K_{pvpl}\left(e_{vpl}(n) - e_{vpl}(n-1)\right) + K_{ivpl}e_{vlm}(n) \\ &= V_{iq}^{*} \end{aligned} \tag{7.36}$$

where, $y(n\text{-}1)$ and $e(n\text{-}1)$ are values of output and error at $(n\text{-}1)^{th}$ sampling instant.

Quadrature voltage templates $\left(u_{sqa}, u_{sqb}, u_{sqc}\right)$ are obtained from in-phase voltage templates as,

$$\begin{bmatrix} u_{sqa} \\ u_{sqb} \\ u_{sqc} \end{bmatrix} = \begin{bmatrix} 0 & -1/\sqrt{3} & 1/\sqrt{3} \\ \sqrt{3}/2 & 1/2\sqrt{3} & -1/2\sqrt{3} \\ -\sqrt{3}/2 & 1/2\sqrt{3} & -1/2\sqrt{3} \end{bmatrix} \begin{bmatrix} u_{sda} \\ u_{sdb} \\ u_{sdc} \end{bmatrix} \tag{7.37}$$

The reference quadrature SSSC voltages ($v_{iqa}^{*}, v_{iqb}^{*}, v_{iqc}^{*}$) are obtained by multiplying $V_{iq}^{*}$ with quadrature voltage templates ($u_{sqa}$, $u_{sqb}$, $u_{sqc}$) gives as,

$$\begin{bmatrix} v_{iqa}^{*} \\ v_{iqb}^{*} \\ v_{iqc}^{*} \end{bmatrix} = V_{iq}^{*} \begin{bmatrix} u_{sqa} \\ u_{sqb} \\ u_{sqc} \end{bmatrix} \tag{7.38}$$

### *7.5.3.3 Reference Load Voltages*

The reference load voltages are the sum of generator voltages, reference in-phase and quadrature SSSC voltages and are expresses as,

$$\begin{bmatrix} v_{la}^{*} \\ v_{lb}^{*} \\ v_{lc}^{*} \end{bmatrix} = \begin{bmatrix} v_{ga} \\ v_{gb} \\ u_{gc} \end{bmatrix} + \begin{bmatrix} v_{ida}^{*} \\ v_{idb}^{*} \\ v_{idc}^{*} \end{bmatrix} + \begin{bmatrix} v_{iqa}^{*} \\ v_{iqb}^{*} \\ v_{iqc}^{*} \end{bmatrix} \tag{7.39}$$

#### *7.5.3.4 Hysteresis Controller*

The switching function for 'a' phase of SSSC ($S_a$) is derived using $v_{la}$ and $v_{la}^*$ as follows,

$$\text{If } v_{la} < \left(v_{la}^* - HB\right) \; S_1 \text{ OFF}, \; S_4 \text{ ON} \Rightarrow S_a = 0 \tag{7.40}$$

$$\text{If } v_{la} > \left(v_{la}^* + HB\right) \; S_1 \text{ ON}, \; S_4 \text{ OFF} \Rightarrow S_a = 1 \tag{7.41}$$

where, $HB$ is the hysteresis band of the controller. Similarly, the switching function for 'b' and 'c' phases can be derived.

#### *7.5.3.5 DC Bus Capacitor and Filter Inductor Current*

The SSSC is a 3-ϕ CC-VSC with self-supporting DC bus employing DC bus capacitor. The charging/discharging of DC bus capacitor is governed by,

$$pV_{dc} = \frac{\left(i_{ca}S_a + i_{cb}S_b + i_{cc}S_c\right)}{C_{dc}} \tag{7.42}$$

The DC bus voltage reflects on the AC side of the PWM converter in the form of voltages $e_a$, $e_b$ and $e_c$, which are expressed as,

$$\begin{bmatrix} e_a \\ e_b \\ e_c \end{bmatrix} = \frac{V_{dc}}{3} \begin{bmatrix} 2 & -1 & -1 \\ -1 & 2 & -1 \\ -1 & -1 & 2 \end{bmatrix} \begin{bmatrix} S_a \\ S_b \\ S_c \end{bmatrix} \tag{7.43}$$

The filter current equations in state space form are written as,

$$\begin{aligned} pi_{fa} &= \frac{1}{L_f}\left(e_a - v_{ia} - R_f i_{fa}\right) \\ pi_{fb} &= \frac{1}{L_f}\left(e_b - v_{ib} - R_f i_{fb}\right) \\ pi_{fc} &= \frac{1}{L_f}\left(e_c - v_{ic} - R_f i_{fc}\right) \end{aligned} \tag{7.44}$$

where, $e_a$, $e_b$, $e_c$ are the ac side voltage of VSC; and $v_{ia}$, $v_{ib}$, $v_{ic}$ are injected voltage into the supply lines.

### 7.5.4 Load Model

The load model consists of the equations for the following loads,

- Resistive load.

- Resistive-inductive load.
- Resistive-capacitive load.

#### *7.5.4.1 Resistive Load*

The load currents ($i_{la}$, $i_{lb}$, $i_{lc}$) for the star connected resistive $R_l$ load are written as,

$$\begin{aligned} i_{la} &= \frac{(v_{ga} - v_{ia})}{R_l} \\ i_{lb} &= \frac{(v_{gb} - v_{ib})}{R_l} \\ i_{lc} &= \frac{(v_{gc} - v_{ic})}{R_l} \end{aligned} \tag{7.45}$$

#### *7.5.4.2 Resistive-Inductive Load*

The state space current equations for star connected resistive-inductive ($R_l$-$L_l$) load are written as,

$$\begin{aligned} pi_{la} &= \frac{1}{L_l}\left(v_{ga} - v_{ia} - R_l i_{la}\right) \\ pi_{lb} &= \frac{1}{L_l}\left(v_{gb} - v_{ib} - R_l i_{lb}\right) \\ pi_{lc} &= \frac{1}{L_l}\left(v_{gc} - v_{ic} - R_l i_{lc}\right) \end{aligned} \tag{7.46}$$

where, $v_{ia}$, $v_{ib}$, $v_{ic}$ are injected voltages by SSSC.

#### *7.5.4.3 Resistive-Capacitive Load*

The voltages $v_{cla}$, $v_{clb}$, $v_{clc}$ across the load capacitors for star connected series resistive-capacitive ($R_l$-$C_l$) load are written in state space form as,

$$\begin{aligned} pv_{cla} &= \frac{1}{R_l C_l}\left(v_{ga} - v_{ia} - v_{cla}\right) \\ pv_{clb} &= \frac{1}{R_l C_l}\left(v_{gb} - v_{ib} - v_{clb}\right) \\ pv_{clc} &= \frac{1}{R_l C_l}\left(v_{gc} - v_{ic} - v_{clc}\right) \end{aligned} \tag{7.47}$$

The SEIG-battery supported SSSC system model with static loads is therefore represented by the set of state space equations including other important equations from eqn. (7.18) to eqn. (7.31) and eqn. (7.45) to eqn. (7.47).

The SEIG-capacitor supported SSSC model with static R-L load is represented by set of state space equations including important equations from eqn. (7.18) to eqn. (7.20), eqn. (7.32) to eqn. (7.44) and eqn. (7.46). These equations are solved by fourth order Runge-Kutta integration method in MATLAB environment.

### 7.5.5 Algorithm for Simulating SEIG-SSSC Performance

The simulation algorithm is briefly explained for the transient analysis of SEIG-SSSC system feeding static R-L load.

1. Read the SEIG parameter, its magnetizing characteristic, shunt capacitance $C_{sh}$, Static R-L load ($R_l$-$L_l$) parameter, time for connecting the SSSC ($t_{SSSC}$), time for load connection ($t_{RL}$), time for load changing ($t_{RLC}$), total simulation time ($t_T$), time step ($\Delta t$). Also read the SSSC parameters, load voltage PI controller gains.
2. Set $t$=0, $[i_{qs} \quad i_{ds}]^T = [0.0001 \quad 0.0001]^T$ to account residual magnetism, voltage buildup resistance ($R_{lvb}$)=20000.
3. Compute $i_M$, $L_M$ and obtain $[\mathbf{L}]$ and $[\mathbf{G}]$.
4. if $t<t_{SSSC}$ than evaluate eight derivatives as $p[\mathbf{i}]$, $p\omega_r$, $pv_{ga}$, $pv_{gb}$, $pv_{gc}$ for no load voltage buildup and go to step 10.
5. Detect the zero crossing instant and sense the $i_{sa}$, $i_{sb}$, $i_{sc}$ and calculate the peak supply current ($I^*_{sm}$) with the help of eqn. (7.26) from sensed supply currents.
6. Generate the gating signals for the six IGBTs of VSC from the control scheme depicted in Fig. 7.3.
7. If $t<t_{RL}$ than evaluate fourteen derivatives as $p[\mathbf{i}]$, $p\omega_r$, $pv_{ga}$, $pv_{gb}$, $pv_{gc}$, $pi_{fa}$, $pi_{fb}$, $pi_{fc}$, $pv_{ia}$, $pv_{ib}$, $pv_{ic}$ for switching of SSSC in the system.
8. If $t<t_{RLC}$ than evaluate seventeen derivatives as $p[\mathbf{i}]$, $p\omega_r$, $pv_{ga}$, $pv_{gb}$, $pv_{gc}$, $pi_{fa}$, $pi_{fb}$, $pi_{fc}$, $pv_{ia}$, $pv_{ib}$, $pv_{ic}$, $pi_{la}$, $pi_{lb}$, $pi_{lc}$ for connection of R-L load to the SEIG-SSSC system.

9. If $t>t_{RLC}$, change the load parameters $R_l$ and $L_l$.
10. Compute the instantaneous values of variables by fourth order Runge-Kutta method.
11. Express generator currents into phase variables and evaluate line currents and store them along with other variables ($i_{ga}$, $i_{gb}$ $i_{gc}$, $v_{ga}$, $v_{gb}$, $v_{gc}$, $v_{ia}$, $v_{ib}$, $v_{ic}$, $i_{la}$, $i_{lb}$ $i_{lc}$) in a data file.
12. If $t<t_T$ than $t=t+\Delta t$ and go to step 3
13. Plot the required waveforms.

The simulation algorithm of SEIG-SSSC is modified accordingly for other loads.

## 7.6 RESULTS AND DISCUSSION

The performance of the series compensated SEIG for feeding linear static loads has been studied and the results are summarized as follows,

- Steady State Performance of Short Shunt SEIG
- Transient Performance of SEIG-Battery Supported SSSC System Feeding Static Loads
- Transient Performance of SEIG-Capacitor Supported SSSC System Feeding Static Load

### 7.6.1 Steady State Performance of Short Shunt SEIG

The simulation and experimental investigations for steady state performance using short shunt SEIG are carried out on a 3-ϕ, Δ-connected, 415 V, 5.5 kW, induction machine operated as a SEIG. The parameters of induction machine, its magnetizing characteristic are given in Appendix-A, and the parameters of GA are summarized in Appendix-D. The SEIG is driven by 3-ϕ, 415V, 10 kVA, 0.8 pf, 1500 rpm synchronous motor. The $C_{hs}$, $C_{es}$ for speed range between $v^{mx}$ as 1.12 pu and $v^{mn}$ as 0.88 pu are obtained for optimum voltage regulation and optimum performance from the developed optimization algorithm. As discussed in Section 7.4, the optimum performance is considered as the weighted sum of voltage regulation in loading range and loadability. The optimum performance is evaluated for higher weightage to loadability ($K_{ld}>K_{vr}$) and

higher weightage to voltage regulation ($K_{ld}<K_{vr}$). As the SEIG is driven by the synchronous machine, the simulated results for 1.0 pu speed are validated experimentally. The optimization is carried out for feeding resistive and 0.9 pf resistive-inductive loads.

#### *7.6.1.1 Optimum Voltage Regulation of Short Shunt SEIG*

The results of optimum voltage regulation for feasible speed range feeding resistive and 0.9 pf resistive-inductive load are shown in Table 7.3 and Table 7.4 respectively. The voltage regulation optimization is carried out by dividing the rated capacity 5.5 kW at rated voltage into 55 load points '*n*'. Thus, no load corresponds to *n*=0 and rated load corresponds to *n=npr* (55).

***Table 7.3 Summary of optimum voltage regulation for short shunt SEIG fed resistive load***

| $f_1$ | $C_{hs}$ (µF) | $C_{es}$ (µF) | *v* (pu) | Output power at *npr (pu)* | Remark |
|---|---|---|---|---|---|
| 0.994267 | 11.5 | 498.6 | 1.12 | 0.788689 | Maximum output |
| 0.999575 | 15.4 | 248.4 | 1.02 | 0.758152 | Optimum voltage regulation |
| 0.997672 | 17.2 | 268.4 | 1.0 | 0.745259 | Experimentally verified |

***Table 7.4 Summary of optimum voltage regulation for short shunt SEIG fed 0.9 pf R-L load***

| $f_1$ | $C_{hs}$ (µF) | $C_{es}$ (µF) | *v* (pu) | Output power at *npr (pu)* | Remark |
|---|---|---|---|---|---|
| 0.976693 | 18.5 | 161.2 | 1.0 | 0.712384 | Experimentally verified |
| 0.979745 | 21.3 | 212.4 | 0.98 | 0.845898 | Maximum output |
| 0.999994 | 31.3 | 185.0 | 0.88 | 0.723009 | Optimum voltage regulation |

For resistive load, the maximum output power is achieved at 1.12 pu speed with lower value of $C_{hs}$. As the speed decreases from 1.12 pu, the fitness value increases, output at *npr* slightly decreases and the $C_{hs}$ increases. The increase in shunt capacitance supplies the excitation VARs for reduced speed operation and thus maintains the desired voltage. The optimum voltage regulation is achieved above the rated speed at 1.02 pu.

Below this speed, the fitness value and output decrease but $C_{hs}$ continues to increase. The lower value of $C_{hs}$ compared to $C_{es}$ shows the dominance of shunt capacitance to supply the reactive VARs.

For 0.9 pf R-L load, the optimum voltage regulation is obtained at lower limiting speed of 0.88 pu speed with output at rated power *npr* as 0.723 pu, because the load parameters calculated at rated speed is offering higher power factor at reduced speed. The maximum output is resulted at slightly lower than synchronous speed for R-L load, whereas, the corresponding value is higher than synchronous speed for resistive load. The $f_l$ and $C_{hs}$ both are increasing with decreasing ν, whereas output at *npr* first increases to 0.84589 pu at 0.98 pu speed and later decreases with decrease in the speed. The range of $f_l$ is large and $C_{es}$ is small for resistive-inductive load as compared to respective range for resistive load.

The performance characteristics corresponding to optimum voltage regulation at rated speed for resistive and 0.9 pf R-L load are shown in Fig. 7.8 and Fig. 7.9 respectively. The characteristics are drawn for capacitances indicated in Table 7.3 and Table 7.4 respectively.

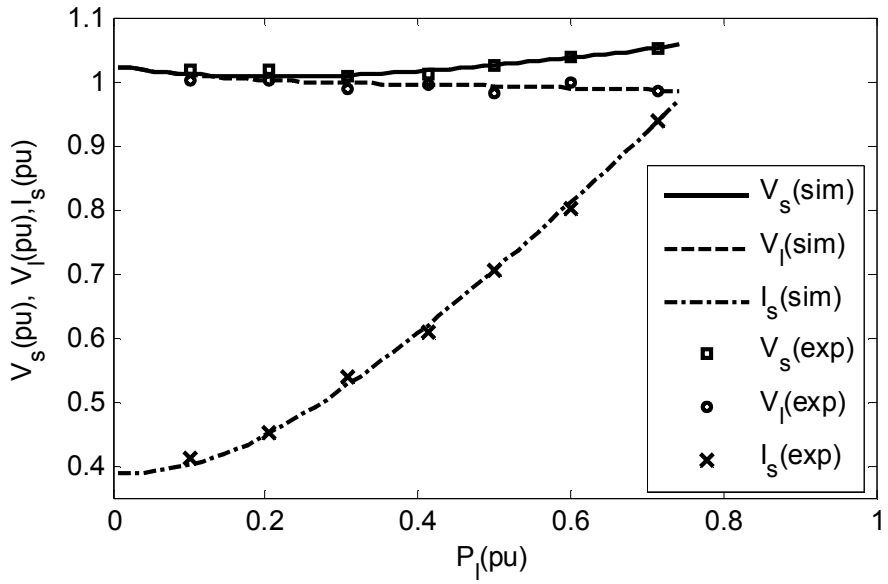


(sim: simulated ; exp: experimental)

***Fig. 7.8 Steady state performance of short shunt SEIG at rated speed with resistive load***

***($C_{hs}$ 17.2 µF and $C_{es}$ 268.4 µF)***

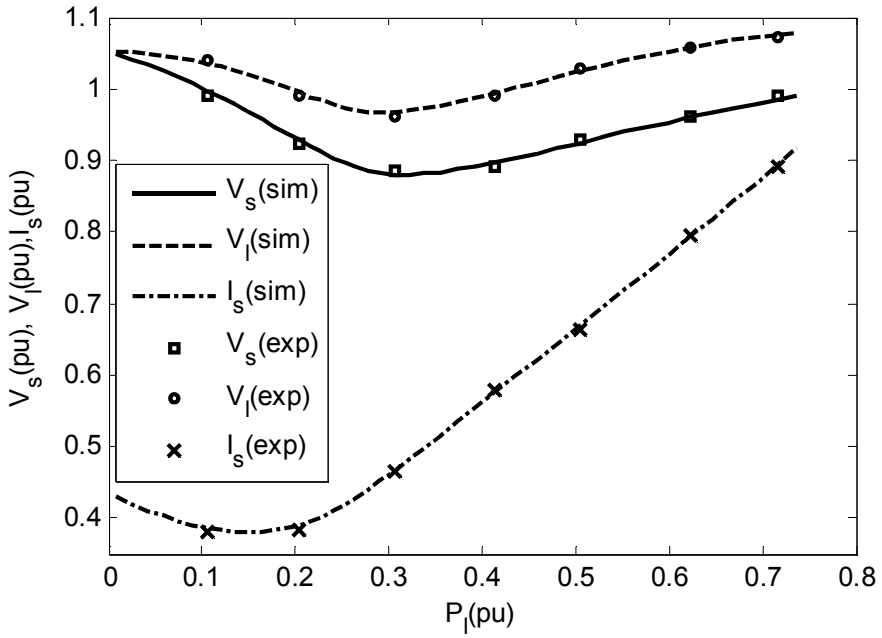


(sim: simulated; exp: experimental)

***Fig. 7.9 Steady state performance of short shunt SEIG at rated speed with 0.9 pf R-L load***

***($C_{hs}$ 18.5 µF and $C_{es}$ 161.2 µF)***

As shown in Fig. 7.8, at no load, $V_s$ and $V_l$ maintain equal value to 1.023 pu. As the load increases, higher $V_s$ is resulted due to higher saturation level and thus maintaining the $V_l$ nearly constant. As shown in Fig. 7.9, the $V_s$ and $V_l$ are same and equal to 1.051 pu at no load. The load and stator voltages decrease initially up to 0.25 pu load and than start increasing. Even the stator voltage is lower than the load voltage is resulted. This feature is different than the corresponding feature for the resistive load because the impedance offered by the combination of series capacitor and the load is changing from inductive to capacitive. For both cases, the increased loading results into increased $I_s$.

### *7.6.1.2 Optimum Performance of Short Shunt SEIG*

The optimum performance results for resistive loads are computed by assigning higher weightage to loadability as compared to voltage regulation firstly and higher weightage to voltage regulation as compared to loadability, and corresponding results are summarized in Table 7.5 and Table 7.6.

The fitness function $f_2$ is designated as $f_{2ld}$ for the weightage factor $K_{ld}$ as 7.0 and $K_{vr}$ as 1.0, i.e. ($K_{ld}$>$K_{vr}$) which indicates higher utilization of the machine. The optimum performance is obtained at upper limiting value of ν, where the loadability is even more

than unity (rated power of machine). As the speed decreases, the fitness $f_{2ld}$ and loadability decreases. As the loadability is varying in wide range, the $f_{2ld}$ is also varying in wide range. The fitness function $f_2$, which is designated as $f_{2vr}$ for the weightage factor $K_{vr}$ as 5.0 and $K_{ld}$ as 1.4, indicates higher preference to voltage regulation. The performance with $f_{2vr}$ is almost identical to the performance with $f_{2ld}$ and an optimum point is also obtained at 1.12 pu speed. However, with $f_{2vr}$, slightly lower loading is resulted. The $f_{2vr}$ varies in narrow range as $f_1$, which is designated for optimum voltage regulation only.

***Table 7.5 Summary of optimum performance ($K_{ld}>K_{vr}$) for short shunt SEIG fed resistive load***

| $f_{2ld}$ | $C_{hs}$ (µF) | $C_{es}$ (µF) | $v$ (pu) | Loadability (pu) | Remark |
|---|---|---|---|---|---|
| 8.293075 | 11.7 | 396.4 | 1.12 | 1.026731 | Optimum performance |
| 7.45274 | 16.7 | 502.6 | 1.0 | 0.906925 | Experimentally verified |

***Table 7.6 Summary of optimum performance($K_{ld}<K_{vr}$) for short shunt SEIG fed resistive load***

| $f_{2vr}$ | $C_{hs}$ (µF) | $C_{es}$ (µF) | $v$ (pu) | Loadability (pu) | Remark |
|---|---|---|---|---|---|
| 6.413069 | 11.2 | 441.3 | 1.12 | 1.021864 | Optimum performance |
| 6.240188 | 17.6 | 364.5 | 1.0 | 0.886928 | Experimentally verified |

The results of optimum performance for feeding 0.9 pf resistive-inductive load are shown in Table 7.7 and Table 7.8. The weightage factor for $f_{2ld}$ and $f_{2vr}$ are kept same as for resistive loads.

***Table 7.7 Summary of optimum performance ($K_{ld}>K_{vr}$) for short shunt SEIG fed 0.9 pf R-L load***

| $f_{2ld}$ | $C_{hs}$ (µF) | $C_{es}$ (µF) | $v$ (pu) | Loadability (pu) | Remark |
|---|---|---|---|---|---|
| 7.420289 | 20.1 | 213.0 | 1.0 | 0.904623 | Optimum performance |
| 7.358339 | 20.6 | 215.3 | 0.99 | 0.914576 | Maximum loading |

***Table 7.8 Summary of optimum performance ($K_{ld}$<$K_{vr}$) for short shunt SEIG fed 0.9 pf R-L load***

| $f_{2vr}$ | $C_{hs}$ (µF) | $C_{es}$ (µF) | $v$ (pu) | Loadability (pu) | Remark |
|---|---|---|---|---|---|
| 6.088911 | 20.2 | 214.5 | 1.0 | 0.903713 | Maximum loading |
| 6.176505 | 23.9 | 231.7 | 0.95 | 0.853534 | Optimum performance |

For $f_{2ld}$, the maximum fitness and maximum loadability are achieved at 1.0 pu and 0.99 pu speed respectively with loading of the machine in the range of 0.90 pu. The optimum value of $f_{2vr}$ is obtained at 0.95 pu speed. As the speed is increasing to 1.0 pu, the $f_{2vr}$ is decreasing but loadability increases. The $f_{2vr}$ is varying in a narrow range as compared to $f_{2ld}$. For optimum performance with R-L load, higher value of shunt capacitance and lower value of series capacitance is resulted as compared to respective value for resistive load.

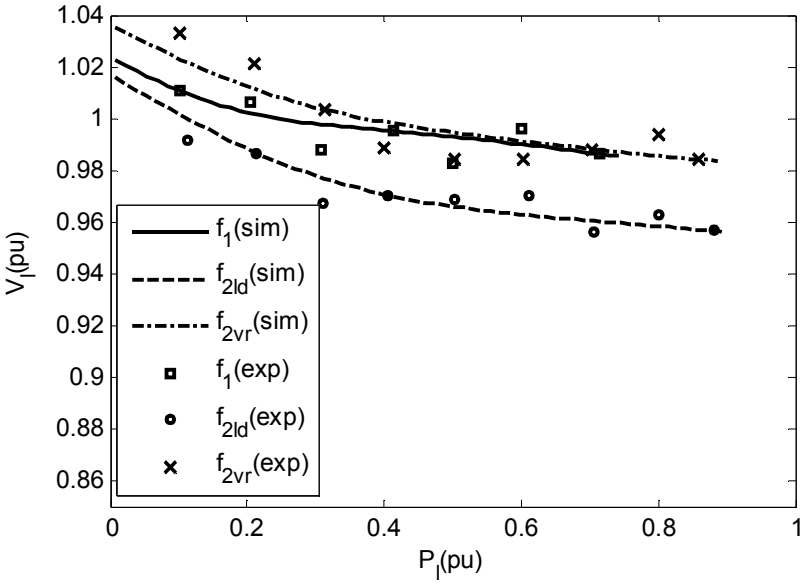


(sim: simulated; exp: experimental)

***Fig. 7.10 Variation in load voltage for different fitness function for resistive load***

The variation of load voltage for optimum capacitance corresponding to fitness value $f_1$, $f_{2ld}$, $f_{2vr}$ at rated speed feeding resistive load is shown in Fig. 7.10. The load voltages $V_l$ for $f_1$ and $f_{2vr}$ are in close proximity at higher load, whereas, voltages for $f_1$ and $f_{2ld}$ are close at lower loading because more weightage to voltage regulation for $f_{2vr}$. The machine has slightly larger loadability for $f_{2ld}$ as compared to $f_{2vr}$. For both $f_{2ld}$ and $f_{2vr}$, the

$I_s^{mx}$ constraint first violates on account of large $I_s$ with loading. The variation of load voltage for optimum capacitances corresponding to fitness function $f_1$, $f_{2ld}$, $f_{2vr}$ at rated speed for feeding 0.9 pf resistive-inductive load is shown in Fig. 7.11. The variation of load voltage for capacitances corresponding to fitness function $f_{2ld}$ and $f_{2vr}$ is almost similar with nearly same loading.

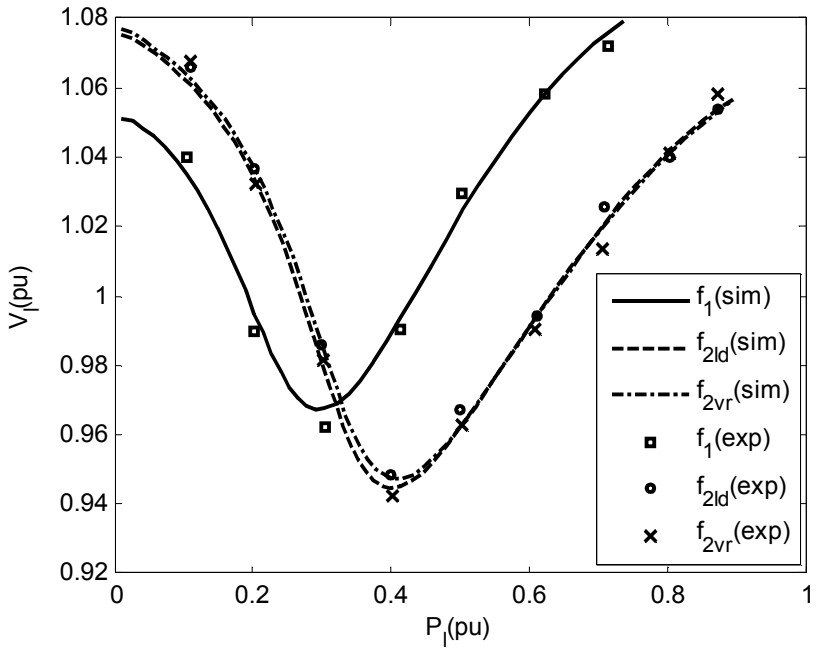


(sim: simulated; exp: experimental)

***Fig. 7.11 Variation in load voltage for different fitness function for R-L load***

### 7.6.2 Transient Performance of SEIG-Battery Supported SSSC System Feeding Static Loads

The investigations are carried out on a 415V, 3.7 kW, 7.6 A, Y-connected squirrel cage induction machine, operating as a SEIG, driven by prime-mover with prime mover torque as $T_P = 6200 - 20\omega_r$ and excited by a star connected capacitor bank. The SSSC parameters for this study are taken corresponding to designed values for static R-L load. The machine and the SSSC PI controller parameters are summarized in Appendix-A and Appendix-H respectively. The capacitance of 48.3 μF/phase is required to obtain rated no load phase voltage of 239 V (peak load voltage $V_{pl}$ is 338 V) and line voltage of 415V. The SEIG is loaded with resistive, resistive-inductive (R-L) and resistive-capacitive (R-C) loads and reactive power requirement is met by SSSC by injecting voltage in series with line. The performance characteristics are studied for the following cases.

- System performance with resistive load
- System performance with R-L load
- Steady state performance for resistive and R-L load
- System performance with R-C load
- Steady state performance for R-C load
- Operating modes of SSSC
- Power quality performance

#### *7.6.2.1 System Performance with Resistive Load*

The performance characteristic of SEIG-battery supported SSSC is shown in Fig. 7.12 for step change in resistive load in terms of generator voltages $v_{gabc}$, generator currents $i_{gabc}$, load voltages $v_{labc}$, load currents $i_{labc}$, injected voltage $v_{iabc}$, peak load voltage $V_{pl}$, prime mover speed $\omega_r$ and battery voltage $v_{bat}$. The SEIG is loaded with 1 kW resistive load. The load is suddenly increased to 2 kW at 2.2 sec. and to 3 kW at 2.4 sec. Correspondingly, $i_{gabc}$ and $i_{labc}$ increase but no appreciable transients in $v_{gabc}$ or $v_{labc}$ are observed. The $V_{pl}$ dips momentarily to 297 V at 2.2 sec. and returns to reference value due to controller action. With 3 kW load at 2.4 sec., $V_{pl}$ drops to 299 V and return to the reference value immediately. There is no appreciable change in $v_{bat}$ during loading. The load is suddenly decreased from 3 kW to 1 kW at 2.6 sec. The obvious transients are observed in various currents and voltages. The $i_{gabc}$ and $i_{labc}$ are decreased, while $V_{pl}$ spikes to around 420 V and gradually settles down to reference value with small ripples.

#### *7.6.2.2 System Performance with R-L Load.*

The performance characteristics of SEIG-battery supported SSSC system are depicted in Fig. 7.13 for 0.8 pf R-L load. The load is increased from 1 kW to 2 kW at 1.8 sec. There is corresponding increase in $i_{gabc}$ and $i_{labc}$ with observable transients in $v_{labc}$ for few cycles. The $V_{pl}$ decreases momentarily to 250V and returns back to reference value gradually in couple of cycles. The $\omega_r$ also decreases slightly due to increase in the load.

At 2.2 sec., the load is reduced to 1 kW. The dynamics of the system changes accordingly and the system returns back to steady state condition after few cycles. The continuous voltage fluctuations are also observed in $v_{bat}$ owing to continuous charging and discharging. With the VAR support provided by SSSC, the SEIG is able to supply 2.0 kW, 0.8 pf R-L load.

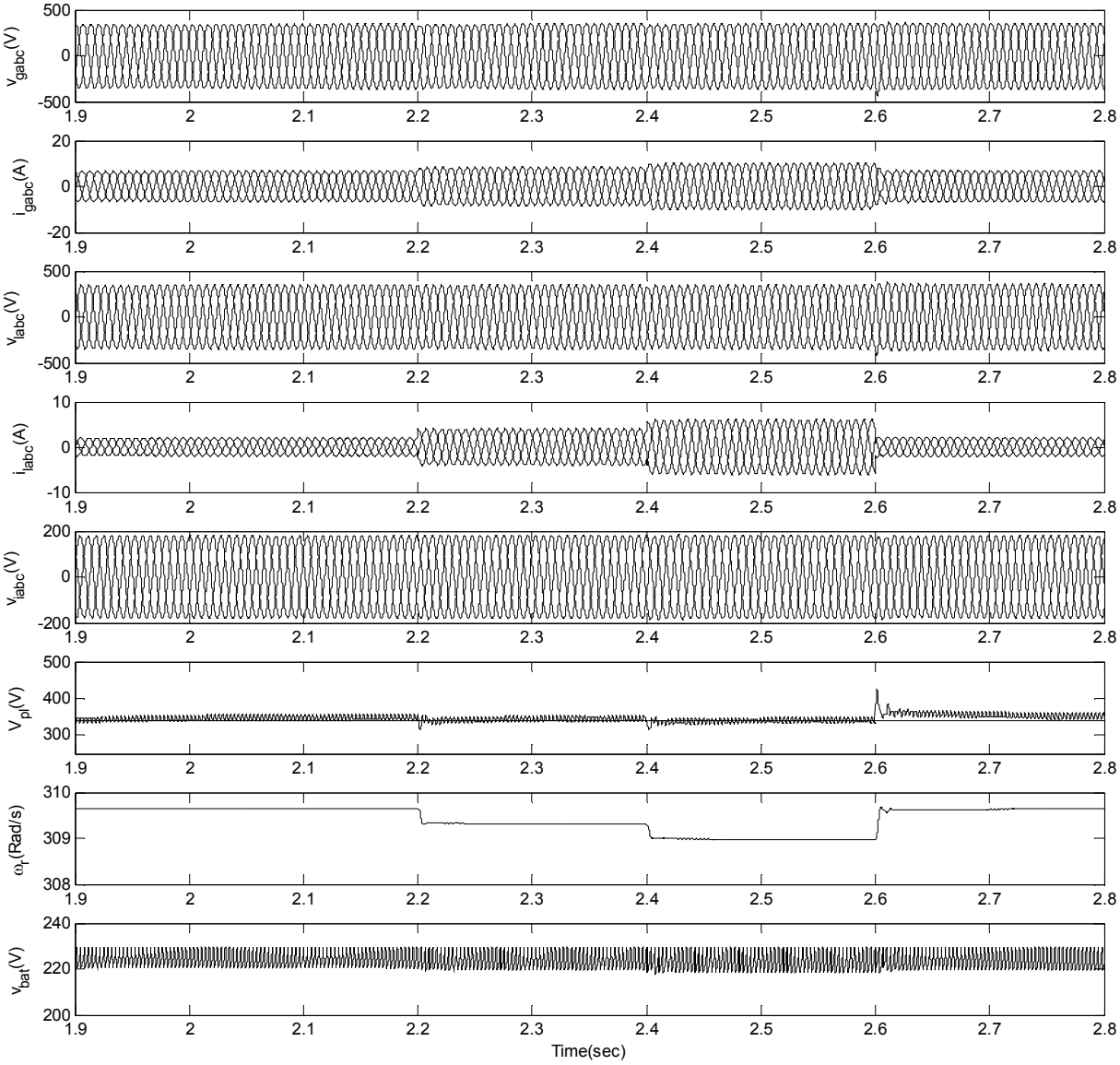


***Fig. 7.12 Transient performance characteristics of SEIG-battery supported SSSC system with resistive load***

***(Load conditions : 2 kW at 2.2 sec., 3 kW at 2.4 sec., and 1 kW at 2.6 sec.)***

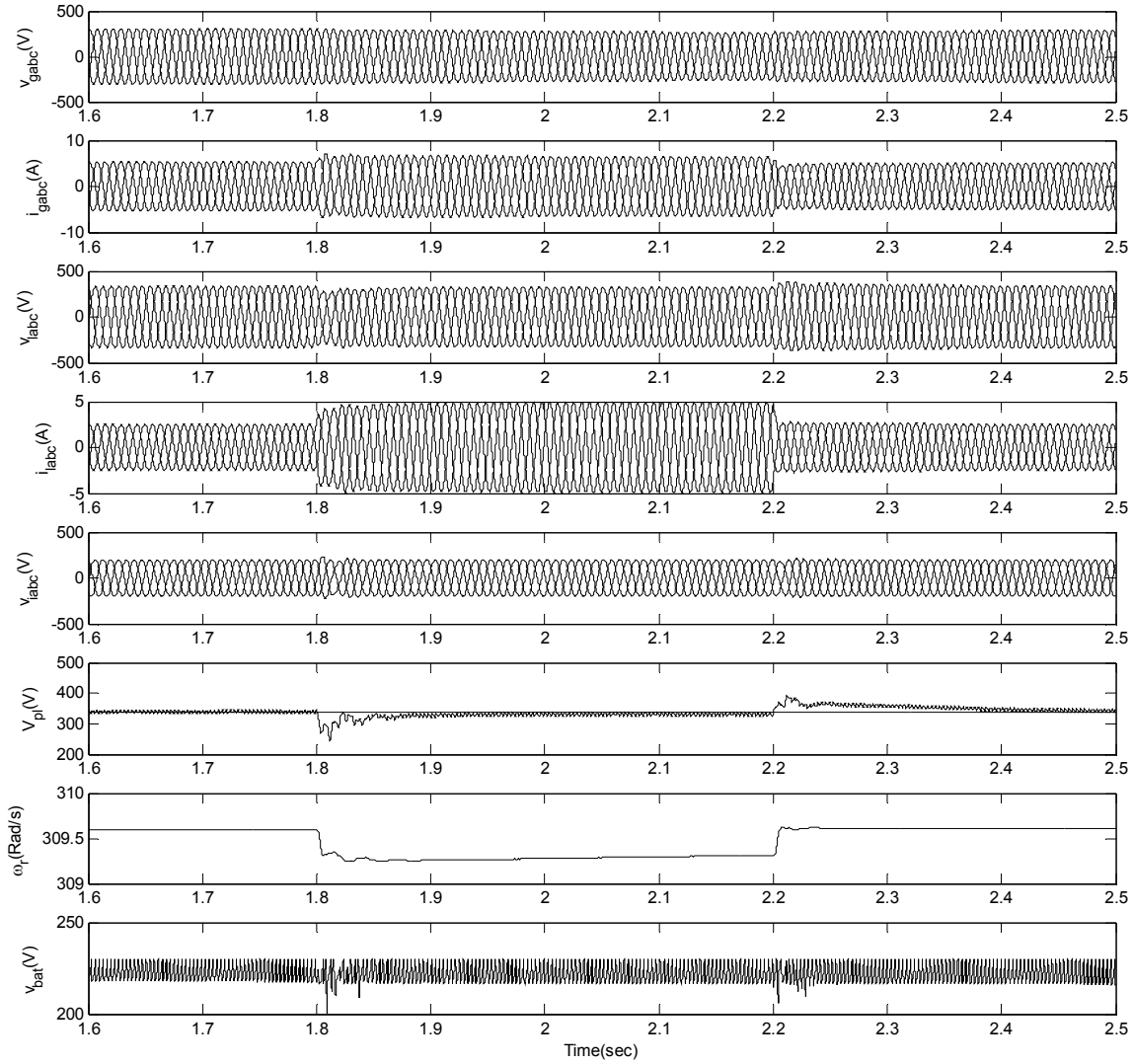


***Fig. 7.13 Transient performance characteristics of SEIG-battery supported SSSC system with 0.8 pf R-L load***

***(Load conditions : 2.0 kW at 1.8 sec. and 1.0 kW at 2.2 sec.)***

### *7.6.2.3 Steady State Performance for Resistive and R-L Load*

The variations in the load voltage ($V_l$), load current ($I_l$) and generator current ($I_g$) with load power during steady state condition of SEIG with and without SSSC, obtained from transient characteristics are shown in Fig. 7.14 for feeding resistive and resistive-inductive loads. The load voltage with SSSC almost remains constant for both resistive and R-L load, while without SSSC $V_l$ falls more sharply, leading to voltage collapse for R-L load (0.8 pf) as compared to resistive load because of the widening of reactive power mismatch for R-L load. With SSSC, the $I_l$ linearly increases with the power, whereas without SSSC, the generator is not able to deliver output power beyond 1.75 kW with resistive load and beyond 1.3 kW with 0.8 pf R-L load.

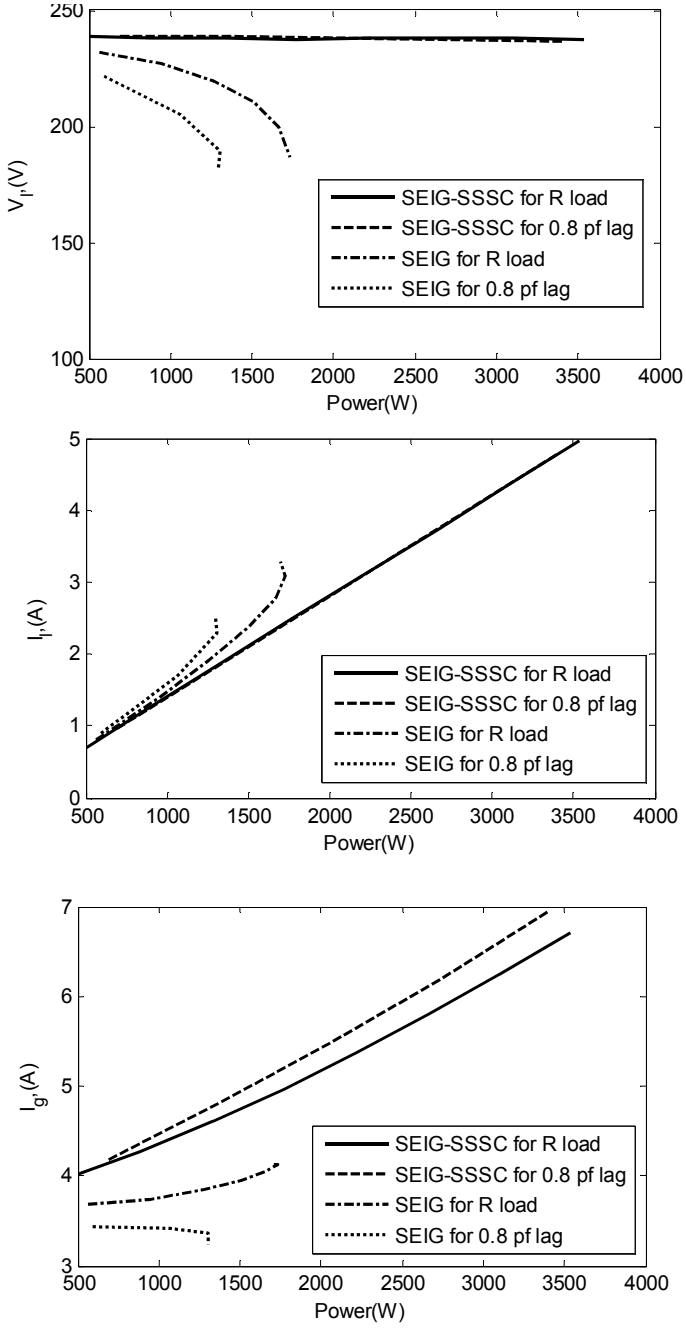


***Fig. 7.14 Steady state performance characteristics of SEIG with and without battery supported SSSC for resistive and 0.8 pf R-L load***

### *7.6.2.4 System Performance with R-C Load*

The performance of SEIG-battery supported SSSC feeding R-C load of 0.8 pf is shown in Fig. 7.15. At 1.6 sec, the load is increased from 1 kW to 2 kW and at 1.8 sec., to 3 kW respectively. With the increased load, the $i_{gabc}$ and $i_{labc}$ are increased correspondingly without any noticeable transients, whereas the $\omega_r$ decreases accordingly. The $V_{pl}$ momentarily increases at the time of increase of the load and after couple of

cycle, settles at reference mark, owing to the controller action. At 2.0 sec, the load is decreased to 1 kW, which results in decrease in $i_{gabc}$ and $i_{labc}$ and an increase in $\omega_r$. The $v_{bat}$ continues to fluctuate because of continuous charging and discharging. As the SSSC is providing the compensated reactive VAR, the load voltage remains constant. However, the load voltage normally increases when SEIG is loaded with R-C load.

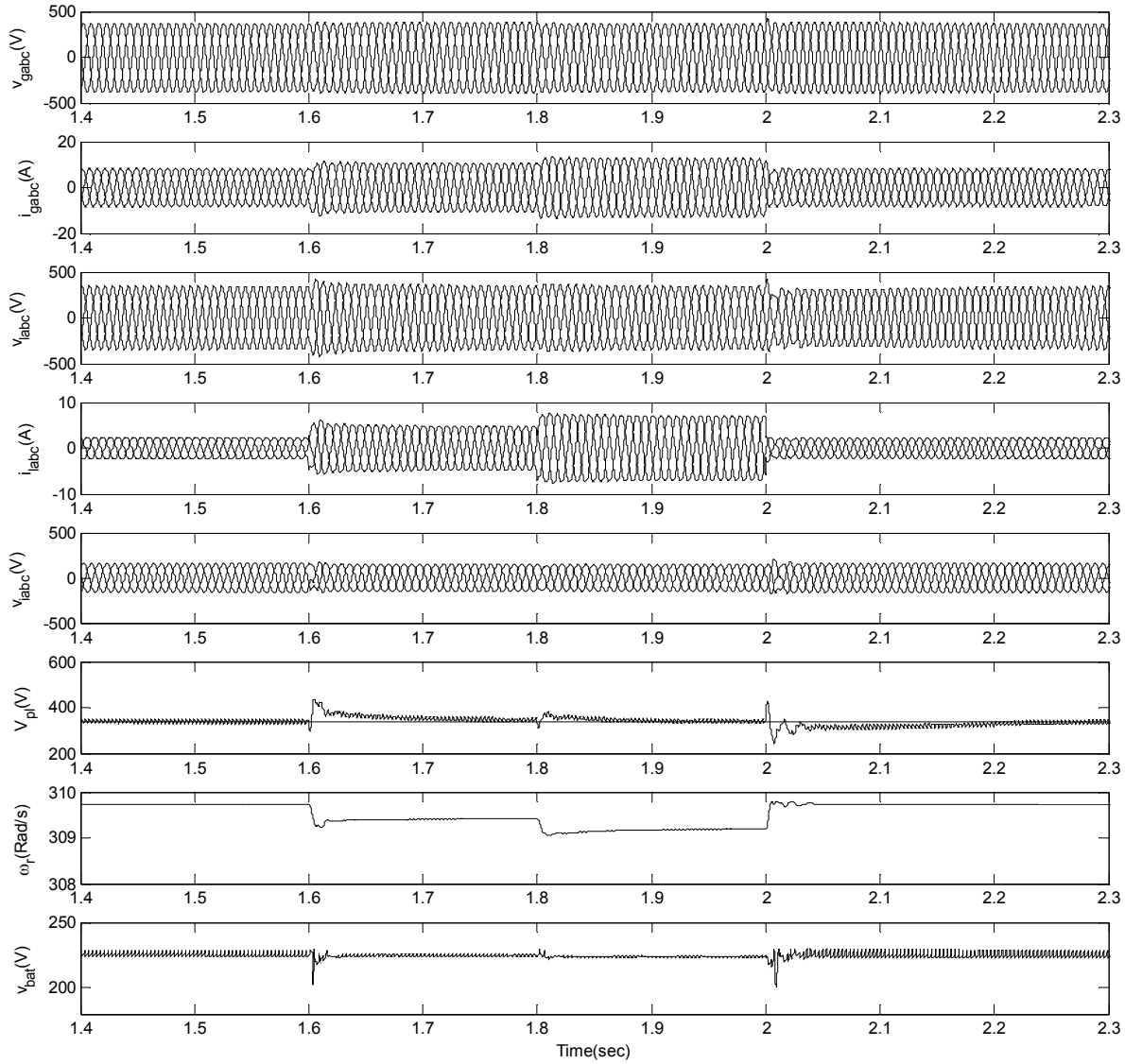


***Fig. 7.15 Transient performance characteristics of SEIG-battery supported SSSC system with 0.8 pf R-C load***

***(Load conditions : 2.0 kW at 1.6 sec., 3 kW at 1.8 sec. and 1 kW at 2.0 sec.)***

### *7.6.2.5 Steady State performance for R-C Load*

The variation in the load voltage ($V_l$), load current ($I_l$) and generator current ($I_g$) with load power during the steady state condition of SEIG with and without SSSC, obtained from the transient characteristics are shown in Fig. 7.16 for feeding resistive-

capacitive load. The load voltage with SSSC almost remains constant and loading up to rated power is achieved. Without SSSC, $V_l$ initially increases rapidly with the load but increases slowly later on due to SEIG operation in deep saturation. With SSSC, the $I_l$, and $I_g$ are more as compared to values without SSSC for same power output because SSSC is operating in the inductive mode, which decreases the load voltage for same power output.

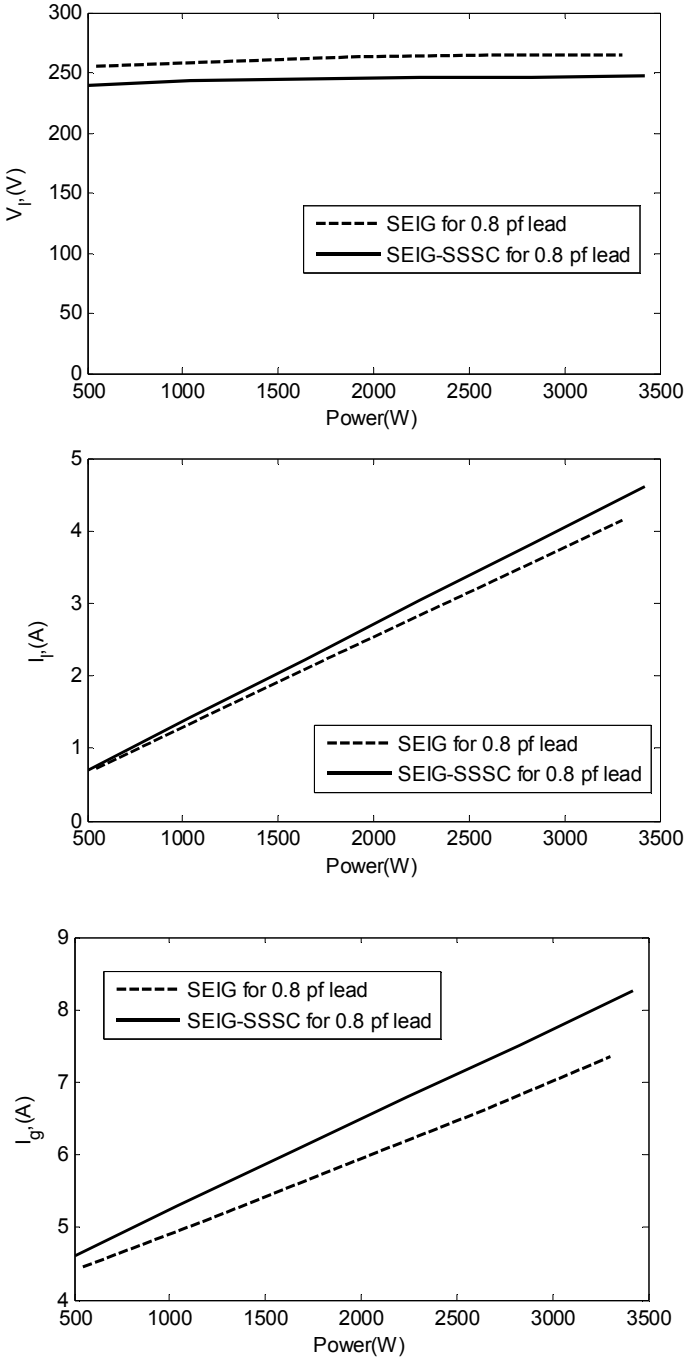


***Fig. 7.16 Steady state characteristics of SEIG with and without battery supported SSSC for R-C load***

### *7.6.2.6 Operating Modes of SSSC*

The operating mode of SSSC on SEIG system for various loads is decided by phase relationship between compensating voltage $v_{ia}$ and line current $i_{la}$. Correspondingly, the enlarged views of $v_{ia}$ and $i_{la}$ during steady state are shown in Fig. 7.17a, Fig. 7.17b and Fig. 7.17c for resistive, resistive-inductive and resistive-capacitive loads respectively.

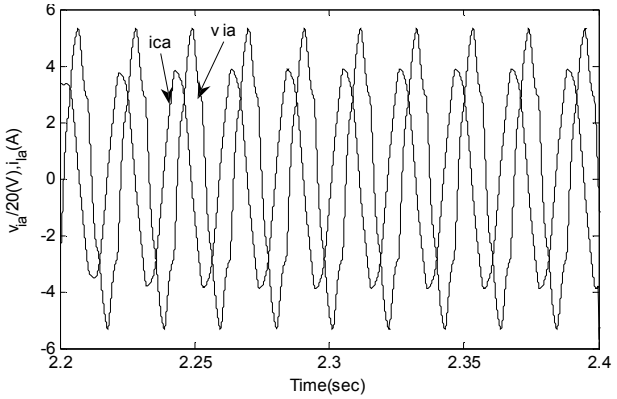


***Fig. 7.17a SSSC injected voltage and line current for 2.0 kW resistive load***

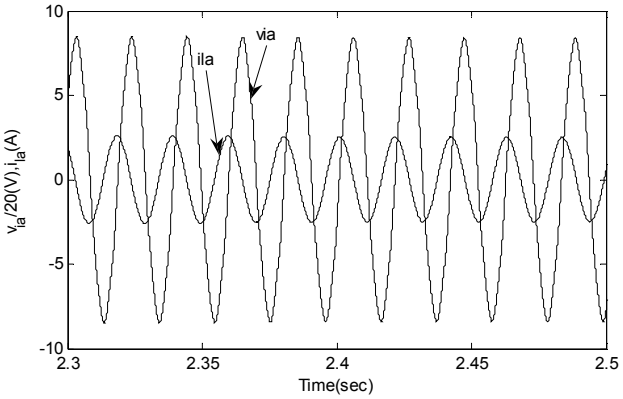


***Fig. 7.17b SSSC injected voltage and line current for 1.0 kW, 0.8 pf R-L load***

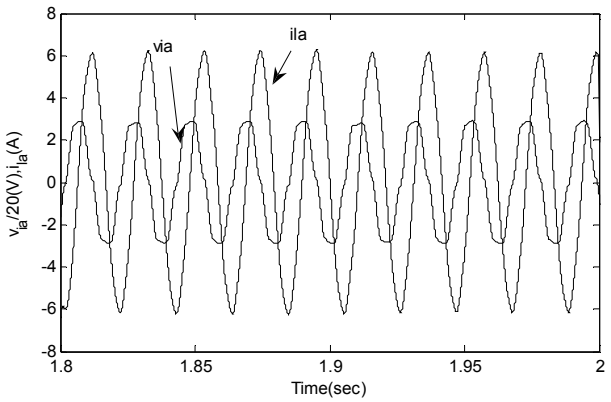


***Fig. 7.17c SSSC injected voltage and line current for 3.0 kW, 0.8 pf R-C load***

***Fig. 7.17 SSSC injected voltage and line current during steady state for various loads***

In Fig. 7.17a and Fig. 7.17b, $v_{ia}$ is almost 90º lagging to $i_{la}$ and thus SSSC is behaving like controlled series capacitor and injecting reactive VAR to regulated the load voltage. With R-C load, Fig. 7.17c, $v_{ia}$ is almost 90º leading to $i_{la}$ and SSSC emulates like controlled series inductor and absorbing the excess reactive VAR, in order to maintain the load voltage at reference value.

### 7.6.3 Transient Performance of SEIG-Capacitor Supported SSSC System Feeding Static Loads

The transient performance of SEIG-capacitor supported SSSC feeding 0.8 pf R-L load is shown in Fig. 7.18 using generator voltages $v_{gabc}$, generator currents $i_{gabc}$, load voltages $v_{la}$, $v_{lb}$, $v_{lc}$, load currents $i_{la}$, $i_{lb}$, $i_{lc}$, injected voltages $v_{ia}$, $v_{ib}$, $v_{ic}$, peak load phase voltage $V_{pl}$, prime mover speed $\omega_r$, DC bus voltage $V_{dc}$. The parameters of capacitor supported SSSC is given in Appendix-H. The 0.8 pf load is increased from 1.0 kW to 2.0 kW at 1.2 sec., which is resulting into increase in $i_{gabc}$ and $i_{la}$, $i_{lb}$ $i_{lc}$; decrease in $\omega_r$. The load voltages ($v_{la}$, $v_{lb}$, $v_{lc}$) stabilizes after experiencing three to four cycles of disturbance. The $V_{dc}$ also fluctuates around the reference value owing to charging and discharging of DC bus capacitor. The load is decreased to 1.0 kW at 1.6 sec., which is resulting into decrease in generator, load currents and increase in $\omega_r$. During The load voltage remains constant irrespective of the increase or decrease of inductive load, which thereby shows the effectiveness of control technique.

### 7.6.4 Power Quality Performance

The performance of the SEIG system with reference to power quality can be assessed by harmonic analysis and total harmonic distortion (THD) of voltages and currents at generator and load terminals. The fast Fourier transformation (FFT) of the waveform is obtained using MATLAB.

#### *7.6.4.1 Harmonic spectra for SEIG-battery supported SSSC fed resistive load*

The voltage and current waveforms under steady state along with their harmonic spectra are shown in Fig. 7.19 for 2 kW resistive load. The generator $v_{ga}$ and $i_{ga}$ are having THD of 0.79% and 1.61%, whereas load $v_{la}$ and $i_{la}$ observing THD of 2.17% each. Thus, both the load and the generator operate satisfactory well within the permissible limit of THD.

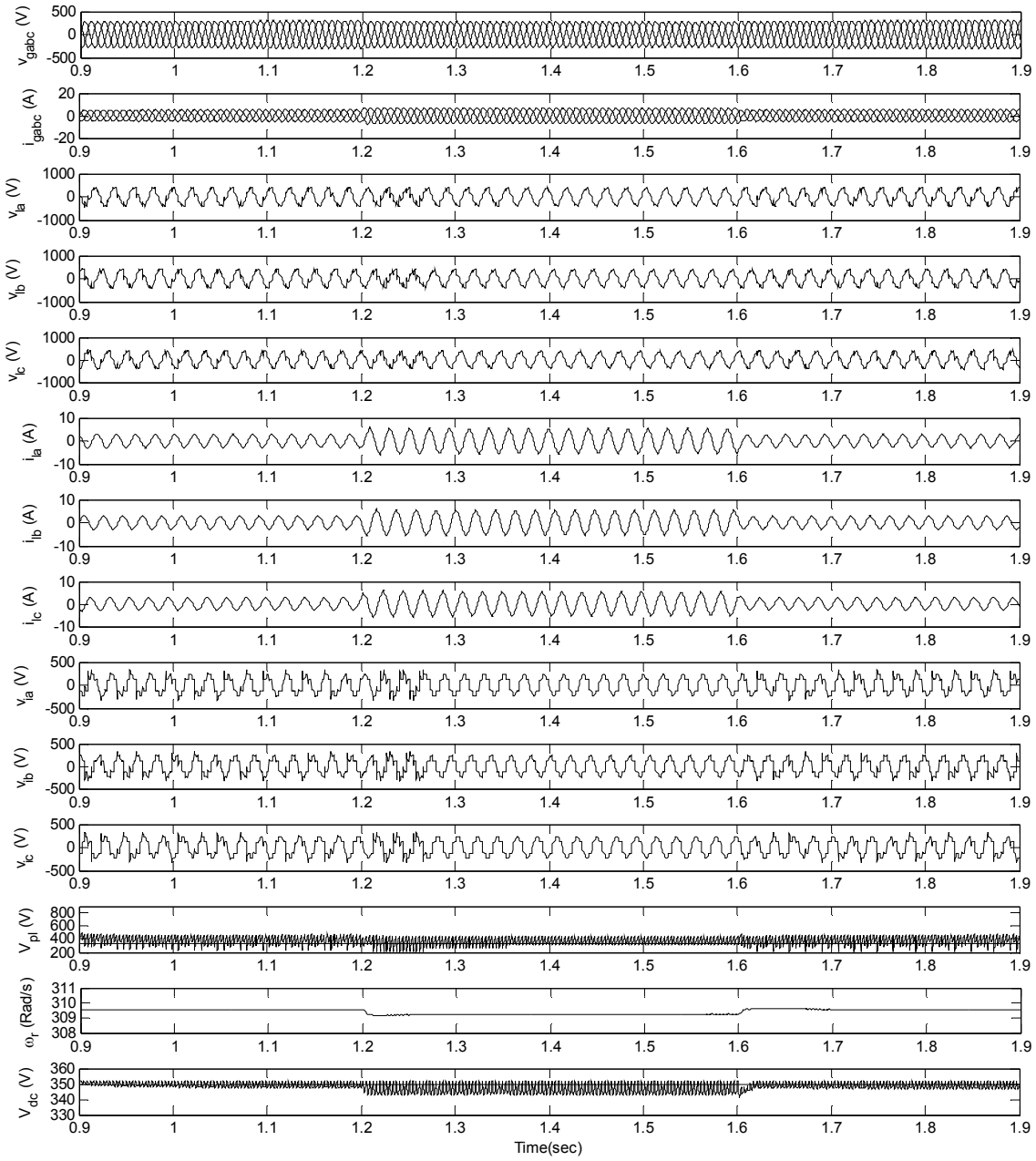


***Fig. 7.18 Performance of SEIG-SSSC system feeding 0.8 pf R-L load***
***(Loading condition: initial load 1.0 kW, 2.0 kW at 1.2 sec. and 1.0 kW at 1.6 sec.)***

### *7.6.4.2 Harmonic spectra for SEIG- battery supported SSSC fed R-L Load*

The steady state system waveforms along with their harmonic spectra are shown in Fig. 7.20 for 2 kW 0.8 pf R-L load. The generator $v_{ga}$ and $i_{ga}$ are having THD of 1.65% and 1.39% respectively, whereas load $v_{la}$ and $i_{la}$ observing THD of 2.53% and 1.77% respectively. These values of THD confirm that the performance both at generator and load sides are satisfactory and well within the permissible limit of THD.

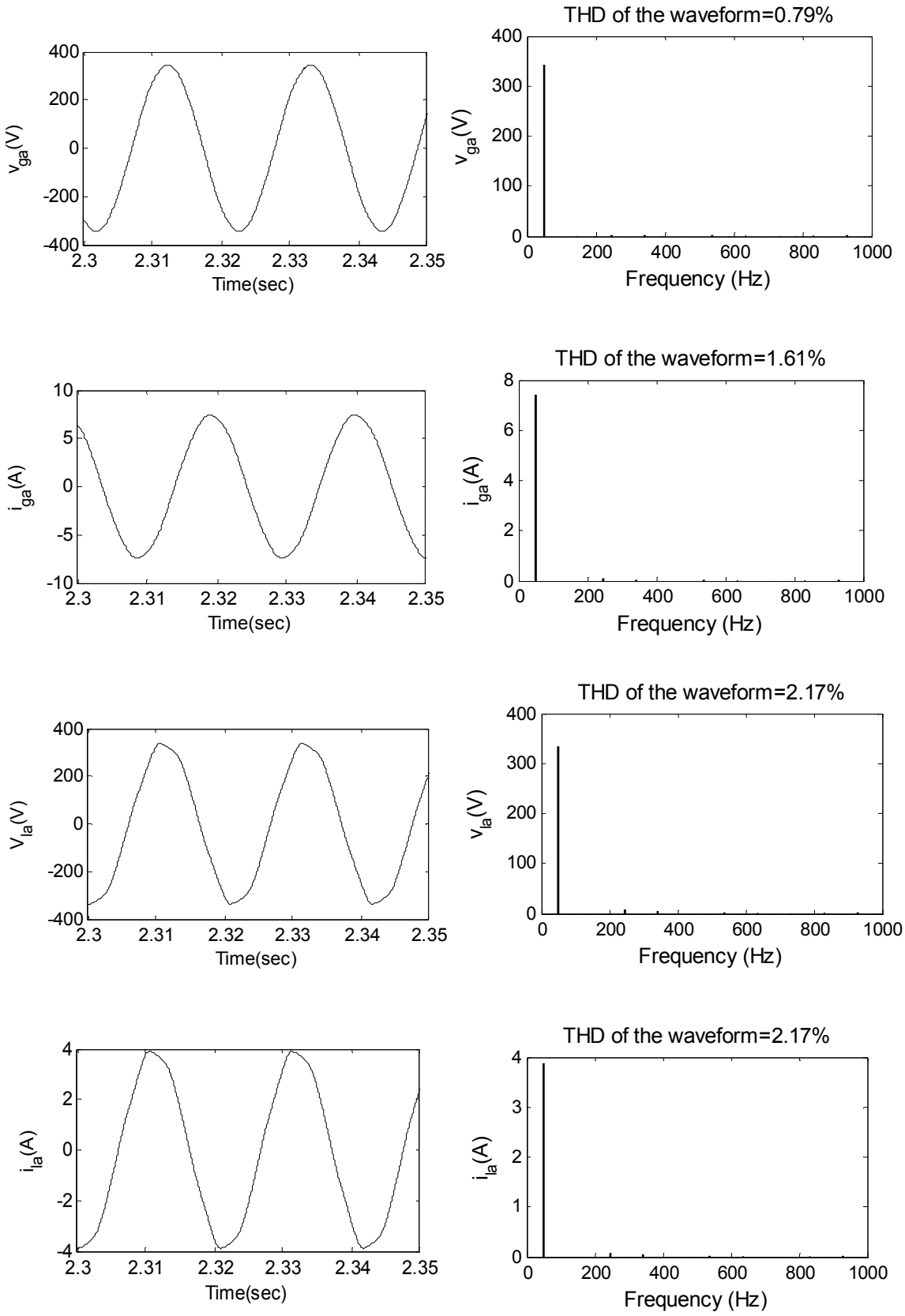


***Fig. 7.19 Harmonic spectra during steady state for SEIG-SSSC fed 2 kW resistive load***

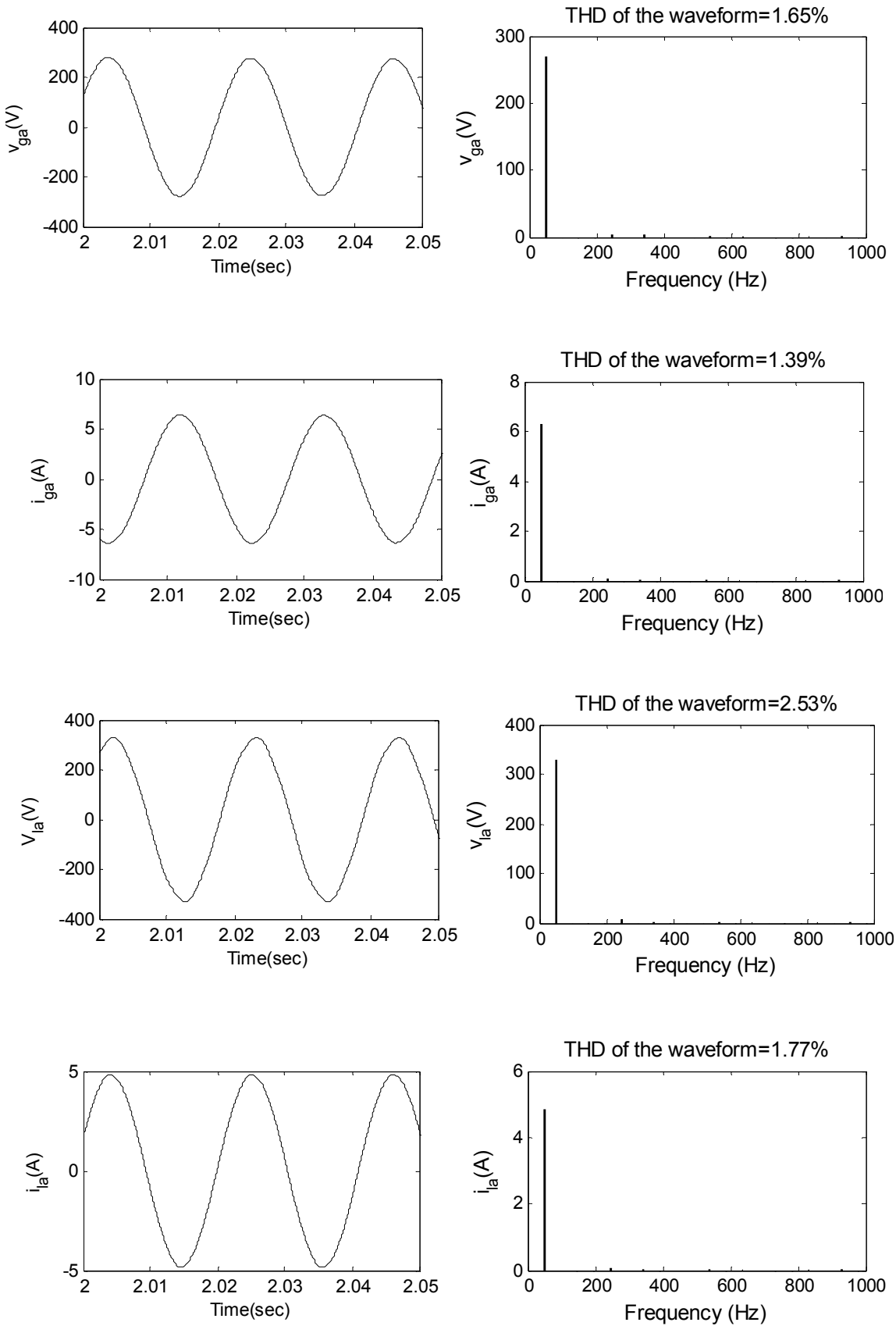


***Fig. 7.20 Harmonic spectra during steady state for SEIG-battery supported SSSC fed 2 kW, 0.8 pf R-L load***

### *7.6.4.3 Harmonic Spectra for SEIG- battery supported SSSC fed R-C Load*

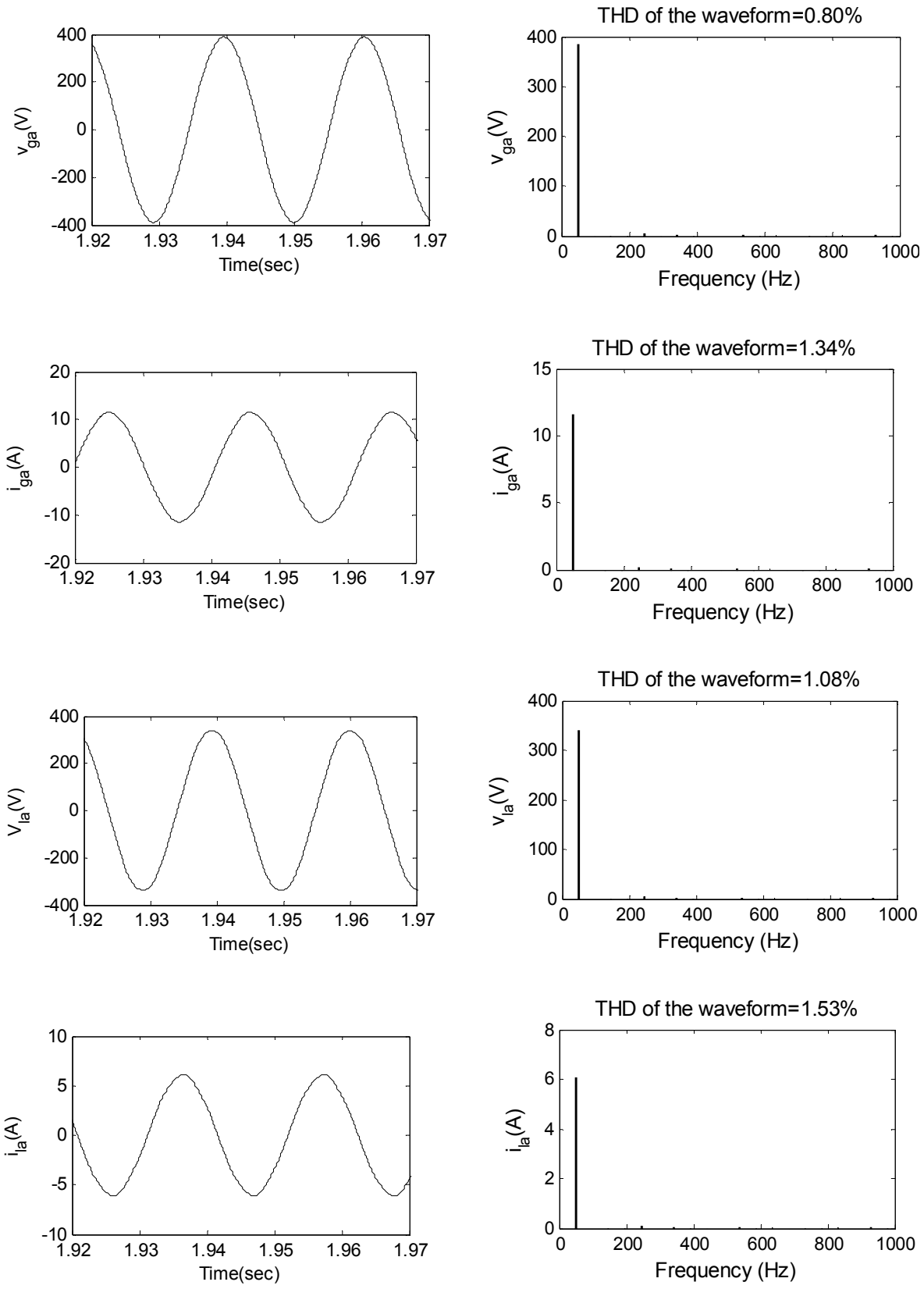


***Fig. 7.21 Harmonic spectra during steady state for SEIG-battery supported SSSC fed 3.0 kW, 0.8 pf R-C load***

The steady state system waveforms along with their harmonic spectrums are shown in Fig. 7.21 for 3 kW 0.8 pf R-C load. The generator $v_{ga}$ and $i_{ga}$ are having THD of 0.8% and 1.34% respectively, whereas load $v_{la}$ and $i_{la}$ observing THD of 1.08% and 1.53% respectively. These values of THD are well within the permissible IEEE-519 limit of THD, therefore confirm that the performance both at generator and load sides are satisfactory.

### *7.6.4.4 Harmonic Spectra for SEIG- capacitor supported SSSC fed R-L Load*

The steady state system waveforms along with their harmonic spectrums are shown in Fig. 7.22 for 2 kW 0.8 pf R-L load. The generator $v_{ga}$ and $i_{ga}$ are having THD of 1.12% and 1.75% respectively, whereas load $v_{la}$ and $i_{la}$ observing THD of 4.98% and 3.24% respectively. These values of THD are well within the permissible IEEE-519 limit of THD, therefore confirm that the performance of SEIG-capacitor supported system is satisfactory.

The THD for various cases are also summarized in Table 7.8. These values of THD are well within the permissible limit, which confirms that the performance both at generator and load sides are satisfactory for both the SEIG-battery supported SSSC and SEIG-capacitor supported SSSC systems.

***Table 7.9 THD values of various static loads on SEIG-SSSC system***

| **Type of System** | **Type of Load** | **Total Harmonic Distortion (THD)** | | | |
|---|---|---|---|---|---|
| | | **Generator** | | **Load** | |
| | | **Voltage** | **Current** | **Voltage** | **Current** |
| SEIG-battery supported SSSC | 2.0 kW R Load | 0.79% | 1.61% | 2.17% | 2.17% |
| | 2.0 kW, 0.8 pf R-L Load | 1.65% | 1.39% | 2.53% | 1.77% |
| | 3.0 kW, 0.8 pf, R-C Load | 0.80% | 1.34% | 1.08% | 1.53% |
| SEIG-capacitor supported SSSC | 2.0 kW, 0.8 pf R-L Load | 1.12% | 1.75% | 4.98% | 3.24% |

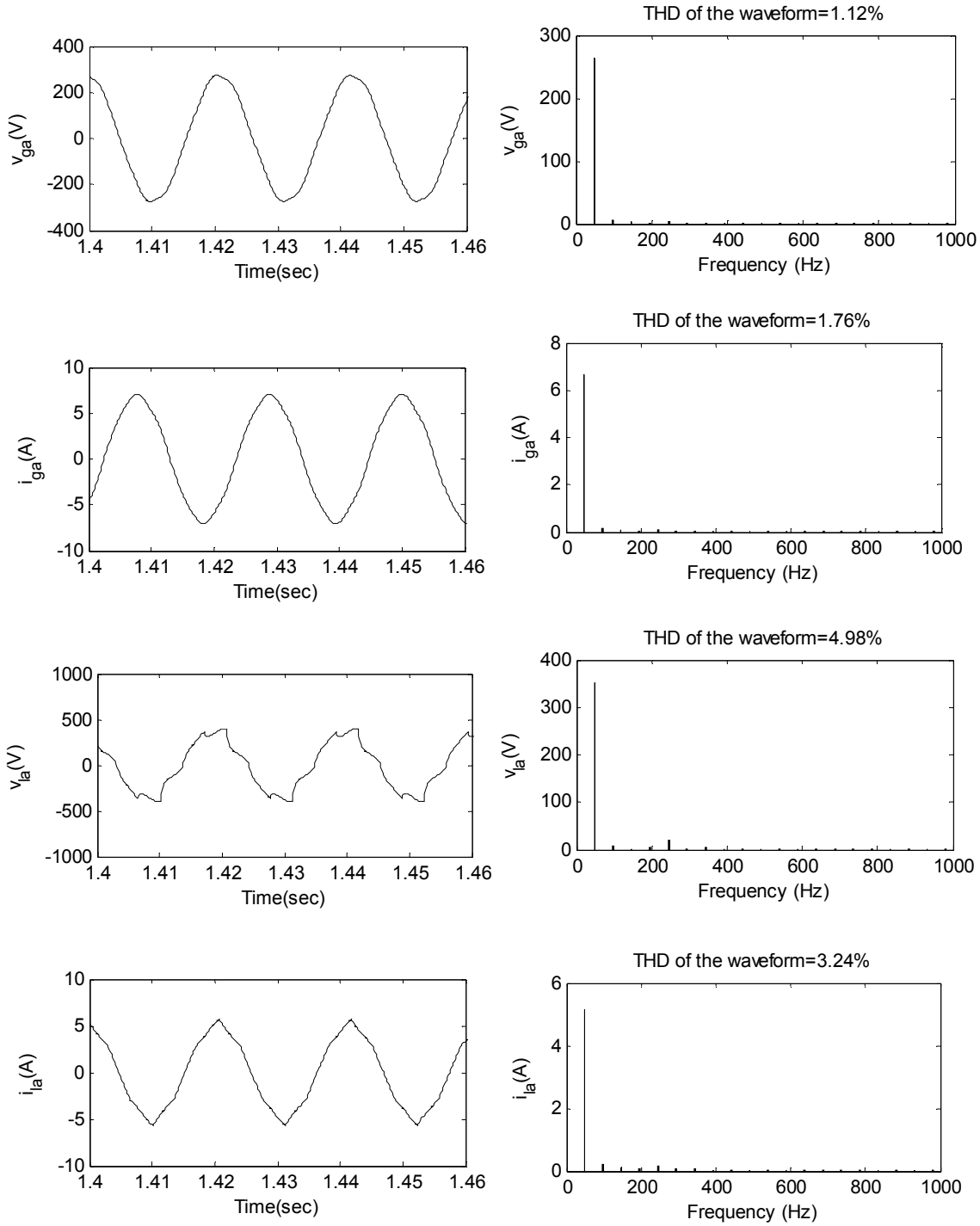


***Fig. 7.22 Harmonic spectra during steady state for SEIG-capacitor supported SSSC fed 2 kW, 0.8 pf R-L load***

## 7.7 CONCLUSIONS

The series compensation methods using series capacitors and SSSC have been applied to SEIG for improving its performance. The steady state performance of short

shunt SEIG feeding resistive, resistive-inductive load and transient performance of SEIG-SSSC system feeding static loads have been carried out in detail.

The shunt and series capacitances for short shunt SEIG have been selected to provide an optimum voltage regulation and optimum performance, a combination of optimum voltage regulation characteristic and loadability for feeding resistive and resistive-inductive loads. These problems have been formulated as optimization problems on the basis of steady state equivalent circuit and have been solved using the proposed strategy based on genetic algorithm. The simulated results corresponding to rated speed have been compared with the experimental results.

The design, modeling and simulation of SEIG-battery supported SSSC system and SEIG-capacitor supported SSSC system have been carried out for static loads. The proposed control technique for battery supported SSSC employs simple and easy PI controller to derive the reference supply current. The PI controller has been employed over peak load voltage, obtained through sensed three-phase load voltages. The hysteresis current controller has been used to generate the gating signals for six IGBTs of SSSC. The simulated characteristics for sudden increase and decrease of the loads on SEIG have been studied to show the effectiveness of control technique. The control technique of the SEIG-capacitor supported SSSC system employed two PI controllers. One PI controller is employed for maintaining DC bus voltage and other for maintaining the load voltage. The following conclusions have been made from the study carried out in this chapter.

- The developed GA based algorithm has been found effective in resulting series and shunt capacitances for optimum voltage regulation and optimum performance for short shunt SEIG feeding static resistive and resistive-inductive load.

- The optimum voltage regulation is obtained at a speed slightly above the rated speed for resistive load, whereas, it is resulted at lower limiting speed for resistive-inductive load.

- The SEIG voltage is more than the load voltage for resistive load, whereas, the SEIG voltage is lower than the load voltage for resistive-inductive load and difference between load and SEIG voltage is increasing with the increase in load.

- The optimum performance has been achieved at higher limiting speed for resistive load, where the loading on SEIG comes out to be more than rated power of machine. While, for resistive-inductive load, the optimum performance has been obtained around rated speed with SEIG loading is lower than rated power of machine.

- The control techniques applied with battery supported SSSC and capacitor supported SSSC are effective in providing compensation for varying loads.

- The SEIG-battery supported SSSC system has exhibited almost flat load voltage characteristic with change in resistive, resistive-inductive, and resistive-capacitive loads. The SSSC operation is demonstrated in inductive mode for capacitive load and in capacitive mode for inductive loads.

- The harmonics on generator side are well within the standard IEEE-519 limits for both the SEIG-battery supported and SEIG-capacitor supported SSSC systems. For all cases, the generator side harmonics are within 2%.

# CHAPTER-VIII

# SEIG OPERATION WITH SSSC FEEDING INDUCTION MOTOR LOAD

## 8.1 GENERAL

The effectiveness of series compensation for improved performance of SEIG has been discussed in the previous chapter. The series compensation has been achieved through classical series capacitors and through advanced converter based static synchronous series compensator (SSSC). However, the investigations have been restricted to only static loads.

The oscillating behavior and high transients are resulted in when the compensated SEIG is loaded with a motor load [127-129]. The problem of unstable behavior during starting and loading of an induction motor by the series capacitor compensated feeder has been referred as an example of sub-synchronous resonance (SSR) [274, 275]. The damping resistors across the series capacitors have been used for stable behavior [129]. However, the damping resistance is associated with additional power loss and complicated selection criterion. The power electronics based scheme famously known as NGH damper is used to mitigate SSR [276]. The effective series compensation, eliminating the SSR has been achieved by SSSC in the power system [249-260].

The investigation on the system performance with dynamic induction motor is very important as it constitutes the majority of practical loads. The induction motor draws excessive current during starting. Due to dynamic nature of the motor load, the performance of compensated SEIG with motor load is bound to be different than the performance with static loads.

In this chapter, the performance of compensated SEIG feeding an induction motor is investigated providing the series compensation by series capacitors and by SSSC. To the best knowledge of the author, this SEIG-SSSC system has not been investigated earlier to feed motor load. The performance of SEIG with SSSC feeding an induction motor load is investigated first time. The employed SSSC is an insulated gate bipolar transistor (IGBT) based pulse width modulated, current controlled-voltage source

converter (CC-VSC) with a battery at DC bus. The proposed control technique based on compensation of fundamental frequency component and is implemented using a proportional-integral (PI) controller. With the employed control technique, the SSSC is injecting a set of three-phase AC voltages in quadrature lagging with respective supply currents in synchronism with the supply voltages through unity ratio injection transformers.

## 8.2 DESIGN OF SSSC FOR FEEDING MOTOR LOAD

The detailed selection and design guidelines for SSSC parameters for static loads have been explained in section 7.3. The brief guidelines to design the SSSC components of the SEIG-SSSC system for feeding an induction motor load are summarized herewith.

- During the starting condition, the motor transient current rises around four-six times of the rated motor current. Due to which, the voltage of SEIG which is operating at rated voltage, collapses during starting of induction motor load. Therefore, the maximum injected voltage in series is taken as rated voltage.

- Volt-ampere (VA) rating of SSSC is equal to the product of maximum injection voltage and the transient motor current drawn from SEIG. Due to cost consideration, the SSSC is designed for three times of the rated motor current.

- Battery voltage $v_{bat}$ is taken with 25% higher over the maximum injection voltage, to account for the voltage drop in the ripple filter.

- The filter inductor depends upon switching frequency $f_s$ and peak ripple current $i_{rpp}$ with associated ripple band $K_{rp}$ [156, 231]. The inductor value is therefore expressed as,

$$L_f = \frac{\left(\frac{\sqrt{3}}{2}\right) v_{bat}}{6af_s K_{rp} i_{rpp}} \tag{8.1}$$

where, constant $a$ lies between 1.2-2.0 to account for transient current and ripple band ($K_{rp}$) =0.05-0.1.

- The ripple filter capacitor $C_f$ is decided on the basis of filtering requirement of compensation voltage. The switching frequency for controller is assumed to be

constant as 10 kHz. The range of $K_{sf}$ (ratio of natural frequency of oscillations of L-C circuit to sampling frequency) is 0.05-0.2 [267]. The $C_f$ is computes as,

$$C_f = \frac{1}{\left(2\pi K_{sf} f_s\right)^2 L_f} \tag{8.2}$$

- The volt-ampere (VA) rating of unity ratio insertion transformer is selected with a factor of 20 % over the VA rating of SSSC for satisfactory performance [265].

- The device voltage and current ratings are selected on the basis of battery voltage and SSSC rating with a factor, which accounts transient conditions and safe operation of device.

On the basis of above design guidelines, the value of designed SSSC components for feeding 415 V, 1.5 kW induction motor load is summarized in Table 8.1. The parameters of 415 V, 1.5 kW induction motor load is given in Appendix-A.

***Table 8.1 Value of SSSC parameters for induction motor load***

| **SSSC Components** | **1.5 kW Induction motor load** |
|---|---|
| SSSC kVA rating | 7.603 |
| Battery voltage (V) | 300 |
| Filter inductor (mH) | 1.812 |
| Filter capacitor (μF) | 13.97 |
| Transformer kVA rating | 8.363 |
| Device selection | IGBT |
| Device voltage rating (V) | 360 |
| Device current rating (A) | 12.67 |

## 8.3 SYSTEM DESCRIPTION AND CONTROL STRATEGY

The schematic of short shunt SEIG feeding an induction motor load is shown in Fig. 8.1. The SEIG consists of a star connected squirrel cage induction machine with a star connected shunt capacitor bank and driven by a prime mover. The induction motor is coupled with mechanical load for its loading.

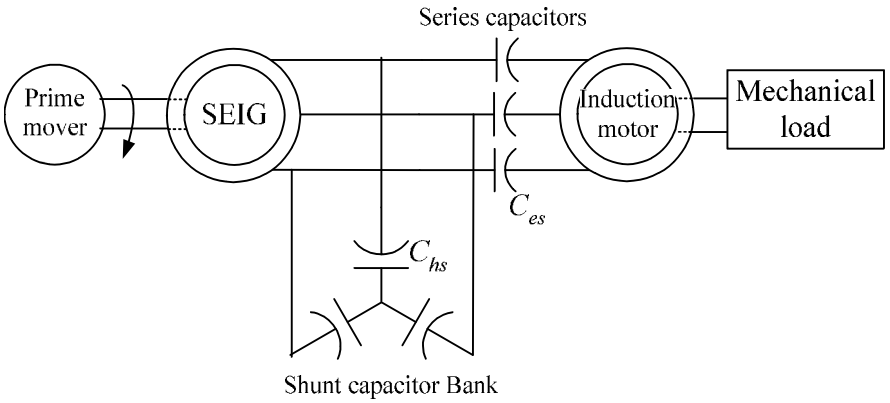


***Fig. 8.1 Schematic of short shunt SEIG feeding induction motor load***

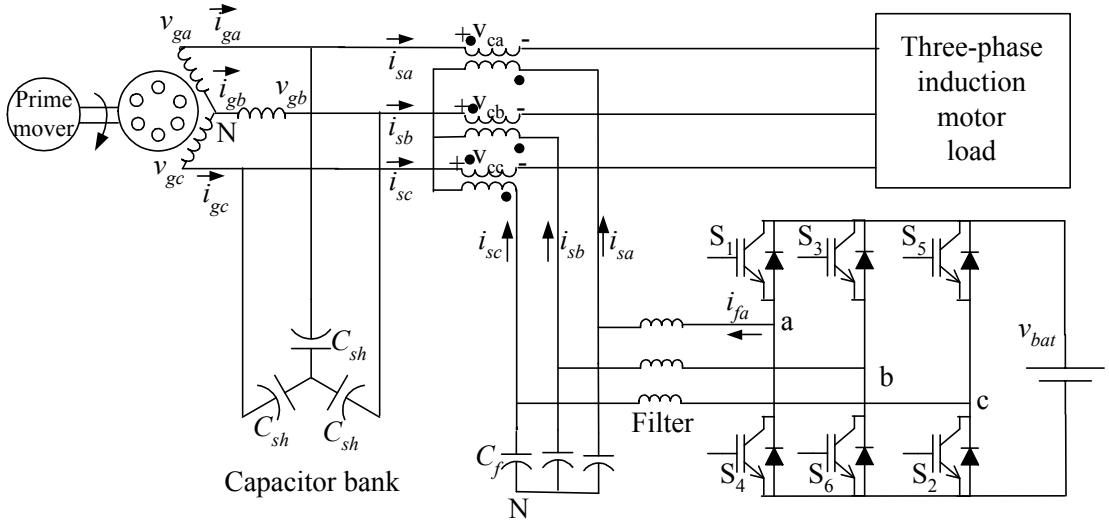


***Fig. 8.2 Schematic of SEIG-SSSC system feeding induction motor load***

The schematic of SEIG-SSSC system feeding an induction motor load is shown in Fig. 8.2. The system consists of following components as,

- Three-phase star connected SEIG
- Static synchronous series compensator
- Unity turn ratio, ideal insertion transformer
- Ripple filter
- DC Bus Battery
- Induction motor load

The three-phase star connected induction machine with star connected capacitor bank works as a SEIG, which is driven by a prime mover. The employed SSSC is a three-phase current controlled-voltage source converter (CC-VSC) with a battery at its DC bus. The AC side voltages of VSC, after filtered through L-C ripple filter, are injected into supply lines through three single-phase series transformers.

The control strategy of generating the gating signals of IGBTs of SSSC is shown in Fig. 8.3. The proposed control strategy employs a proportional-integral (PI) controller in control loop for generating reference supply currents. The load voltage is regulated by injecting the compensating voltage at appropriate phase angle.

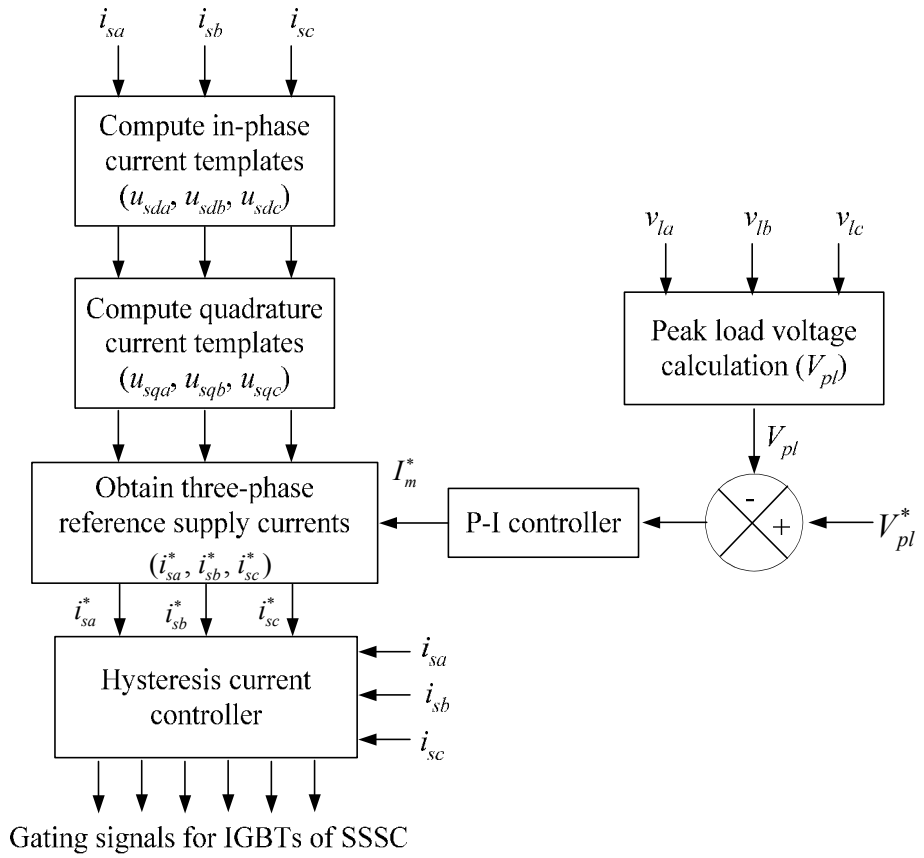


***Fig. 8.3 Control strategy for generating the gating signals of SSSC***

The peak load voltage $V_{pl}$ is calculated from the sensed load voltages. The inputs to PI controller are peak load voltage and corresponding reference voltage $V^*_{pl}$ and its output is taken as reference peak current $I^*_m$, which is responsible for maintaining load voltage. In-phase current templates ($u_{sda}$, $u_{sdb}$, $u_{sdc}$) are generated from supply currents ($i_{sa}$, $i_{sb}$, $i_{sc}$) and the quadrature current templates ($u_{sqa}$, $u_{sqb}$, $u_{sqc}$) are obtained from in-phase

current templates. The quadrature current templates are multiplied by $I_m^*$ to obtain reference supply currents ($i_{sa}^*, i_{sb}^*, i_{sc}^*$). The gating signals for IGBTs of VSC are obtained by comparing sensed and reference supply currents through the hysteresis current controller.

## 8.4 SYSTEM MODELING

The system comprises of SEIG, SSSC with associated control technique and an induction motor load. The dynamic model of system components are briefed herewith.

### 8.4.1 SEIG Model

The self-excited induction generator model in stationary q-d reference frame considering the effect of both main and cross flux saturation is already explained in previous chapters. The model equations are replicated herewith for ready reference as,

$$p[\mathbf{i}] = [\mathbf{L}]^{-1}\left([\mathbf{v}] - [\mathbf{r}][\mathbf{i}] - [\mathbf{G}][\mathbf{i}]\right) \tag{8.3}$$

$$p\omega_r = \frac{P}{2J}\left(T_P - T_{em}\right) \tag{8.4}$$

where, $[\mathbf{v}]$, $[\mathbf{i}]$, $[\mathbf{r}]$, $[\mathbf{L}]$, $[\mathbf{G}]$ and $T_{em}$ are defined in Appendix-B.

The SEIG phase voltages ($v_{ga}$, $v_{gb}$, $v_{gc}$) obtained from shunt capacitance $C_{sh}$ are expressed as,

$$\begin{aligned} v_{ga} &= \frac{(i_{ga} - i_{sa})}{C_{sh}} \\ v_{gb} &= \frac{(i_{gb} - i_{sb})}{C_{sh}} \\ v_{gc} &= \frac{(i_{gc} - i_{sc})}{C_{sh}} \end{aligned} \tag{8.5}$$

### 8.4.2 SSSC Model and Gating Signal Generation

The model of SSSC components and reference supply current equations are already explained in previous chapter. The major equations are reproduced herewith for ready reference.

#### *8.4.2.1 Filter Inductor Currents*

The filter currents ($i_{fa}$, $i_{fb}$, $i_{fc}$) equations in state space form are written as,

$$pi_{fa} = \frac{(e_a - v_{ia} - R_f i_{fa})}{L_f}$$
$$pi_{fb} = \frac{(e_b - v_{ib} - R_f i_{fb})}{L_f} \quad (8.6)$$
$$pi_{fc} = \frac{(e_c - v_{ic} - R_f i_{fc})}{L_f}$$

### *8.4.2.2 AC Side PWM Voltages*

The DC bus voltage $v_{bat}$ is reflected on the ac side of the VSC as $e_a$, $e_b$, $e_c$, as,

$$\begin{bmatrix} e_a \\ e_b \\ e_c \end{bmatrix} = \frac{v_{bat}}{3} \begin{bmatrix} 2S_a & -S_b & -S_c \\ -S_a & 2S_b & -S_c \\ -S_a & -S_b & 2S_c \end{bmatrix} \quad (8.7)$$

### *8.4.2.3 Filter Capacitor*

Ripple filter capacitor voltages ($v_{ia}$, $v_{ib}$, $v_{ic}$) equations in terms of filter currents $i_{fa}$, $i_{fb}$, $i_{fc}$ and unity turn ratio injection transformer secondary currents, which are equal to supply currents $i_{sa}$, $i_{sb}$, $i_{sc}$, are given as,

$$pv_{ia} = \frac{(i_{fa} - i_{sa})}{C_f}$$
$$pv_{ib} = \frac{(i_{fb} - i_{sb})}{C_f} \quad (8.8)$$
$$pv_{ic} = \frac{(i_{fc} - i_{sc})}{C_f}$$

### *8.4.2.4 PI Controller*

The voltage error is the difference between reference peak load voltage $V_{pl}^*$ and actual peak load voltage $V_{pl}$. At n$^{th}$ sampling instant, the voltage error *e(n)* and output *y(n)* are expressed as,

$$e(n) = V_{pl}^*(n) - V_{pl}(n)$$
$$y(n) = y(n-1) + K_p \{e(n) - e(n-1)\} + K_i e(n) \quad (8.9)$$
$$= I_m^*$$

### *8.4.2.5 Reference Supply Currents*

The control technique for generating reference supply currents is depicted in Fig. 8.3. In-phase current templates are obtained as,

$$u_{sda} = \frac{i_{sa}}{i_{sm}}$$
$$u_{sdb} = \frac{i_{sb}}{i_{sm}} \tag{8.10}$$
$$u_{sdc} = \frac{i_{sc}}{i_{sm}}$$

where, $i_{sm} = \sqrt{\frac{2}{3}\left(i_{sa}^2 + i_{sb}^2 + i_{sc}^2\right)}$ (8.11)

Quadrature current templates are obtained from in-phase current templates (derived in Appendix-F) as,

$$u_{sqa} = \frac{\left(-u_{sdb} + u_{sdc}\right)}{\sqrt{3}}$$
$$u_{sqb} = \frac{\sqrt{3}u_{sda}}{2} + \frac{1}{2\sqrt{3}}\left(u_{sdb} - u_{sdc}\right) \tag{8.12}$$
$$u_{sqc} = -\frac{\sqrt{3}u_{sda}}{2} + \frac{1}{2\sqrt{3}}\left(u_{sdb} - u_{sdc}\right)$$

The PI controller with inputs as peak load voltage and corresponding reference voltage, results output as reference peak current $I_m^*$. It is multiplied by quadrature current templates to obtain reference supply currents as,

$$i_{sa}^* = I_m^* u_{sqa}$$
$$i_{sb}^* = I_m^* u_{sqb} \tag{8.13}$$
$$i_{sc}^* = I_m^* u_{sqc}$$

### *8.4.2.6 Hysteresis Current Controller*

The switching functions to obtain gating signals for IGBTs of the CC-VSC are derived from the Hysteresis controller having *HB* current band. The switching function $S_a$ for phase '*a*' is expressed as,

$$\text{if } i_{sa} < \left(i_{sa}^* - HB\right): S_1 \text{ OFF}, S_4 \text{ ON} \Rightarrow S_a = 0$$
$$\text{if } i_{sa} > \left(i_{sa}^* + HB\right): S_1 \text{ ON}, S_4 \text{ OFF} \Rightarrow S_a = 1 \tag{8.14}$$

Similarly, switching functions $S_b$ and $S_c$ can be derived for phase '*b*' and phase '*c*' respectively.

### 8.4.3 Series Capacitors Model

The equations for series capacitors voltages ($v_{ia}$, $v_{ib}$, $v_{ic}$) in short shunt SEIG are written as,

$$\begin{aligned} pv_{ia} &= \frac{i_{sa}}{C_{es}} \\ pv_{ib} &= \frac{i_{sb}}{C_{es}} \\ pv_{ic} &= \frac{i_{sc}}{C_{es}} \end{aligned} \tag{8.15}$$

### 8.4.4 Induction Motor Model

The state space q-d model equations of an induction motor are similar to eqn. (8.3), when expressed with motor variables and are written as,

$$p[\mathbf{i}_m] = [\mathbf{L}_m]^{-1}\left([\mathbf{v}_m] - [\mathbf{r}_m][\mathbf{i}_m] - [\mathbf{G}_m][\mathbf{i}_m]\right) \tag{8.16}$$

$$p\omega_{rm} = \frac{P_m}{2J_m}\left(T_{emm} - T_L\right) \tag{8.17}$$

The load voltages can be obtained with the help of shunt capacitance and SSSC (or series capacitor) are expressed in phase variables as,

$$\begin{aligned} v_{la} &= v_{ga} - v_{ia} \\ v_{lb} &= v_{gb} - v_{ib} \\ v_{lc} &= v_{gc} - v_{ic} \end{aligned} \tag{8.18}$$

The load voltage in phase variables transformed into q-d variables to obtain load voltage vector $\boldsymbol{v}_m$ in q-d reference frame, as required in eqn. (8.16).

### 8.4.5 Battery Model

The detailed Thevenin discharge electrical model of the battery [263] is already been explained in previous chapter. The equation governing the behavior of the battery is reproduced herewith for ready reference. For RC discharge time constant $\tau_0$ (=$R_0C$), the $v_{bat}$ is expressed as,

$$v_{bat} = E_p - i_{bat}(R_p + R_0) + i_{bat}R_0 e^{(-t/\tau_0)} \tag{8.19}$$

where, $E_p$ signifies the equilibrium electromotive force of the battery under no load condition, $R_P$ represents ohmic polarization, resistance $R_0$ signifies charge transfer losses and capacitance C signifies the double layer effect dynamics.

The short shunt SEIG with an induction motor load model is represented by the set of equations from eqn. (8.3) to eqn. (8.5) and eqn. (8.15) to eqn. (8.18).

The SEIG-SSSC system with an induction motor load model is therefore represented by the set of equations from eqn. (8.3) to eqn. (8.14) and eqn. (8.16) to eqn. (8.19). Both the short shunt SEIG and the SEIG-SSSC system model equations are solved by fourth order Runge-Kutta integration method in MATLAB environment.

## 8.5 ALGORITHM FOR SIMULATING SEIG-SSSC PERFORMANCE

The flow chart showing main algorithmic steps for simulating the transient performance of SEIG-SSSSC system feeding induction motor load is shown in Fig. 8.4 and corresponding algorithm is explained as,

1. Read the SEIG and an induction motor parameter, shunt capacitance $C_{sh}$, their magnetizing characteristic. Moreover read the SSSC parameters and load voltage PI controller gains.

2. Set $t$=0, $[i_{qs} \quad i_{ds}]^T = [0.0001 \quad 0.0001]^T$ to account residual magnetism, voltage buildup resistance ($R_{lvb}$)=20000.

   Also set time for connecting the SSSC ($t_{SSSC}$), time for connecting an induction motor load ($t_{ms}$), time for mechanical loading on induction motor ($t_{ml}$), total simulation time ($t_T$), time step ($\Delta t$).

3. Compute $i_M$, $L_M$ and obtain $[\mathbf{L}]$ and $[\mathbf{G}]$.

4. If ($t<t_{SSSC}$) than evaluate differential equations of SEIG for no load voltage buildup and go to step 10.

5. Detect the zero crossing, calculate the peak supply current from sensed supply currents and generate the gating signals from control strategy.

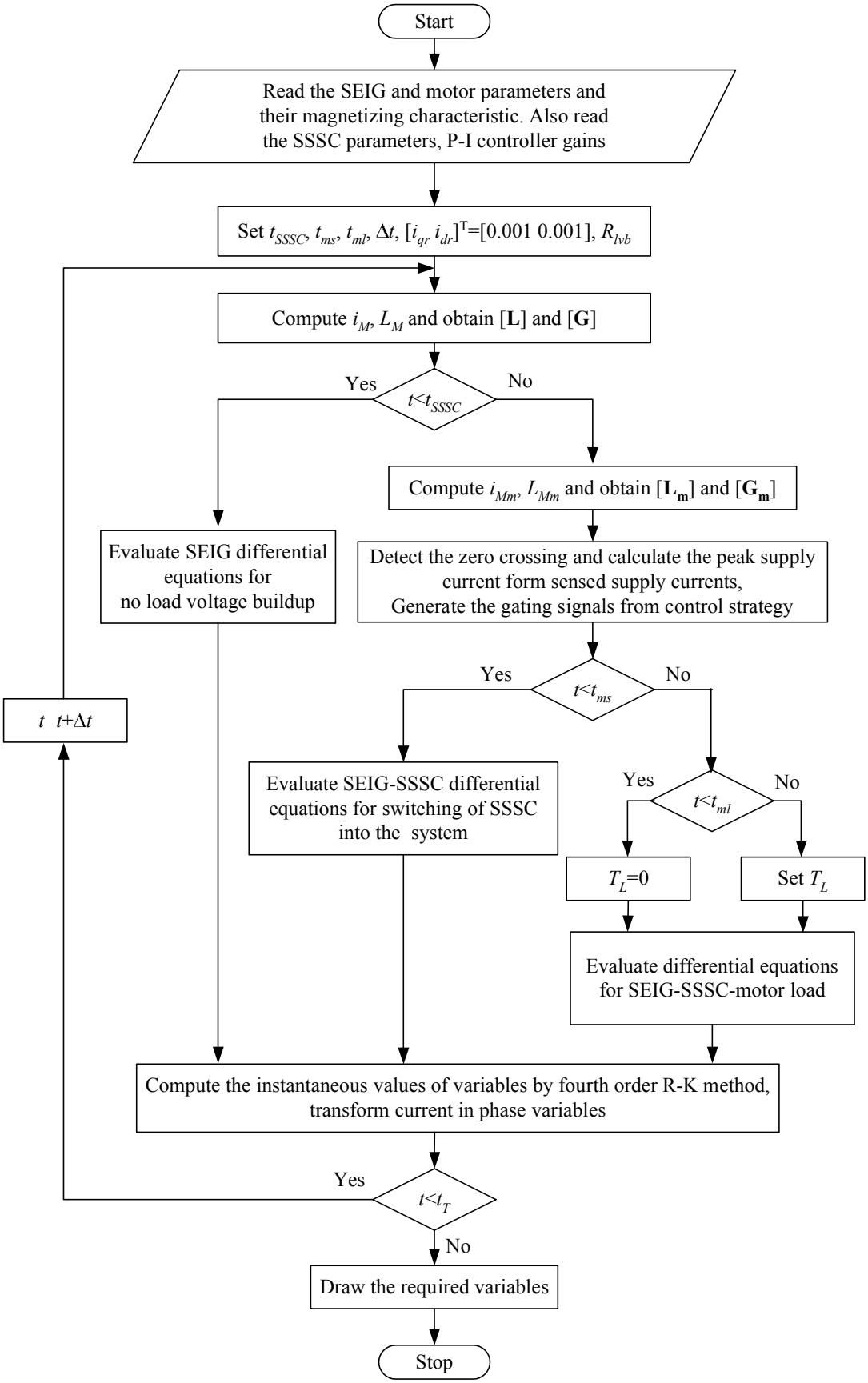


***Fig. 8.4 Flow chart for simulating transient performance of SEIG-SSSC system feeding induction motor load***

6. If ($t<t_{ms}$) than evaluate differential equations to simulate SEIG-SSSC switching of SSSC and go to step 10.

7. $i_{Mm}$, $L_{Mm}$ and deduce [$\mathbf{L}_m$] and [$\mathbf{G}_m$].

8. If ($t<t_{ml}$) than set $T_L$=0 otherwise $T_L$=rated motor torque.

9. Evaluate differential equations to simulate the SEIG-SSSC system feeding an induction motor load.

10. Compute the instantaneous values of variables by fourth order Runge-Kutta method and transform currents in phase variables.

11. If $t<t_T$ than $t=t+\Delta t$ and go to step 3.

12. Draw the waveforms for the SEIG-SSSC system feeding induction motor load.

## 8.6 RESULTS AND DISCUSSION

The investigations have been carried out on 415V, 3.7 kW, 7.6 A, Y-connected squirrel cage induction machine working as a SEIG driven by prime-mover with prime mover torque as $T_P = 6200 - 20\omega_r$ and excited by a star connected capacitor bank. The 48.3 μF/phase capacitance is required to obtain rated no load voltage of 239 V (peak phase voltage 340 V). The performance of short shunt SEIG and SEIG-SSSC configurations are studied for feeding an induction motor load. These configurations are loaded with 415 V, 1.5 kW, 3.2 A, Δ-connected induction motor. The successful starting of the motor load by SEIG requires shunt capacitance of 109 μF/phase. The shunt capacitance of 109μF/phase is resulting into very high voltage during no load and therefore the shunt capacitance $C_{sh}$, as obtained from steady state equivalent circuit at full load is taken as 80 μF/phase and the remaining reactive VARS are supplied by SSSC or series capacitors in short shunt SEIG. The optimization technique and the problem formulation for calculating the shunt capacitance are summarized in Appendix-G. The parameters of the induction machine operated as a SEIG and an induction motor load are given in Appendix-A, whereas, the SSSC parameters are summarized in Appendix-H. The following investigations are carried out,

- Short shunt SEIG performance with motor load

- SEIG- SSSC performance with motor load
- Power quality performance

### 8.6.1 Short Shunt SEIG Performance with Motor Load

The starting of an induction motor by short shunt SEIG is studied in terms of generator voltages $v_{gabc}$, generator currents $i_{gabc}$, load voltages $v_{labc}$, motor currents $i_{mabc}$, motor electromagnetic torque $T_{emm}$, peak load voltage $V_{pl}$ and motor speed $\omega_{rm}$ for $C_{hs}$ (=$C_{sh}$) as 80 μF and two values of $C_{es}$ as 400 μF and 300 μF and the transient performance characteristics are shown in Fig. 8.5 and Fig. 8.6 respectively. As shown in Fig. 8.5, with higher value of $C_{es}$ as 400 μF, the higher magnitude oscillations are resulted in $i_{gabc}$, $i_{mabc}$, $v_{labc}$ and $T_{em}$. The oscillations remains sustained for long duration until the voltage collapses. Therefore, the unstable behavior is due to high magnitude oscillations and voltage collapse.

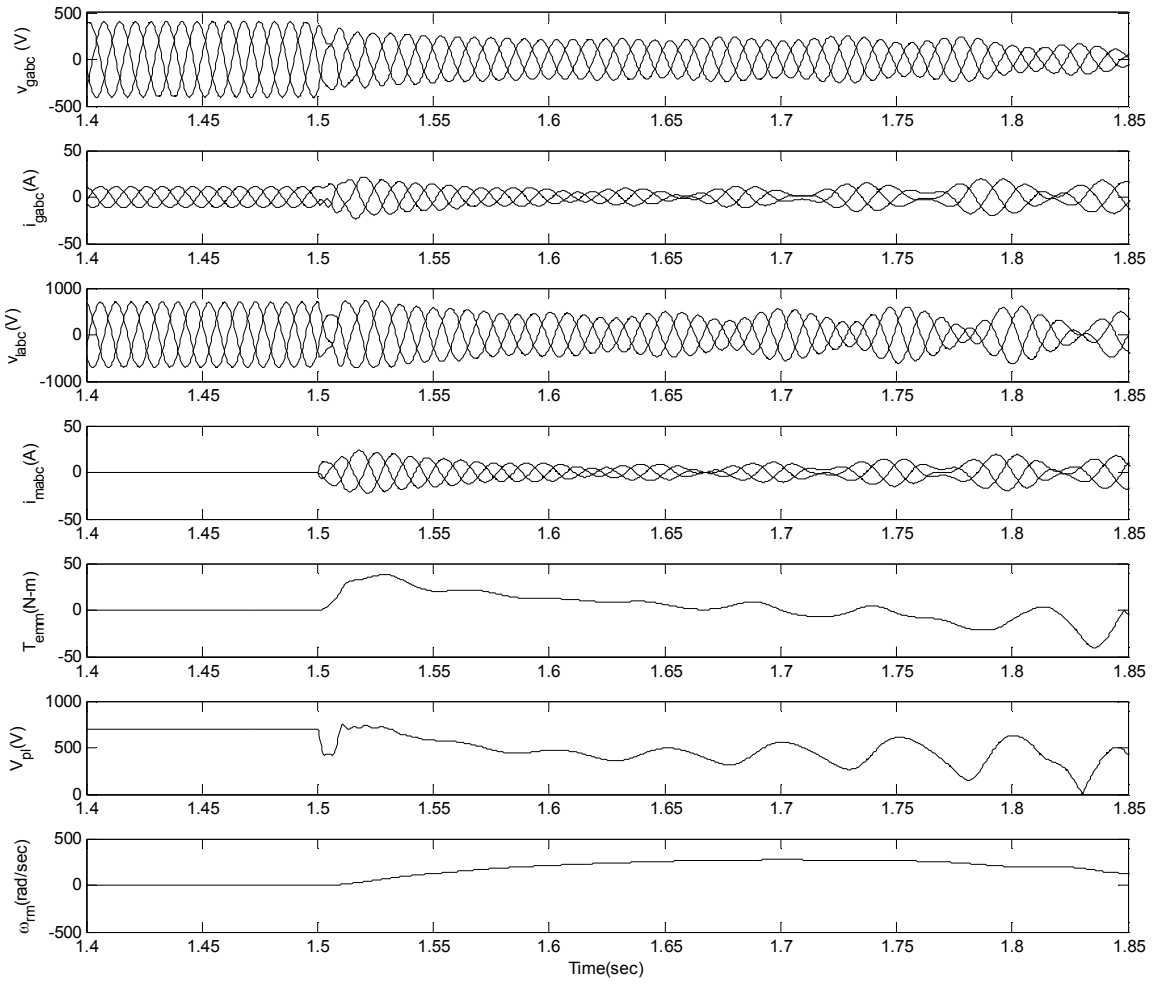


***Fig. 8.5 Transient performance characteristic during unsuccessful starting of motor load by short shunt SEIG due to voltage collapse resulted by high $C_{es}$***

As shown in Fig. 8.6, after the initial transients of 0.4 sec., $i_{gabc}$ of four times to rated generator current and $i_{mabc}$ of seven times to rated motor current are observed causing large stress on insulation life. Therefore, the unsuccessful starting of motor load is due to sustained and excessively high $i_{gabc}$ and $i_{mabc}$ currents.

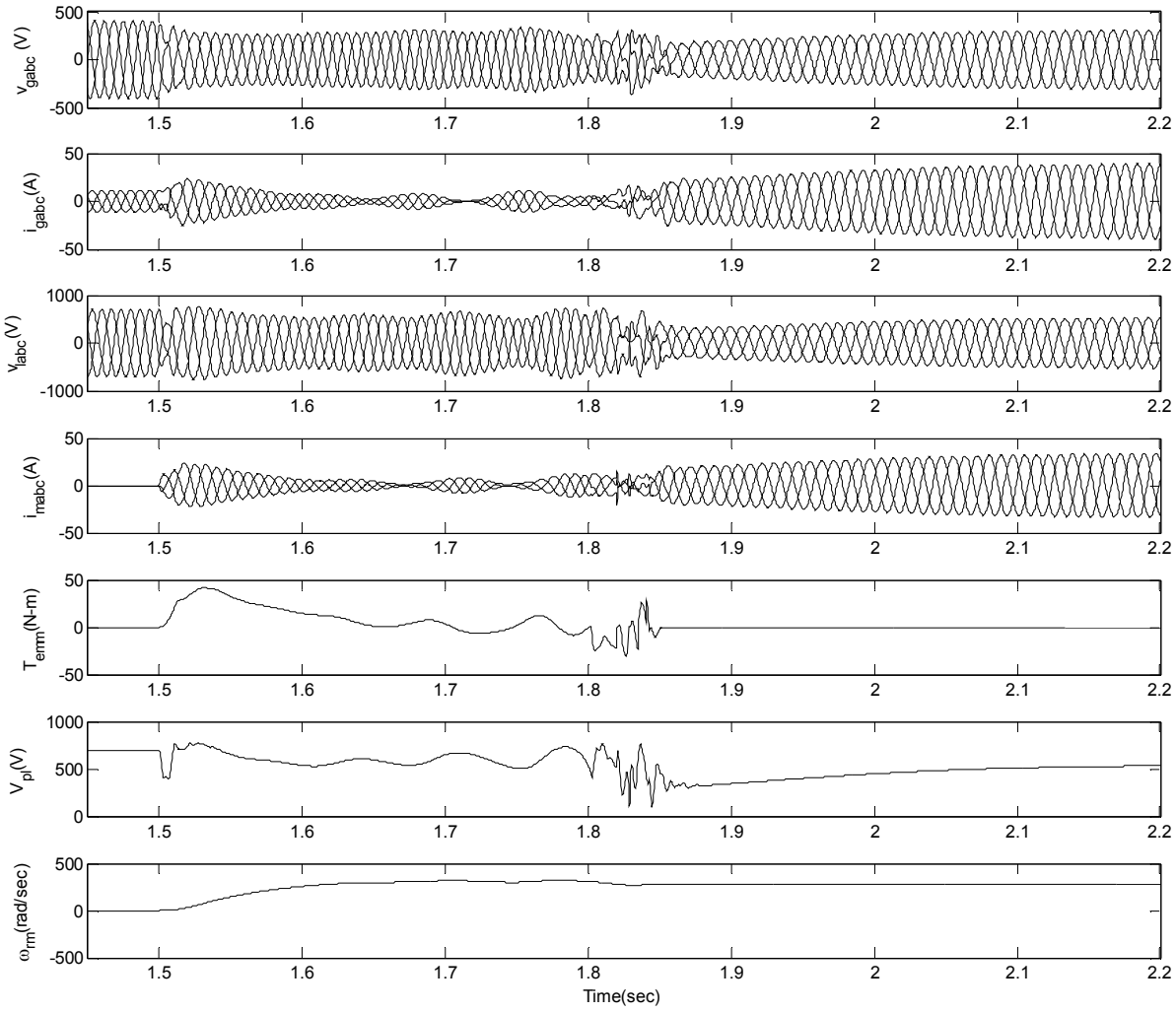


***Fig. 8.6 Transient Performance characteristic during unsuccessful starting of motor load by short shunt SEIG due to sustained large currents resulted by low $C_{es}$***

As evident from this study, with both low and high values of series capacitance, the unstable behavior is resulted in either due to excessive high current of sustained nature or high magnitude oscillations and voltage collapse due to the phenomenon like sub-synchronous resonance.

### 8.6.2 SEIG- SSSC Performance with Motor Load

The performance of SEIG-SSSC system feeding an induction motor load is shown in Fig. 8.7 in terms of generator voltages $v_{gabc}$, generator currents $i_{gabc}$, load voltages $v_{labc}$,

motor electromagnetic torque $T_{emm}$, induction motor speed $\omega_{rm}$, peak load voltage $V_{pl}$, prime mover speed $\omega_r$, battery voltage $v_{bat}$. The induction motor is connected at 0.8 sec, which attains the rated speed after the successful starting in 0.3 sec. The starting motor current $i_{ma}$ is only three times to rated motor current.

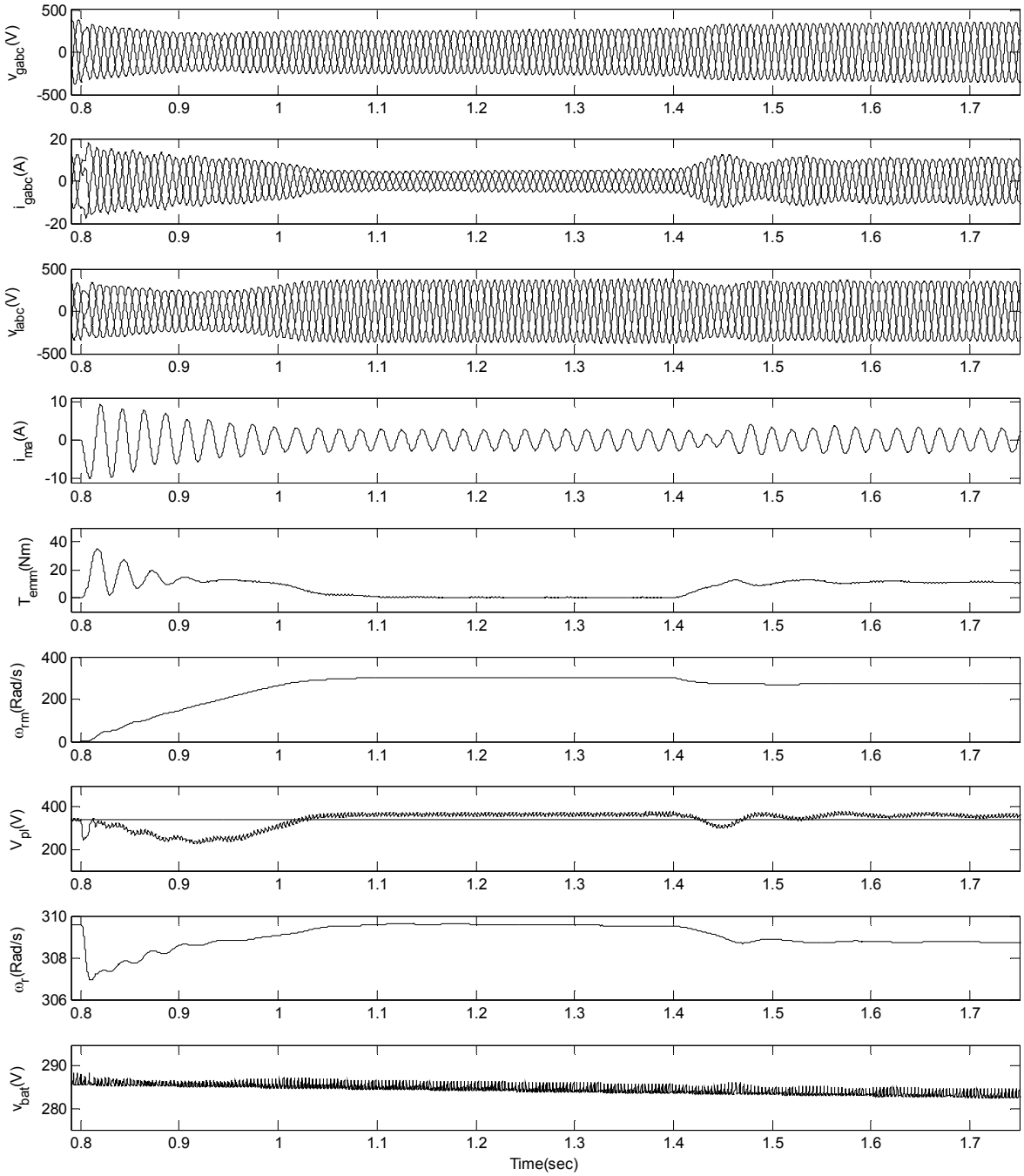


***Fig. 8.7 Transient performance characteristic of SEIG-SSSC during successful startup of motor load and full mechanical loading***

***(Load conditions : $T_L$=0 at 0.8 sec. and $T_L$=rated torque at 1.4 sec.)***

During the starting of motor load, the $V_{pl}$ droops to 240 V which gradually increases to reference value under the PI controller action. When SEIG is operated without any load, higher generator current $i_{gabc}$ is resulted in because $C_{hs}$ is higher than required for rated voltage at no load. The $i_{gabc}$ decreases with the connection of motor load. During starting, appreciable transients are also exhibited in motor torque $T_{em}$ which are settled after few cycles. The prime mover speed $\omega_r$ also decreases during starting of an induction motor load.

At 1.4 sec, the induction motor is loaded with rated mechanical load, correspondingly, $i_{gabc}$, $i_{ma}$, $T_{em}$ increase and $\omega_{rm}$ and $\omega_r$ are decreased. With this increased mechanical load, steady state condition is resulted in 0.2 sec. after some oscillations in $i_{gabc}$. As the stable operation is achieved with SEIG-SSSC configuration supplying a motor load, it is observed that SSSC provides effective damping to oscillating transients, which are resulting in with short shunt SEIG.

### 8.6.3 Power Quality Performance

The performance of the SEIG-SSSC system with reference to power quality is assessed by harmonic spectrum and total harmonic distortion (THD) of voltages and currents of the generator and load terminal using the fast Fourier transformation (FFT)in MATLAB. The voltage and current waveforms under steady state along with their harmonic spectra during induction motor operation with and without mechanical load are shown in Fig. 8.8 and Fig. 8.9 respectively. The obtained values of THD, as summarized in Table 8.2, are well within the permissible limits. The THD value for generator quantities with full mechanical loading is also calculated which comes out within the acceptable range. Based on the THD values, it is observed that the performance both at generator and load terminals are satisfactory as far as power quality is concerned.

***Table 8.2 THD values for SEIG-SSSC system feeding induction motor load***

| **Loading condition** | **THD in $v_{ga}$ (%)** | **THD in $i_{ga}$ (%)** | **THD in $v_{la}$ (%)** | **THD in $i_{ma}$ (%)** |
|---|---|---|---|---|
| No load | 0.10 | 0.63 | 0.82 | 1.23 |
| Full load | 0.74 | 1.19 | 1.62 | 0.83 |

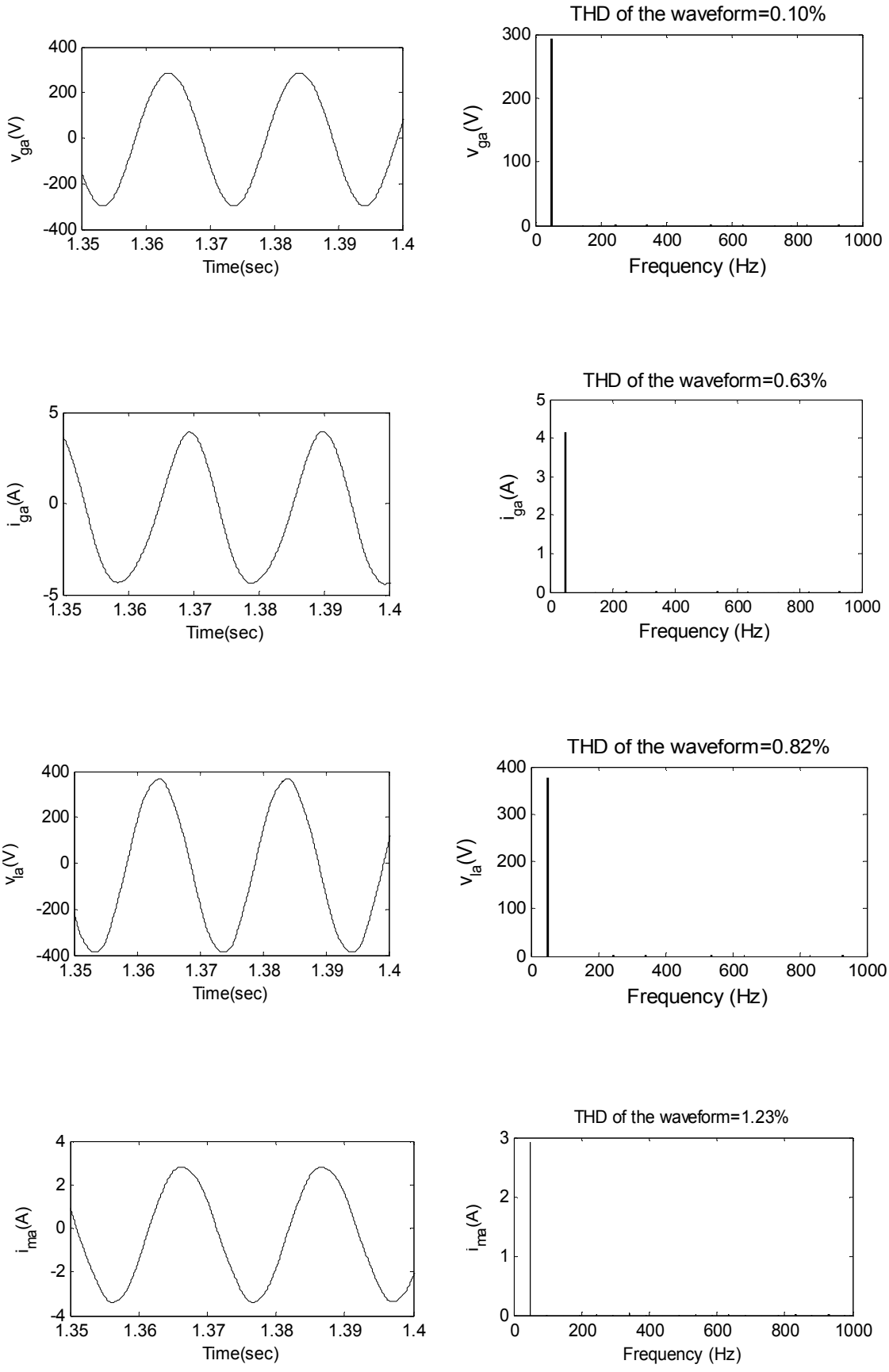


***Fig. 8.8 Harmonic spectra during steady state for SEIG-SSSC fed induction motor at no load***

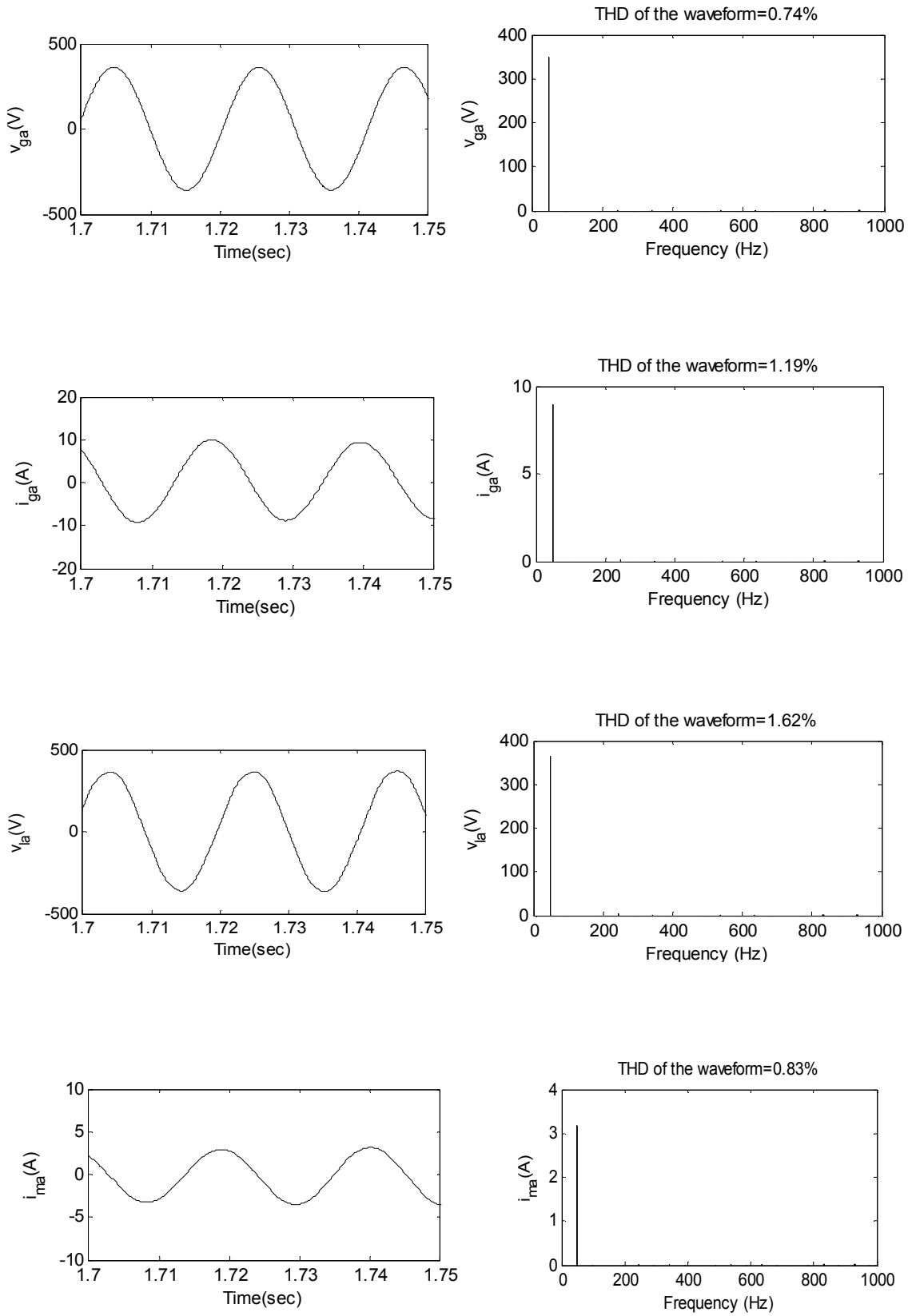


***Fig. 8.9 Harmonic spectra during steady state for SEIG-SSSC fed induction motor at full mechanical load***

## 8.7 CONCLUSIONS

The design, modeling and simulation of SEIG-SSSC system have been carried out and the performance has been studied for feeding an induction motor load. The simplified model equations of each system component have been presented in detail. The proposed SSSC has employed IGBTs based, three-phase current controlled-voltage source converter. The control technique, which has employed only a PI control loop to calculate the reference supply currents, injects controllable voltage in series with the load. The gating signals of IGBTs of SSSC have been generated using a hysteresis current controller. The control scheme of SSSC has been found effective in mitigating the unstable behavior like SSR, which is the major problem with the series capacitor compensated SEIG feeding an induction motor load. The following conclusions have been deduced from the study carried out in this chapter.

- The larger series capacitance in short shunt SEIG has caused the oscillating behavior leading to voltage collapse, whereas smaller series capacitor has caused the dangerously high generator voltage and current.

- The SEIG-SSSC system has resulted in satisfactory performance with an induction motor load during starting and mechanical loading on the induction motor. The capability of SSSC has been shown in damping out the oscillating and unstable behavior, observed during loading of compensated SEIG with an induction motor load.

# CHAPTER-IX

# MAIN CONCLUSIONS AND SUGGESTIONS FOR FURTHER WORK

## 9.1 GENERAL

The self-excited induction generator (SEIG) is emerging potentially to harness small capacity resources due to its various inherent advantages. The application of SEIG is helpful for the electrification of remote locations. It can also be used as standby power supply to feed critical loads. The inherent poor voltage regulation is one of the major bottlenecks for its wider applicability. The advances in power electronic devices, their improved characteristics, power converter topologies, digital processors and improved control algorithms have resulted in usage of non-linear loads and static converters for improved performance. The research work has been carried out with the objective to investigate the performance of static controllers namely STATCOM and SSSC for improving the performance of SEIG while supplying various linear, non-linear, balanced and unbalanced loads. The objectives outlined in the thesis have been attempted through the various studies that are detailed in different chapters. The various studies carried out are as,

- The study on the classification and operational aspects of the regulating schemes has been summarized in Chapter-III.
- The investigations on the steady state performance of SEIG for feeding static and dynamic loads and the transient performance of SEIG feeding linear and non-linear loads have been summarized in Chapter-IV.
- The investigations on SEIG-STATCOM system for feeding balanced static resistive-inductive, induction motor and three-phase fully controlled rectifier fed DC motor loads have been summarized in Chapter-V.
- The study on SEIG-STATCOM system operating as a four-wire isolated supply system for feeding various static linear and nonlinear loads has been detailed in Chapter-VI.

- The study on series compensation, which is realized through series capacitors and through static synchronous series compensator (SSSC) for SEIG feeding static loads have been detailed in Chapter-VII.

- The investigations on SEIG-SSSC system feeding induction motor load for the stable operation have been detailed in Chapter-VIII.

## 9.2 MAIN CONCLUSIONS

The detailed conclusions of various studies have been given in the respective chapters. The main concluding remarks of each study are encapsulated herewith,

**1. Study on the classification and operational aspects of the regulating schemes**

The regulating schemes have been classified on the basis of voltage, frequency and voltage-frequency control. As the terminal voltage is governed by the reactive power compensation, the voltage regulating (VR) schemes have been classified into shunt and series regulating schemes; each one is further sub classified into classical, switching device based and converter based voltage regulating schemes. The loads on SEIG have also been classified on the basis of number of phases or nature of loads as linear or non-linear loads. The broad application areas of SEIG have been summarized. The following conclusions are drawn from this study.

- The saturable core reactor is the best among the classical shunt schemes from view point of the stability, the reliability and the cost for feeding linear loads.

- Among solid state switching device based shunt compensation schemes, the SVC based VR scheme is suited to supply sensitive loads. In this VR scheme, the TCR branch can be eliminated and an effective control can be achieved with only TSC.

- Among the converter based shunt compensation VR schemes, the voltage source converter based STATCOM is best suited due to the fast and an effective control. It can also supply the nonlinear unbalanced loads

- For the effective series compensation, the short shunt SEIG is good option to supply static loads whereas the SSSC based scheme is effective to supply sensitive loads.

- Scheme employing a shunt active filter (AF), bidirectional current battery converter (BC) and electronic load controller (ELC) is the most generalized arrangement for voltage-frequency control.

**2. Steady state performance of SEIG for feeding static and dynamic loads and the transient performance of SEIG feeding linear and non-linear loads**

The steady state performance of SEIG has been studied for static and dynamic loads. An optimization problem has been formulated for voltage regulation, using steady state equivalent circuit, subjected to various inequality constraints related to performance and solved for shunt capacitance and speed using genetic algorithm (GA). The performance for optimum voltage regulation of SEIG feeding static resistive and resistive-inductive loads has been studied in detail.

The transient performance of SEIG has been studied feeding linear and non-linear load. The dynamic model of SEIG and induction motor has been developed in q-d variables in stationary reference frame, by considering main and cross flux saturation. The dynamic model of three-wire and four wire uncontrolled rectifier fed resistive, resistive-capacitive non-linear loads have been developed in phase variables. The power quality performance of system quantities has been studied using harmonic spectrum and total harmonic distortion (THD). The following conclusions are deduced from this study.

- The developed voltage regulation optimization algorithm employing GA is effective in providing the optimum values of the shunt capacitance and the speed.

- In spite of optimum capacitance selection, the SEIG exhibits drooping terminal voltage with loads.

- Better voltage regulation with high loading capacity has been obtained with resistive load as compared to inductive loads.

- The large voltage drop and large starting time are serious power quality problems for the SEIG feeding induction motor load, which suggest the use of static controllers for supplying the reactive power.

- The THD on generator side due to non linear load is resulted in higher than specified IEEE 519 standard. Therefore, the SEIG should not be run for prolong time with non-linear loads to avoid any damage.

## 3. SEIG-STATCOM system for feeding balanced static resistive-inductive, induction motor and three-phase fully controlled rectifier fed DC motor loads

The performance of SEIG-STATCOM system have been studied for feeding balanced resistive-inductive, induction motor and fully controlled rectifier fed DC motor loads. A methodology has been proposed to design STATCOM parameters and the STATCOM has been designed for two cases namely full rating STATCOM and reduced rating STATCOM. The control scheme has been proposed, which consists of two proportional-integral (PI) controllers. One PI controller is applied to regulate the DC link voltage to the reference value and the other PI controller is applied to regulate the terminal voltage by regulating the required reactive power. The hybrid model has been developed for the system, where, the induction machine model has been modeled in q-d variables in stationary reference frame and the STATCOM and controlled rectifier fed DC machine have been modeled in phase variables. The following conclusions are made form this study.

- The starting time and the voltage dip due to starting of induction motor on SEIG-STATCOM system are reduced as compared to respective values resulting due to the application of induction motor on SEIG system.

- The SEIG-STATCOM system is able to supply controlled rectifier fed DC motor load. The soft starting action limits the generator current, DC motor current and developed electromagnetic torque.

- The performance of both full rating and reduced rating STATCOM are found commendable as far as starting, voltage dip during transient period and THD components under steady state condition are concerned.

## 4. SEIG-STATCOM system operated as a four-wire isolated supply system for feeding various static linear and nonlinear loads

The performance of SEIG-STATCOM system has been studied as a four-wire isolated system for feeding various static linear and non-linear loads. The induction machine model in q-d variables and shunt capacitance and load model in phase variables

have been used for the study. The control technique consists of two PI controllers, which take cares of unbalanced and non-linear loads. The three-wire uncontrolled rectifier fed resistive, three-wire uncontrolled rectifier fed resistive-capacitive and four-wire uncontrolled rectifier fed resistive-capacitive loads have been considered as non-linear loads. The following conclusions are drawn from this study.

- The capability of the STATCOM has been demonstrated as a voltage regulator, a load balancer, a harmonic eliminator and a neutral current compensator.

- The harmonics content and THD are lower than the standard IEEE-519 limit for generator side, which validate the effectiveness of control technique.

- With the support of STATCOM, the SEIG system can operate as an ideal four-wire isolated supply feeding linear and non-linear loads.

**5. Operation of series compensated SEIG feeding static loads using series capacitors and static synchronous series compensator (SSSC)**

The steady state performance of short shunt SEIG has been studied for feeding resistive and resistive-inductive loads. Based on the steady state equivalent of short shunt SEIG, an optimization problem has been formulating for short shunt SEIG with objective function for voltage regulation characteristic and for performance characteristic, a combination of voltage regulation characteristic and loadability, subjected to various equality and inequality constraints related to SEIG performance. The series and shunt capacitances at a specified speed have been calculated for both the objective functions using genetic algorithm.

The transient performance of SEIG-battery supported SSSC and SEIG-capacitor supported SSSC system have been studied for feeding static loads. The design methodology to decide the battery supported and capacitor supported SSSC parameters has been explained and SSSC has been designed for static loads. A simplified PI based control technique has been proposed for SEIG-battery supported SSSC system to regulate the terminal voltage and the performance is studied for resistive, resistive-inductive and resistive-capacitive loads. The control technique of the SEIG-capacitor supported SSSC system employed two PI controllers and the system is studied for static resistive-inductive load. The following conclusions have been drawn from this study.

- The developed GA based algorithm is found effective for the selection of series and shunt capacitances for short shunt SEIG feeding static resistive and resistive-inductive load.

- The optimum voltage regulation is obtained at a speed slightly more than rated speed for resistive load, whereas, the optimum voltage regulation is obtained at lower limiting value of the speed for resistive-inductive loads.

- The SEIG voltage is more than the load voltage for resistive load, whereas, the SEIG voltage is lower than the load voltage and difference between them is increasing with the increase in loads.

- For performance characteristic, the optimum performance has been achieved at an upper limiting speed for resistive load, where the loading on SEIG comes out to be more than rated power of machine, irrespective of the considered weightage factors. While, for resistive-inductive load, the optimum performance has been obtained in the range of unity with loading on SEIG is less than unity.

- The SEIG-battery supported SSSC system has exhibited almost flat load voltage characteristic with change in resistive, resistive-inductive, and resistive-capacitive loads. The inductive mode operation for capacitive load and capacitive mode operation for both resistive and inductive loads have been demonstrated, which shows the effectiveness of control technique.

- The load voltage for SEIG-capacitor supported SSSC system feeding static R-L load shows the flat characteristic during change of load, which thereby showing the effectiveness of control technique.

- The harmonics on generator side are well within the standard IEEE-519 limits for both the SEIG-battery supported and SEIG-capacitor supported SSSC systems.

## 6. SEIG-SSSC system feeding induction motor load for the stable operation

The transient performance of SEIG-SSSC system feeding induction motor load has been studied. The SSSC parameters have been designed for induction motor load. The hybrid dynamic model of short shunt SEIG and SEIG-SSSC system and feeding induction

motor load has been developed to study the transient performance with an induction motor load. The following conclusions have been deduced from this study.

- The larger series capacitance in short shunt SEIG caused the oscillating behavior leading to voltage collapse, whereas smaller series capacitor caused the dangerously high generator voltage and current.

- The SEIG-SSSC system has resulted in satisfactory performance with induction motor load during starting and mechanical loading on the induction motor. The capability of SSSC has been shown in damping out the oscillating and unstable behavior, observed during loading of compensated SEIG with the induction motor load.

## 9.3 SUGGESTIONS FOR FURTHER WORK

The research work is a continuous process for the improvement in the existing and exploration of further work. As a consequence of the investigations carried out in this thesis on regulating schemes for three-phase SEIGs, steady state and transient analysis of three-phase SEIG, SEIG operation with STATCOM feeding static and dynamic loads, SEIG-STATCOM operation as an isolated four-wire supply system, short shunt SEIG operation for optimum performance, SEIG operation with SSSC feeding static and induction motor loads, the research objectives have been achieved successfully and the following areas have been identified for further work in this research area-

- The steady state performance of SEIG have been carried out for feeding static and dynamic loads and transient state performance of SEIG feeding linear and non-linear load. The study can be extended for unbalanced steady state and transient state performance, which is important for designing of small isolated system and devising protection strategy.

- The SEIG-static compensator (STATCOM) system driven by constant speed prime mover has been thoroughly investigated for linear and non-linear loads for voltage regulation, harmonics elimination, load balancing and neutral current compensation through the reactive power compensation. The study can be extended for the variable speed prime mover for the potential applications in wind energy conversion systems.

- The extensive study has been carried out for the reactive power compensation by the STATCOM to improve the SEIG performance. The active power control aspect can be explored by considering the load controller.

- The steady state performance of short shunt SEIG has been examined by selecting shunt and series capacitance for optimum voltage regulation and for optimum performance. The performance of short shunt SEIG can be evaluated while considering the effect of frequency regulation, which is important for standby power supply applications driven by constant speed prime mover as diesel internal combustion (IC) engine or variable speed prime mover as wind turbine etc.

- The SEIG-SSSC system has been analyzed under balanced conditions for feeding static and dynamic loads. There is a scope to extend the work under unbalanced condition operation such as load unbalanced, capacitor unbalanced etc. Furthermore, the study can be extended for feeding non-linear loads.

- The performance of battery supported SSSC and capacitor supported SSSC has been investigated for the linear loads. The battery supported SSSC has also been considered for the analysis of linear loads. The capacitor supported SSSC and associated control algorithm can be extended for feeding induction motor load and non-linear loads.

- The study carried out on SEIG-STATCOM and SEIG-SSSC systems can be useful for the field installation of SEIG-STATCOM and SEIG-SSSC proto-models for supplying various loads.

# REFERENCES


[1] E. D. Bassett and F. M. Potter, "Capacitive excitation for induction generators," *AIEE Trans. on Electrical Engineering*, vol. 54, pp. 540-545, 1935.

[2] C. F. Wagner, "Process of self-excitation of induction motors," *AIEE Trans. on Electrical Engineering*, vol. 58, pp. 47-51, 1939.

[3] J. E. Barkle and R. W. Ferguson, "Induction generator theory and application," *AIEE Trans. on Electrical Engineering*, vol. 58, pp. 12-19, 1954.

[4] B. C. Doxey, "Theory and application of the capacitor excited induction generator," *The Engineers*, vol. 216, pp. 893-897, 1963.

[5] Bhim Singh, "Induction generator-a prospective," *Electrical Machines and Power Systems*, vol. 23, pp. 163-177, 1995.

[6] R. C. Bansal, T. S. Bhatti and D. P. Kothari, "Bibliography on the application of induction generators in non conventional energy systems," *IEEE Trans. on Energy Conversion,* vol. 18, no. 3, pp. 433-439, 2003.

[7] R. C. Bansal, T. S. Bhatti and D. P. Kothari, "Induction generator for isolated hybrid power system applications: a review," *Institute of Engineers (India), Electrical*, vol. 83, pp. 262-269, 2003.

[8] R. C. Bansal, "Three-phase self-excited induction generators: an overview," *IEEE Trans. on Energy Conversion*, vol. 20, no. 2, pp. 292-299, 2005.

[9] G. K. Singh, "Self-excited induction generator research-a survey," *Elect. Power Sys. Res*., vol. 69, pp. 107-114, 2003.

[10] L. B. Shilpakar, "Analysis of self-excited induction generators supplying single-phase and three-phase loads," *Ph. D.* Thesis, *Department of Electrical Engineering*, *IITD*, New Delhi, 1997.

[11] S. K. Jain, "Isolated and grid mode operation of induction generators," *Ph. D. Thesis, Department of Electrical Engineering*, *IIT* Roorkee, 2000.

[12] S. Gupta, "Analysis and development of load controller and static compensator for self-excited induction generator based autonomous generating system," *Ph. D. Thesis, Department of Electrical Engineering*, *IITD*, New Delhi, 2004.

[13] P. Vas, *Electrical machines and drives: a space vector theory approach*, Oxford, Clarendon Press, 1992.

[14] I. J. Nagrath and D. P. Kothari, *Electrical machines*, Second edition, New Delhi, Tata McGraw Hill, 1997.

[15] M. G. Simoes and F. A. Farret, *Renewable energy systems: design and analysis with induction generators*, Boca Raton, CRC Press, 2004.

[16] S. S. Murthy, O. P. Malik and A. K. Tandon, "Analysis of self-excited induction generators," *IEE Proc. Gener., Transm. and Distrib.,* vol. 129, no. 6, pp. 260-265, 1982.

[17] A. K. Tandon, S.S. Murthy and G. J. Berg, "Steady state analysis of capacitor self-excited induction generators," *IEEE Trans. on Power Apparatus and Systems,* pp. 612-618, 1984.

[18] N. H. Malik and S. E. Haque, "Steady state analysis and performance of an isolated self-excited induction generator," *IEEE Trans. on Energy Conversion,* vol. 1, no. 3, pp. 134-139, 1986.

[19] S. S. Murthy, B. P. Singh, C. Nagamani and K. V. V. Satyanarayana, "Studies on the use of conventional induction motors as self-excited induction generators," *IEEE Trans. on Energy Conversion,* vol. 3, no. 4, pp. 842-848, 1988.

[20] S. P. Singh, Bhim Singh and M. P. Jain, "Comparative study on the performance of a commercially designed induction generator with induction motors operating as self excited induction generators," *IEE Proc.-C*, vol. 140, no. 5, pp. 374-380, 1993.

[21] L. Ouazene and G. J. McPherson, "Analysis of the isolated induction generator," *IEEE Trans. on Power Apparatus and Systems,* vol. 102, no. 8, pp. 2793-2798, 1983.

[22] J. A. A. Melkebeek and D.W. Novotny, "Steady state modelling of regeneration and self-excitation in induction machines," *IEEE Trans. on Power Apparatus and Systems,* vol. 102, no. 8, pp. 2725-2733, 1983.

[23] A. Al-Jabri, "Direct evaluation of output frequency and the magnetizing reactance of the three-phase isolated self-excited induction generators," *Electric Machines and Power Systems,* vol. 8, pp. 113-131, 1990.

[24] S. P. Singh, Bhim Singh and M. P. Jain, "Performance characteristics and optimum utilization of a cage machine as capacitor excited induction generator," *IEEE Trans. on Energy Conversion,* vol. 5, no. 4, pp. 679-684, 1990.

[25] T. F. Chan, "Steady state analysis of self-excited induction generator," *IEEE Trans. on Energy Conversion,* vol. 9, no. 2, pp. 288-296, 1994.

[26] X. S. Chen, A. J. Flechsig, C. W. Pang and L. M. Zhuang, "Digital modelling of an induction generator," in *Proc. IEE Int. Conf. Advances in power system control, operation and management,* Hong Kong, pp. 720-726, 1991.

[27] N. Ammasaigounden, M. Subbiah and M. R. Krishnamurthy, "Wind driven self-excited pole changing induction generators," *IEE Proc. Electr. Power Appl.,* vol. 133, no. 5, pp. 315-321, 1986.

[28] S. S. Yegnanarayanan and V. J. Johnny, "Contributions to the steady state analysis of wind turbine driven self-excited induction generators," *IEEE Trans. on Energy Conversion*, vol. 1, no. 1, pp. 169-176, 1986.

[29] S. M. Alghuwainem, "Steady state analysis of an isolated self-excited induction generator driven by regulated and unregulated turbines," *IEEE Trans. on Energy Conversion,* vol. 14, no. 3, pp. 718-723, 1999.

[30] S. M. Alghuwainem, "Performance analysis of a PV powered DC motor driving a 3-phase self-excited induction generator," *IEEE Trans. on Energy Conversion,* vol. 11, no. 1, pp. 155-161, 1996.

[31] S. M. Alghuwainem, "Speed control of a PV powered DC motor driving a self-excited 3-phase induction generator for maximum utilization efficiency," *IEEE Trans. on Energy Conversion,* vol. 11, no. 4, pp. 768-773, 1996.

[32] T. F. Chan, "Steady-state analysis of self-excited induction generators," *IEEE Trans. on Energy Conversion,* vol. 9, no. 2, pp. 288-296, 1994.

[33] T. F. Chan, "Analysis of self-excited induction generators using an iterative method," *IEEE Trans. on Energy Conversion,* vol. 10, no. 3, pp. 502-507, 1995.

[34] T. F. Chan, "Self-excited induction generators driven by regulated and unregulated turbines," *IEEE Trans. on Energy Conversion*, vol. 11, no. 2, pp. 338-343, 1996.

[35] L. Wang and C. H. Lee, "A novel analysis on the performance of an isolated self-excited induction generator," *IEEE Trans. on Energy Conversion,* vol. 12, no. 2, pp. 109-117, 1997.

[36] K. S. Sandhu and S. K. Jain, "Operational aspects of self-excited induction generator using a new model," *Electrical Machines and Power Systems*, vol. 27, pp. 169-178, 1997.

[37] S. Rajakaruna and R. Bonert, "A technique for the steady state analysis of a self-excited induction generator with variable speed," *IEEE Trans. on Energy Conversion*, vol. 8, no. 4, pp. 757-761, 1993.

[38] S. S. Murthy and S. Acharya, "MATLAB based steady state analysis of self excited induction generator," in *Proc. 5$^{th}$ Int. Conf. Power Electronics and Drive Systems,* vol. 1, pp. 749-853, Nov. 17-20, 2003.

[39] A. L. Alolah and M. A. Alkanhal, "Optimization-based steady state analysis of three phase self-excited induction generator," *IEEE Trans. on Energy Conversion,* vol. 15, no. 1, pp. 61-65, 2000.

[40] Y. N. Anagreh and I. S. Al-Kofahi, "Genetic algorithm based performance analysis of self-excited induction generator," *International Journal of Modelling and Simulation*, vol. 26, no. 2, pp. 175-179, 2006.

[41] Bhim Singh, S. S. Murthy, Madhusudan, M. Goel and A. K. Tandon, "A steady state analysis on voltage and frequency control of self-excited induction generator in micro-hydro system," *Int. Conf. Power Electronics, Drives and Energy Systems,* New Delhi, India, pp. 1-6, Dec. 12-15, 2006.

[42] M. H. Haque, "A novel method of evaluating performance characteristics of a self-excited induction generator," *IEEE Trans. on Energy Conversion*, vol. 24, no. 2, pp. 358- 365, 2009.

[43] R. H. Park, "Two reaction theory of synchronous machines, Part-I: Generalised method of analysis," *AIEE Trans. on Electrical Engineering.,* vol. 48, pp. 716-727, 1929.

[44] P. C. Krause, *Analysis of electrical machinery*, McGraw-Hill Book Company, 1986.

[45] P. C. Krause and C. H. Thomas, "Simulation of symmetrical induction machinery," *IEEE Trans. on Power Apparatus and Systems,* vol. 84, no. 11, pp. 1038-1053, 1965.

[46] J. A. A. Melkebeek and D. W. Novotny, "Small signal dynamic analysis of regeneration and self-excitation in induction machines," *Electric Machines and Power Systems,* vol. 8, pp. 259-280, 1983.

[47] J. A. A. Melkebeek, "Magnetizing field saturation and dynamic behaviour of induction machines, Part-I : Improved calculation method for induction machine dynamics, Part-II : Stability limit of a voltage feed induction motor and self excited induction generator," *IEE Proc. Electr. Power Appl.*, vol. 130, no. 1, pp. 1-17, 1983.

[48] P. Vas, K. E. Hallenius and J. E. Brown, "Cross saturation in smooth air gap electrical machines," *IEEE Trans. on Energy Conversion,* vol. 1, no. 1, pp. 103-109, 1986.

[49] E. Levi and V. Vuckovid, "Magnetizing curve representation methods in digital simulation of induction machine dynamics," *International Journal Modelling and Simulation,* vol. 10, no. 2, pp. 52-56, 1990.

[50] E. Levi, "Application of the current space model in analysis of saturated induction machine," *Elect. Power Sys. Res*., vol. 31, pp. 203-216, 1994.

[51] J. Reynaud and P. Pillay, "Reclosing transients in induction machines including the effects of saturation of magnetizing branch and a practical case study," *IEEE Trans. on Energy Conversion,* vol. 9, no. 2, pp. 383-389, 1994.

[52] A. C. Smith, R. C. Healey and S. Williamson, "A transient induction motor model including saturation and deep bar effect," *IEEE Trans. on Energy Conversion,* vol. 11, no. 1, pp. 8-15, 1996.

[53] K. E. Hallenius, P. Vas and J. E. Brown, "The analysis of a saturated self-excited asynchronous generator," *IEEE Trans. on Energy Conversion,* vol. 6, no. 2, pp. 336-344, 1991.

[54] C. Grantham, D. Sutanto and B. Mismail, "Steady state and transient analysis of self-excited induction generators," *IEE Proc. Electr. Power Appl.,* vol. 136, no. 2, pp. 61-68, 1989.

[55] L. Wang and C. H. Lee, "A novel analysis of the performance of an isolated self excited induction generator," *IEEE Trans. on Energy Conversion,* vol. 12, no. 2, pp. 109-117, 1997.

[56] L. Wang and J. Y. Su, "Dynamic performances of an isolated self-excited induction generator under various loading conditions," *IEEE Trans. on Energy Conversion,* vol. 14, no. 1, pp. 93-100, 1999.

[57] D. Bispo, L. Martins, J. T. N. Resende and D. A. D. Andrade, "A new strategy for induction machine modeling taking into account the magnetic saturation," *IEEE Trans. on Industry Applications,* vol. 37, no. 6, pp. 1710-1719, 2001.

[58] R. Wamkeue and I. Kamwa, "Numerical modeling and simulation of saturated unbalanced electromechanical transients of self-excited induction generators," in

*Proc. Conf. Electrical and Computer Engg.,* Halifax, NS, Canada, vol. 2, pp. 1147–1151, March 7-10, 2000.

[59] S. S. Murthy and A. J. P. Pinto, "A generalized dynamic and steady state analysis of self excited induction generator (SEIG) based on MATLAB," in *Proc. 8th Int. Conf. Electrical Machines and Systems,* New Delhi, vol. 3, pp. 1933-38, Sept. 27-29, 2005.

[60] G. S. Kumar and A. Kishore, "A generalized dynamic modeling and analysis of self-excited induction generator using state-space approach with ANN-model of magnetizing inductance**,"** in *Proc. IEEE Int. Conf. Industrial Technology,* Mumbai, India, pp. 2698-2703, Dec. 15-17, 2006.

[61] A. Kishore and G. S. Kumar, "A generalized state-space modeling of three phase self-excited induction generator for dynamic characteristics and analysis,**"** in *Proc. 1st IEEE Int. Conf. Industrial Electronics and Applications,* Singapore, pp. 1-6, May 2006.

[62] M. M. Neam, F. F. M. El-Sousy, M. A. Ghazy and M. A. Abo-Adma, "The dynamic performance of an isolated self-excited induction generator driven by a variable-speed wind turbine," in *Proc. Int. Conf. Clean Electrical Power,* Capri, Italy, pp. 536 – 543, May 21-23, 2007.

[63] L. Shridhar, B. Singh, C. S. Jha and B. P. Singh, "Analysis of self-excited induction generator feeding induction motor," *IEEE Trans. on Energy Conversion,* vol. 9, no. 2, pp. 390-396, 1994.

[64] S. M. Alghuwainem, "Steady-state analysis of an isolated self-excited induction generator supplying an induction motor load," in Proc. *IEEE Int. Conf. Electric Machines and Drives,* Seattle, WA, USA, pp. 351-353, May 9-12, 1999.

[65] S. C. Kuo and L. Wang, "Steady-state performance and dynamic stability of a self-excited induction generator feeding an induction motor," in *Proc. IEEE PES Winter Meeting,* vol. 1, pp. 277-280, 2000.

[66] S. C. Kuo and L. Wang, "Dynamic eigen value analysis of a self-excited induction generator feeding an induction motor," in *Proc. IEEE Power Engineering Society Winter Meeting,* vol.3, pp. 1393 -1397, 2001

[67] S. C. Kuo and L. Wang, "Steady-state performance and dynamic stability of a self-excited induction generator feeding an induction motor**,"** in Proc. *IEEE Int. Conf. Power Engineering Society, Winter Meeting,* vol. 3, pp. 277-280, Jan.23-27, 2001.

[68] S. C. Kuo and L. Wang, "Analysis of isolated self-excited induction generator feeding a rectifier load," *IEE Proc. Gener., Transm. and Distrib.,* vol. 149, no.1, pp. 90-97, 2002.

[69] N. Kumaresan, "Analysis and control of three phase self-excited induction generators supplying single phase AC and DC loads," *IEE Proc.-Electr. Power Appl.*, vol. 152, no. 3, PP. 739-747, 2005.

[70] N. H. Malik and A. A. Mazi, "Capacitance requirements for isolated self-excited generators," *IEEE Trans. on Energy Conversion,* vol. 2, no. 1, pp. 62-69, 1987.

[71] T. F. Chan, "Capacitance requirements of self-excited induction generators," *IEEE Trans. on Energy Conversion,* vol. 8, no. 2, pp. 304-311, 1993.

[72] A. Al-Jabri and A. I. Alolah, "Limits on the performance of the three-phase self-excited induction generators," *IEEE Trans. on Energy Conversion,* vol. 5, no. 2, pp. 350-357, 1990.

[73] C. Chakraborty, S. N. Bhadra and A. K. Chattopadhyay, "Excitation requirements for stand-alone three-phase self-excited induction generator," *IEEE Trans. on Energy Conversion*, vol. 13, no. 4, pp. 358-365, 1998.

[74] R. J. Harrington and F. M. M. Bassiouny, "New approach to determine the critical capacitance for self-excited induction generators," *IEEE Trans. on Energy Conversion,* vol. 13, no. 3, pp. 244-249, 1998.

[75] L. Wang and J. Y. Su, "Determination of minimum and maximum capacitances of an isolated SEIG using eigen value sensitivity approach," in *Proc. Conf. Power*

*System Technology*, POWERCON '98, Beijing, China, vol. 1, pp. 610-614, Aug. 18-21, 1998.

[76] A. M. Eltamaly, "New formula to determine the minimum capacitance required for self-excited induction generator," in *Proc. 33rd IEEE Power Electronics Specialists Conf.*, vol. 1, pp. 106-110, June 23-27, 2002.

[77] D. Seyoum, C. Grantham, F. Rahman and M. Nagrial, "An insight into the dynamics of loaded and free running isolated self-excited induction generators," in *Proc. Int. Conf.* Power *Electronics, Machines and Drives*, pp. 580-585, June 4-7, 2002.

[78] D. Seyoum, C. Grantham and F. Rahman, **"**The dynamic characteristics of an isolated self-excited induction generator driven by a wind turbine," *IEEE Trans. on Industry Applications,* vol. 39, no. 4, pp. 936-944, 2003.

[79] A. H. Al-Bahrani and N. H. Malik, "Voltage control of parallel operated self excited induction generators," *IEEE Trans. on Energy Conversion,* vol. 8, no. 2, pp. 236-242, 1993.

[80] L. B. Shilpakar, B. Singh and K. S. P. Rao, "Transient analysis of parallely operated self-excited induction generators," in *Proc. Int. Conf. Power Electronics, Drives and Energy Systems for Industrial Growth,* New Delhi, India, pp. 470-476, Jan. 8-11, 1996.

[81] C. H. Lee and L. Wang, "A novel analysis of parallel operated self-excited induction generators," *IEEE Trans. on Energy Conversion,* vol. 13, no. 2, pp. 117-123, 1998.

[82] C. Chakraborty, S. N. Bhadra and A. K. Chattopadhyay, "Analysis of parallel-operated self excited induction generators," *IEEE Trans. on Energy Conversion,* vol. 14, no. 2, pp. 209-216, 1999.

[83] C. Chakraborty, M. Ishida, S. N. Bhadra and A. K. Chattopadhyay, "Performance of parallel-operated self-excited induction generators with the variation of machine parameters," in *Proc. IEEE Power Electronics and Drive Systems*, vol. 1, pp. 86-91, 1999.

[84] L. Wang and C. H. Lee, "Dynamic analyses of parallel operated self-excited induction generators feeding an induction motor load," *IEEE Trans. on Energy Conversion,* vol. 14, no. 3, pp. 479-485, 1999.

[85] B. Palle, M. G. Simoes and F. A. Farret, "Dynamic simulation and analysis of parallel self-excited induction generators for islanded wind farm systems," *IEEE Trans. on Industry Applications,* vol. 41, no. 4, pp. 1099-1106, 2005.

[86] F.A. Farret, B. Palle and M.G. Simoes, "State space modeling of parallel self-excited induction generators for wind farm simulation," in *Proc. 39th IAS Annual Meeting, Industry Applications,* vol. 4, pp. 2801-2807, Oct. 3-7, 2004.

[87] O. J. M. Smith, "Three-phase induction generator for single-phase line," *IEEE Trans. on Energy Conversion,* vol. 2, no. 3, pp. 382-387, 1987.

[88] M. O. Durham and R. Ramakumar, "Power system balancers for an Induction generator," *IEEE Trans. on Industry Applications,* vol. 23, no. 6, pp. 1067-1072, 1987.

[89] J. L. Bhattacharya and J. L. Woodward, "Excitation balancing of self-excited induction generator for maximum power output," *IEE Proc. Gener., Transm. and Distrib.,* vol. 135, no. 2, pp. 88-97, 1988.

[90] A. H. Al-Bahrani and N. H. Malik, "Steady state analysis and performance characteristics of a three-phase induction generator self excited with a single capacitor," *IEEE Trans. on Energy Conversion,* vol. 5, no. 4, pp. 725-732, 1990.

[91] Y. H. A. Rahim, "Excitation of isolated three-phase induction generator by a single capacitor," *IEE Proc. Electr. Power Appl.*, vol. 140, no. 1, pp. 44-50, 1993.

[92] T. F. Chan, "Performance analysis of a three-phase induction generator self-excited with a single capacitance," *IEEE Trans. on Energy Conversion,* vol. 14, no. 4 pp. 894-900, 1999.

[93] L. Wang and R. Y. Deng, "Transient performance of an isolated induction generator under unbalanced excitation capacitors," *IEEE Trans. on Energy Conversion,* vol. 14, no. 4, pp. 887-893, 1999.

[94] L. Wang and C. M. Cheng, "Excitation capacitance required for an isolated three-phase induction generator supplying a single-phase load," in *Proc. IEEE Power Engineering Society, Winter Meeting,* vol. 1, pp. 299 -303, 2000.

[95] T. F. Chan and L. L. Lai, "Phase balancing for a self-excited induction generator," in *Proc. Int. Conf. Electric Utility Deregulation and Restructuring and Power Technologies*, London, UK, pp. 602-607, April. 4-7, 2000.

[96] T. F. Chan and L. L. Lai, "Steady-state analysis and performance of a stand-alone three-phase induction generator with asymmetrically connected load impedances and excitation capacitances," *IEEE Trans. on Energy Conversion,* vol. 16, no. 4, pp. 327 -333, 2001.

[97] Sanjay. K. Jain, J. D. Sharma and S. P. Singh, "Transient performance of three-phase self-excited induction generator during balanced and unbalanced faults," *IEE Proc. Gener., Transm. and Distrib.*, vol. 149, no.1, pp. 50-57, 2002.

[98] A. I. Alolah and M. A. Alkanhal, "Excitation requirements of three phase self-excited induction generator under single phase loading with minimum unbalance," in *Proc. IEEE Int. Conf. Power Engineering Society Winter Meeting*, vol. 1, pp. 257-259, Jan. 23-27, 2000.

[99] Y. J. Wang and Y. S. Huang, "Analysis of a stand-alone three-phase self-excited induction generator with unbalanced loads using a two-port network model," *IET Electr. Power Appl.*, vol. 3, no. 5, pp. 445-452, 2009.

[100] S. S. Murthy, "A novel self-induced self-regulated single phase induction generator. I. Basic system and theory," *IEEE Trans. on Energy Conversion,* vol. 8, no. 3, pp. 377-382, 1993.

[101] L. Shridhar, Bhim Singh and C. S. Jha, "Options for single-phase power generation in isolated applications using cage generators," *Institute of Engineers. (India), Electrical,* 1996.

[102] Y. N. Anagreh, "A new approach for steady-state analysis of single-phase self-excited induction generator," in *Proc. 8$^{th}$ Int. Conf. Power Engineering*, vol. 2, pp. 509-512, Sept. 6-8, 2004.

[103] T. Ahmed, K. Nishida and M. Nakaoka, "Static VAr compensator-based voltage regulation implementation of single-phase self-excited induction generator," in *Proc. 39th IAS Annual Meeting, Industry Applications,* vol. 3, pp. 2069-2076, Oct. 3-7, 2004.

[104] O. Ojo and I. Bhat, "An analysis of single-phase self-excited induction generators: model development and steady-state calculations," *IEEE Trans. on Energy Conversion,* vol. 10, no. 2, pp. 254-260, 1995.

[105] O. Ojo, "The transient and qualitative performance of a self-excited single-phase induction generator," *IEEE Trans. on Energy* Conversion. vol. 10, no. 3, pp. 493-501, 1995.

[106] O. Ojo, "Performance of self-excited single-phase induction generators with shunt, short-shunt and long-shunt excitation connections," *IEEE Trans. on Energy Conversion,* vol. 11, no. 3, pp. 477-482, 1996.

[107] T. F. Chan and L. L. Lai, "A novel single-phase self-regulated self-excited induction generator using a three-phase machine," *IEEE Trans. on Power Engineering Review,* vol. 21, no. 5, pp. 62-62, 2001.

[108] T. Ahmed, K. Ogura, K. Soshin, E. Hiraki and M. Nakaoka, "Small-scale wind turbine coupled single-phase self-excited induction generator with SVC for isolated renewable energy utilization," in *Proc. 5th Int. Conf. Power Electronics and Drive Systems,* vol. 1, pp. 781-786, Nov. 17-20, 2003.

[109] C. J. Kim, K. Y. Lee, Y. T. Kim and H. K. Shin, "Design and performance analysis of single-phase self-excited induction generators," in *Proc.* 8th *Int. Conf. Electrical Machines and Systems, vol. 2,* pp. 974-977, Sept. 27-29, 2005.

[110] D. K. Palwalia and S. P. Singh, "Design and implementation of induction generator controller for single phase self excited induction generator," in *Proc. 3rd IEEE Conf. Industrial Electronics and Applications,* Singapore, pp. 400-404, June 3-5, 2008.

[111] L. B. Shilpakar and Bhim Singh, "Dynamic behaviour of a three-phase induction generator for single-phase power generation," *Electric Power Syst. Res.*, vol. 48, pp. 37-44, 1998.

[112] T. F. Chan and L. L. Lai, "A novel excitation scheme for a stand-alone three-phase induction generator supplying single-phase loads," *IEEE Trans. on Energy Conversion,* vol. 19, no. 1, pp. 136-143, 2004.

[113] S. N. Mahato, M. P. Sharma and S. P. Singh, "Transient performance of a single-phase self regulated induction generator using a three-phase machine," *Electric Power Syst. Res*., vol. 77, no. 7, pp. 839–850, 2007.

[114] S. N. Mahato, M. P. Sharma and S. P. Singh, "Transient Analysis of a Single-Phase Self-Excited Induction Generator using a Three-Phase Machine feeding Dynamic Load," in Proc. *Int. Conf. Power Electronics, Drives and Energy Systems,* New Delhi*,* India, pp. 1-6, Dec. 12-15, 2006.

[115] S. N. Mahato, S. P. Singh and M. P. Sharma, "Capacitors required for maximum power of a self-excited single-phase induction generator using a three-phase machine," *IEEE Trans. on Energy Conversion,* vol. 23, no. 2, pp. 372-381, 2008.

[116] T. Fukami, M. Imamura, Y. Kaburaki and T. Miyamoto, "A new self-regulated self-excited single-phase induction generator using a squirrel cage three-phase induction machine," in *Proc. Int. Conf. Energy Management and Power Delivery,* vol. 1, pp. 308-312, Nov. 21-23, 1995.

[117] Bhim Singh, S. P. Singh and M. P. Jain, "Design optimization of capacitor self-excited induction generator," *Elect. Power Sys. Res*., vol. 22, pp. 71-76, 1991.

[118] L. Shridhar, Bhim Singh and C. S. Jha, "A step towards improvements in the characteristics of self excited induction generator," *IEEE Trans. on Energy Conversion,* vol. 8, no. 1, pp. 40-46, 1993.

[119] J. Faiz, A. A. Dadgari, S. Horning and A. Keyhani, "Design of a three-phase self-excited induction generator," *IEEE Trans. on Energy Conversion,* vol. 10, no. 3, pp. 516-523, 1995.

[120] B. Sawetsakulanond and V. Kinnares, "Investigation of skew effect on the performance of self-excited induction generators," in *Proc. 7th Int. Conf. Power Electronics and Drive Systems,* Bangkok, Thailand, pp. 1167-1173, Nov. 27-30, 2007.

[121] B. Sawetsakulanond and V. Kinnaraes, **"**Analysis and comparative study on the performance between standard and high efficiency induction machines operating as self-excited induction generators," in *Proc*. 7th Int. Conf. Power Electronics and Drive Systems, Bangkok, Thailand, pp. 1313-1318, Nov. 27-30, 2007.

[122] E. Bim, J. Szajner and Y. Burian, "Voltage compensation of an induction generator with long shunt connection," *IEEE Trans. on Energy Conversion,* vol. 4, no. 3, pp. 526-530, 1989.

[123] L. Shridhar, Bhim Singh and C. S. Jha, "Transient performance of the self regulated short shunt self-excited induction generator," *IEEE Trans. on Energy Conversion,* vol. 10, no. 2, pp. 261-267, 1995.

[124] L. Shridhar, B. Singh, C. S. Jha, B. P. Singh and S. S. Murthy, "Selection of capacitors for the self regulated short shunt self-excited induction generator," *IEEE Trans. on Energy Conversion*, vol. 1, no. 1, pp.10-17, 1995.

[125] F. Tadashi, K. Yuichi, K. Satoru and M. Toshio, "Performance analysis of a self regulated self-excited induction generator using a three-phase machine," *IEEE Trans. on Energy Conversion,* vol. 14, no. 3, pp. 622-627, 1999.

[126] Bhim Singh, L. Shridhar and C. S. Jha*,* "Improvements in the performance of self-excited induction generator through series compensation," *IEE Proc. Gener., Transm. and Distrib.,* vol. 146, no. 6, pp. 602-608, 1999.

[127] L. Wang and J. Y. Su, "Effect of long shunt and short shunt connections on voltage variations of a self-excited induction generator," *IEEE Trans. on Energy Conversion,* vol. 12, no. 4, pp. 368-374, 1997.

[128] L. Wang and C. H. Lee, "Long-shunt and short-shunt connections on dynamic performance of a SEIG feeding an induction motor load," *IEEE Trans. on Energy Conversion,* vol. 15, no. 1, pp. 1-7, 2000.

[129] S. P. Singh, Sanjay. K. Jain and J. Sharma, "Voltage regulation optimization of compensated self-excited induction generator with dynamic load," *IEEE Trans. on Energy Conversion,* vol. 19, no. 4, 724–732, 2004.

[130] M. H. Haque, "Selection of capacitors to regulate voltage of a short-shunt induction generator," *IET Gener., Transm. and Distrib.*, vol. 3, no. 3, pp. 257-265, 2009.

[131] T. J. E. Miller, *Reactive power control in electric systems*, John Wiley and Sons, Toronto, 1982.

[132] S. S. Murthy, O. P. Malik and P. Walsh, "Capacitive requirements of self-excited induction generator to achieve desired voltage regulation," in *Proc. IEEE Conf. Industrial and Commercial Power Systems,* Milwaukee, 1983.

[133] J. M. Elder, J. T. Boys and J. L. Woodward, "Self-excited induction generator as a small low cost generator," *IEE Proc. Gener., Transm. and Distrib.,* vol. 131, no. 2, pp. 33-40, 1984.

[134] S. M. Alghuwainem, "Steady state analysis of an induction generator self-excited by a capacitor in parallel with a saturable reactor," *Electric Machines and Power Systems,* vol. 26, pp. 617-625, 1998.

[135] S. M. Alghuwainem, "Steady-state analysis of a self-excited induction generator including transformer saturation," *IEEE Trans. on Energy Conversion,* vol. 14, no. 3, pp. 667–672, 1999.

[136] R. K. Mishra, B. Singh and M. K. Vasantha, "Voltage regulator for isolated self-excited cage induction generators," *Elect. Power Sys. Res.,* vol. 24, pp. 75-83, 1992.

[137] H. C. Rai, A. K. Tandon, S. S. Murthy, B. Singh and B. P. Singh, "Voltage regulation of self excited induction generator using passive elements," in *Proc. Int. Conf. Elect. Machines and Drives, Rec.* no. 376, pp. 240 -245, 8-10 Sep. 1993.

[138] M. A. Al-Saffar, N. Eui-Cheol and T. A. Lipo*,* "Controlled shunt capacitor self-excited induction generator," in *Proc. 33rd IAS Annual Meeting Industry*

*Applications Conference,* vol. 2, pp. 1486 -1490, St. Louise, USA, 12-15 Oct, 1998.

[139] E. C. Quispe, R. D. Arias and J. E. Quintero, "A new voltage regulator for self-excited induction generator-design, simulation, and experimental results," in *Proc. IEEE Int. Conf. Electric Machines and Drives Con. Record,* Milwaukee, USA, pp. TB3/7.1 -TB3/7.3, 18-21 May, 1997.

[140] O. Chtchetinine, "Voltage stabilization system for induction generator in stand alone mode," *IEEE Trans. on Energy Conversion,* vol. 14, no. 3, pp. 298-303, 1999.

[141] J. K. Chatterjee, P. K. S. Khan, A. Anand and A. Jindal, "Performance evaluation of an electronic lead-lag VAr compensator and its application in brushless generation," in *Proc. Int. Conf. Power Electronics and Drive Systems, vol. 1,* pp. 59-64, 26-29 May, 1997.

[142] P. K. S. Khan and J. K. Chatterjee, "Modelling and control design for self-excited induction generator with solid-state lead-lag VAR compensator in micro-hydro energy conversion scheme," in *Proc. IEEE Int. Conf. Global Connectivity in Energy, Computer, Communication and Control, TENCON '98,* vol. 2, pp. 398-401, New Delhi, 1998.

[143] P. K. S. Khan, J. K. Chatterjee, M. A. Salam and H. Ahmad, "Transient performance of unregulated prime mover driven stand alone self-excited induction generator with solid-state lead-lag VAr compensator," in Proc. *Conf. TENCON 2000*, Kuala Lumpur, Malaysia, vol. 1, pp. 235-239, Sept. 24-27, 2000.

[144] P. K. S. Khan, J. K. Chatterjee and G. Ramasamy, "Inductively loaded current controlled solid-state lead-lag VAr compensator: special feature and performance," in Proc. *Int. Conf. Power Electronics and Drives Systems,* vol. 2*,* pp. 1333-1338, Nov. 28-01, 2005.

[145] O. P. Malik, D. Divan, S. S. Murthy, T. Grant and P. Walsh, "A solid state voltage regulator for self-excited induction generators," in *Proc. IEEE Conf. Industrial and Commercial Power System,* Milwaukee, 1983.

[146] D. K. Jain, A. P. Mittal and B. Singh, "Advanced controlled series compensated self-excited induction generator," in *Proc. Int. Conf. Power Electronics, Drives and Energy Systems for Industrial Growth,* vol. 2, pp. 707 -712, New Delhi, 8-11 Jan 1996.

[147] T. Ahmed, O. Noro, E. Hiraki and M. Nakaoka**, "**Terminal voltage regulation characteristics by static var compensator for a three-phase self-excited induction generator," *IEEE Trans. on Industry Appications.,* vol. 40, no. 4, pp. 978-988, 2004.

[148] T. Ahmed, O. Noro, K. Matsuo, Y. Shindo and M. Nakaoka, **"**Wind turbine coupled three-phase self-excited induction generator voltage regulation scheme with static VAR compensator controlled by PI controller," in *Proc. 6th Int. Conf. Electrical Machines and Systems,* vol. 1, pp. 293-296, Nov. 9-11, 2003.

[149] F. D. Wijaya, T. Isobe, K. Usuki, J. A. Wiik and R. Shimada, "A new automatic voltage regulator of self-excited induction generator using SVC magnetic energy recovery switch (MERS)," in *Proc. IEEE Int. Conf. Power Electronics Specialists Conference,* Rhodes, pp. 697-703, June 15-19, 2008.

[150] J. M. Elder, J. T. Boys and J. L. Woodward, "Integral cycle control of stand alone generators," *IEE Proc. Gener., Transm. and Distrib.*, vol. 132, no. 2, pp. 57–66, 1985.

[151] S. S. Murthy, A. J. P. Pinto and A. R. Beig, "Novel integral cycle voltage controller for self excited induction generators," in *Proc. Int. Conf. Power Electronics, Drives and Energy Systems,* New Delhi, India, pp. 1-4, Dec. 12-15, 2006.

[152] S. S. Murthy and A. J. P. Pinto, "Theory, simulation and experimental verification of a new integral cycle robust control strategy for self excited induction generators," in Proc. *7th Int. Conf. Power Electronics and Drive Systems,* pp. 924-929, Nov. 27-30, 2007.

[153] D. H. Lee, T. H. Kim and J. W. Ahn, "Control of digital AVR in stand alone generator for improved dynamic characteristics," in Proc. *IEEE Conf. Power Electronics Specialists,* pp. 1978-1982, June 15-19, 2008.

[154] Bhim Singh and L. B. Shilpakar, "Analysis of a novel solid state voltage regulator for a self-excited induction generator," *IEE Proc. Gener., Transm. and Distrib,* vol. 145, no. 6, pp. 647-655, 1998.

[155] S. C. Kuo and L. Wang, "Analysis of voltage control for a self-excited induction generator using a current-controlled voltage source inverter (CC-VSI)," *IEE Proc. Gener., Transm. and Distrib,* vol. 148, no. 5, pp. 431-438, 2001.

[156] Bhim Singh, S. S. Murthy and S. Gupta, "Analysis and design of STATCOM-based voltage regulator for self-excited induction generators," *IEEE Trans. on Energy Conversion,* vol. 19, no. 4, pp. 783–790, 2004.

[157] Bhim Singh, S. S. Murthy and S. Gupta, **"**Modelling and analysis of STATCOM based voltage regulator for self-excited induction generator with unbalanced loads," in *Proc. Conf. on Convergent Technologies for Asia-Pacific Region,* vol. 3, pp. 1109-1114, Oct. 15-17, 2003.

[158] Bhim Singh, S. S. Murthy and S. Gupta, "STATCOM-based voltage regulator for self-excited induction generator feeding nonlinear loads," *IEEE Trans. on Industry Applications,* vol. 53, no. 5, pp. 1437-1452, 2006.

[159] Bhim Singh, S. S. Murthy and S. Gupta, **"**Modelling of STATCOM based voltage regulator for self-excited induction generator with dynamic loads," in *Proc. Int. Conf. Power Electronics, Drives and Energy Systems,* New Delhi, India, pp. 1-6, Dec. 12-15, 2006.

[160] Bhim Singh, Madhusudan, V. Verma and A. K. Tandon, "Rating reduction of static compensator for voltage control of three-phase self-excited induction generator," in Proc. *IEEE Int. Symp. Industrial Electronics*, Montreal, Que., vol. 2, pp. 1194-1199, July 2006.

[161] H. R. Karshenas and A. Abdolahi, "Analysis of a voltage regulator for self-excited induction generator employing current-type static compensator," in *Proc. Canadian Conf. Electr. and Comp. Engineering,* vol. 2, pp.1053 -1058, 2001.

[162] S. Wekhande and V. Agarwal, "Wind driven self-excited induction generator with simple de-coupled excitation control," in *Proc. 34th IAS Annual Meeting, Industry Applications,* Phoenix, AZ, USA, vol. 3, pp. 2077-2083, Oct. 3-7, 1999.

[163] S. Wekhande and V. Agarwal, "A simple wind driven self-excited induction generator with regulated output voltage," in *Proc. 21st Int. Conf. Telecommunications Energy*, Copenhagen, Denmark, pp. 396-403, June 6-9, 1999.

[164] S. Wekhande and V. Agarwal, "A new variable speed constant voltage controller for self-excited induction generator," *Elect. Power Sys. Res*., vol. 59, pp. 157-164, 2001.

[165] G. V. Jayaramaiah and B. G. Fernandas, **"**Analysis of voltage regulator for a three-phase self-excited induction generator using current controlled voltage source inverter," in *Proc. 4th Int. Conf. Power Electronics and Motion Control,* vol. 3, pp. 1404-1408, Aug. 14-16, 2004.

[166] Bhim Singh and G. K. Kasal, "Neural network-based voltage regulator for an isolated asynchronous generator supplying three-phase four-wire loads," *Electric Power Systems Research*, vol. 78, pp. 985-994, 2008.

[167] S. S. Murthy, B. Singh, A. Kulkarni, R. Sivarajan and S. Gupta, "Field experience on a novel picohydel system using self excited induction generator and electronic load controller," in Proc. *5th Int. Conf. Power Electronics and Drive Systems,* vol. 2, pp. 842-847, Nov. 17-20, 2003.

[168] Bhim Singh, S. S. Murthy and S. Gupta, "An improved electronic load controller for self-excited induction generator in micro-hydel applications," in *Proc. 29th IEEE Int. Conf. Industrial Electronics Society, IECON-2003*, vol. 3, pp. 2741-2746, Nov. 2-6, 2003.

[169] Bhim Singh, S. S. Murthy and S. Gupta, "Transient analysis of self-excited induction generator with electronic load controller (ELC) supplying static and dynamic loads" *IEEE Trans. on Industry Applications,* vol. 41, no. 5, pp. 1194-1204, 2005.

[170] S. S. Murthy, M. S. L. Ramrathnam, K. Gayathri and U. N. Siva, "A novel digital control technique of electronic load controller for SEIG based micro hydel power generation," in *Proc. Int. Conf. Power Electronics, Drives and Energy Systems for Industrial Growth,* New Delhi, India, pp. 1-5, Dec. 12-5, 2006.

[171] S. S. Murthy, R. Jose and B. Singh, "A practical load controller for stand alone small hydro systems using self excited induction generator," in *Proc. Int. Conf. Power Electronics, Drives and Energy Systems,* vol. 1, pp. 359-364, Dec. 1-3, 2006.

[172] Bhim Singh, S. S. Murthy and S. Gupta, "Analysis and design of electronic load controller for self-excited induction Generators," *IEEE Trans. on Energy Conversion,* vol. 21, no. 1, pp. 285-293, 2006.

[173] Bhim Singh, S. S. Murthy and S. Gupta, "An electronic voltage and frequency controller for single-phase self-excited induction generators for pico hydro applications," in Proc. *Int. Conf. Power Electronics and Drives Systems,* vol. 1, pp. 240-245, Jan. 16-18, 2006.

[174] J. M. Ramirez and M. E. Torres., "An electronic load controller for the self-excited induction generator," *IEEE Trans. on Energy Conversion,* vol. 22, no. 2, pp. 546-548, 2007.

[175] D. W. Novotny, D. J. Gritter and G. H. Studtmann, "Self-excitation in inverter driven induction machines," *IEEE Trans. on Power Apparatus and Systems,* vol. 96, no. 4, pp. 1117-1125, 1977.

[176] R. M. Hilloowala and A. M. Sharaf, "A rule-based fuzzy logic controller for a PWM inverter in a stand alone wind energy conversion scheme," *IEEE Trans. on Industry Applications,* vol. 32, no. 1, pp. 57-65, 1996.

[177] E. G. Marra and J. A. Pomilio, "Self-excited induction generator controlled by a VS-PWM bidirectional converter for rural applications," *IEEE Trans. on Industry Applications,* vol. 35, no. 4, pp. 877-883, 1999.

[178] E. Suarez and G. Bortolotto, "Voltage and frequency control of self-excited induction generator," *IEEE Trans. on Energy Conversion*, vol. 14, no. 3, pp. 394-401, 1999.

[179] V. M. Pereira, J. A. Pomilio and P. A. V. Ferreira, "Induction generator driven by internal combustion engine with voltage and frequency regulation," in *Proc. IEEE Conf. Industrial Electronics*, vol. 3, pp. 834-839, May 26-29, 2002.

[180] W. L. Chen, Y. H. Lin, H. S. Gau and C. H. Yu, "STATCOM controls for a self-excited induction generator feeding random loads," *IEEE Trans. on Power Delivery,* vol. 23, no. 4, pp. 2207-2215, 2004.

[181] D. Joshi, K. S. Sandhu and M. K. Soni, "Constant voltage constant frequency operation for a self-excited induction generator," *IEEE Trans. on Energy Conversion,* vol. 21, no.1, pp. 228-234, 2006.

[182] B. Singh and G. K. Kasal, "Voltage and frequency controller for isolated asynchronous generators feeding three-phase four-wire loads," in *Proc. IEEE Int. Conf. Industrial Technology,* pp. 2773-2778, Dec. 15-17, 2006.

[183] B. V. Perumal and J. K. Chatterjee, "Analysis of a self excited induction generator with STATCOM/battery energy storage system," in *Proc. IEEE Conf. Power India*, pp. 1-6, April 10-12, 2006.

[184] J. K. Chatterjee, B. V. Perumal and N. R. Gopu, "Analysis of operation of a self-excited induction generator with generalized impedance controller," *IEEE Trans. on Energy Conversion,* vol. 22, no. 2, pp. 307-315, 2006.

[185] B. V. Perumal and J. K. Chatterjee, "SVPWM implementation in dSPACE for generalized impedance controller used for self-excited induction generation system," in Proc. *Conf. Power Electronics, Drives and Energy Systems,* New Delhi, India, pp. 1-6, Dec. 12-15, 2006.

[186] B. V. Perumal and J. K. Chatterjee, "Voltage and frequency control of a stand alone brushless wind electric generation using generalized impedance controller," *IEEE Trans. on Energy Conversion,* vol. 23, no. 2, pp. 632-641, 2008.

[187] J. K. Chatterjee, A. Bansal and D. Sarkar, "Performance evaluation of synchronous impedance controller based self excited induction generator system," in *Proc. IEEE Conf. Power India*, pp. 1-6, April 10-12, 2006.

[188] L. A. C. Lopes and R.G. Almeida, "Wind-driven self-excited induction generator with voltage and frequency regulated by a reduced-rating voltage source inverter," *IEEE Trans. on Energy Conversion,* vol. 21, no. 2, pp. 297-304, 2006.

[189] K. H. Youssef, M. A. Wahba, H. A. Yousef and O. A. Sebakhy, "A new method for voltage and frequency control of stand-alone self-excited induction generator using PWM converter with variable DC link voltage," in *Proc. American Control Conference,* Seattle, WA, USA, pp. 2486-2491, June 11-13, 2008.

[190] S. G. Kumar, S. A. Rahman and G. Uma, "Operation of self-excited induction generator through Matrix Converter," in *Proc. 23rd IEEE Conf. Power Electronics Conference and Exposition,* Austin, TX, USA, pp. 999-1002, Feb. 24-28, 2008.

[191] G. K. Kasal and B. Singh, "Decoupled voltage and frequency controller for isolated asynchronous generators feeding three-phase four-wire loads," *IEEE Trans. on Power Delivery,* vol. 23 no. 2, pp. 966-973, 2008.

[192] J. A. Barrado, R. Grino and H. Valderrama, "Standalone self-excited induction generator with a three-phase, four-wire active filter and energy storage system', in *Proc. IEEE Int. Symp. on Industrial Electronics*, Vigo, Spain, pp.697-703, 2008.

[193] D. B. Watson, J. Arrillaga and T. Dansem, "Controlled DC power supply from wind driven self-excited induction machines," *IEE Proc.* vol. 126, no. 12, pp. 1245-1248, 1979.

[194] E. H. Watanabe and A. N. Barreto, "Self-excited induction generator/forced commutated rectifier system operating as a DC power supply," *IEE Proc.-B*, vol. 134, no. 5, pp. 154-159, 1990.

[195] E. H. Watanabe and A. N. Barreto, "Self-excited induction generator/forced-commutated rectifier system operating as a DC power supply," *IEE Proc.-B*, vol. 134, no. 5, pp. 255-260, 1987.

[196] C. Chakraborty, S. N. Bhadra and A. K. Chattopadhyay, "Controllable DC power from self-excited induction generator through series connected single phase force-commutated rectifiers," in *Proc. IEEE Conf. Industry Applications Society Annual Meeting*, Dearborn, MI, USA, pp. 1624-1629, Sept. 28-Oct. 4, 1991.

[197] S. P. Singh, M. P. Jain and Bhim Singh, "Steady state analysis of a self-excited induction generator with an AC-DC conversion scheme for small scale generation," *Elect. Power Sys. Res*., vol. 20, pp. 95-104, 1991.

[198] T. L. Maguire and A. M. Gole, "Apparatus for supplying an isolated DC load from a variable-speed self-excited induction generator," *IEEE Trans. on Energy Conversion,* vol. 8, no. 3, pp. 468-475, 1993.

[199] J. C. Wu, "AC /DC power conversion interface for self-excited induction generator," *IET Renew. Power Gener.*, vol. 3, no. 2, pp. 144-151, 2009.

[200] K. Nishida, T. Ahmed and M. Nakaoka, "Induction generator hybrid applications with active power filter," *IEE Proc. Electr. Power Appl*, vol. 153, no. 2, pp.197-205, 2006.

[201] M. S. S. Miranda, R. O. C. Lyra and S. R. Siva, "An alternative isolated electric pumping system using induction machines', *IEEE Trans. on Energy Conversion*, vol. 14, no. 4, pp.1611-1616, 1999.

[202] S. S. Murthy, R. Jose and B. Singh, "Experience in the development of micro hydel grid independent power generation scheme using induction generators for Indian conditions," in *Proc. IEEE Int. Conf. Global Connectivity in Energy, Computer, Communication and Control, vol. 2,* pp. 461-465, Dec. 17-19, 1998.

[203] J. B. Ekanayake, "Induction generators for small hydro schemes," *Power Engineering Journal,* pp. 61-67, 2002.

[204] J. Faria, E. Margato and M.J. Resende, "Self-excited induction generator for micro-hydro plants using water current turbines Type," in *Proc. 27th Int. Conf. Telecommunications, INTELEC '05,* Berlin, Germany, pp. 107-112, 2005.

[205] G. K. Singh, K. B. Yadav and R. P. Saini, "Capacitive self-excitation in a six-phase induction generator for small hydro power: an experimental investigation," in Proc. *Int. Conf. Power Electronics, Drives and Energy Systems*, pp. 1-6, Dec. 12-15, 2006.

[206] G. Raina and O. P. Malik, "Wind energy conversion using a self-excited induction generator," *IEEE Trans. on Power Apparatus and Systems,* vol. 102, no. 12, pp. 3933-3936, 1983.

[207] N. Ammasaigounden and M. Subbiah, "Microprocessor-based voltage controller for wind-driven induction generators," *IEEE Trans. on Industrial Electronics,* vol. 37, no. 6, pp. 531-537, Dec. 1990.

[208] S. M. Alghuwainem, R. A. Hammouda and A. R. M. Al-Farhan, "Transient analysis of a wind-driven induction generator," in *Proc. Conf. Electrical and Computer Engg.,* Toronto, Ont., Canada, vol. 2, pp. 805-809, May 13-16, 2001.

[209] G. K. Singh, K.B. Yadav and R. P. Saini, "A self-excited six-phase induction generator for stand-alone renewable energy generation," in *Proc. Aegean Int. Conf. Electrical Machines and Power Electronics*, Bodrum, Turkey, pp. 690-695, Sept. 10-12, 2007.

[210] K. Hafiz, G. Nanda and N. C. Kar, "Skin effect modeling of self excited induction generator in wind power application," in *Proc. Conf. Electrical and Computer Engineering,* Niagara Falls, ON, Canada, pp. 1587 – 1590, May 4-7, 2008.

[211] M. A. Al-Geelani and S. P. Gupta, "Cyclo-converter excited squirrel cage machine as a wind power converter," *Electric Power Components and Systems*, vol. 30, no. 1, pp. 57-76, 2002.

[212] R. Datta and V. T. Ranganathan, "A method of tracking the peak power points for a variable speed wind energy conversion system," *IEEE Trans. on Energy Conversion*, vol. 18, no. 1, pp. 163-168, 2003.

[213] A. Kishore, R. C. Prasad and B.M. Karan, "Design of field oriented controller to improve dynamic characteristics of three phase self excited induction generator," in *Proc. 1st IEEE Int. Conf. Power Electronics, Drives and Energy Systems*, Singapore, pp. 1-6, May 2006.

[214] G. S. Kumar and A. Kishore, "Dynamic analysis and control of output voltage of a wind turbine driven isolated induction generator," in *Proc. IEEE Int. Conf. Industrial Technology*, Mumbai, India, pp. 494-499, Dec. 15-17, 2006.

[215] F. El-Sousy, M. Orabi and H. Godah, "Indirect field orientation control of self-excited induction generator for wind energy conversion system," in *Proc. IEEE Int. Conf . Industrial Technology,* vol. 1, pp. 480-485, Dec. 8-10, 2004.

[216] T. Satish, K. K. Mohapatra and N. Mohan, "Speed sensor-less direct power control of a matrix converter fed induction generator for variable speed wind turbines," in *proc. Int. IEEE Conf. Power Electronics, Drives and Energy Systems*, Dec. 12-15, 2006, New Delhi, pp. 1-6., 2006

[217] G. V. Jayaramaiah and B. G. Fernandes, "Analysis of voltage and frequency controller for grid connected 3-phase self-excited induction generator using current controlled voltage source inverter," in *Proc. IEEE Int. Conf . Industrial TENCON-2004, vol. 3,* pp. 468-471, Nov. 21-24, 2004.

[218] R. K. Varma and S. Auddy, "Mitigation of subsynchronous oscillations in a series compensated wind farm with static VAr compensator," in *Proc. IEEE Power Engineering Society General Meeting*, pp. 1-7, June 18-22, 2006.

[219] R. K. Varma, S. Auddy and Y. Semsedini, "Mitigation of subsynchronous resonance in a series-compensated wind farm using FACTS controllers," *IEEE Trans. on Power Delivery*, vol. 23, no. 3, pp. 1645-1654, 2008.

[220] J. A. Baroudi, V. Dinavahi and A. M. Knight, "A review of power converter topologies for wind generators," *Renewable Energy*, vol. 32, pp. 2369-85, 2007.

[221] E. L. Owen and G. R. Griffith, "Induction generator applications for petroleum and chemical plants," *IEEE Trans. on Industry Applications*, vol. 19, no. 6, pp. 1003-1013, 1983.

[222] W. D. Bolin, "Power cost reduction using small induction generators," *IEEE Trans. on Industry Applications*, vol. 20, no.5, pp. 1352-1354, 1984.

[223] R. L. Nailen, "Watts from waste heat-induction generators for the process industries," *IEEE Trans. on Industry Applications*, vol. 19, no. 3, pp. 470-475, 1983.

[224] J. R. Parsons, "Co-generation application of induction generator," *IEEE Trans on Industry Applications*, vol. 20, pp. 497-503, 1984.

[225] W. P. Smith, "Cogeneration: small turbine-generator case study," *IEEE Trans. on Industry Applications*, vol. 22, no. 1, pp. 121-125, 1986.

[226] R. Wamkeue, S. Moraogue and L. Kamwa, "Distribution network fed in co-generation by induction generators: incidence of self-excitation phenomenon," in *Proc. IEEE Int. Conf. Electric Machines and Drives*, Cambridge, MI, UK, pp. 594-603, 2001.

[227] A. Bellini, G. Franceschini, E. Lorenzani, C. Tassoni and M. Tomaiuolo, "Field oriented control of self-excited induction generator for distributed cogeneration plants," in *Proc. 41$^{th}$ IAS Annual Meeting, Industry Applications,* Tampa, FL, USA, vol. 4 pp. 1738-1744, Oct. 8-12, 2006.

[228] M. Naidu and J. Walters, "A 4-kW 42-V induction-machine-based automotive power generation system with a diode bridge rectifier and a PWM inverter," *IEEE Trans. on Industry Applications,* vol. 39, no. 5, pp. 1287-1293, 2003.

[229] E. Erdelyi, E. E. Kolatorowicz and W. R. Moller, "The limitations of induction generator in constant frequency aircraft system," *AIEE Trans. on Electrical Engineering*, vol. 77, pp. 384-351, 1958.

[230] M. Chiragwin and L. J. Stratton, "Variable speed constant frequency generator system for aircraft," *AIEE Trans. on Electrical Engineering*, pp. 304-310, 1959.

[231] N. Mohan, T. M. Undeland and W. P. Robbins, *Power electronics: Converters, Applications and Design*, John *Wiley and Sons, New York, Second Edition*, 1995.

[232] Y. H. Song and A. T. Johns, *Flexible AC transmission systems*, IEE London, 1999.

[233] N. G. Hingorani and L. Gyugyi, *Understanding FACTs: concepts and technology of flexible AC transmission systems*, New York, IEEE Power Engineering Society Inc., 2000.

[234] L. Gyugyi and E. R. Taylor, "Characteristics of static thyristor controlled shunt compensators for power transmission system applications," *IEEE Trans. on Power Apparatus and Systems*, vol. 99, no. 5, pp. 1795-1804, 1980.

[235] H. Akagi, Y. Kanazawa and A. Nabae, "Instantaneous reactive power compensators comprising switching devices without energy storage components," *IEEE Trans. on Industry Applications*, vol. 20, no. 3, pp. 625-630, 1984.

[236] L. H. Walker, "Forced commutated reactive power compensators," *IEEE Trans. on Industry Applications*, vol. 22, no. 6, pp. 1091-1104, 1986.

[237] L. T. Moran, P. D. Ziogaz and G. Joos, "Analysis and design of a three-phase synchronous solid-state VAR compensator," *IEEE Trans. on Industry Applications*, vol. 25, no. 4, pp. 598-608, 1989.

[238] G. D. Galanos, C. I. Hatziadoniu, X. J. Cheng and D. Maratukulam, "Advanced static compensator for flexible AC transmission," *IEEE Trans. on Power Systems*, vol. 8, no. 1, pp. 113-120, 1993.

[239] C. Schauder and H. Mehta, "Vector analysis and control of advanced static VAR compensator," *IEE Proc.- C*, vol. 140, no. 4, pp. 299-306, 1993.

[240] J. B. Ekanayaka, N. Jenkins and C. B. Cooper, "Experimental investigation of an advanced static VAR compensator," *IEE Proc. Gener., Transm. and Distrib.*, vol. 142, no. 2, pp. 202-210, 1995.

[241] J. W. Dixon, J. J. Garcia and L. Moran, "Control system for three-phase active power filter which simultaneously compensates power factor and unbalanced loads," *IEEE Trans. on Industrial Electronics*, vol. 42, no. 6, pp. 636-641, 1995.

[242] C. Schauder, M. Gernhardt, T. W. Cease and A. Edris, "Operation of ±100 MVAR STATCON," *IEEE Trans. on Power Delivery*, vol. 12, no. 4, pp. 1805-1811, 1997.

[243] J. B. Ekanayaka and N. Jenkins, "Selection of passive elements for a three-level inverter based static synchronous compensator," *IEEE Trans. on Power Delivery*, vol. 14, no. 2, pp. 655-661, 1999.

[244] A. Chandra, B. Singh, B. N. Singh and K. Al-Haddad, "An improved control algorithm of shunt active filter for voltage regulation, harmonic elimination, power factor correction, and balancing of nonlinear loads," *IEEE Trans. on Power Electronics*, vol. 15, no. 3, pp. 495-507, 2000.

[245] S. K. Jain, P. Agrawal and H. O. Gupta, "Fuzzy logic controlled shunt active power filter for power quality improvement," *IEE Proc.-Electr. Power. Appl*. vol. 149, no. 5, pp. 317-328, 2002.

[246] S. K. Jain, P. Agrawal and H. O. Gupta, "A control algorithm for compensation of customer-generated harmonics and reactive power," *IEEE Trans. on Power Delivery*, vol. 19, no. 1, pp. 357-366, 2004.

[247] A. Jain, K. Joshi, A. Behal and N. Mohan, "Voltage regulation with STATCOM: modeling, control and results," *IEEE Trans. on Power Delivery*, vol. 21, no. 2, pp. 726-735, 2006.

[248] Bhim Singh, V. Verma, A. Chandra and K. Al-Haddad, "Hybrid filters for power quality improvement," *IEE Proc.-Gener., Transm. and Distrib.*, vol. 152, no. 3, pp. 365-378, 2005.

[249] L. Gyugyi, C. D. Schauder and K. K. Sen, "Static synchronous series compensators. A solid-state approach to the series compensation of transmission lines," *IEEE Trans. on Power Delivery,* vol. 12, no. 1, pp. 406-417, 1997.

[250] L. Gyugyi, "Application characteristics of converter-based FACTS controllers," in *Proc. IEEE Int. Conf. Power System Technology, PowerCon 2000,* Perth, vol. 1, pp. 391-396, Dec. 4-7, 2000.

[251] K. K. Sen, "SSSC-static synchronous series compensator-Theory, modelling, and applications," *IEEE Trans. on Power Delivery,* vol. 13, no. 1, pp. 241-246, 1998.

[252] R. Mihalic, "Power flow control with controllable reactive series elements," *IEE Proc. Gener., Transm. and Distrib.,* vol. 145, no. 5, pp. 493-498, 1998.

[253] B. A. Renz, A. Keri, C. Schauder, E. Stacey and A. Edris, "AEP unified power flow controller performance," *IEEE Trans. on Power delivery,* vol. 14, no. 4, pp. 1347-1381, 1999.

[254] B. M. Han, J. K. Park, S. L. Moon and G. G. Karady, "Switching-level simulation model for SSSC with EMTP," in *Proc. IEEE Winter Meeting Power Engineering Society,* vol.2, pp. 1259-1263, Jan. 31-Feb.04, 1999.

[255] B. N. Singh, A. Chandra, K. Al-Haddad and B. Singh, "Performance of sliding mode and fuzzy controllers for a static synchronous series compensators," *IEE Proc. Gener., Transm. and Distrib.,* vol. 146, no. 2, pp. 200-206, 1999.

[256] I. Papic, "Mathematical analysis of FACTS devices based on a voltage source converter, Part-I. Mathematical model, Part-II Steady state operation characteristics," *Elect. Power Sys. Res., 56,* pp. 139-157, 2000.

[257] Y. Ye, M. Kazerani and V. Quintana, "Current-source converter based SSSC modelling and control," in *Proc. IEEE Power Engineering Society Summer Meeting,* pp. 949-954, July 15-19, 2001.

[258] V. K. Sood, "Static synchronous series compensator model in EMTP," in *Proc. IEEE Conf. Electrical and Computer Engineering,* pp. 207-211, 2002.

[259] F. W. Huang, B. S. Rigby and R. G. Harley, "A static synchronous series compensator model for EMTDC," in *Proc. 6th IEEE Africon Conf.,* Africa, vol. 2, pp.933-939, Oct. 2-4, 2002.

[260] U. Gabrijel and R. Mihalic, "Direct Method for transient stability assessment on power systems comprising controllable series devices," *IEEE Trans. on Power Systems,* vol. 17, no. 4, pp. 1116-1122, 2002.

[261] S. J. Lee, H. Kim, S. K. Sul and F. Blaabjerg, "A novel control algorithm for static series compensators by use of PQR instantaneous power theory," *IEEE Trans. on Power Electronics*, vol. 19, no. 3, pp. 814-827, 2004.

[262] C. J. Zhan, V. K. Ramachandramurthy, A. Arulampalam, C. Fitzer, S. Kromlidis, M. Barnes and N. Jenkins, "Dynamic voltage restorer based on voltage-space-vector PWM control," *IEEE Trans. on Industry Applications*, vol. 37, no. 6, pp. 1855-1863, 2001.

[263] C. J. Zhan, X. G. Wu, S. Kromlidis, V.K. Ramachandramurthy, M. Barnes, N. Jenkins and A.J. Rudell, "Two electrical models of the lead-acid battery used in a dynamic voltage restorer," *IEE Proc.-Gener., Transm., and Distrib*, vol. 150, no. 2, pp. 175-182, 2003.

[264] A. Ghosh, A. K. Jindal and A. Joshi, "Design of a capacitor-supported dynamic voltage Restorer (DVR) for unbalanced and distorted loads," *IEEE Trans. on Power Delivery*, vol. 19, no. 1, pp. 405-413, 2004.

[265] S. Sasitharan, M. K. Mishra, B. K. Kumar and V. Jayashankar, "Rating and design issues of DVR injection transformer," in *Proc. IEEE Conf.* TENCON 2008, pp. 449-455, 19-21 Nov. Chennai, India, 2008.

[266] M. Vilathgamuwa, A. A. D. Ranjith Perera and S. S. Choi, "Performance improvement of the dynamic voltage restorer with closed-loop load voltage and current-mode control," *IEEE Trans. on Power Electronics*, vol. 17, no. 5, pp. 824-834, 2002.

[267] C. N. Ho, H. S. H. Chung and K. T. K. Au, "Design and Implementation of a Fast Dynamic Control Scheme for Capacitor-Supported Dynamic Voltage Restorers," *IEEE Trans. on Power Electronics*, vol. 23, no. 1, pp. 237-251, 2008.

[268] P. Jayaprakash, Bhim Singh and D. P. Kothari, "Current mode control of dynamic voltage restorer for power quality improvement in distribution system," in *Proc. IEEE Int. Conf. on Power and Energy (PECon 08)*, Dec. 1-3, 2008, pp. 301-306, Johor Baharu, Malaysia, 2008.

[269] S. R. Naidu and D. A. Fernandes, "Dynamic voltage restorer based on a four-leg voltage source converter," *IET Gener., Transm., and Distrib*., vol. 3, no. 5, pp. 437-447, 2009.

[270] K. F. Man, K. S. Tang and S. Kwong, "Genetic algorithms: concepts and applications," *IEEE Trans. on Industrial Electronics*, vol. 43, no. 5, pp. 519-533, 1996,

[271] K. Dev, *Optimization for engineering design*: *algorithm and examples*, N. Delhi, India: Prentice Hall, 1995.

[272] S. S. Rao, *Engineering optimization, theory and practice*, New Delhi, India, New Age International (P) Limited, 1998.

[273] D. E. Goldberg, *Genetic algorithms in search, optimization, and machine learning*, N. Delhi, India: Pearson Education, 2001.

[274] A. A. Mahmoud, T. H. Ortmeyer, R. G. Harley and C. Calabrese, "Effects of reactive compensation on induction motor dynamic performance," *IEEE Trans. on Power App. Syst.*, vol. 99, pp. 841–846, 1980.

[275] S. E. M. DeOliveira, "Starting transients of saturated induction motors with series capacitors on the supply," *IEEE Trans. on Energy Conversion*, vol. 1, pp. 205–210, 1986.

[276] N. G. Hingorani, "A new scheme for subsynchronous resonance damping of torsional oscillations and transient torque - part I," *IEEE Trans. on Power Apparatus and Systems*, vol. 100, pp. 1852-1855, 1981.

[277] C. T. Chen, *Analog and digital control system design: transfer function state-space and algebraic method*s, New York, Saunders College Publishers.

[278] M. H. Rashid, *Power electronics: circuits, devices, and applications*, Second edition, New Delhi, Prentice Hall of India, 1996.

[279] M. G. Say, *Alternating current machines*, Fifth edition, London, Sir Isaac Pitman, 1983.

[280] A. E. Fitzgerald, C. Kingsley and S. D. Uman, *Electrical machinery*, Fifth edition, New York, McGraw Hill, 1991.

[281] A. S. Langsdorf, *Theory of alternating current machinery*, Second edition, New York: McGraw-Hill, 1995.

# APPENDIX-A

## PARAMETERS OF MACHINES

The squirrel cage induction machines of different ratings have been used for the investigations. The machine parameters have been obtained with the help of no load, blocked rotor and DC test on these machines [279-281]. The stator resistance is obtained by DC test. The rotor resistance is obtained using blocked rotor test. It is assumed that stator and rotor leakage reactance is equal. The magnetizing characteristic, which is relating air gap voltage with magnetizing reactance ($V_g$ v/s $X_M$) or magnetizing inductance with magnetizing current ($L_M$ v/s $I_M$) is obtained from the synchronous speed test. Let the voltage ($V$), current ($I$) and power ($P$) are the phase quantities during synchronous speed test.

From the measured parameters, the power factor ($\cos\theta$) is calculated as,

$$\cos\theta = \frac{P}{VI} \tag{A.1}$$

Airgap voltage ($V_g$) is computed as,

$$V_g = \text{Abs}\left(V\angle 0 - \left(R_s + jX_s\right)I\angle\theta\right) \tag{A.2}$$

Core loss $P_c$ is obtained as,

$$P_c = P - I^2 R_s \tag{A.3}$$

Core loss resistance $R_c$ is computed as,

$$R_c = \frac{V_g^2}{P_c} \tag{A.4}$$

Core loss current $I_c$ is calculated as,

$$I_c = \frac{V_g}{R_c} \tag{A.5}$$

Magnetizing current $I_M$ is achieved as,

$$I_M = \sqrt{I^2 - I_c^2} \tag{A.6}$$

Magnetizing reactance $X_M$ or inductance $L_M$ is obtained as,

$$X_M = \frac{V_g}{I_M};\ L_M = \frac{V_g}{2\pi f I_M} \tag{A.7}$$

The magnetizing characteristic ($L_M$ v/s $I_M$) is obtained by calculating $I_M$ and $L_M$ with the help of eqns. (A.6) and (A.7) from the test data and by applying polynomial curve fitting technique.

**Induction Machine-1**

*Specifications*: Δ-connected, 415 V, 5.5 kW, 10.1 A, 4-Pole, 50 Hz, 1450 rpm, $J$=0.10 kg-m$^2$

*Parameters*: $R_s$ = 0.0632 pu, $R_r$ = 0.0247 pu, $X_{ls}$ = 0.0633 pu, $X_{lr}$ = 0.0633 pu, $X_M^{uns}$ =3.48 pu, $Z_b$ = 71.168 Ω

*Magnetizing* characteristic: $L_M = -0.0003 i_M^3 + 0.0198 i_M^2 - 0.2472 i_M + 1.1816$

**Induction Machine-2**

*Specifications*: Δ-connected, 415 V, 3.7 kW, 7.6 A (line), 4 pole, 50 Hz, 1430 rpm, $J$ = 0.0842 kg-m$^2$

*Parameters*: $R_s$ = 0.0585 pu, $R_r$ = 0.06196 pu, $X_{ls}$ = 0.1015 pu, $X_{lr}$ = 0.1015pu, $X_M^{uns}$ = 2.858 pu, $Z_b$ = 94.57 Ω

*Magnetization characteristic*: $L_M = 0.0013 i_M^2 - 0.0364 i_M + 0.3555$

**Induction Machine-3**

*Specifications*: Δ-connected, 415 V, 2.2 kW, 4.8 A (line), 4 pole, 50 Hz, 1415 rpm, $J$ = 0.03 kg-m$^2$

*Parameters*: $R_{sm}$ = 0.115 pu, $R_{rm}$ = 0.072 pu, $X_{lsm}$ = 0.0941 pu, $X_{lrm}$ = 0.0941 pu, $X_{Mm}^{uns}$ =2.142 pu, $Z_b$ = 149.75 Ω

*Magnetizing characteristic*: $L_{Mm} = -0.0123 i_{Mm}^2 - 0.1174 i_{Mm} + 1.101$

**Induction Machine-4**

*Specifications*: Δ-connected, 415 V, 1.5 kW, 3.2 A (line), 4 pole, 50 Hz, 1430 rpm, $J$ = 0.0205 kg-m$^2$

*Parameters*: $R_{sm}$ = 0.0832 pu, $R_{rm}$ = 0.0853 pu, $X_{lsm}$ = 0.1101 pu, $X_{lrm}$ = 0.1101 pu, $X_{Mm}^{uns}$ = 1.83 pu, $Z_b$ = 149.75 Ω

*Magnetizing characteristic*: $L_{Mm} = K_{m1} i_{Mm}^4 + K_{m2} i_{Mm}^3 + K_{m3} i_{Mm}^2 + K_{m4} i_{Mm} + K_{m5}$

where, $K_{m1}$ = -0.0849, $K_{m2}$ = 0.4298, $K_{m3}$ = -0.9924, $K_{m4}$ = 0.6847, $K_{m5}$ =1.171

**DC Dynamic Motor Load**

*Specifications*: 220 V, 1.5 kW, 8.0 A, 1500 rpm,

*Parameters*: $R_a$ = 4.5 Ω, $L_a$ = 0.10 H, $J_d$ = 0.10 kg-m$^2$, sep. excited motor, $k_a$ = 1.27 V/(Rad/sec) at rated field current.

# APPENDIX-B

## INDUCTION MACHINE MODEL WITH MAIN AND CROSS FLUX SATURATION

The dynamic model of induction machine is developed in stationary reference frame while considering the effect of both main flux and cross flux saturation.

The generalized q axis and d axis equivalent circuit of induction machine [44] are shown in Fig. B.1 and Fig. B.2 respectively.

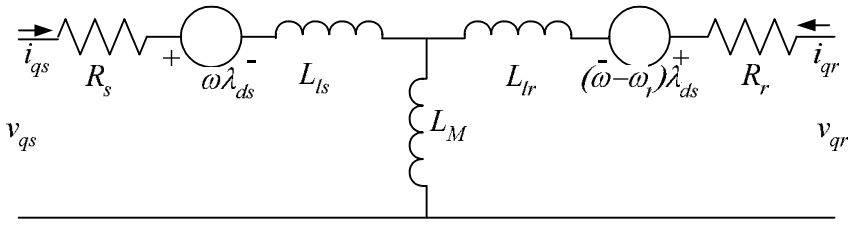


***Fig. B.1 q-axis equivalent circuit***

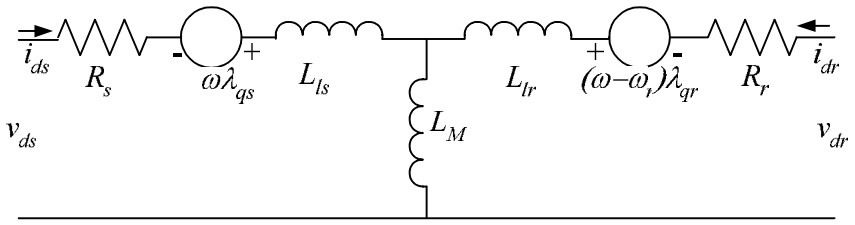


***Fig. B.2 d-axis equivalent circuit***

The stator and rotor voltage equations in arbitrary q-d reference frame are expressed as,

$$\mathbf{v}_{qd0s} = \mathbf{R}_s \mathbf{i}_{qd0s} + \omega \boldsymbol{\lambda}_{dqs} + p\boldsymbol{\lambda}_{qd0s} \tag{B.1}$$

$$\mathbf{v}_{qd0r} = \mathbf{R}_r \mathbf{i}_{qd0r} + (\omega - \omega_r)\boldsymbol{\lambda}_{dqr} + p\boldsymbol{\lambda}_{qd0r} \tag{B.2}$$

where,

$$\mathbf{v}_{qd0s} = \begin{bmatrix} v_{qs} & v_{ds} & v_{0s} \end{bmatrix}^T \qquad \mathbf{v}_{qd0r} = \begin{bmatrix} v_{qr} & v_{dr} & v_{0r} \end{bmatrix}^T$$

$$\mathbf{i}_{qd0s} = \begin{bmatrix} i_{qs} & i_{ds} & i_{0s} \end{bmatrix}^T \qquad \mathbf{i}_{qd0r} = \begin{bmatrix} i_{qr} & i_{dr} & i_{0r} \end{bmatrix}^T$$

$$\lambda_{dqs} = \begin{bmatrix} \lambda_{ds} & \lambda_{qs} & 0 \end{bmatrix}^T \qquad \lambda_{dqr} = \begin{bmatrix} \lambda_{dr} & \lambda_{qr} & 0 \end{bmatrix}^T$$

The flux linkages used in eqns (B.1) and (B.2) are expressed as,

$$\begin{aligned} \lambda_{qs} &= \left(L_{ls} + L_M\right) i_{qs} + L_M i_{qr} \\ \lambda_{qr} &= \left(L_{lr} + L_M\right) i_{qr} + L_M i_{qs} \\ \lambda_{ds} &= \left(L_{ls} + L_M\right) i_{ds} + L_M i_{dr} \\ \lambda_{dr} &= \left(L_{lr} + L_M\right) i_{dr} + L_M i_{ds} \end{aligned} \tag{B.3}$$

The eqns (B.1) and (B.2) are written in expanded form as,

$$\begin{aligned} v_{qs} &= R_s i_{qs} + \omega\lambda_{ds} + p\lambda_{qs} \\ v_{ds} &= R_s i_{ds} - \omega\lambda_{qs} + p\lambda_{ds} \end{aligned} \tag{B.4}$$

$$\begin{aligned} v_{qr} &= R_r i_{qr} + \left(\omega - \omega_r\right)\lambda_{dr} + p\lambda_{qr} \\ v_{dr} &= R_r i_{dr} - \left(\omega - \omega_r\right)\lambda_{qr} + p\lambda_{dr} \end{aligned} \tag{B.5}$$

In stationary reference frame, the eqns. (B.4) and (B.5) are written in an alternative vector form as,

$$[\mathbf{v}] = [\mathbf{R}][\mathbf{i}] + [\mathbf{L}]p[\mathbf{i}] + [\mathbf{G}][\mathbf{i}]$$

where, the $[\mathbf{v}], [\mathbf{i}], [\mathbf{r}], [\mathbf{L}]$ and $[\mathbf{G}]$ has the form as follows-

$$[\mathbf{v}] = \begin{bmatrix} v_{qs} & v_{ds} & v_{qr} & v_{dr} \end{bmatrix}^T \tag{B.6}$$

$$[\mathbf{i}] = \begin{bmatrix} i_{qs} & i_{ds} & i_{qr} & i_{dr} \end{bmatrix}^T \tag{B.7}$$

$$[\mathbf{R}] = \begin{bmatrix} R_s & 0 & 0 & 0 \\ 0 & R_s & 0 & 0 \\ 0 & 0 & R_r & 0 \\ 0 & 0 & 0 & R_r \end{bmatrix} \tag{B.8}$$

$$[\mathbf{G}] = \begin{bmatrix} 0 & 0 & 0 & 0 \\ 0 & 0 & 0 & 0 \\ 0 & -\omega_r L_M & 0 & L_r \\ -\omega_r L_M & 0 & L_r & 0 \end{bmatrix} \tag{B.9}$$

Due to cross flux saturation, magnetic coupling exists between q axis and d axis and transformer inductance matrix $[\mathbf{L}]$ [50] is defined as,

$$[\mathbf{L}] = \begin{bmatrix} L_{sq} & L_{dq} & L_{Mq} & L_{dq} \\ L_{dq} & L_{sd} & L_{dq} & L_{Md} \\ L_{Mq} & L_{dq} & L_{rq} & L_{dq} \\ L_{dq} & L_{Md} & L_{dq} & L_{rd} \end{bmatrix} \tag{B.10}$$

For SEIG, the air gap voltage does not remain constant and therefore the magnetizing reactance also varies accordingly. For the purpose, the magnetizing current is calculated as,

$$i_M = \sqrt{\left(i_{qs} + i_{qr}\right)^2 + \left(i_{ds} + i_{dr}\right)^2} \tag{B.11}$$

The magnetizing inductance $L_M$ is calculated using magnetizing characteristic, which is obtained from synchronous speed test of the machine.

The main and cross flux saturation depended coefficients [50] are evaluated as,

$$\begin{aligned} L_M &= \frac{\lambda_M}{i_M} \\ L &= \frac{d\lambda_M}{di_M} \end{aligned} \tag{B.12}$$

$$\begin{aligned} \cos\mu &= \frac{i_{dM}}{i_M} \\ \sin\mu &= \frac{i_{qM}}{i_M} \end{aligned} \tag{B.13}$$

$$\begin{aligned} L_{dq} &= (L - L_M)\cos\mu\sin\mu \\ L_{Mq} &= L\cos^2\mu + L_M\sin^2\mu \\ L_{Md} &= L\sin^2\mu + L_M\cos^2\mu \end{aligned} \tag{B.14}$$

$$\begin{aligned} L_{sq} &= L_{ls} + L_{Mq} \\ L_{sd} &= L_{ls} + L_{Md} \\ L_{rq} &= L_{lr} + L_{Mq} \\ L_{rd} &= L_{lr} + L_{Md} \end{aligned} \tag{B.15}$$

# APPENDIX-C

## COEFFICIENTS OF LOOP IMPEDANCE FOR SEIG FEEDING RESISTIVE-INDUCTIVE LOAD

The coefficients '*A'* and '*B'* are calculated for the real and imaginary part of loop impedance $Z_{LS}$ for SEIG feeding resistive-inductive load. The coefficients 'A' are corresponding to $G_S$ polynomial of real part and coefficients 'B' are corresponding to $H_S$ polynomial of imaginary part and are expressed as,

$$G_S = \sum_{m=0}^{3}\left(A^{2m+1} + A^{2m+2}X_M\right)F^m = 0$$
$$H_S = \sum_{m=0}^{3}\left(B^{2m+1} + B^{2m+2}X_M\right)F^m = 0 \quad \text{(C.1)}$$

The coefficients '*A*' and '*B*' are expressed as,

$$A^1 = -\nu X_{lr}[R_l X_{sh} + R_s X_{sh}] \quad \text{(C.2)}$$

$$A^2 = -\nu[R_s X_{sh} + R_l X_{sh}] \quad \text{(C.3)}$$

$$A^3 = X_{sh}(R_s X_{lr} + R_r X_{ls}) + R_r(R_s R_l + X_l X_{sh}) + X_{lr} X_{sh} R_l \quad \text{(C.4)}$$

$$A^4 = R_s X_{sh} + X_{sh}(R_s + R_r) \quad \text{(C.5)}$$

$$A^5 = \nu X_{lr}(X_{ls} R_l + R_s X_l) \quad \text{(C.6)}$$

$$A^6 = \nu[R_s X_l + R_l(X_{ls} + X_{lr})] \quad \text{(C.7)}$$

$$A^7 = X_l(R_r X_{ls} + R_s X_{lr}) + X_{ls} X_{lr} R_l \quad \text{(C.8)}$$

$$A^8 = R_s(X_{ls} + X_{lr}) + X_l(R_s + R_r) \quad \text{(C.9)}$$

$$B^1 = -[X_{sh} R_2 R_l + R_s R_r X_{sh}] \quad \text{(C.10)}$$

$$B^2 = -X_{sh} \quad \text{(C.11)}$$

$$B^3 = -\nu X_{lr}[X_{sh} X_l + X_{ls} X_{sh} + X_{ls} R_l] \quad \text{(C.12)}$$

$$B^4 = -\nu[X_{sh} X_l + R_s R_l + X_{sh}(X_{ls} + X_{lr})] \quad \text{(C.13)}$$

$$B^5 = X_{lr}(R_s R_l + X_{sh} X_l + X_{lr} X_{sh} + R_r(R_s X_l + X_{ls} R_l) \quad \text{(C.14)}$$

$$B^6 = R_l(R_s + R_r) + X_{sh} X_l + (X_{ls} + X_{lr}) X_{sh} \quad \text{(C.15)}$$

$$B^7 = \nu X_{ls} X_{lr} X_l \quad \text{(C.16)}$$

$$B^8 = \nu X_l (X_{ls} + X_{lr}) \quad \text{(C.17)}$$

$$B^9 = -X_{ls} X_{lr} X_l \quad \text{(C.18)}$$

$$B^{10} = -X_l (X_{ls} + X_{lr}) \quad \text{(C.19)}$$

# APPENDIX-D

## GENETIC ALGORITHM PARAMETERS

- Population size for each variable=150
- String length of each variable=28 bit
- Cross over probability=0.8
- Mutation probability=0.05

# APPENDIX-E

## EQUATION OF DIGITAL PI CONTROLLER

The proportional-integral (PI) controller equation can be deduced from the general proportional-integral-derivative (PID) controller equation in discrete time domain. In one of the form, the transfer function of analog PID controller [277] is written as,

$$G(s) = k_p\left(1+\frac{1}{T_i s}+T_d s\right) \tag{E.1}$$

Where, $T_i$ and $T_d$ are the integral and derivative time constants.

Using trapezoidal approximation for the integrator and the backward difference for the differentiator, eqn. (E.1) in z-domain is written as,

$$G(z) = k_p\left[1+\frac{T_s}{2T_i}\left(\frac{z+1}{z-1}\right)+\frac{T_d}{T_s}\left(\frac{z-1}{z}\right)\right] \tag{E.2}$$

$$G(z) = k_p\left[1-\frac{T_s}{2T_i}+\frac{T_s}{T_i}\left(\frac{1}{1-z^{-1}}\right)+\frac{T_d}{T_s}\left(1-z^{-1}\right)\right] \tag{E.3}$$

where, $T_s$ is the sampling time.

Now define

$$\text{Proportional Gain}=K_P = k_p\left(1-\frac{T_s}{2T_i}\right)$$

$$\text{Integral Gain}= K_I = k_p\frac{T_s}{T_i} \tag{E.4}$$

$$\text{Derivative Gain}=K_D = k_p\frac{T_d}{T_s}$$

Therefore, eqn. (E.3) is written as,

$$G(z) = K_P+\frac{K_I}{(1-z^{-1})}+K_D(1-z^{-1}) = \frac{U(z)}{E(z)} \tag{E.5}$$

The eqn. (E.5) is a general expression of the digital PID controller. After rearranging, the equation takes the form as,

$$(1-z^{-1})U(z) = K_P(1-z^{-1})E(z) + K_I E(z) + K_D(1-2z^{-1}+z^{-2})E(z) \quad \text{(E.6)}$$

Let *e(k)* and *u(k)* are the input and output, eqn. (E.6) in discrete time domain is expresses as,

$$u(k) = u(k-1) + K_P\left[e(k) - e(k-1)\right] + K_I e(k) + K_D\left[e(k) - 2e(k-1) + e(k-2)\right] \quad \text{(E.7)}$$

The eqn. (E.7) suggests that derivative (D) controller should have terms *e(k*-2*)* in addition to *e(k)* and *e(k*-1*)*, while the PI controller has the terms *e(k)* and *e(k*-1*)* only.

By substituting $K_D$=0 in the eqn. (E.7), the discrete PI controller equation takes the form as,

$$u(k) = u(k-1) + K_P\left[e(k) - e(k-1)\right] + K_I e(k) \quad \text{(E.8)}$$

# APPENDIX-F

## QUADRATURE AND IN-PHASE COMPONENTS RELATIONSHIP

The phasor relationship of quadrature templates ($u_{sqa}$, $u_{sqb}$ and $u_{sqc}$) and in-phase templates ($u_{sda}$, $u_{sdb}$ and $u_{sdc}$) are shown in the Fig. F.1 as,

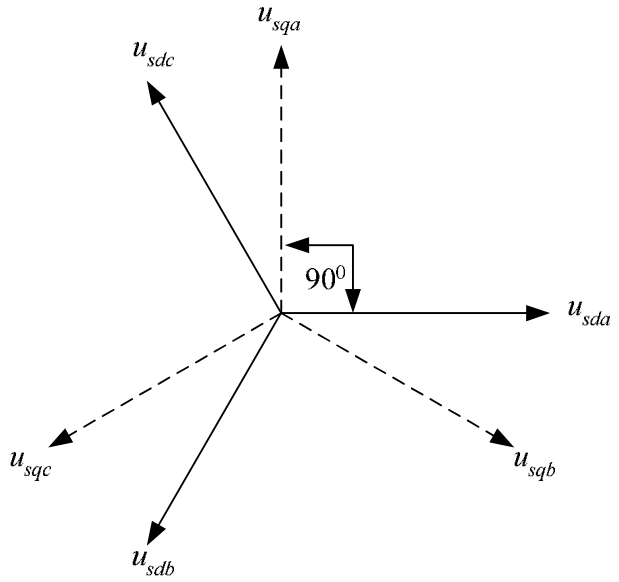


***Fig. F.1 Phasor diagram relating in-phase and quadrature components***

The quadrature template $u_{sqa}$ can be obtained as,

$$u_{sqa} = \frac{2}{3}(u_{sdb}\cos 150 + u_{sdc}\cos 30) = \frac{1}{\sqrt{3}}(-u_{sdb} + u_{sdc}) \tag{F.1}$$

The 2/3 factor is used in eqn. (F.1) on account of equating the peak values of in-phase and quadrature templates to unity.

Similarly, the $u_{sqb}$ and $u_{sqc}$ can be obtained as,

$$u_{sqb} = \frac{2}{3}(u_{sdc}\cos 150 + u_{sda}\cos 30) = \frac{1}{\sqrt{3}}(-u_{sdc} + u_{sda}) \tag{F.2}$$

$$u_{sqc} = \frac{2}{3}(u_{sda}\cos 150 + u_{sdb}\cos 30) = \frac{1}{\sqrt{3}}(-u_{sda} + u_{sdb}) \tag{F.3}$$

In vector form, the eqns. (F.1) to (F.3) can also be written as,

$$\begin{bmatrix} u_{sqa} \\ u_{sqb} \\ u_{sqc} \end{bmatrix} = \frac{1}{\sqrt{3}} \begin{bmatrix} 0 & -1 & 1 \\ 1 & 0 & -1 \\ -1 & 1 & 0 \end{bmatrix} \begin{bmatrix} u_{sda} \\ u_{sdb} \\ u_{sdc} \end{bmatrix} \tag{F.4}$$

For balanced sinusoidal templates,

$$u_{sqa} + u_{sqb} + u_{sqc} = 0 \tag{F.5}$$

Therefore, $u_{sqa}$, $u_{sqb}$ and $u_{sqc}$ summarized in eqn. (F.4), are rewritten as,

$$u_{sqa} = \frac{1}{\sqrt{3}}(-u_{sdb} + u_{sdc}) \tag{F.6}$$

$$u_{sqb} = \frac{1}{\sqrt{3}}(u_{sda} - u_{sdc}) = \frac{1}{2\sqrt{3}}(3u_{sda} + u_{sdb} - u_{sdc}) = \frac{\sqrt{3}}{2}u_{sda} + \frac{1}{2\sqrt{3}}(u_{sdb} - u_{sdc}) \tag{F.7}$$

$$u_{sqc} = \frac{1}{\sqrt{3}}(-u_{sda} + u_{sdb}) = \frac{1}{2\sqrt{3}}(-3u_{sda} + u_{sdb} - u_{sdc}) = -\frac{\sqrt{3}}{2}u_{sda} + \frac{1}{2\sqrt{3}}(u_{sdb} - u_{sdc}) \tag{F.8}$$

In vector form, the eqns. (F.6) to (F.8) are written as,

$$\begin{bmatrix} u_{sqa} \\ u_{sqb} \\ u_{sqc} \end{bmatrix} = \begin{bmatrix} 0 & -1/\sqrt{3} & 1/\sqrt{3} \\ \sqrt{3}/2 & 1/2\sqrt{3} & -1/2\sqrt{3} \\ -\sqrt{3}/2 & 1/2\sqrt{3} & -1/2\sqrt{3} \end{bmatrix} \begin{bmatrix} u_{sda} \\ u_{sdb} \\ u_{sdc} \end{bmatrix} \tag{F.9}$$

The eqn. (F.9) represents the standard form relating quadrature and in-phase templates.

# APPENDIX-G

## SUMT WITH ROSENBROCK'S METHOD APPLIED TO SEIG-INDUCTION MOTOR LOAD

### G.1 Rosenbrock's Method of Rotating Coordinates

The brief algorithm of Rosenbrock's method of rotating coordinate [272], which is a direct search method, is summarized as follows,

1. Define a set of initial step lengths $\lambda_1$ and $\lambda_2$ along the search directions $S_1^{(1)} = \begin{bmatrix} 1 \\ 0 \end{bmatrix}$ and $S_2^{(1)} = \begin{pmatrix} 0 \\ 1 \end{pmatrix}$ respectively, $\alpha$>1, 0<$\beta$<1, Max. iteration $j^{mx}$, small number $\varepsilon$, base point $X_b$ and iteration $j$=1.

2. A step of length $\lambda_1$ is taken in the direction $S_1^{(j)}$ from the base point $X_b$, new point $X = X_b + \lambda_1 S_1^{(j)}$

3. if $f(X)<f(X_b)$, then $\lambda_1 = \lambda_1 \alpha$, $X = X_b$, $\Delta_1 = \Delta_1 + \lambda_1$, record the success, otherwise, $\lambda_1 = -\lambda_1 \beta$, record the failure.

4. Continue the search along the $S_2^{(j)}$ direction, until at least one step has been successful and one step has failed in each of the direction.

   Compute the new set of directions as $S_1^{(j+1)}$, $S_2^{(j+1)}$ for use in ($j$+1) iteration of minimization by using Gram-Schmidt orthogonalization procedure as,

$$P = [P_1 \quad P_2] = \begin{bmatrix} S_1^{(1)} & S_2^{(1)} \end{bmatrix} \begin{bmatrix} \Delta_1 & 0 \\ \Delta_2 & \Delta_2 \end{bmatrix} \tag{G.1}$$

$$S_1^{(1+j)} = \frac{P_1}{\|P_1\|} \tag{G.2}$$

$$Q_2 = P_2 - P_2^T S_1^{(1+j)} S_1^{(1+j)} \tag{G.3}$$

$$S_2^{(1+j)} = \frac{Q_2}{\|Q_2\|} \tag{G.4}$$

5. Take the best point obtained in the present stage as the best point for the next stage and increase the iteration number to ($j$+1).

6. if $j<j^{mx}$ or $|\Delta_i| \le \varepsilon$ for all $i$, go to step 2 otherwise stop.

## G.2 Sequential Unconstrained Minimization Technique (SUMT)

The SUMT, which is also known as penalty function method [272], transforms the constrained optimization problem into alternative unconstrained minimization formulation. The basic optimization problem has the form as,

Find $X$ which minimizes $f(X)$, subjected to $g_j(X) \le 0, j = 1,2,....,m$ .

The problem is converted into an unconstrained minimization problem by formulating the alternative function of the form as,

$$\phi_k = \phi(X, r_k) = f(X) + r_k \sum_{j=1}^{m} G_j[g_j(X)] \qquad \text{(G.5)}$$

Where, $G_j$ is the function of constraints $g_j$, and $r_k$ is a positive constant known as the penalty constant. The second function of above equation is called penalty term. The unconstrained minimization of the $\phi$ function is repeated for the sequence of values of the penalty constant $r_k$ ($k$=1, 2, …), the solution will be converged to that of original function.

The algorithmic steps of the SUMT are as,

1. Select the initial feasible point $X_1$, satisfying all the constraints that is $g_j(X_1)<0$, $j$=1, 2...$m$. and initial value of $r_1>0$, small number ε. Set $k$=1.

2. Minimize $\phi(X, r_k)$ by using Rosenbrock's method of rotating coordinate and obtain the solution $X_k^*$.

3. If $f(X_k^*) - f(X) \le \varepsilon$, than $X_k^*$ is the optimum solution of $f(X)$ and terminate the process, otherwise go to next step.

4. Change the penalty constant $r_{k+1}=c\ r_k$, where $c<1$

5. Change $X_1$ as $X_1 = X_k^*$.

6. Increase the iteration as $k=k+1$ and go to step 2.

## G.3 Computation of Capacitance for SEIG Fed Induction Motor Load

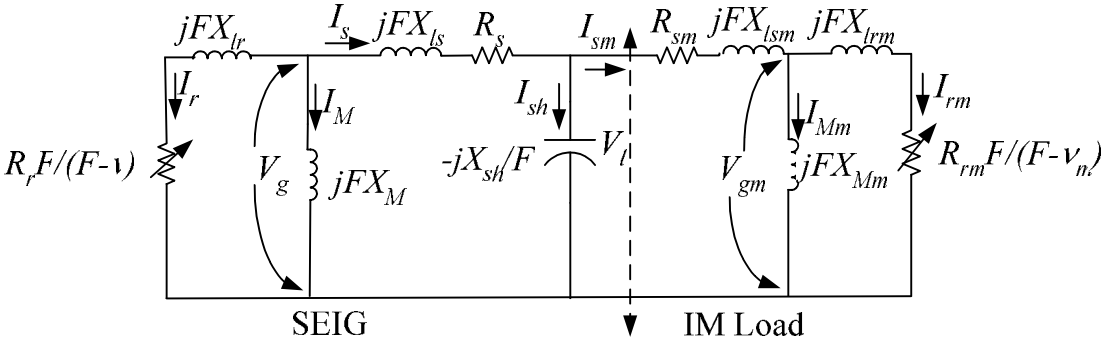


***Fig. G.1 Equivalent circuit of SEIG with IM Load***

Let the impedances are defined as follows,

$$Z_s = R_s + jFX_{ls} \tag{G.6}$$

$$Z_M = jFX_M \tag{G.7}$$

$$Z_{sh} = -\frac{jX_{sh}}{F} \tag{G.8}$$

$$Z_r = \frac{R_r F}{\left(F - \nu\right)} + jFX_{lr} \tag{G.9}$$

$$Z_{sm} = R_{sm} + jFX_{lsm} \tag{G.10}$$

$$Z_{Mm} = jFX_{Mm} \tag{G.11}$$

$$Z_{rm} = \frac{R_{rm} F}{\left(F - \nu_m\right)} + jFX_{lrm} \tag{G.12}$$

$$Z_{mtr} = Z_{sm} + \frac{Z_{rm} Z_{Mm}}{Z_{rm} + Z_{Mm}} \tag{G.13}$$

Applying KVL on stator side loop of induction generator results –

$$Z_{Lm}\, I_s = 0 \tag{G.14}$$

$$\text{where, } Z_{Lm} = \frac{Z_M Z_r}{Z_M + Z_r} + Z_s + \frac{Z_{sh} Z_{mtr}}{Z_{sh} + Z_{mtr}} \tag{G.15}$$

Under steady state condition, $I_s$ can not be zero and therefore $Z_{Lm}$ from eqn. (G.15) should be zero. An optimization problem with objective function as $Z_{Lm}$ has been

formulated to obtain the unknown variables $X_{sh}$ and $F$. The objective function $F_n(X_{sh}, F)$ is as,

$$F_n(X_{sh}, F) = \left| \frac{Z_M Z_r}{Z_M + Z_r} + Z_s + \frac{Z_{sh} Z_{mtr}}{Z_{sh} + Z_{mtr}} \right| \tag{G.16}$$

The bound on variables are as,

$$F^{mn} \le F \le F^{mx}$$
$$X_{sh}^{mn} \le X_{sh} \le X_{sh}^{mx}$$

The superscript *mn* and *mx* indicates the minimum and maximum values.

The above problem is solved through SUMT (sequential unconstraint minimization technique) in conjunction with the Rosenbroack method of direct search technique. The objective function should converge to a very small value closer to zero. Indeed, the capacitance can be computed as $C_{sh} = \frac{1}{2\pi F_b X_{sh}}$

# APPENDIX-H

## PARAMETERS OF STATIC CONTROLLERS

### H.1 STATCOM and PI Controllers Parameters for STATCOM Feeding Static and Dynamic Loads

Full rating STATCOM parameters:

AC side inductor filter: $R_f = 0.5\Omega$, $L_f = 3.4$ mH

DC bus capacitor $C_{dc} = 285$ μF

Reduced rating STATCOM parameters:

AC side inductor filter: $R_f = 0.5\Omega$, $L_f = 6.8$ mH

DC bus capacitor $C_{dc} = 145$ μF

DC link voltage PI controller gains: $K_{pvdc} = 0.0051$, $K_{ivdc} = 0.00652$

Terminal voltage PI controller gains: $K_{pvps} = 0.003$, $K_{ivps} = 0.0056$

### H.2 STATCOM and PI Controllers Parameters for Three-Phase Four-Wire Isolated System

AC side inductor filter: $R_f = 0.5\Omega$, $L_f = 6.0$ mH

DC bus capacitor $C_{dc} = 500$ μF

PI controller gains for DC bus voltage control: $K_p = 0.045$, $K_i = 0.0009$

PI controller gains for SEIG terminal voltage control: $K_p = 0.055$, $K_i = 0.003$

### H.3 SSSC and PI Controller Parameters for SEIG-SSSC Feeding Static Loads

Battery voltage $v_{bat} = 231$ V

Ripple filter parameters: $R_f = 0.1\Omega$, $L_f = 3.4$ mH, $C_f = 8.0$ μF

PI Controller gains for load voltage control: $K_p = 0.0085$, $K_i = 0.0098$

## H.4 SSSC and PI Controllers Parameters for SEIG-Capacitor Supported SSSC Feeding Static R-L Load

Reference DC bus voltage = 350 V

Ripple filter parameters: $R_f$ = 0.1Ω, $L_f$ = 7.75 mH, $C_f$ = 3.3 μF

DC bus capacitance $C_{dc}$ = 491 μF

Load voltage PI controller gains:

$K_{pvpl}$ = 0.00091; $K_{ipvl}$ = 0.009190

DC bus PI controller gains:

$K_{pvdc}$ = 0.001; $K_{ivdc}$ = 0.00070

## H.5 SSSC and PI Controller Parameters for SEIG-SSSC Feeding Induction Motor Load

Battery voltage $v_{bat}$ = 300 V

Ripple filter parameters: $R_f$ = 0.1Ω, $L_f$ = 1.812 mH, $C_f$ = 13.97 μF

PI Controller gains for load voltage control, $K_p$ = 0.0068, $K_i$=0.0022

# APPENDIX-I

## COEFFICIENTS OF LOOP IMPEDANCE FOR SHORT SHUNT SEIG FEEDING RESISTIVE-INDUCTIVE LOAD

The coefficients '*C'* and '*D'* from the loop impedance $Z_{LH}$ for short shunt SEIG configuration is given below. The coefficients '*C*' for $G_H$ polynomial of real part and coefficients '*D*' for $H_H$ polynomial of imaginary part are as,

$$C^1 = -r_s X_{hs} X_{es} \tag{I.1}$$

$$C^2 = 0 \tag{I.2}$$

$$C^3 = -\nu X_{lr}[R_l X_{hs} + R_s(X_{hs} + X_{es})] \tag{I.3}$$

$$C^4 = -\nu[R_s(X_{hs} + X_{es}) + R_l X_{hs}] \tag{I.4}$$

$$C^5 = (X_{hs} + X_{es})(R_s X_{lr} + R_r X_{ls}) + R_r(R_s R_l + X_l X_{hs}) + X_{lr} X_{hs} R_l \tag{I.5}$$

$$C^6 = R_s X_{hs} + (X_{hs} + X_{es})(R_s + R_r) \tag{I.6}$$

$$C^7 = \nu X_{lr}(X_{ls} R_l + R_s X_l) \tag{I.7}$$

$$C^8 = \nu[R_s X_l + R_l(X_{ls} + X_{lr})] \tag{I.8}$$

$$C^9 = X_l(R_r X_{ls} + R_s X_{lr}) + X_{ls} X_{lr} R_l \tag{I.9}$$

$$C^{10} = R_s(X_{ls} + X_{lr}) + X_l(R_s + R_r) \tag{I.10}$$

$$D^1 = \nu X_{es} X_{hs} X_{lr} \tag{I.11}$$

$$D^2 = \nu X_{es} X_{hs} \tag{I.12}$$

$$D^3 = -[X_{hs}(R_2 R_l + X_{lr} X_{es}) + R_s R_r(X_{hs} + X_{es})] \tag{I.13}$$

$$D^4 = -(X_{hs} + X_{es}) \tag{I.14}$$

$$D^5 = -\nu X_{lr}[X_{hs} X_l + X_{ls}(X_{hs} + X_{es}) + X_{ls} R_l] \tag{I.15}$$

$$D^6 = -\nu[X_{hs} X_l + R_s R_l + (X_{hs} + X_{es})(X_{ls} + X_{lr})] \tag{I.16}$$

$$D^7 = X_{lr}(R_s R_l + X_{hs} X_l + X_{lr}(X_{hs} + X_{es}) + R_r(R_s X_l + X_{ls} R_l) \quad \text{(I.17)}$$

$$D^8 = R_l(R_s + R_r) + X_{hs} X_l + (X_{ls} + X_{lr})(X_{hs} + X_{es}) \quad \text{(I.18)}$$

$$D^9 = \nu X_{ls} X_{lr} X_l \quad \text{(I.19)}$$

$$D^{10} = \nu X_l(X_{ls} + X_{lr}) \quad \text{(I.20)}$$

$$D^{11} = -X_{ls} X_{lr} X_l \quad \text{(I.21)}$$

$$D^{12} = -X_l(X_{ls} + X_{lr}) \quad \text{(I.22)}$$

# LIST OF PUBLICATIONS

**International Journal Papers**

1. "Static VAR Compensator for Self-Excited Induction Generator Feeding Dynamic Load," *Electric Power Components and Systems*, vol. 36, no. 10, pp. 1080-1101, 2008.

2. "A Prospective on Voltage Regulation of SEIG for Industry Applications," *IEEE Transactions on Industry Applications,* vol. 46, no. 2, pp. 720-730, 2010.

**IEEE International Conference Papers**

3. "Transient Performance of Three-Phase Four-Wire Stand Alone Supply System with Static Converter Employed for Industrial Loads*," in Proc. IEEE Conf. POWERCON-2008*, 13-15 Oct. 2008, New Delhi.

4. "A Prospective on Voltage Regulation of SEIG for Industrial Applications," *in Proc*. *IEEE Conf. IAS-PCIC 2004*, 9-10 Nov. 2004, New Delhi.

**Research papers under Review**

5. "Genetic Algorithm Based Optimum Performance of Compensated Self-excited Induction Generator," **Revised manuscript has been submitted** in *International Journal of Modelling and Simulation, Acta Press.*

6. "Voltage and Frequency Regulating Schemes for Three-Phase Self-Excited Induction Generators," *International Journal of Energy Technology and Policy, Inderscience Publications.*